Fall 10-1-2021

Expanding the Reliable Paleomagnetic Constraints on Configurations of Pre-Pangean Supercontinents

Zheng Gong
Yale University Graduate School of Arts and Sciences, njugongzheng@gmail.com

Abstract

Expanding the Reliable Paleomagnetic Constraints on Configurations of Pre-Pangean Supercontinents

Zheng Gong

2021

Supercontinents embody perhaps the longest cyclic process on our planet, profoundly influencing the evolution of Earth's biosphere, geosphere, and atmosphere on timescales of hundred-million years or more. Yet, the configurations of pre-Pangean supercontinents, Rodinia, Nuna, and/or Kenorland, as well as their transition processes remain the subjects of debate, hampering the understanding of the interactions between the global tectonics and Earth's evolution in deep time. Compared to other approaches, paleomagnetism is the only quantitative method to reconstruct pre-Pangean supercontinents in an absolute paleogeographic framework. However, a recent summary of global paleomagnetic data of Precambrian age reveals two problems. First is that discordant paleomagnetic records exist in some cratons' datasets, thus rendering paleogeographic interpretations difficult. Second is that some cratons (e.g., West African Craton) have heretofore essentially no reliable Precambrian paleomagnetic records, yielding large uncertainties in their paleogeography.

This dissertation is dedicated to addressing these problems. Specifically, we studied three cases of discordant paleomagnetic records, one from Tonian data in Baltica, and a pair of Orosirian datasets from the Slave craton. By adding new data and carefully compiling and evaluating published results, we thoroughly discussed the possible causes of discordance

in the paleomagnetic directions. For Baltica, using detailed laboratory demagnetization techniques on samples from the Dalarna-Blekinge dolerite dike suite, we attributed an abnormal direction within the Dalarna-Blekinge mafic dikes to unremoved overprints. In addition, by comparing our new Baltica poles around ~950 Ma with coeval poles from Laurentia, we proposed rapid latitudinal motions of these two cratons in early Tonian time. For the Slave craton, we proposed that although basin- or local-scale vertical-axis rotations could account for some discrepancies among time-correlative 2.02-1.88 Ga poles, the overall pattern of the Orosirian apparent polar wander path of the Slave craton is better explained by true polar wander. These findings are helpful for studying the dynamic movements of Rodinia and the amalgamation of Nuna.

In addition, we reviewed the Precambrian paleomagnetic records of the West African Craton to understand the limitations of previous studies. We found that most of the low-quality published results from the West African Craton suffer from inadequate sampling, poor dating, and the lack of field tests. We conducted a paleomagnetic study on Proterozoic mafic dike swarms in the Anti-Atlas Belt, Morocco, combined with U-Pb geochronology. After detailed field and laboratory work, we provided two reliable paleomagnetic poles for the West African Craton, one at 2.04 Ga and the other at 1.4–1.36 Ga. These new poles help fill the large gaps in the paleomagnetic dataset of the West African Craton. Using the two poles, we proposed a new connection between the West African Craton and Amazonia before and within Nuna, of which the relative position between the two cratons is 180° different from their connection in Gondwana. Incorporating paleomagnetic and geological constraints from other major cratons, we revised the configuration of supercontinent Nuna.

Our new reconstruction model sheds light on the plate motion pattern between neighboring cratons in deep time, as well as the style of Nuna-Rodinia supercontinental transition.

To summarize, the outcome of this dissertation expands the reliable paleomagnetic constraints on configurations of pre-Pangean supercontinents, and promotes an understanding of the Earth's evolution in a spatial perspective. The final establishment of a global paleogeographic framework in the Precambrian still awaits further integrations of robust paleomagnetic studies with geochronological, stratigraphical, geochemical, and paleontological constraints.

Expanding the Reliable Paleomagnetic Constraints on Configurations of Pre-Pangean Supercontinents

A Dissertation

Presented to the Faculty of the Graduate School

of

Yale University

in Candidacy for the Degree of

Doctor of Philosophy

by

Zheng Gong

Dissertation Director: David A. D. Evans

December, 2021

Acknowledgments

This dissertation would not be possible without the help and support that I have received from my supervisors, colleagues, and friends over the course of my Ph.D. First and foremost, I would like to thank my advisor, David Evans. I have learned so much by working with him in both the laboratory and field. Most importantly, he has encouraged me to become an independent scientist and has allowed me to study the topics I am interested in, even though some of them are not always directly relevant to my dissertation. I am fortunate to have been a student of Dave. In addition, I want to thank my dissertation committee, Mark Brandon, Noah Planavsky, Jun Korenaga, and Alan Rooney, for giving me invaluable research suggestions and career advice.

I also want to thank our department for fostering a friendly and supportive research community and being generous in funding research, colloquiums, as well as field trips. I have made so many friends who have helped, inspired, and encouraged me in many ways in the past five years. I'd like to thank Bin Wen, Xianqing Jing, Jikai Ding, Chao Wang, Seamus Houlihan, Chiara Chung-Halpern, Vuong Mai, James Pierce, and Eliza Poggi for being great lab mates. It was a pleasure to serve as Dana Club officers with Sophie Westacott and Ryan Li. I thank Nicole Shibley and Alexie Millikin for co-organizing a successful and fun Yukon-Alaska field trip. Peng Sun and William Frazer were great office mates. I thank Zhongtian Zhang, Meng Guo, Yu Liang, Jie Deng, Ryan Li, Bowen Zhao, Guangyi Wei, Mingyu Zhao, Qinting Jiang, Zhiyuan Li, Yantao Luo, and many more Chinese postdocs, graduate students, and visiting scholars for creating such a lovely and supportive Chinese community.

Additionally, I am grateful to have worked with so many brilliant geoscientists from other institutions in the laboratory and field. Their constructive ideas and invaluable insights have significantly improved my research. I would like to thank Sten-Åke Elming, Ulf Söderlund, and Johanna Salminen for their help with my project in Sweden; Ross Mitchell, Paul Hoffman, Wouter Bleeker, and Alessandro Ielpi for working with me on my project in Nunavut, Canada; Nasrrddine Youbi, Ulf Söderlund, Kevin Chamberlain, Abdelhak Ait Lahna, Malika Ait Malek, Madeleine Palassia, Bin Wen, Xianqing Jing, Jikai Ding, Moulay Boumehdi, and Richard Ernst for their help in my project in Morocco. I also want to acknowledge the financial support that I have received over the past few years. My fieldwork in Sweden was partially funded by the travel grant of the Yale EPS Department. Research in Morocco was funded by the National Science Foundation (Grant EAR-1953549), the Swedish MENA Research Program, the Russian Mega-Grant (14.Y26.31.0012), as well as the LIPs–Industry Consortium Project (Industry support matched by a Canadian NSERC grant CRDPJ 523131-17). My fieldwork in Canada was funded by the GSA Graduate Research Grant Outstanding Mention Award, the GSA Geophysical Division Student Research Award, and Yale University.

Last but not least, I want to thank my parents, Sihong Gong and Xiangmei Duan, for always encouraging me to pursue my dreams. Even though we have to be separated by wide oceans, their endless and unconditional love enables me to face the difficulties and struggles in my life bravely, always stay positive, and be kind and thankful to this world.

TABLE OF CONTENTS

(282 pp.)

Introduction

Cyclicities are commonly observed phenomena in the Earth system, occurring on a wide range of time scales (Fig. 1). Among these, the supercontinental cycle has perhaps the longest cyclicity, which occurs roughly every 600 million years (Fig. 1; Evans, 2013; Mitchell et al., 2021). The concept of supercontinental cycles has been widely promoted, in which the amalgamation and breakup of each supercontinent are considered to have profoundly shaped the directions of the Earth's biological, geological and climate evolutions (Nance et al., 2014).

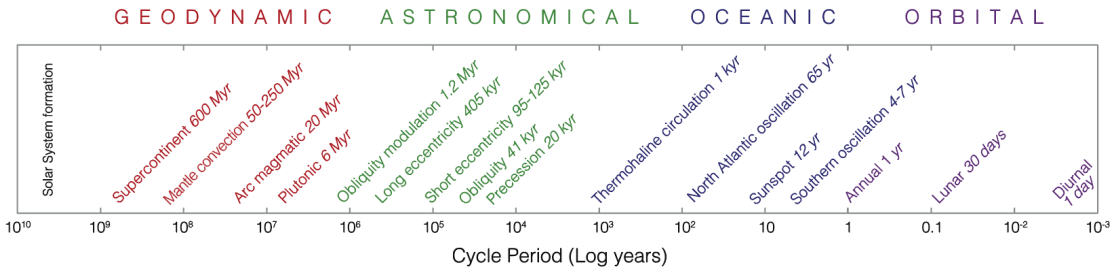

Figure 1 Cyclicities in Earth system on various time scales (modified from Mitchell et al., 2019).

According to numerous pieces of evidence, the configuration of the most recent supercontinent, Pangea, and how its building blocks were assembled and dispersed have been understood with strong confidence. However, due to the less-commonly preserved geological records in deep time, the configurations of pre-Pangean supercontinents, namely Rodinia, Nuna, and/or Kenorland, are still highly debated (Fig. 2; Evans, 2013). The last decade has witnessed continuing refinements of Rodinia, and many new speculations on Nuna (reviewed in Evans, 2021; Elming et al., 2021). These new reconstruction models benefit from increasingly well-constrained Precambrian geological records worldwide,

advances in the visualization of kinematic reconstructions such as GPlates animations (Müller et al., 2018), and the inventions and improvements of techniques in the field and laboratory.

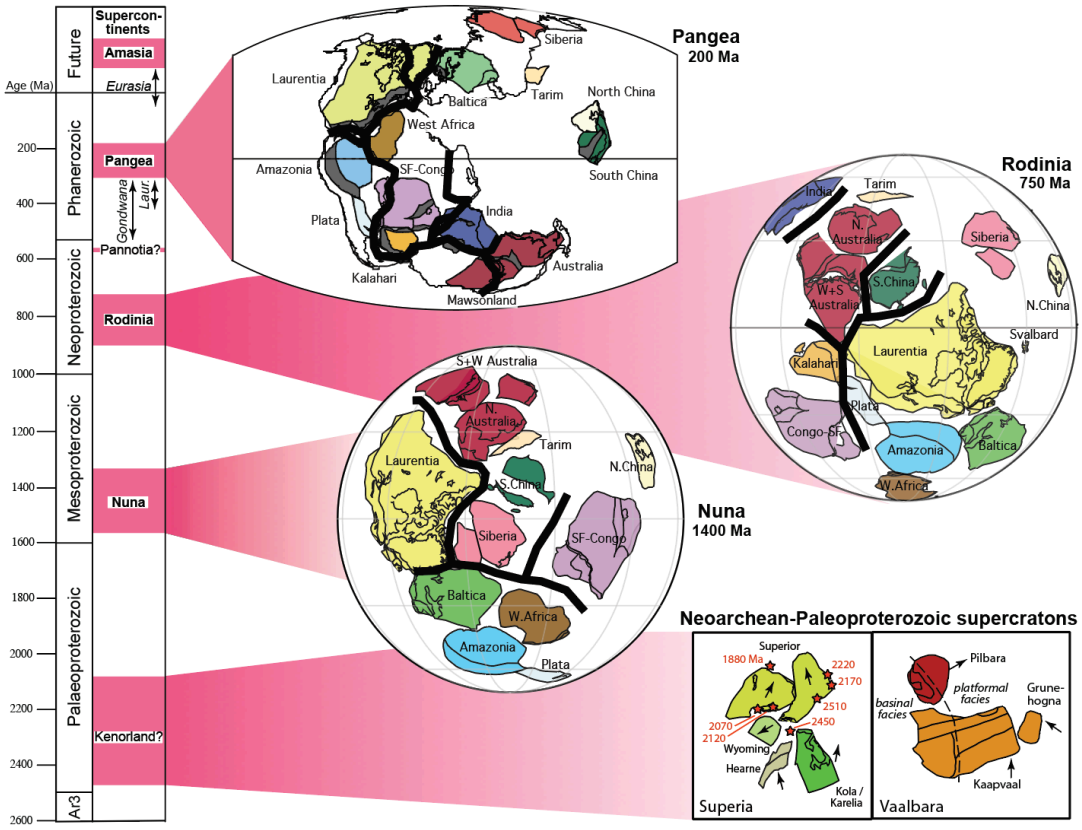

Figure 2 Graphical summary of Earth's supercontinents (adapted from Evans et al. 2016). Abbreviations: Ar3, Neoarchean; Laur., Laurussia. Semi-supercontinents are named in italics. Bold black curves show incipient rifts developed during the breakup of supercontinents.

Aside from geological evidence, many reconstruction models rely heavily on paleomagnetism, which is the only quantitative tool to constrain the paleolatitude and

orientation of cratons in Precambrian time. Assuming that the ancient geomagnetic field was a geocentric-axial dipole (GAD), the magnetic remanence of rocks from a given craton is a function of its paleoposition, varying with age. Specifically, the inclination can inform the paleolatitude of the craton, that is, a steep inclination would indicate a high latitudinal position, and a shallow inclination would indicate a low latitudinal position, in a normal polarity scenario following Equation (1).

$$\tan(\text{inclination}) = 2 \times \tan(\text{paleolatitude}) \qquad (1)$$

Furthermore, under the GAD assumption, declination is zero everywhere on the Earth, as shown in Equation (2).

$$\text{declination} = 0° \qquad (2)$$

Therefore, a non-zero declination of remanence means that the craton must have had a different orientation relative to Earth's rotation axis from the present-day position. Recovering the primary magnetization that was acquired during the formation of the rocks is thus key for using paleomagnetism for paleogeographic reconstructions. A time-series of paleomagnetic poles can be connected to provide an apparent polar wander (APW) path of a given craton, and comparing the APW paths of multiple cratons can constrain their relative distance and orientations as shown in Fig. 3.

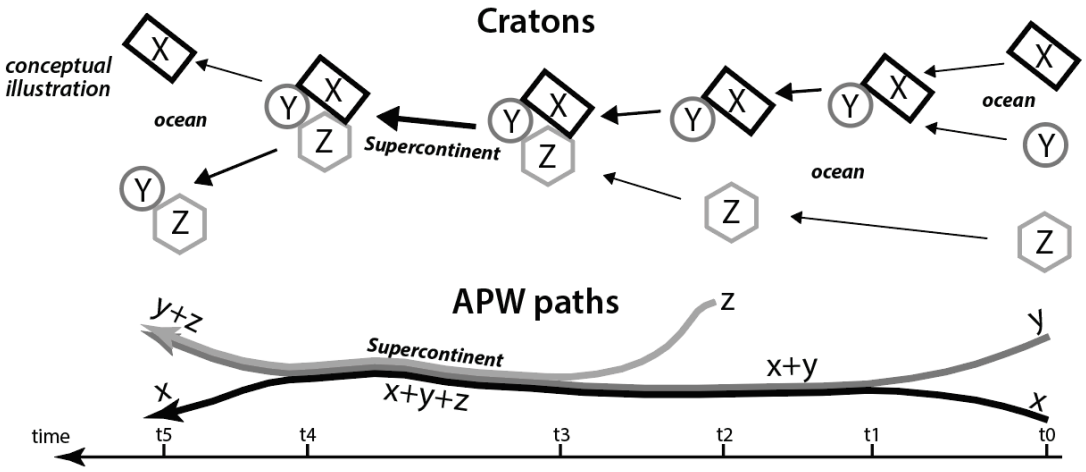

Figure 3 A schematic cartoon of the paleomagnetic record of supercontinental amalgamation and dispersal, involving cratons X, Y, and Z (adapted from Pesonen et al. 2021). Time becomes younger from right to left. A supercontinent is formed when three cratons collide at t3, and it is destroyed when X rifts away from Y+Z at t4. APW = apparent polar wander.

Paleomagnetic data are only useful if they are reliable, with constraints from rigorous field tests and precise geochronology. In order to evaluate the quality of the paleomagnetic data, Van der Voo (1990) proposed seven criteria that have been widely used in the community. These criteria have been recently updated by Meert et al. (2020) to accommodate new developments of paleomagnetism over three decades. Basically, these criteria are designed (1) to constrain the age of the rocks and the age of the magnetization; (2) to guarantee an adequate sampling of the rocks; (3) to ensure an appropriate demagnetization of the rocks using modern techniques; (4) to establish field tests that constrain the age of magnetization; (5) to understand the magnetic mineralogy of the rocks; (6) to verify if the rocks are tectonically coherent with the block that is studied; (7) to exclude the possibility of

remagnetization. Recently, global Precambrian paleomagnetic databases have been thoroughly evaluated by expert community workshops (Brown et al., 2018; Evans et al., 2021), following the updated criteria, and the most reliable paleomagnetic poles are compiled and recommended for paleogeographic reconstructions (Fig. 4). The compilation shows that Laurentia, Baltica, Siberia, and Australia have robust paleomagnetic pole coverage over the longevity of pre-Pangean time. India, Kalahari, Congo/São Francisco, North China, and Amazonia are more sparsely covered by poles, while West Africa stands alone as the only large craton with essentially no paleomagnetic constraints prior to the compilation.

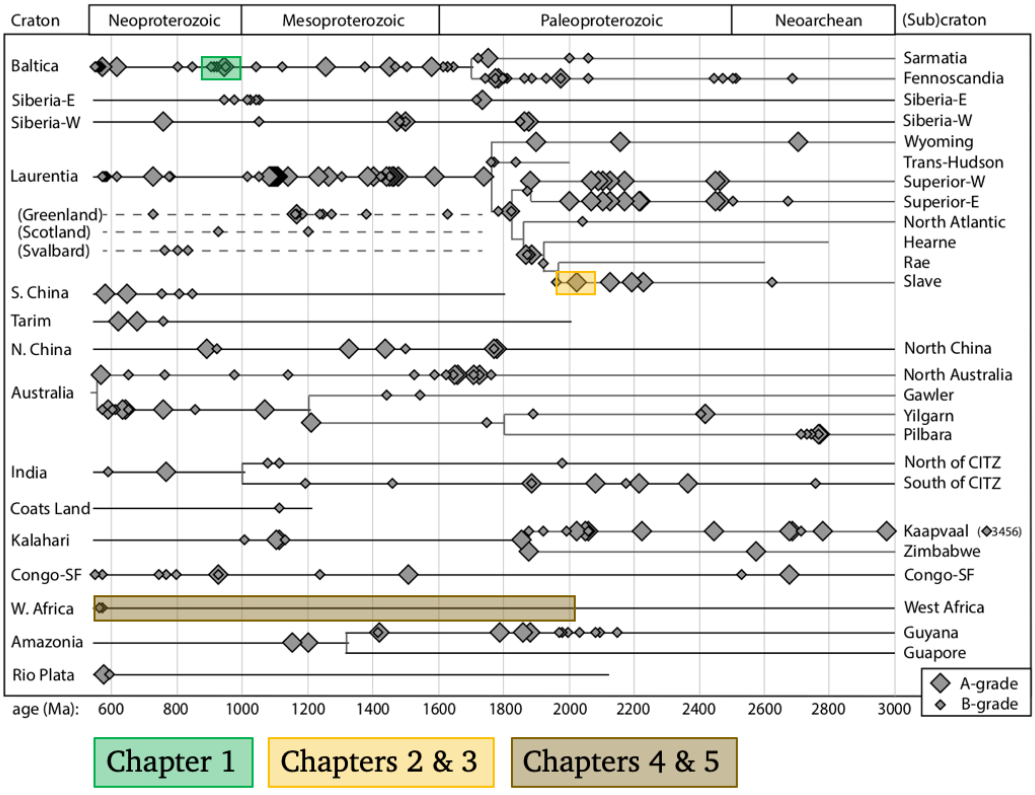

Figure 4 Distribution of A-grade and B-grade poles in time and space, according to the compilation from the Seventh Nordic Paleomagnetism Workshop, modified from Evans et al. (2021). CITZ=Central Indian Tectonic Zone; SF=São Francisco. Green bar covers the

studied interval of Chapter 1, yellow bar indicates the studied interval of Chapters 2 and 3, and brown bars mark the studied intervals of Chapters 4 and 5.

However, some paleomagnetically well-constrained cratons still contain several instances of discordant records, which are obtained from rocks with very similar ages but show distinct paleomagnetic signatures. These discordant paleomagnetic records are, often, unlikely to be simply interpreted as rapid plate motions. Alternative interpretations vary, case by case, including (1) unresolved secondary overprints, (2) unrecognized local structural anomalies, (3) anomalous geomagnetic field behaviors, or (4) true polar wander. Resolving the origin of these discordant paleomagnetic records could not only help us better constrain the configuration of pre-Pangean supercontinents, but also shed light on geodynamic processes. Part I of this dissertation focuses directly on three Proterozoic case studies of discordant paleomagnetic poles obtained from Baltica and Slave craton.

Chapter 1 focuses on testing the veracity of an early Neoproterozoic paleomagnetic pole from Baltica, in an attempt to provide robust quantitative constraints on its paleogeography in supercontinent Rodinia. Detailed paleomagnetic, rock magnetic, anisotropy of magnetic susceptibility and U-Pb baddeleyite geochronological studies were conducted on the Blekinge-Dalarna dolerite (BDD) dykes in Sweden, in order to resolve large variances found in previous paleomagnetic results of the BDD dykes (Gong et al., 2018a). By positive baked-contact tests and reversal tests, a reliable 951–935 Ma key pole for Baltica is proposed. A new 971 Ma virtual paleomagnetic pole for Baltica is also provided. Comparing the coeval poles from Baltica and Laurentia, it is suggested that these two

continents drifted together in Rodinia from high to low latitude between 970–960 Ma and 950–935 Ma, and back to high latitude by 920–870 Ma. Some anomalous directions of the BDD dykes, including the 947 Ma Nornäs dyke, are attributed to a partial remagnetization and should not be used for paleogeographic reconstruction in the future. In addition, by combining our new geochronological data with published ages of mafic intrusions in the Fennoscandian Shield, we argue that origin of the BDD dykes are unlikely a giant circumferential swarm generated by a mantle plume, but more likely results from the tectonic extension at the waning stage of the Sveconorwegian orogeny.

Chapter 2 aims to test the veracity of APW path of the Slave craton during 2.0–1.8 Ga time interval, which is defined by paleomagnetic poles distributed along a >110° arc. This APW path, also known as the Coronation loops, shows an oscillatory pattern that is difficult to reconcile with an actualistic style of plate tectonics, and has been alternatively attributed to rapid plate motion, localized vertical-axis rotation, or true polar wander. By a detailed paleomagnetic and rock magnetic study of 1.87 Ga Pearson Formation (basalt) from different areas in the Great Slave basin, Northwest Territories, Canada, it is observed that paleomagnetic declinations reveal a one-to-one correlation with local structural attitudes, indicating that vertical-axis rotation associated with the dextral displacement along the McDonald Fault system possibly deflects primary paleomagnetic directions up to 60° (Gong et al., 2018b). This study also highlights the possibility of vertical-axis rotation as the cause of the discordant Stark and Tochatwi poles on the Coronation loops, given that they were obtained from rocks in areas with anomalous structural attitudes. Discussions of true polar wander or anomalous geomagnetic field as the alternative explanation for

variances among Coronation poles were also developed but considered to be less parsimonious in this instance. Therefore, it is suggested that adequate consideration of localized structural anomalies must be taken in future paleomagnetic studies in the Great Slave basin.

Chapter 3 is designed to directly test another pole within the Coronation loops of the Slave craton. In the Kilohigok basin, Nunavut, Canada, the 1.963-Ga Rifle Formation has previously yielded a paleopole lying substantially east of the other Coronation poles. Samples from that previous study were collected from aa shallowly dipping homocline about 30 km west of the Bathurst Fault, so large rotation of the Rifle Formation produced by the shearing of the Bathurst Fault is considered unlikely. In this study (Gong and Evans, in review), we collected ~300 samples of the Rifle Formation and adjacent strata of the Goulburn Supergroup, in shallowly dipping autochthonous sections east of the Bathurst Fault. Magnetic mineralogy and anisotropy were studied by various rock magnetic experiments. Paleomagnetic results of this study yield a total of seven Orosirian preliminary poles, including one from the Rifle Formation. Adding these new poles to the Coronation loops makes the APW path even more complicated. After a careful evaluation, we suggest that basin- or local-scale vertical-axis rotations could lead to some oscillatory patterns of the Coronation loops, but could not explain the large declination variations observed in the homoclinal sections of the Rifle Formation. Therefore, true polar wander could potentially be the major contributor to the large, and back-and-forth swings of the Coronation loops (other than 1.88-Ga Stark and Tochatwi poles).

Part II of this dissertation is dedicated to provide robust Proterozoic paleomagnetic poles for West African Craton (WAC), in order to help fill the large gap in its current paleomagnetic dataset and to better constrain its paleogeography and its relationships with other cratons in pre-Pangean supercontinents.

Chapter 4 provides a thorough review of paleogeographic constraints of WAC in the Precambrian, including a summary of its basement geology, large igneous province records, and paleoclimate indicators (Gong and Evans, 2021). Importantly, all available paleomagnetic data of WAC have been carefully evaluated to understand the reasons why they fail to yield reliable paleomagnetic poles of pre-Ediacaran age. We found that many previous WAC paleomagnetic data suffer from poorly dated ages, inadequate sampling and the lack of field tests. All these aspects could be improved in future studies of WAC. Fortunately, mafic intrusions are commonly observed in WAC and many of them have been precisely dated, which could be promising targets for paleomagnetism. We conclude this chapter by summarizing and discussing various reconstruction models of WAC within supercontinents Nuna and Rodinia, and propose the ways to test these models.

Chapter 5 adds two reliable and precisely-dated paleomagnetic poles for WAC by studying the Proterozoic mafic dikes in Anti-Atlas Belt, Morocco (Gong et al., 2021). Using these new poles, we tested the position of WAC in supercontinent Nuna. Previously, many reconstruction models placed southern WAC close to northeast Amazonia, similar to how they were connected in Gondwana. We proposed a new model, which inverts WAC and juxtaposes its northern margin to northeast Amazonia. This inverted WAC-Amazonia

connection persists through the Nuna time interval, and is supported by paleomagnetic data from many neighboring cratons as well as the distribution pattern of correlative large igneous provinces. The inverted WAC-Amazonia connection indicates that through supercontinental cycles, the relative position of these two cratons experienced substantial changes; the proposed pattern of relative motion facilitates the understanding of the broader styles of plate motions in deep time.

Results of this dissertation expand the reliable paleomagnetic constraints on configurations of pre-Pangean supercontinents. Establishing a robust and testable global paleogeographic framework in Precambrian time still requires further high-quality and well-dated paleomagnetic studies from areas with complicated and scarce paleomagnetic data, as well as an integration of geological, geochemical, and paleontological constraints. With such a framework, the evolution of the Earth could be understood in not only a temporal, perspective, but a spatial one as well.

References to Introduction

Brown, M., Torsvik, T., and Pesonen, L., 2018. Nordic workshop takes on major puzzles of paleomagnetism. Eos, v. 99, doi:10.1029/ 2018eo094671.

Elming, S. -Å., Salminen, J. M., & Pesonen, L. J. (2021). Paleo-Mesoproterozoic Nuna supercycle. In: Pesonen, L. J., Salminen, J. M., Evans, D. A. D., Elming, S. -Å., Veikkolainen, T. (eds.), *Ancient Supercontinents and the Paleogeography of Earth*. Elsevier.

Evans, D. A. D. (2013). Reconstructing pre-Pangean supercontinents. *GSA Bulletin*, 125(11-12), 1735-1751.

Evans, D. A. D., Eglington, B. M., Elming, S. -Å., Gong, Z., Li, Z. X., McCausland, P. J., Meert, J. G., Mertanen, S., Pesonen, L. J., Pisarevsky, S. A., Pivarunas, A. F., Salminen, J. M., Swanson-Hysell, N., Torsvik, T. H., Trindade, R. I. F., Veikkolainen, T., & Zhang, S. (2021). An expanding list of reliable paleomagnetic poles for Precambrian tectonic reconstructions. In: Pesonen, L. J., Salminen, J. M., Evans, D. A. D., Elming, S. -Å., Veikkolainen, T. (eds.), *Ancient Supercontinents and the Paleogeography of Earth*. Elsevier.

Evans, D. A. D. (2021). Meso-Neoproterozoic Rodinia supercycle. In: Pesonen, L. J., Salminen, J. M., Evans, D. A. D., Elming, S. -Å., Veikkolainen, T. (eds.), *Ancient Supercontinents and the Paleogeography of Earth*. Elsevier.

Gong, Z., Evans, D. A., Elming, S. Å., Söderlund, U., & Salminen, J. M. (2018a). Paleomagnetism, magnetic anisotropy and U-Pb baddeleyite geochronology of the early Neoproterozoic Blekinge-Dalarna dolerite dykes, Sweden. *Precambrian Research*, 317, 14-32.

Gong, Z., Xu, X., Evans, D. A., Hoffman, P. F., Mitchell, R. N., & Bleeker, W. (2018b). Paleomagnetism and rock magnetism of the ca. 1.87 Ga Pearson Formation, Northwest Territories, Canada: A test of vertical-axis rotation within the Great Slave basin. *Precambrian Research*, 305, 295-309.

Gong, Z. & Evans, D. A. D. (in review). Paleomagnetic survey of the Goulburn Supergroup, Kilohigok Basin, Nunavut, Canada: Toward an understanding of the Orosirian apparent polar wander path of the Slave craton. *Precambrian Research*.

Gong, Z. & Evans, D. A. D. (2021). Constraints on the Precambrian paleogeography of West African Craton. In: Pesonen, L. J., Salminen, J. M., Evans, D. A. D., Elming, S. Å. & Veikkolainen, T. (eds.), *Ancient Supercontinents and the Paleogeography of Earth*. Elsevier, in press.

Gong, Z., Evans, D. A. D., Youbi, N., Ait Lahna, A., Söderlund, U., Ait Malek, M., Wen, B., Jing, X. Q., Ding, J. K., Boumehdi, M. & Ernst, R. E. (2021). Reorienting the West African Craton in Paleoproterozoic-Mesoproterozoic supercontinent Nuna. *Geology*, v. 49, in press.

Meert, J. G., Pivarunas, A. F., Evans, D. A., Pisarevsky, S. A., Pesonen, L. J., Li, Z. X., ... & Salminen, J. M. (2020). The magnificent seven: A proposal for modest revision of the quality index. *Tectonophysics*, 790, 228549.

Mitchell, R. N., Spencer, C. J., Kirscher, U., He, X. F., Murphy, J. B., Li, Z. X., & Collins, W. J. (2019). Harmonic hierarchy of mantle and lithospheric convective cycles: Time series analysis of hafnium isotopes of zircon. *Gondwana Research*, 75, 239-248.

Mitchell, R. N., Zhang, N., Salminen, J., Liu, Y., Spencer, C. J., Steinberger, B., ... & Li, Z. X. (2021). The supercontinent cycle. *Nature Reviews Earth & Environment*, 2(5), 358-374.

Pesonen, L. J., Evans, D. A. D., Veikkolainen, T., Salminen, J. M., & Elming, S. -Å. (2021). Precambrian supercontinents and supercycles – an overview. In: Pesonen, L. J., Salminen, J. M., Evans, D. A. D., Elming, S. -Å., Veikkolainen, T. (eds.), *Ancient Supercontinents and the Paleogeography of Earth*. Elsevier.

Van der Voo, R. (1990). The reliability of paleomagnetic data. *Tectonophysics*, 184(1), 1-9.

Part I

Discordant Paleomagnetic Poles and Their Geodynamic Implications: Proterozoic Case Studies

Chapter 1

Paleomagnetism, magnetic anisotropy and U-Pb baddeleyite geochronology of the early Neoproterozoic Blekinge-Dalarna dolerite dykes, Sweden [1]

Zheng Gong [a], David A. D. Evans [a], Sten-Åke Elming [b], Ulf Söderlund [c,d], Johanna M. Salminen [e]

[a] Department of Geology and Geophysics, Yale University, 210 Whitney Avenue, New Haven, CT 06511, USA

[b] Department of Civil, Environmental and Natural Resources Engineering, Luleå University of Technology, SE-971 87 Luleå, Sweden

[c] Department of Geology, Lund University, SE-223 62 Lund, Sweden

[d] Swedish Museum of Natural History, Laboratory of Isotope Geology, SE-104 05 Stockholm, Sweden

[e] Department of Geosciences and Geography, University of Helsinki, Helsinki 00014, Finland

---

[1] Chapter 1 published in Gong, Z., Evans, D. A. D., Elming, S. Å., Söderlund, U., & Salminen, J. M. (2018). Paleomagnetism, magnetic anisotropy and U-Pb baddeleyite geochronology of the early Neoproterozoic Blekinge-Dalarna dolerite dykes, Sweden. *Precambrian Research*, v. 317, pp. 14-32.

Abstract

Paleogeographic proximity of Baltica and Laurentia in the supercontinent Rodinia has been widely accepted. However, robust paleomagnetic poles are still scarce, hampering quantitative tests of proposed relative positions of the two cratons. A recent paleomagnetic study of the early Neoproterozoic Blekinge-Dalarna dolerite (BDD) dykes in Sweden provided a 946-935 Ma key pole for Baltica, but earlier studies on other BDD dykes discerned large variances in paleomagnetic directions that appeared to indicate more complicated motion of Baltica, or alternatively, unusual geodynamo behavior in early Neoproterozoic time. We present combined paleomagnetic, rock magnetic, magnetic fabric and geochronological studies on BDD dykes in the Dalarna region, southern Sweden. Positive baked-contact and paleosecular variation tests support the reliability of the 951-935 Ma key pole (Plat. = -2.6°N, Plon. = 239.6°E, A_{95} = 5.8°, N = 12 dykes); and the ancient magnetic field was likely a stable geocentric axial dipole at that time, based on a positive reversal test. Detailed analysis of the 947 Ma Nornäs dyke, one of the dykes previously showing anomalous directions, suggests a partial viscous remagnetization. Therefore, the observed large variances in nearly coeval BDD dykes are suspected to result from present-day overprints that were not adequately removed in earlier studies. In addition, we obtained a 971 Ma virtual geomagnetic pole (Plat. = -27.0°N, Plon. = 230.4°E, A_{95} = 14.9°, N = 4 dykes) for Baltica. Comparing similar-aged poles from Laurentia, we suggest that Baltica and Laurentia drifted together from high to low latitude between 970-960 Ma and 950-935 Ma, and returned back to high latitude by 920-870 Ma. In this scenario, the apparent polar wander paths of Baltica and Laurentia may be more complicated than the previously proposed, solitary Sveconorwegian and Grenville loops. The new U-Pb

baddeleyite ages do not support BDD dykes as a giant circumferential swarm generated by a mantle plume, and the prolonged timespan of dyke intrusion is likely associated with the plate boundary forces as causing gravitational extension at the waning stage of the Sveconorwegian orogeny.

1. Introduction

Although the existence of the Proterozoic supercontinent Rodinia has long been suggested, its configuration is still highly debated, and new studies continue to paint different pictures regarding the shape of Rodinia (e.g., Slagstad et al., 2013; Wen et al., 2017; Wen et al., 2018). Nonetheless, the juxtaposition of Laurentia and Baltica in Rodinia is widely adopted in various reconstruction models (e.g., Dalziel, 1997; Pisarevsky et al., 2003; Cawood and Pisarevsky, 2006; Li et al., 2008; Evans, 2009), in order to account for geological similarities between the two cratons. As the only quantitative method to constrain the paleolatitude and the orientation of pre-Pangea continents, paleomagnetism plays an important role in testing current reconstruction models of Laurentia and Baltica. The apparent polar wander (APW) paths of Laurentia and Baltica, including the Grenville and Sveconorwegian loops, respectively, show a broad agreement during post-1.0-Ga Rodinia assembly (Li et al., 2008), supporting the paleogeographic proximity of the two cratons. However, most paleomagnetic poles on the Grenville and Sveconorwegian loops derive from high-grade metamorphic rocks, making the determination of the age of remanence acquisition difficult (Brown and McEnroe, 2012; Brown and McEnroe, 2015). Compilation of paleomagnetic poles with ages between 1.3 Ga and 0.9 Ga (Veikkolainen et al., 2017) shows that even though numerous poles have been generated for Baltica and Laurentia,

high-quality poles with quality criteria Q_{Voo} value larger than 4 are scarce (Fig.1a), and most poles have no field tests to constrain the age of remanence (Fig. 1b). As a result, large uncertainties remain regarding the shapes and younging directions of the Grenville and Sveconorwegian loops (Hyodo and Dunlop, 1993; Elming et al., 1993; Weil et al., 2006; Elming et al., 2014).

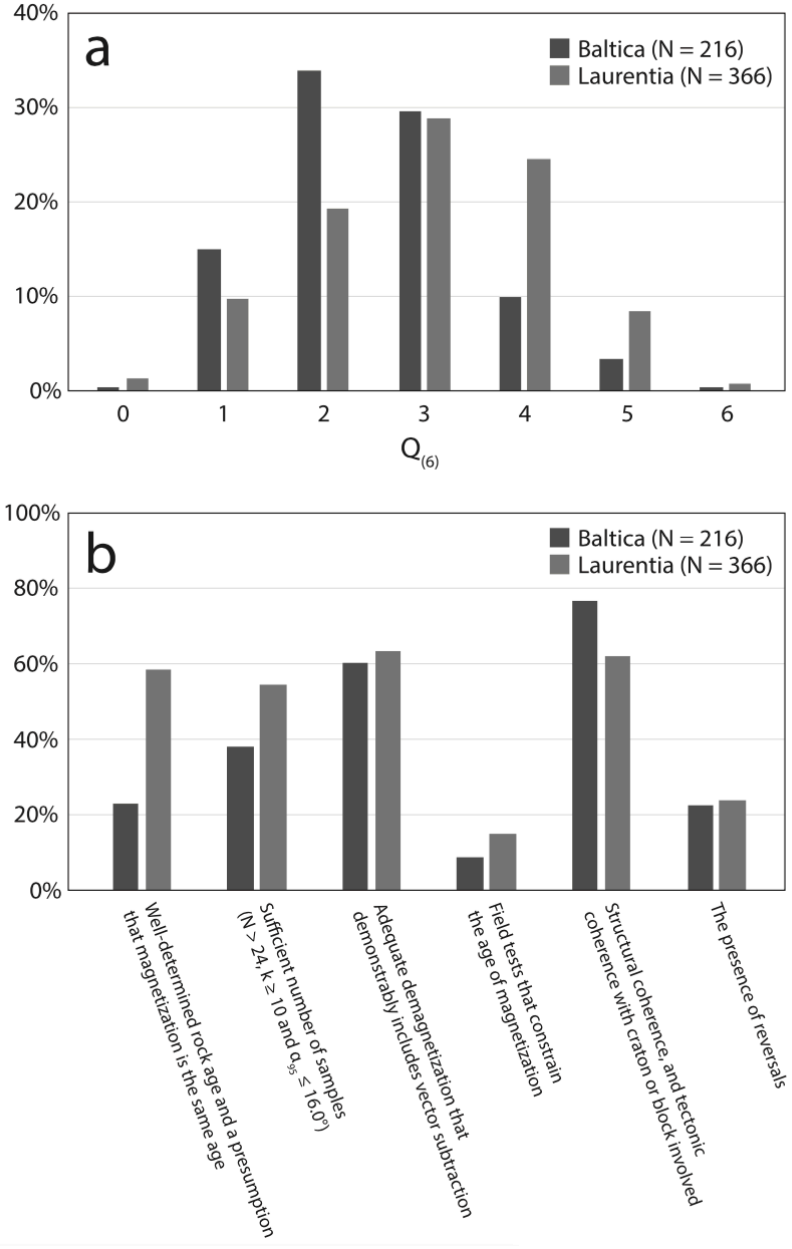

Figure 1 Compilation of paleomagnetic poles from Baltica and Laurentia within the 1.3-0.9 Ga interval (Veikkolainen et al., 2017). (a) Sum of quality criteria $Q_{(6)}$ (Van der Voo, 1990), excluding the seventh criterion as in the Precambrian paleomagnetism database PALEOMAGIA. (b) Individual quality criteria (Van der Voo, 1990). N = number of paleomagnetic poles.

Mafic intrusions are promising targets for yielding high-quality poles since they are usually enriched in magnetite grains. Also, baddeleyite grains in mafic intrusions can be directly dated by U-Pb method with high precision (Söderlund et al., 2005). A recent study of the Blekinge-Dalarna dolerite (BDD) dykes in southern Sweden generated a 946-935 Ma low-latitude pole that has been proposed as a key pole for Baltica (Elming et al., 2014). However, earlier studies of BDD dykes show large variances in paleomagnetic directions (Patchett and Bylund, 1977; Bylund, 1985; Bylund and Elming, 1992) that might indicate unusual cratonic motions or complicated geomagnetic behavior. Here we present detailed paleomagnetic, rock magnetic and magnetic fabric studies on a number of BDD dykes in the Dalarna region, southern Sweden, in order to better understand the paleogeography of Baltica in early Neoproterozoic time. We also present new U-Pb baddeleyite ages that shed light on the tectonic origin of BDD dykes.

2. Geologic background, previous work and sampling

Following the Svecofennian orogeny (2.0-1.75 Ga), Baltica grew outward as a result of accretionary tectonics manifested by the 1.81-1.76 Ga Transscandinavian Igneous Belt (TIB; Bogdanova et al., 2015). Afterwards, there was a protracted interval of mafic

magmatism peaked at 1.6 Ga, 1.57 Ga, 1.47-1.44 Ga, 1.27-1.26 Ga, 1.22 Ga, and 0.98-0.95 Ga, respectively (Söderlund et al., 2005; Brander and Söderlund, 2007). The 1.47-1.44 Ga magmatism, referred to as the Danopolonian event (Bogdanova et al., 2001), is largely coeval with dynamic high-grade metamorphism in southwestern Sweden, and is suggested to be related to convergent active margin processes called the Hallandian event (Christoffel et al., 1994; Söderlund et al., 2002; Möller et al., 2007; Brander and Söderlund, 2007). After the Hallandian event, the 1.1-0.9 Ga Sveconorwegian orogeny (e.g., Bingen et al., 2008) extensively reworked the basement rocks west of the Protogine Zone (PZ) and the Sveconorwegian Frontal Deformation Zone (SFDZ) in southwest Scandinavia (Fig. 2; Wahlgren et al., 1994). Later, Caledonian allochthons were thrust onto the northwest margin of Baltica at 0.6-0.4 Ga (Fig. 2; Gaál and Gorbatschev, 1987; Bingen and Solli, 2009).

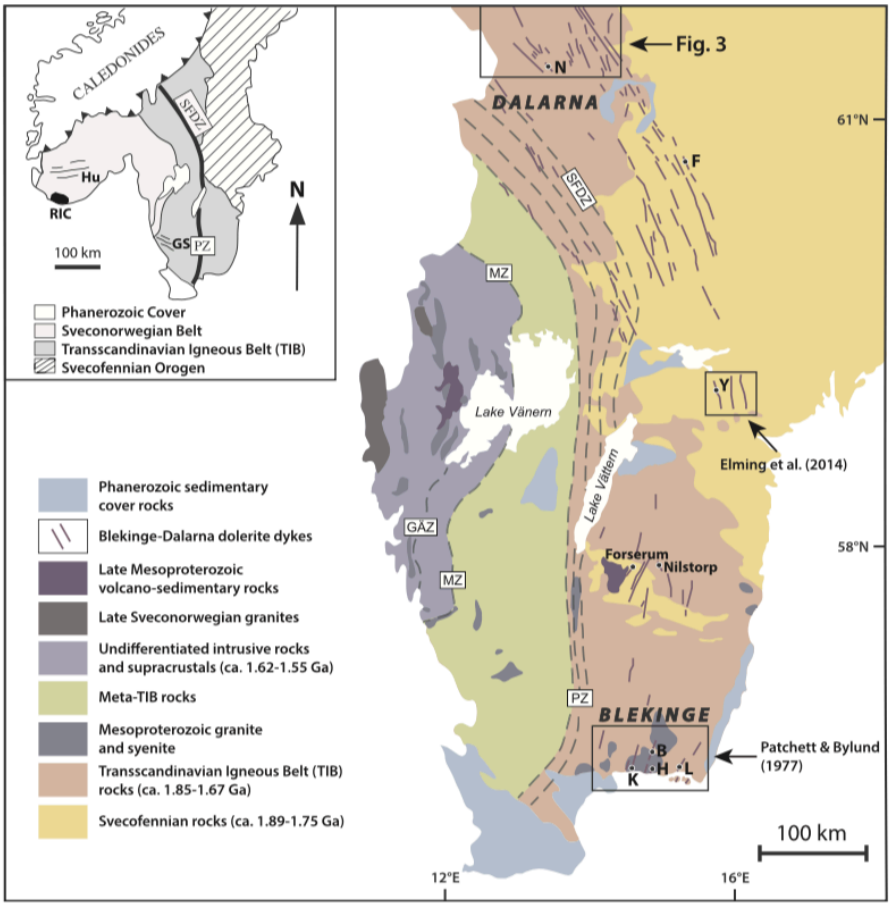

Figure 2 Geologic map of southern Sweden. GÄZ = Göta Älv Zone, MZ = Mylonite Zone, PZ = Protogine Zone, SFDZ = Sveconorwegian Frontal Deformation Zone. Inset map shows the major tectonic divisions of southern Sweden (modified from Söderlund et al., 2004b). GS = Göteborg-Slussen dykes, Hu = Hunnedalen dykes, RIC = Rogaland Igneous Complex. Small boxes show the locations of Y1, Y2 (Y), and Falun (F) dykes in Elming et al. (2014); and Lösen-Fäjö (L), Bräkne-Hoby (B), Karlshamn (K), and Härsjön (H) dykes in Patchett and Bylund (1977); and Nornäs dyke (N) in this study.

Partly coincident with the Sveconorwegian orogeny, the early Neoproterozoic BDD dykes intruded the TIB and Svecofennian rocks east of the PZ and SFDZ, over an extent of 750

km (Fig. 2). One prominent feature of BDD dykes is their arcuate shape, trending NE-SW in the Blekinge region, and deflected ~60° to NW-SE in the Dalarna region (Fig. 2). The ages of BDD dykes are well established by U-Pb baddeleyite geochronology and $^{40}Ar/^{39}Ar$ whole-rock dating, ranging from 978 Ma to 939 Ma (Söderlund et al., 2005; Elming et al., 2014). The origin of BDD dykes is debated. Different models have been proposed, including fracturing due to late Sveconorwegian uplift (Patchett and Bylund, 1977), gravitational collapse at the final stage of the Sveconorwegian orogeny (Pisarevsky and Bylund, 2006), and the giant circumferential system of a mantle plume (Buchan and Ernst, 2016). Petrological studies show that BDD dykes are fine- to medium-grained with slight alteration, and the major minerals consist of plagioclase, olivine, clinopyroxene, orthopyroxene, biotite, ilmenite, and titanomagnetite (Johansson and Johansson, 1990; Solyom et al., 1992).

Previous paleomagnetic work focused on the southern and central part of BDD dykes (e.g., Patchett and Bylund, 1977; Bylund, 1985; Bylund and Elming, 1992), while the northern part is relatively less studied. Recently, Elming et al. (2014) proposed a low-latitude pole for Baltica at 946-935 Ma, combining the results of several BDD dykes in the Norrköping and Falun areas with the 935 Ma Göteborg-Slussen dykes in southwestern Sweden (Fig. 2; Pisarevsky and Bylund, 2006). The reliability of this low-latitude pole is supported by a positive baked-contact test and the appearance of antipodal directions. However, large variances still remain in the paleomagnetic results of BDD dykes, complicating the application of the low-latitude pole to paleogeographic reconstruction of Baltica. For example, the 947 Ma Nornäs dyke yields a high-latitude pole (Piper and Smith, 1980;

Bylund, 1985), which apparently contradicts with the result of Elming et al. (2014). It is also difficult to explain their difference by plate tectonics because they are very similar in age and would imply extremely rapid continental motions. Alternative interpretations have been suggested, such as late-stage selective remagnetization, true polar wander, a non-dipole geomagnetic field or the non-averaged paleosecular variation (Pesonen and Klein, 2013). However, none of these has been fully examined. Notably, the result of the Nornäs dyke was obtained more than three decades ago when modern laboratory treatment and data analysis of paleomagnetism had not been fully developed. Hence, it is necessary to restudy the Nornäs dyke with more detailed and sophisticated techniques.

Since more than 90% of the bedrock in the Dalarna region is covered by glacial deposits, aeromagnetic data (Ripa et al., 2012) and data from geological mapping of the Swedish Geological Survey (Ripa, personal communication) were used to help delineate dykes in the field. For detailed mapping of the outcrops, a portable magnetic susceptibility meter was used to determine the extension of the dykes and contacts to host rocks. A number of NW-SE trending dykes in the Dalarna region were sampled using a portable gasoline-powered rock drill (Fig. 3). Host rocks (ca. 1.46 Ga Öje basalt and ca. 1.46 Ga Dala sandstone) were collected in two sites for baked-contact tests, the former where a clear intrusive contact was observed, and the latter where the concealed contact could be triangulated to within about a meter of the baked host-rock samples. Core samples were oriented with a Brunton compass, and sun-compass readings were also taken in order to correct any small-scale magnetic anomaly in the outcrop. Block samples were collected from the central parts of dykes for U-Pb baddeleyite geochronology.

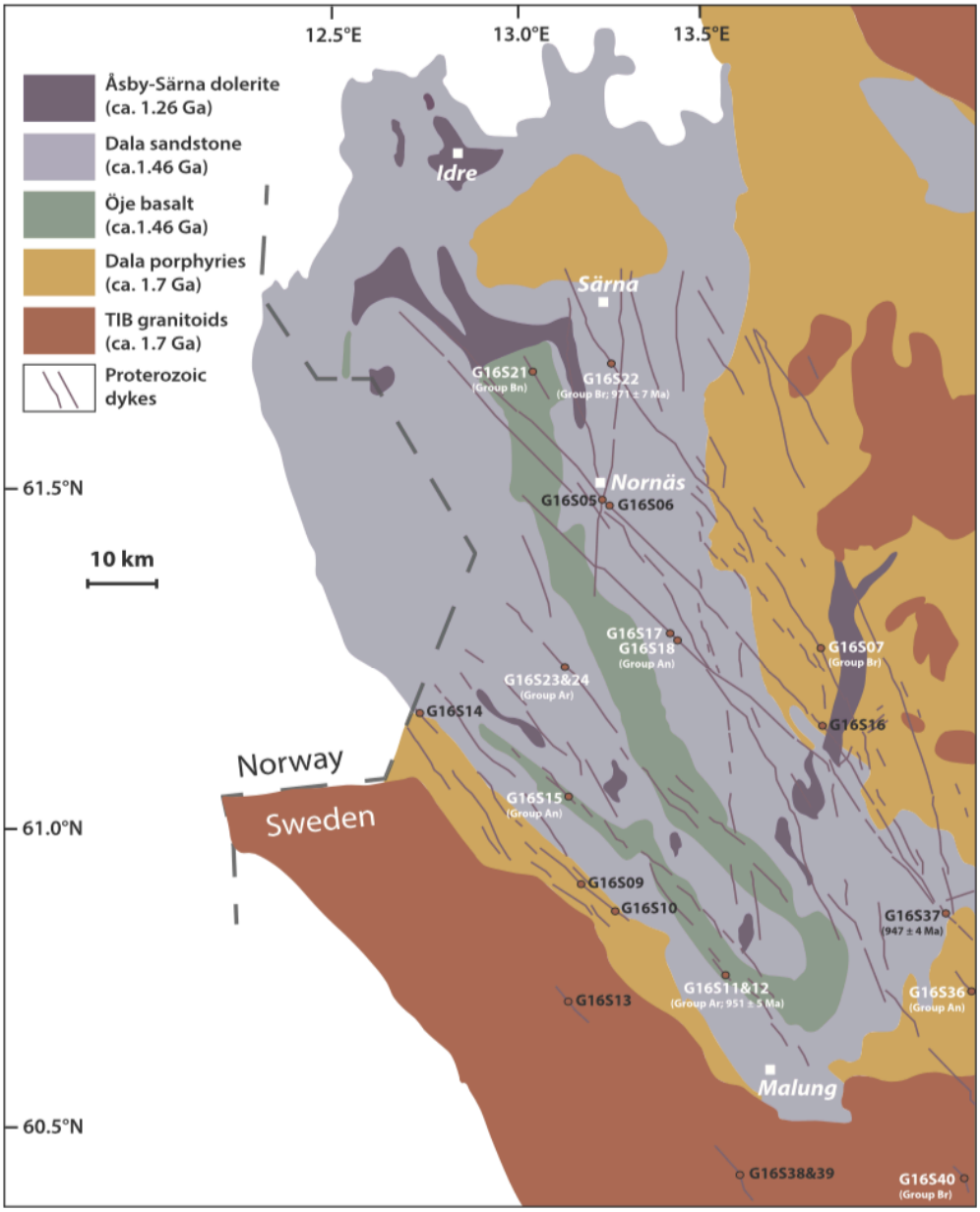

Figure 3 Geologic map of the western Dalarna region (modified from Lundmark and Lamminen, 2016). Proterozoic dyke locations are based on Ripa et al. (2012). Sites yield interpretable paleomagnetic results (white) and sites give paleomagnetically unstable directions/partial remagnetization (black) are differentiated by colors.

3. Methods

3.1 U-Pb baddeleyite geochronology

All samples were crushed, and baddeleyite grains were separated using the Wilfley table technique following Söderlund and Johansson (2002) at Lund University in Sweden. The extracted baddeleyite grains are dark to moderately brown. Grains from all samples are fresh without any trace of alteration. About 1-5 grains per fraction were combined and transferred to clean Teflon capsules. Grains were washed in numerous steps using 3 M HNO_3, including one step on a hotplate (~30 minutes). One drop of the ^{205}Pb-$^{233-236}U$ tracer solution and 10 drops of HF-HNO_3 (10:1) were added to each capsule. Baddeleyite grains were completely dissolved after 3 days in an oven under high pressure at a temperature of ~190°C. The samples were evaporated on a hotplate and then dissolved in 10 drops of 6.2 M HCl. One drop of 0.25 M H_3PO_4 was added to each capsule before it dried down. U and Pb were loaded on an outgassed Re filament together with a small amount of silica gel.

Thermal Ionization Mass Spectrometry (TIMS) was performed at the Laboratory of Isotope Geology at the Swedish Museum of Natural History in Stockholm, Sweden, using a Thermo Finnigan Triton TIMS system. An ETP SEM detector equipped with a RPQ filter was used to measure the Pb and U isotope intensities in dynamic (peak-switching) mode. Pb-isotopes were measured at a filament temperature in the 1200-1230°C range, while U-isotopes were measured in dynamic mode on the SEM with filament temperatures exceeding 1300°C. Data reduction was performed using the Excel add-in "Isoplot" of Ludwig (2003); decay constants for ^{238}U and ^{235}U follow those of Jaffey et al. (1971). All errors in age and isotopic ratios are quoted at 2σ. Initial Pb isotope compositions were corrected according to the global common Pb evolution model of Stacey and Kramers

(1975). U-Pb data are presented in Table 1 and the fractions are plotted in the concordia diagrams in Fig. 4.

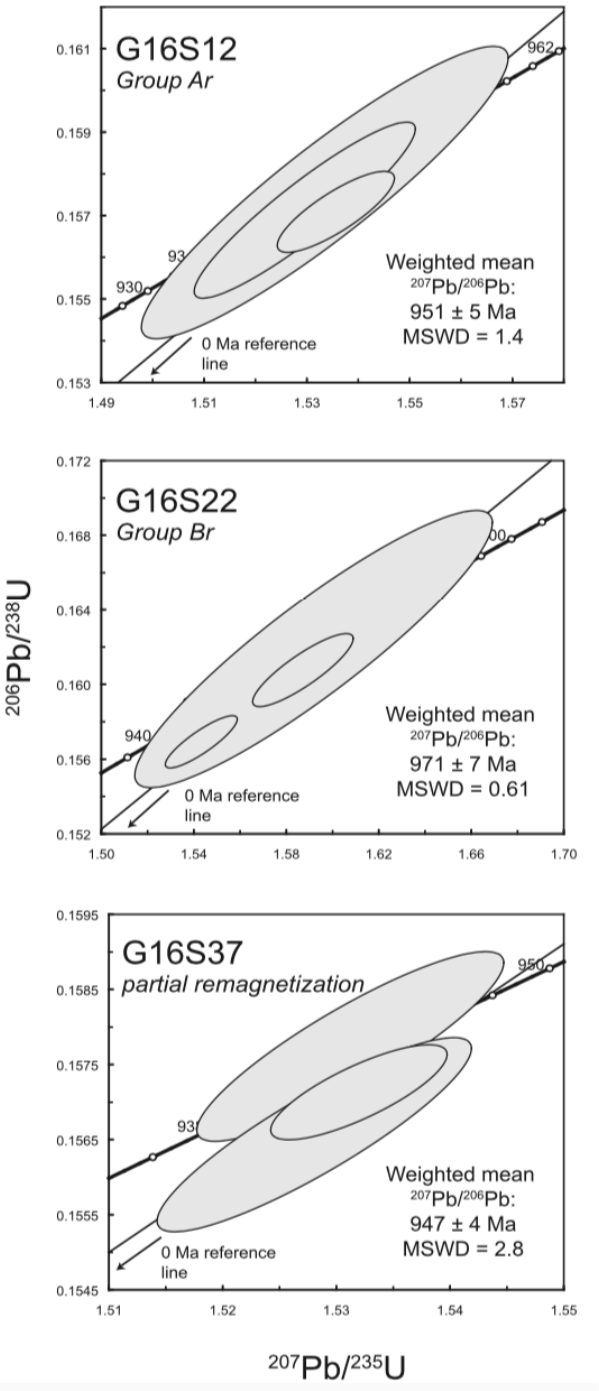

Figure 4 U-Pb concordia diagrams of dated BDD dykes.

3.2 Magnetic measurements

Magnetic measurements were conducted in the Paleomagnetic Laboratory and Archaeomagnetism Laboratory at Yale University, USA. In order to understand the pattern of dyke propagation and to discern the possible alteration or deformation of dykes (Hrouda, 1982; Rochette et al., 1992), anisotropy of magnetic susceptibility (AMS) was measured for each dyke using an AGICO Kappabridge KLY-4S susceptibility meter. AMS data were analyzed in Anisoft42 software. To characterize magnetic mineralogy, representative samples were subjected to thermomagnetic susceptibility analysis. Temperature ranges from 25°C to 700°C and is controlled by a CS3 high temperature furnace apparatus. Bulk magnetic susceptibility was measured during heating and cooling in an argon gas environment in order to subdue magnetic phase transition. Magnetic grain size was inferred by the Day plot (Day et al., 1977) constructed by magnetic parameters, which are determined by hysteresis loop measurement using a MicroMag 2900 alternating gradient magnetometer (AGM). After the measurement of natural remanent magnetization (NRM), samples were cooled to liquid nitrogen temperature (~77 K) in a magnetic shielded container to demagnetize the remanence carried by multidomain grains (Muxworthy and McClelland, 2000). Thermal demagnetization was conducted in an ASC Scientific TD-48 thermal demagnetizer with stepwise heating up to 580°C in 15-20 steps in a nitrogen gas environment. Sister samples from each dyke were demagnetized using alternating field (AF) in a Molspin tumbler demagnetizer. After each thermal or AF demagnetization step, remanence was measured by a 2G Enterprises cryogenic DC-SQuID magnetometer with automatic sample-changing device (Kirschvink et al., 2008). Paleomagnetic vectors were calculated using principal component analysis (Kirschvink, 1980) and the great circle

method (McFadden and McElhinny, 1988), and were plotted using vector-endpoint diagrams (Zijderveld, 1967) in PaleoMag X software (Jones, 2002). Paleogeographic reconstruction was carried out using GPlates software (Boyden et al., 2011).

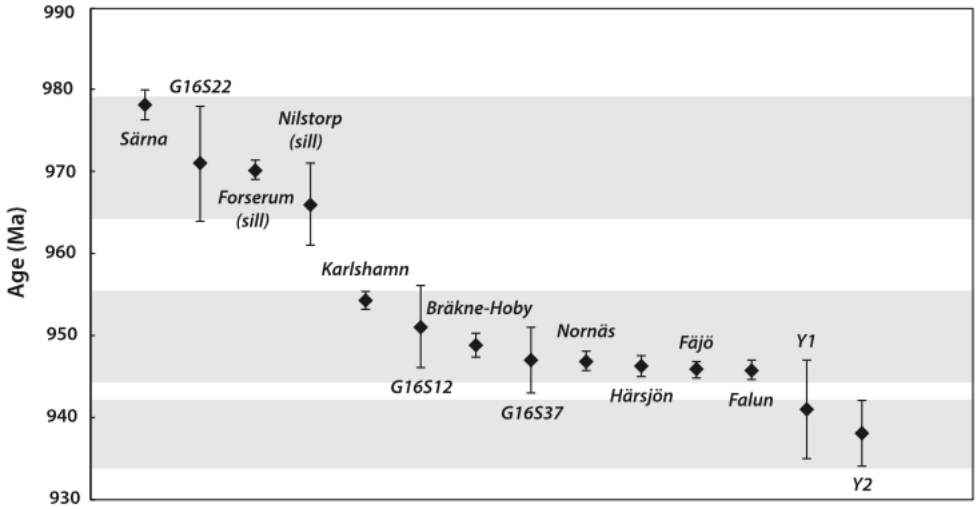

Figure 5 Summary of ages from 980-930 Ma BDD-related intrusions in southern Sweden. Age references are listed in Table 2. Shaded areas show age ranges of possible pulses of BDD intrusions.

4. Results

4.1 U-Pb baddeleyite geochronology

We report U-Pb baddeleyite TIMS ages of three NW-SE trending BDD dykes from the Dalarna region. Data are summarized in Table 1, and concordia diagrams are shown in Fig. 4. Three baddeleyite fractions of dyke G16S12, which is intrusive into the Öje basalt (G16S11), are concordant at 951 ± 5 Ma (2σ, mean square weighted deviates [MSWD] = 1.4). This age is calculated as the weighted mean of $^{207}Pb/^{206}Pb$ dates for these fractions. Three fractions of dyke G16S22 were analyzed, of which two are concordant within uncertainty whereas one analysis is slightly discordant. The weighted mean of $^{207}Pb/^{206}Pb$

dates is 971 ± 7 Ma (2σ, MSWD = 0.61). Three fractions of dyke G16S37, which is probably the southern extension of the Nornäs dyke, cluster at and just below the concordia curve. The weighted mean is 947 ± 4 Ma (2σ, MSWD = 2.8). These age estimates are interpreted as dating the crystallization of the rocks.

Before this study, a total of 11 ages of BDD dykes/sills were published, with nine U-Pb baddeleyite ages (Söderlund et al., 2004a; Söderlund et al., 2005) and two $^{40}Ar/^{39}Ar$ whole-rock ages (Elming et al., 2014). We provide an additional three U-Pb baddeleyite ages. Collectively, they demonstrate a ~40 million-year range of BDD intrusions with probably three magmatic pulses, extending from 978 Ma to 939 Ma (Fig. 5).

4.2 Rock magnetism

AMS data show that the degree of anisotropy (P_j) of BDD dykes is typically below 6%, which is a common value for primary fabric of igneous rocks (Hrouda, 1982). Low P_j values indicate that these rocks have not experienced significant deformation, hence, have a reasonable chance of retaining primary magnetization. The majority of dykes exhibit oblate fabrics with K_1 and K_2 axes dispersed in the NW-SE oriented, vertical or sub-vertical plane (Fig. 6e). Some dykes show prolate fabrics with K_1 axis pointing to the NW-SE direction (Fig. 6a). The orientation of magnetic anisotropy ellipsoid genuinely reflects the trends (NW-SE) of these dykes (Knight and Walker, 1988), which is also supported by field observations and the aeromagnetic anomaly map (Fig. 3; Ripa et al., 2012). AMS of Öje basalt is expected to have a horizontal oblate fabric; the K_3 axis shows a transition from steep to shallow directions (Fig. 6c). Samples with shallow K_3 axes are close to the

contact and the chilled margin of dyke G16S12. It is suspected that some secondary magnetic minerals might grow along the basalt contact zone due to the migration of reducing fluids, and cause anomalously shallow K_3 axes. But the remanences of the secondary magnetic minerals are adequately removed by thermal demagnetization and have no effect on primary paleomagnetic signals (see discussion below). AMS of the Dala sandstone (G16S24) shows a typical depositional fabric (oblate and horizontal), with K_3 axis perpendicular to the bedding plane and K_1 and K_2 axes distributed parallel to the bedding plane (Fig. 6h).

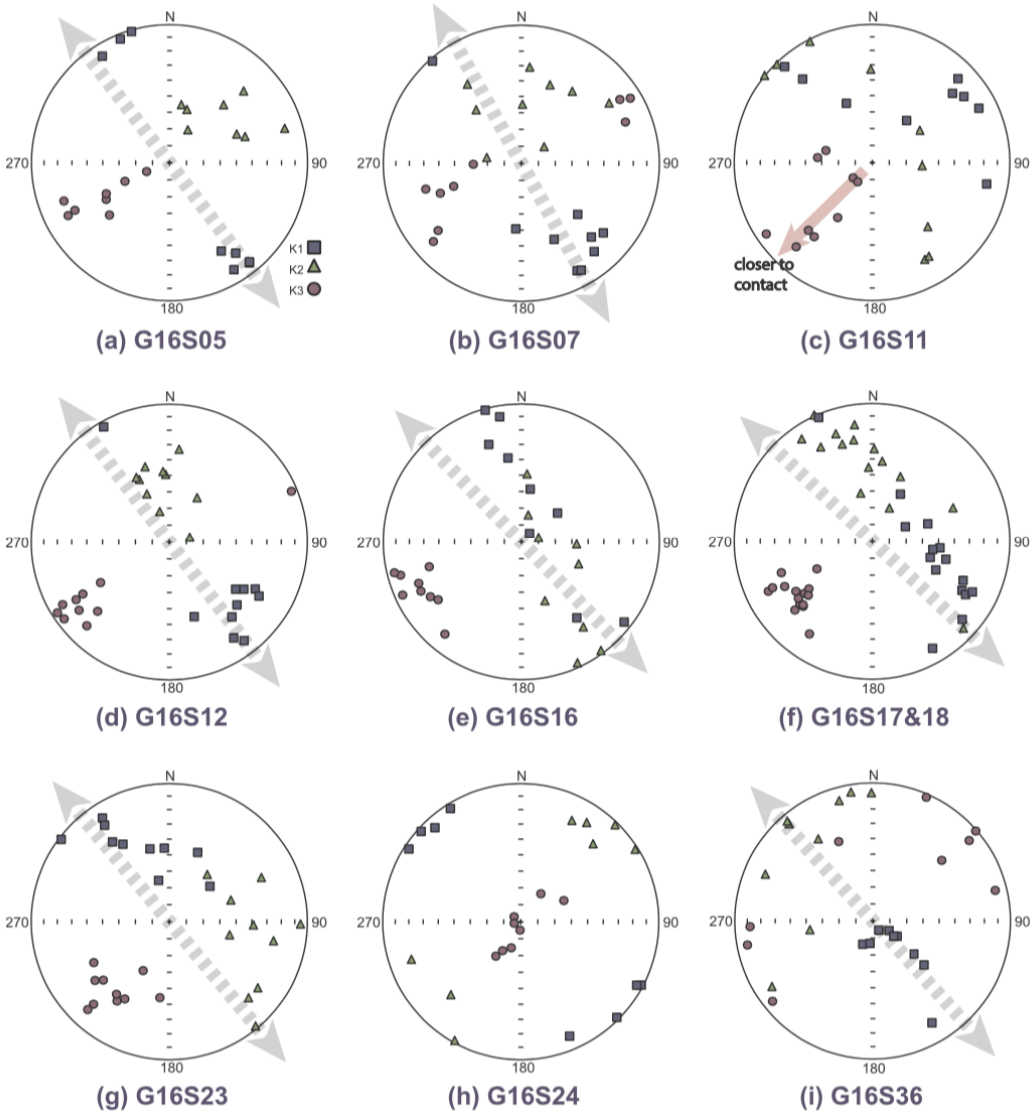

Figure 6 Representative stereonet projections of the anisotropy of magnetic susceptibility (AMS) data. Squares, triangles and circles show the principal axes of AMS ellipsoids. Grey arrows indicate the trends of dykes inferred from aeromagnetic anomalies (Ripa et al., 2012). Red arrow represents the evolution of AMS ellipsoid of Öje basalt.

Thermomagnetic susceptibility analysis of BDD dykes shows that heating and cooling curves are generally reversible (Fig. 7). During heating, the magnetic susceptibility decreases substantially between 580°C and 600°C, which provides clear evidence for the presence of magnetite. Minor drops in magnetic susceptibility are also noticed between 600°C and 700°C, indicating small amounts of hematite or maghemite. Exceptions are Öje basalt (G16S11) and dyke G16S12, which yields a distinct susceptibility hump and a large decline between 300°C and 400°C on the heating curve (Fig. 7c-d). This temperature range coincides with the Curie temperature of magnetic sulfides (pyrrhotite or greigite). During heating, the magnetic sulfides were broken down to form new magnetite, as suggested by the sharply increased susceptibility at 580°C on the cooling curve. The magnetic sulfides are likely the reason for shallow K_1 axis observed in the AMS data of Öje basalt (G16S11). Dala sandstone (G16S24) has a low magnetic susceptibility and shows a gradual decrease in susceptibility between 600°C and 700°C (Fig. 7g), suggesting the major magnetic phase is hematite or titano-hematite.

The coercivity of remanence of BDD dykes determined by hysteresis loop measurement is typically less than 30 mT, which is a normal value for magnetite. Only dyke G16S12 gives slightly higher coercivity (~80 mT), showing the contribution from magnetic sulfides (Fig.

8b). The typical grain size of magnetic phases in BDD dykes falls in pseudo-single domain (PSD) region on the Day plot. According to Dunlop (2002)'s theoretical estimates, the magnetic grains are mixtures of single domain (SD) and multidomain (MD) minerals with varying SD content ranging from 20% to 60% (Fig. 8c).

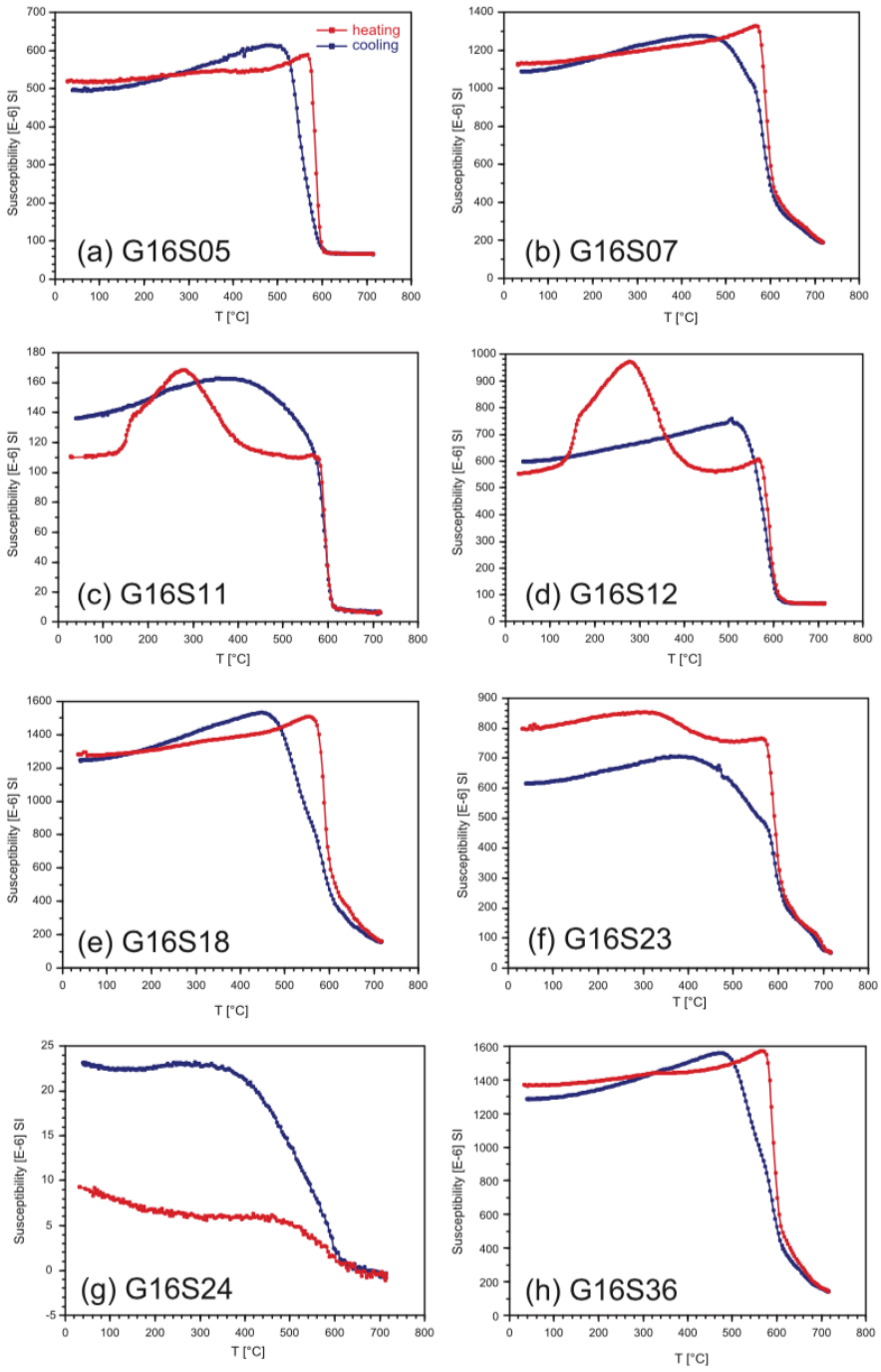

Figure 7 Results of thermomagnetic susceptibility analysis. Heating and cooling curves are represented by red and blue colors, respectively.

4.3 Paleomagnetism

Paleomagnetic results show that during heating, most samples exhibit a significant decline of remanence at ~580°C, close to the unblocking temperature for pure magnetite (Fig. 9). Samples that were subjected to liquid nitrogen bath show a large decrease of remanence, indicating that the viscous remanence carried by MD grains has been effectively removed (Fig. 9). Some samples show a gradual loss of remanence at lower temperatures, which could be either due to the demagnetization of larger size grains or magnetic sulfides. Most samples yield a clear decay-to-origin component between 500°C and 580°C, which is defined as the characteristic remanent magnetization (ChRM). Only samples from sites G16S17 and G16S18 (two sites were collected from the same dyke) were analyzed by the combination of principal component analysis and great circle method, owing to the overlapping unblocking temperatures of different-sized grains.

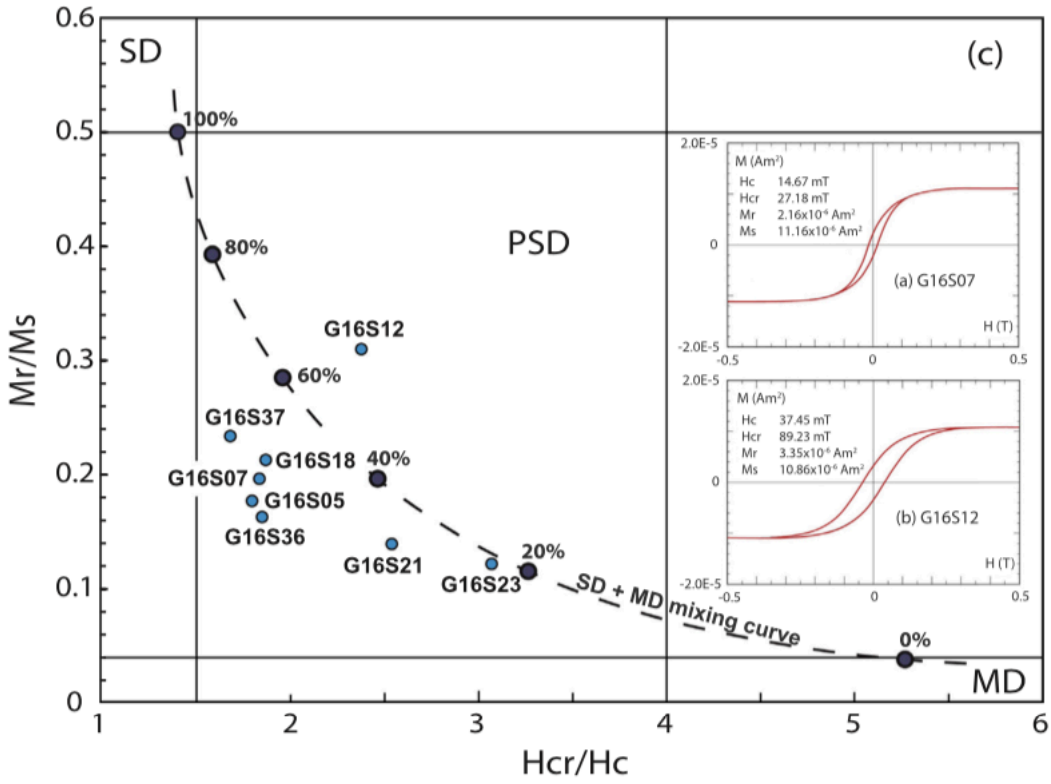

Figure 8 Hysteresis ratios of BDD dykes displayed in the Day plot (Day et al., 1977). The dashed line shows the SD/MD theoretical mixing curve (Dunlop, 2002). Inset plots are representative hysteresis loops after the correction of paramagnetic slope.

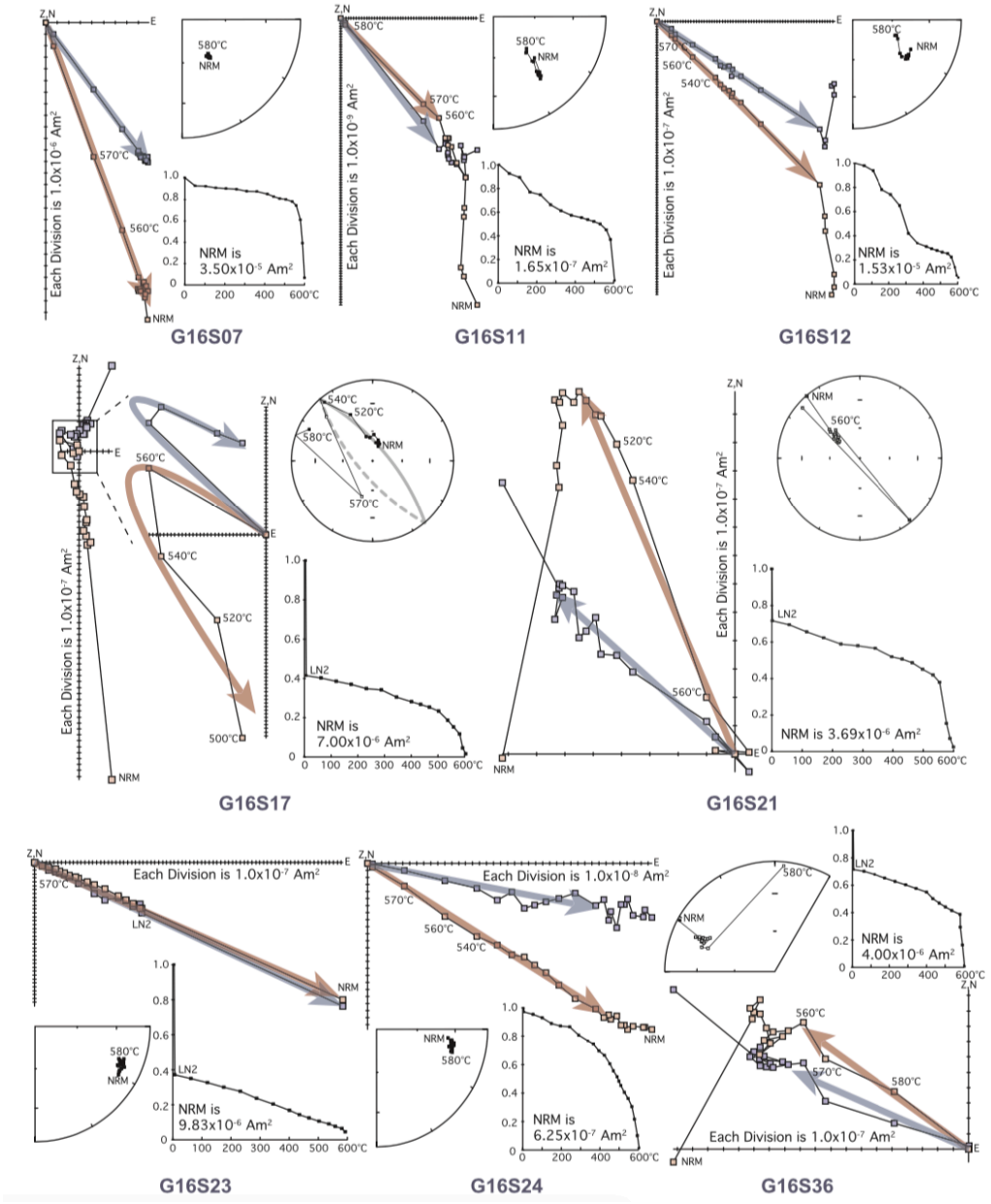

Figure 9 Representative thermal demagnetization results of BDD dykes. Vector-endpoint diagrams are shown (Zijderveld, 1967), with equal-area stereonet plots and remanence intensity (J/J_0) plots. ChRMs are plotted with blue and red arrows representing declinations and inclinations, respectively.

Usable paleomagnetic directions of BDD dykes fall into two statistically different groups (Fig. 10a), one with shallower inclinations (Group A) and another with steeper inclinations (Group B). Importantly, the dating results also show that the two groups are different in age. Group A is about 951 ± 5 Ma, ~20 million years younger than Group B (971 ± 7 Ma). Both groups show two polarities. Following Precambrian paleomagnetism database PALEOMAGIA's nomenclature (Veikkolainen et al., 2017), we assign reverse polarity to sites with southeasterly declinations (Groups Ar, Br) and normal polarity to sites with northwesterly declinations (Groups An, Bn; Table 2). Paleomagnetic directions of Group A are resemble those of the Y1, Y2 and Falun dykes obtained in Elming et al. (2014). A positive baked-contact test supports the primary origin of the NW-up direction (Group An; Elming et al., 2014), In addition, we have two positive baked-contact tests for the SE-down direction (Group Ar). The baked areas of the Öje basalt (G16S11) and the Dala sandstone (G16S24), which were intruded by dykes G16S12 and G16S23 respectively, show similar remanence to BDD dykes, but are very different from their primary (unbaked) directions (Piper and Smith, 1980; Fig. 10a). We performed a reversal test on Group A, together with Y1, Y2 and Falun dykes from Elming et al. (2014) and the Tuve, Small, Hjuvik and Slussen dykes from Pisarevsky and Bylund (2006); the test is demonstrated to be positive with classification C (γ/γ_c = 8.7°/13.9°; McFadden and McElhinny, 1990). On the basis of the similar ages and paleomagnetic results of Pisarevsky and Bylund (2006), Elming et al. (2014), and our data, we obtained a new mean 951-935 Ma paleomagnetic pole: Plat. = -2.6°N, Plon. = 239.6°E, A_{95} = 5.8° (N = 12 dykes; Table 2). There is no baked-contact test for the four dykes in Group B, but their demagnetization patterns, such as the square-shouldered thermal decay curve with the unblocking temperature closed to 580°C, suggest

that their ChRMs are probably primary (Fig. 9). The number of dykes in Group B is insufficient for the reversal test, but quasi-antipodal directions have been observed, also supporting the notion that dykes in Group B carry primary remanence. We calculated a 971 Ma virtual geomagnetic pole (VGP) from Group B, which is Plat. = -27.0°N, Plon. = 230.4°E, A_{95} = 14.9° (N = 4 dykes; Table 2).

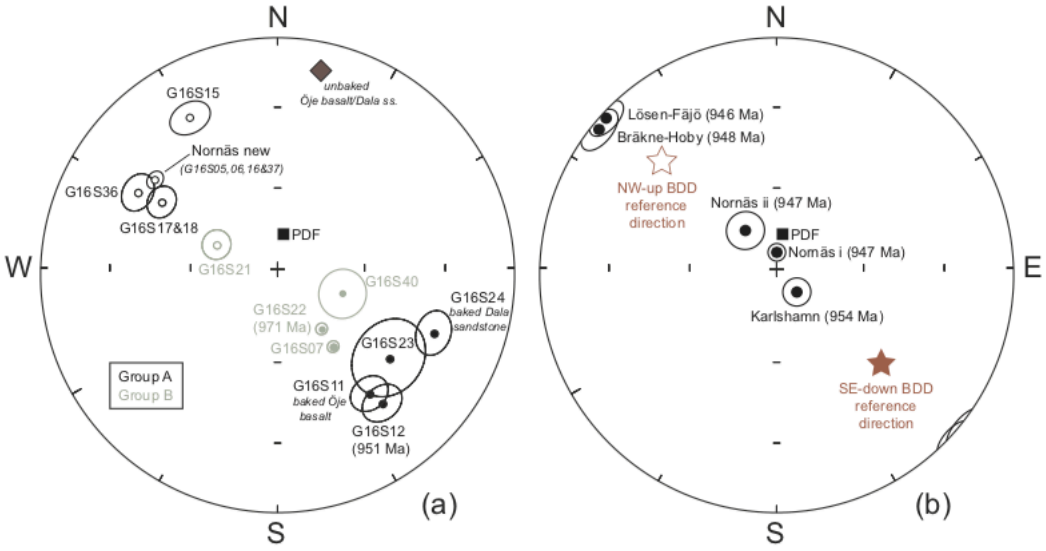

Figure 10 (a) Equal-area stereonet projection summarizing the ChRMs of BDD dykes with corresponding 95% confidence cones. Unbaked paleomagnetic direction of Öje basalt and Dala sandstone is suggested by the purple diamond. Present-day field direction of sampling area is indicated by the black square. Closed and open circles show the downwards and upwards paleomagnetic inclinations. PDF = present-day field. (b) Equal-area stereonet projection of anomalous BDD dyke directions. Red stars indicate the BDD reference directions.

Paleomagnetic results of the Nornäs dyke (G16S05 and G16S06; 946.8 ± 1.2 Ma) show that the natural remanent magnetization (NRM) direction is very close to the steep ChRM

yielded from previous work (Piper and Smith, 1980; Bylund, 1985). The steep ChRM is also very close to present-day field (PDF) direction (Fig. 10b). However, as temperature or AF intensity increases, the inclination gradually decreases (Fig. 11). It is noteworthy that the direction of remanences of some samples are able to migrate towards the upper hemisphere at ~570°C or ~30 mT. The remanence becomes unstable when approaching the unblocking temperature or coercivity of magnetite, so it is hard to isolate a decay-to-origin component. However, the directions move towards the NW-up BDD-reference direction (Group An; Fig. 10). The pattern of vector-endpoint diagrams clearly shows a partial remagnetization. Based on the aeromagnetic anomaly map and geochronology, it is likely that sites G16S16 and G16S37 (947 ± 4 Ma) are from a southeastward extension of the Nornäs dyke, and they also give identical paleomagnetic results and similar ages. Therefore, we interpret that the Nornäs dyke consists of some PSD grains that carry a PDF overprint, difficult to be adequately removed due to the strong overlap of unblocking temperature or coercivity with SD magnetite grains. Since a clear decay-to-origin component cannot be isolated from sites G16S05, G16S06, G16S16 and G16S37, we tried to use great circle method for paleomagnetic analyses. Combining all great circles from these four sites of the Nornäs dyke, we obtained a mean direction of Declination = 307.9°, Inclination = -35.3°, α_{95} = 2.9°, which we named it as "Nornäs new", the direction of which is very close to the NW-up BDD-reference direction (Group An; Fig. 10; Table 2). The Nornäs new direction is likely the primary remanence of the Nornäs dyke. However, without any sample bearing a clear decay-to-origin component, we prefer to exclude this Nornäs new mean direction from the paleomagnetic statistics of this study. The steep ChRM direction of previous work was calculated from the minimum scatter in magnetic directions after demagnetization in

AF intensities of 10-20 mT (Piper and Smith, 1980; Bylund, 1985; Table 2), which is too low to remove the PDF overprint. Another dyke, G16S14, yields similar demagnetization pattern as the Nornäs dyke and is also likely affected by partial remagnetization in the PDF direction.

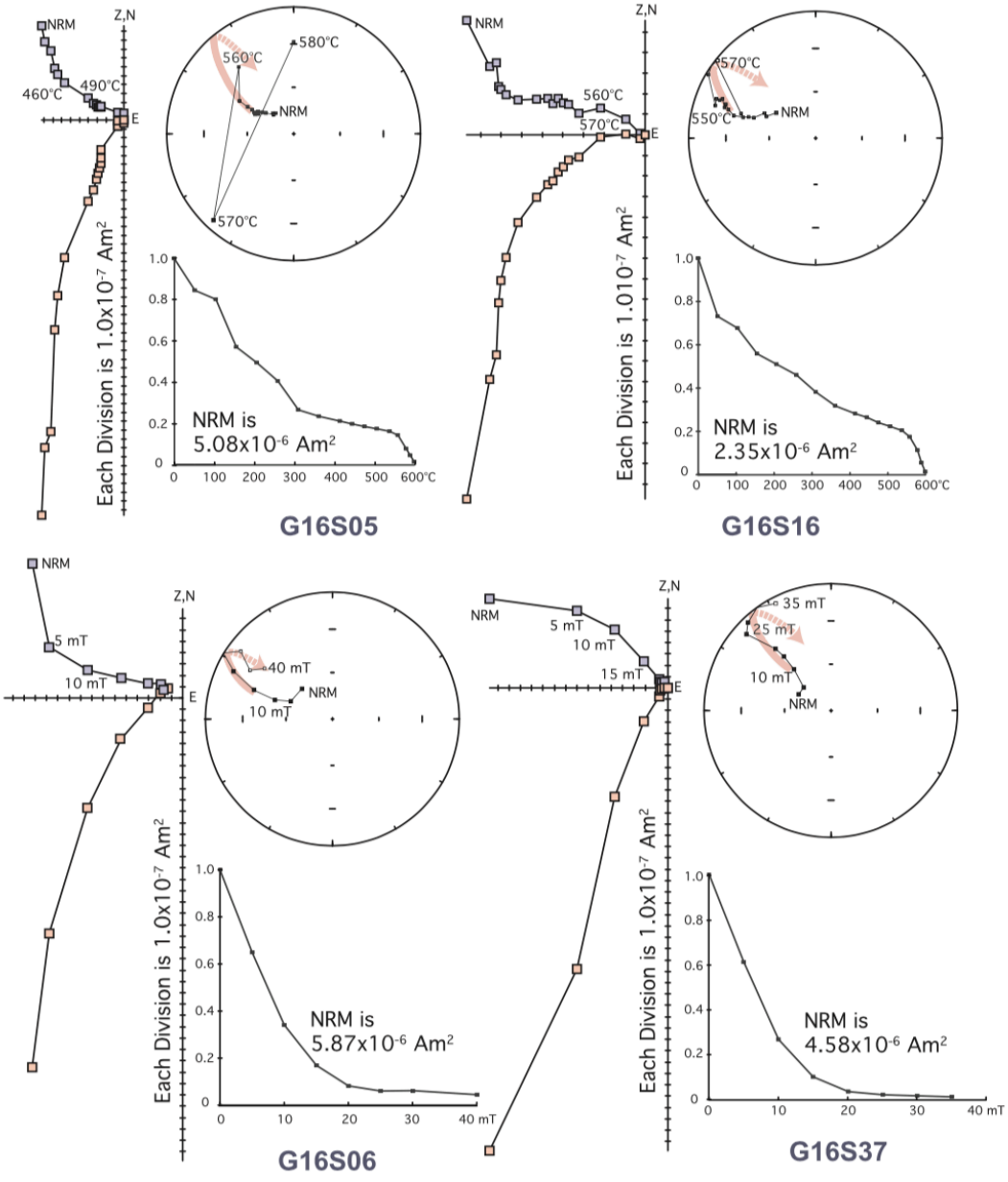

Figure 11 Typical thermal and alternating-field demagnetization behaviors of the Nornäs dyke. Vector-endpoint diagrams (Zijderveld, 1967), equal-area stereonet plots and

remanence intensity (J/J_0) plots are shown. Red solid/dashed lines indicate the trending of remanent directions in lower/upper hemisphere.

5. Discussion

5.1 Origin of BDD dykes – A giant circumferential swarm?

Arcuate-shaped swarms have been increasingly reported in different geological settings with various intrusion ages (Denyszyn et al., 2009; Mäkitie et al., 2014; Buchan and Ernst, 2018). However, the physical mechanism explaining the unusual geometry is still under debate. Interestingly, the coronae on Venus are also characterized by similar ring-shaped surface expressions and are thought to be associated with tectono-magmatic processes (Squyres et al., 1992). Are the arcuate-shaped swarms on Earth and Venusian coronae intrinsically related in terms of their origin?

Venusian coronae have two components: a radiating system and a circumferential system, both of which are presumably underlain by dykes (Ernst et al., 2003). In order to explain their distinctive tectonic and topographic features, Stofan and Head (1990) suggested a mantle plume origin for coronae. The radiating system is argued to be related to the upwelling of hot magma, causing surface uplift and dyke intrusion, while the circumferential system is due to gravitational collapse as the mantle upwelling ceases. If this mechanism is true, it is expected that the radiating system would predate the circumferential system.

Ernst and Buchan (1998) first proposed that the arcuate-shaped swarms on the Earth could be analogous to Venusian coronae. They defined any arcuate-shaped swarm as a giant circumferential swarm if it has a primary circular or elliptical geometry with an arc of > 45° and a diameter > 60 km (Buchan and Ernst, 2016). Based on these criteria, BDD dykes would be classified as a giant circumferential swarm, accounting for their 750-km long, ~60° arcuate geometry. The primary curved geometry is supported by tectonic coherence of southern Sweden since Neoproterozoic time, and also the demonstrably high-quality BDD paleomagnetic data, which discern no structural rotation following emplacement. Therefore, the critical test of this hypothesis hinges on another two aspects. Is there a corresponding radiating system? And if so, is the radiating system older than BDD dykes, as required by Stofan and Head (1990)'s model?

The available ages of BDD dykes/sills suggest prolonged intrusions (Fig. 5). Given the distribution of these ages, there seems to be 3 possible pulses of BDD intrusions, first pulse from 980 Ma to 965 Ma; second from 955 Ma to 945 Ma; third from 942 Ma to 935 Ma (Fig. 5), although definitive conclusion still needs more geochronological studies. Any radiating-system candidate should be older or at least very close to the first pulse of BDD intrusions. The Göteborg-Slussen dykes in southwestern Sweden were proposed as the radiating system linked to the purported mantle plume, because their trends are sub-orthogonal to those of the BDD dykes (Fig. 2; Buchan and Ernst, 2016). However, the Tuve dyke, which belongs to the Göteborg-Slussen dyke suite, is dated to be 935 ± 3 Ma by the U-Pb baddeleyite method (Hellström et al., 2004), which approaches equivalency to the youngest members of BDD dykes but is tens of millions of years younger than the majority

of BDD dykes. Another candidate for the radiating system might be the Hunnedalen dykes in western Norway (Fig. 2), trending NE-SW, sub-orthogonal to BDD dykes. But the Hunnedalen dykes are ~100 million years younger than BDD dykes (Walderhaug et al., 1999), excluding their possibility of being the radiating component. In general, geochronological data do not support Buchan and Ernst (2016)'s mantle plume model. The prolonged intrusion interval of BDD dykes is more likely connected with the plate boundary forces causing gravitational extension in the Baltic foreland during protracted waning stages of the Sveconorwegian orogeny. Variable orientation of the regional stress field might be the cause for the primary arcuate geometry (Wahlgren et al., 1994).

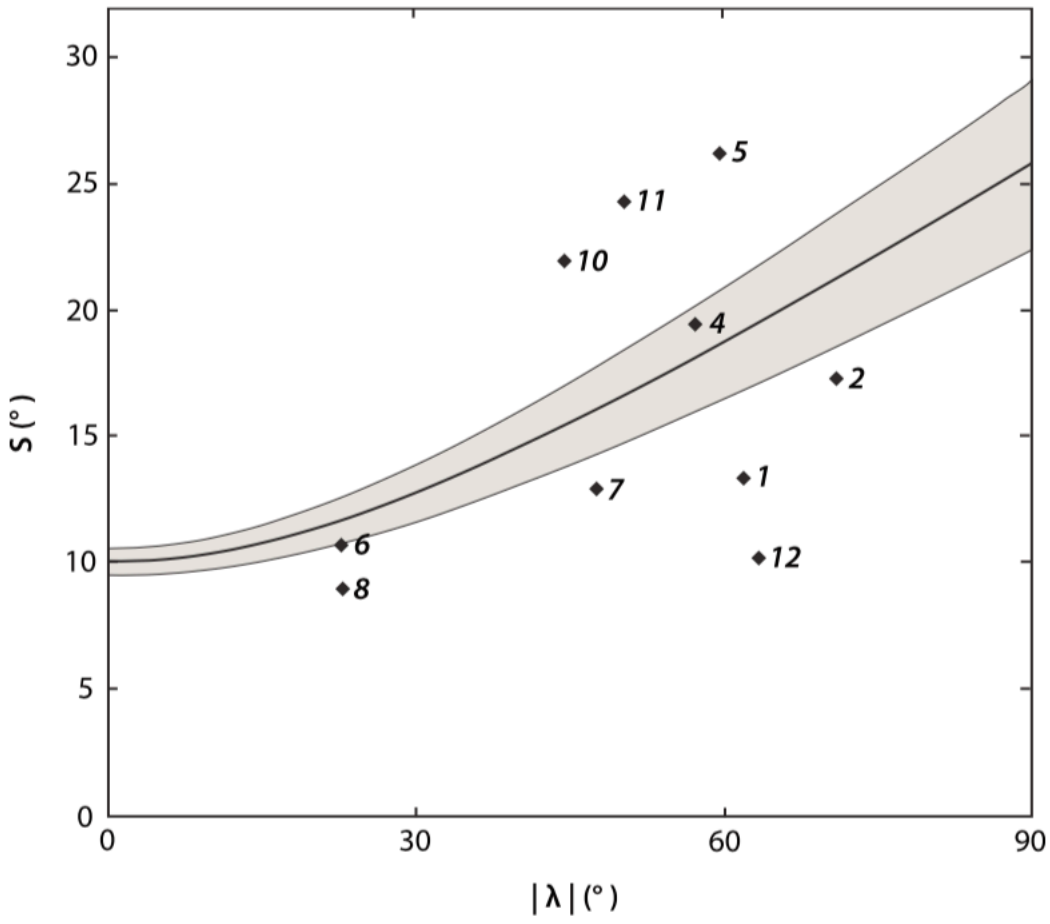

Figure 12 Paleosecular variation (PSV) test. The thick black line is the 1.5-0.5 Ga model G curve from Veikkolainen and Pesonen (2014). The gray area is the corresponding error limits (2σ). Numbers are paleomagnetic poles used in the paleogeographic reconstruction, which are listed in Table 3.

5.2 Implications for paleogeography of Baltica

Large variances have been observed in the paleomagnetic results of BDD dykes (Fig. 10b; Table 2), which have been interpreted differently in previous studies (e.g., Pesonen and Klein, 2013). Here, we summarize available paleomagnetic and geochronological data of BDD dykes in the literature (Fig. 5; Table 2), in an attempt to examine each proposed model, and then discuss their implications. First, if we assume that all BDD results are reliable without any remagnetization/contamination, the variance in BDD dyke remanences would be substantial (Table 2), for instance, the very steep inclinations of 947 Ma Nornäs dyke and 954 Ma Karlshamn dyke, and the very shallow inclinations of 946 Ma Fäjö dyke and 948 Ma Bräkne-Hoby dyke (Fig. 10b). This variance, occurring within a fairly short time interval (< 10 Ma), if interpreted as plate motion, would require unrealistically fast drift rates of Baltica, contradicting geologically younger plate tectonic speeds. Even true polar wander, which might occur as fast as ~6° per Myr (Rose and Buffett, 2017), is insufficient to reconcile the variances in BDD remanences. Another possibility might be a non-GAD field, but even then, the entire BDD dataset would be difficult to explain unless departures from GAD were extreme. For example, Pesonen et al. (2012) show that with 11% octupole field (relative to a dominant GAD field), the inclination shallowing effect will approach a maximum ~10° at mid-paleolatitudes. However, the

inclination differences among BDD remanences are mostly larger than 10°, and some even reach 70-80° (Table 2). Only if the transient ancient magnetic field was totally dominated by octupole component (Tauxe, 2005) or by an ephemeral equatorial dipole field (Abrajevitch and Van der Voo, 2010) can the large inclination differences be explained.

After the experience gained from careful demagnetization procedures in our study, we are suspicious that the large variances of remanence in the entire BDD dataset likely result from selective remagnetization. The 947 Ma Nornäs dyke, after being subjected to detailed demagnetization, shows that the remanence gradually moves away from the previously determined ChRM and towards the NW-up BDD-reference direction (Figs. 10 and 11). In fact, based on the great circle analyses, the primary remanence of the Nornäs dyke should be the same as that of Group An, and the low-temperature or low-AF remanence component of Nornäs dyke is NNW and steep down, very close to the PDF direction. Hence, it is very likely that the Nornäs dyke was affected by partial remagnetization and component mixing due to overlapping coercivity and/or unblocking temperature spectra. That concept impels us to doubt the robustness of other anomalous directions, especially the 954 Ma Karlshamn dyke, for which the published ChRM direction is very close to the PDF direction (Fig. 10b). Also, as the remanences of 946 Ma Lösen-Fäjö and 948 Ma Bräkne-Hoby dykes are half-way between the PDF direction and the NW-up BDD-reference direction (Group An), they could possibly carry substantial PDF overprints as well. Besides, the previously published directions of the Nornäs, Lösen-Fäjö, Karlshamn and Bräkne-Hoby dykes were calculated using the minimum scatter of data at 10 mT, 20 mT, 30 mT or 40 mT (Patchett and Bylund, 1977; Piper and Smith, 1980; Bylund, 1985;

Table 2). AF demagnetization below 30 mT is generally too low to be pertinent to Precambrian paleomagnetic remanence preservation. If two components have strongly overlapping demagnetization spectra, higher AF intensities do not necessarily guarantee a successful removal of a partial overprint. With more sophisticated laboratory equipment and more accurate analytical methods (principal component analysis, great circle method etc.) now available, we suggest a re-study of these dykes before using their directions for geophysical interpretations.

Because we suspect the reliability of some results of BDD dykes in previous studies, either due to the inadequate demagnetization (e.g., low AF field) or outdated analytical methods (e.g., least scatter method for averaging paleomagnetic directions), for subsequent discussion we only focus on the results that we can be assured to lack an overprint/contamination. This would yield 12 dykes in Group A (6 dykes in Group An and 6 dykes in Group Ar; Table 2) and 4 dykes in Group B (1 dyke in Group Bn and 3 dykes in Group Br; Table 2). We admit that by this treatment the paleomagnetic dataset of BDD dykes is reduced, but we can test for averaging out the paleosecular variation (PSV) by calculating the angular dispersion (*S*) for each of the two poles we obtained from Groups A and B, respectively, following the approximation equation:

$$S = \frac{81°}{\sqrt{K}}$$

where *K* is the best estimate of precision parameter (Butler, 1992).

The calculated *S* values are plotted against the 1.5-0.5 Ga model G curve fitted by Veikkolainen and Pesonen (2014). It is noted that the 951-935 Ma pole obtained from

Group A matches the model G curve very well (Fig. 12; Table 3), which means that even though we used a smaller dataset, the number of dykes seems sufficient to average out the PSV. In contrast, the 971 Ma pole obtained from Group B falls below the model G curve (Fig. 12; Table 3). Since there are only 4 dykes in Group B, this pole is considered merely as a VGP, and more dykes in this group are needed to provide a paleomagnetic pole in future studies. Further geochronology on Group B dykes would also be useful to assess whether they are restricted to a narrow age range.

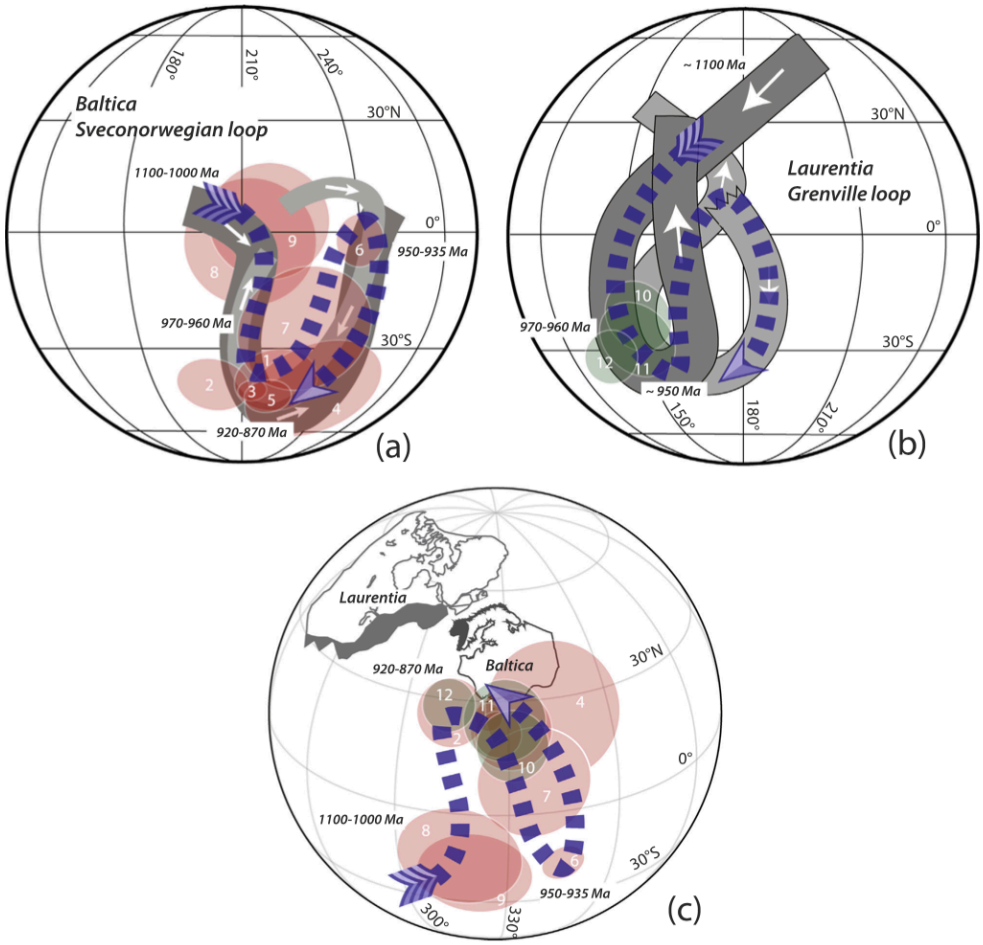

Figure 13 (a) Sveconorwegian loop for Baltica. Counterclockwise motion is from Elming et al. (1993) and clockwise motion is from Elming et al. (2014). (b) Grenville loop for Laurentia. Counterclockwise motion is from Weil et al. (1998) and clockwise motion is

from Hyodo and Dunlop (1993). (c) Coeval 1000-850 Ma paleomagnetic poles from Baltica and Laurentia in present North America reference frame. White arrows indicate the younging directions of apparent polar wander paths. Blue dash lines indicate new loop proposed by this study. Red poles are from Baltica and green poles are from Laurentia. Poles' numbers are listed in Table 3.

The early Neoproterozoic apparent polar wander (APW) path of Baltica, known as the Sveconorwegian loop, is under debate in terms of its shape and form. Previously, the Sveconorwegian loop (as shown in the South Pacific) was generally assumed to exhibit counterclockwise motion (Fig. 13a; Elming et al., 1993). However, some have suggested that the southernmost part of the Sveconorwegian loop represents a post-900 Ma delayed remanence acquisition during slow exhumation of the deep-seated igneous rocks (Walderhaug et al., 1999; Brown and McEnroe, 2004). Pisarevsky and Bylund (2006) speculated that the delayed acquisition is probably caused by low-temperature chemical alteration. Elming et al. (2014) proposed a clockwise motion of the south-Pacific polarity representation of the Sveconorwegian loop, incorporating the 945 Ma equatorial pole and assuming that the southernmost part of the loop is post-900 Ma (Fig. 13a). Similarly, the early Neoproterozoic APW path of Laurentia (also viewed in the south-Pacific polarity representation) is also interpreted as either clockwise (Hyodo and Dunlop, 1993) or counterclockwise (Weil et al., 2006). Regardless of uncertainties in the APW paths of two cratons, geological evidence supports a proximity of Baltica and Laurentia during the Neoproterozoic time (Cawood and Pisarevsky, 2006).

Our results from the BDD dykes support the equatorial pole for Baltica at 951-935 Ma, similar to the result of Elming et al. (2014). In addition, we obtained a 971 Ma VGP for Baltica, suggesting a high-paleolatitude position. Brown and McEnroe (2012) studied paleomagnetism of the igneous and metamorphic rocks in the Adirondack Highlands of Laurentia. Performing careful rock-magnetic and petrological studies, they generated several poles with modeled cooling ages of 990-960 Ma. We also performed the PSV test of the 970 Ma and 960 Ma poles from Brown and McEnroe (2012), which suggests that the PSV has been averaged out from these two poles (Fig. 12; Table 3). Cratonic reconstruction using these poles and our new 971 Ma VGP permits a close position between Baltica and Laurentia at 970-960 Ma. The reconstructed positions of two cratons allow the Sveconorwegian and Grenville orogenies be a continuous belt, which has been suggested in many other studies (e.g., Li et al., 2008; although see Gower et al., 2008, for cautionary details). The Sveconorwegian and Grenville loops seem to have some oscillatory components (Fig. 13), which could be attributed to plate motions or true polar wander (Evans, 2009). In this scenario, the paleogeographic evolution of the two cratons is characterized by high- to low-latitude drift between 970-960 Ma and 950-935 Ma, and a return from low to high latitude by 920-870 Ma (Fig. 14). Notably, all three pole groups include at least one result that appears to average paleosecular variation adequately (Fig. 12). The implied drifting speed is of ~100-150 km/Ma, which is fast but is a reasonable rate for either plate tectonics or true polar wander. Deconvolving those two processes will require more detailed paleomagnetic work from Baltica, Laurentia, and other cratons with suitably complete early Neoproterozoic geological records.

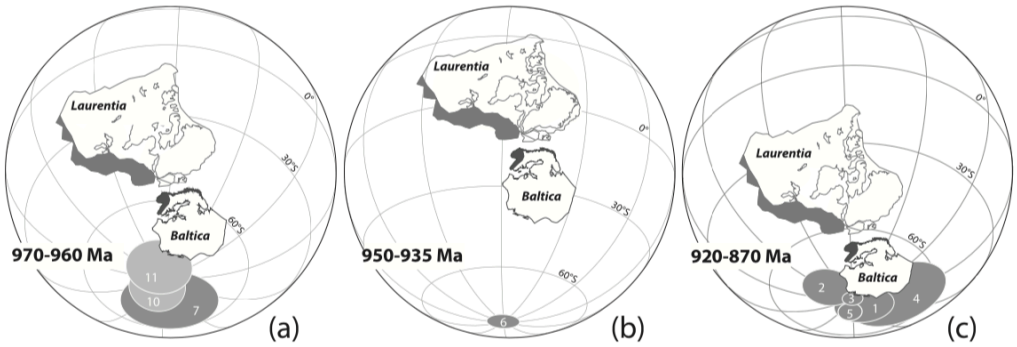

Figure 14 Paleogeographic reconstructions of Baltica and Laurentia. (a) 970-960 Ma (Euler pole of Laurentia to absolute reference: 22.4°N, 100.6°E, 127.6°; Euler pole of Baltica to Laurentia: 75.8°N, 95.7°E, -59.2°); (b) 950-935 Ma (Euler pole of Laurentia to absolute reference: -37.9°N, -65.5°E, -99.8°; Euler pole of Baltica to Laurentia: 75.8°N, 95.7°W, -59.2°); (c) 920-870 Ma (Euler pole of Laurentia to absolute reference: -15.6°N, -93.5°E, -125.9°; Euler pole of Baltica to Laurentia: 75.8°N, 95.7°W, -59.2°). Paleomagnetic poles used for reconstruction are listed and numbered in Table 3. Dark and light gray poles are from Baltica and Laurentia, respectively.

6. Conclusions

We present a detailed paleomagnetic, rock magnetic and anisotropy of magnetic susceptibility, and geochronological study of the Blekinge-Dalarna dolerite dykes, which leads to following conclusions:

(1) Positive baked-contact, reversal and PSV tests support the reliability of the equatorial paleomagnetic pole for Baltica at 951-935 Ma (Plat. = -2.6°N, Plon. = 239.6°E, A_{95} = 5.8°, N = 12 dykes), which can be used as a key pole to constrain the paleogeography of Baltica.

(2) The anomalous paleomagnetic direction obtained from the 947 Ma Nornäs dyke is probably due to a PDF overprint that was not adequately removed by low alternating-field demagnetization levels in previous studies, instead of originating from true polar wander, or abnormal geomagnetic field behaviors. PDF component contamination is suspected in other anomalously-directed BDD dykes.

(3) A well-dated 971 Ma VGP (Plat. = -27.0°N, Plon. = 230.4°E, A_{95} = 14.9°) from four BDD dykes, in concert with same-age poles from Laurentia, suggests a high-latitude position for Baltica in proto-Rodinia. Paleogeographic reconstruction demonstrates that Baltica and Laurentia drifted together towards low latitude between 970-960 Ma and 950-935 Ma, and moved back to high latitude by 920-870 Ma. In this scenario, the apparent polar wander path would be more complicated than either the Sveconorwegian and Grenville loops considered in isolation.

(4) Based on published ages of BDD dykes and adjacent dykes sub-orthogonal to it, it seems that the requirement of a single mantle plume model is not satisfied. The BDD dykes more likely result from plate boundary forces associated with the Sveconorwegian orogeny. The arcuate geometry could be associated with a spatially varying regional stress distribution.

Acknowledgements

We would like to thank Anna Sartell at Lund University for preparing baddeleyite grains for U-Pb dating, and Stephen Victor for helping with hysteresis loop measurement in Yale

Archaeomagnetism Laboratory. Thanks are also due to Magnus Ripa at the Geological Survey of Sweden for the geological data and information of outcrops, and to Torkhild Rasmussen at Luleå University of Technology for help in creating maps of outcrops. Two anonymous reviewers are gratefully acknowledged for constructive reviews that improved the quality of the manuscript.

Table 1 Results of U-Pb baddeleyite geochronology.

Sample (number of grains)	U/Th	Pb_c/Pb_{tot}[1]	$^{206}Pb/^{204}Pb$	$^{207}Pb/^{235}U$	± 2s% Error	$^{206}Pb/^{238}U$	± 2s% Error	$^{207}Pb/^{235}U$	$^{206}Pb/^{238}U$	$^{207}Pb/^{206}Pb$	± 2σ	Concordance
			[Raw][2]	[Corr][3]				[Age, Ma]				
G16S12												
Bd-1 (2 grains)	27.4	0.085	818.2	1.5298	1.15	0.15711	1.10	942.4	940.7	946.5	9.2	0.994
Bd-2 (4 grains)	14.3	0.046	1449.3	1.5358	0.61	0.15707	0.51	944.8	940.4	955.1	7.0	0.985
Bd-3 (3 grains)	7.3	0.174	375.2	1.5337	1.90	0.15753	1.82	944.0	943.1	946.1	15.4	0.997
G16S22												
Bd-1 (2 grains)	5.9	0.311	214.3	1.5922	3.96	0.16185	3.75	967.2	967.1	967.4	33.6	1.000
Bd-2 (5 grains)	12.3	0.080	820.0	1.5437	0.82	0.15688	0.73	948.0	939.4	968.0	8.4	0.970
Bd-3 (5 grains)	9.0	0.168	365.5	1.5875	1.12	0.16072	0.99	965.3	960.8	975.8	11.6	0.985
G16S37												
Bd-1 (1 grains)	13.0	0.033	2026.6	1.5314	0.41	0.15714	0.33	943.0	940.8	948.2	5.2	0.992
Bd-2 (2 grains)	17.1	0.070	947.4	1.5281	0.74	0.15656	0.68	941.7	937.6	951.4	6.9	0.986
Bd-3 (2 grains)	7.6	0.119	520.8	1.5312	0.72	0.15773	0.65	943.0	944.1	940.3	7.0	1.004

[1] Pb_c = common Pb, Pb_{tot} = total Pb (radiogenic + blank + initial).

[2] Measured ratios, corrected for fractionation and spike.

[3] Isotopic ratios corrected for fractionation (0.1% per amu for Pb), spike contribution, blank (0.4 pg Pb and 0.04 pg U), and initial common Pb. Initial common Pb corrected with isotopic compositions from the model of Stacey and Kramers (1975) at the age of the sample.

Table 2 Summary of paleomagnetic results of BDD dykes (from North to South).

Dyke	Slat (°N)	Slon (°E)	Age (Ma)	Dec (°)	Inc (°)	α_{95} (°)	N/n	Plat (°N)	Plon (°E)	A_{95} (°)	Group	Reference	Comment
G16S22	61.6043	13.2260	971 ± 7	140.6	66.1	2.0	1/10	-24.5	220.8	3.0	Br	This study	NW-SE trending (324°)
G16S21	61.5937	13.0047		296.5	-66.5	5.0	1/8	-32.1	236.3	7.5	Bn	This study	NW-SE trending
Nornäs ii	61.42	13.21	946.8 ± 1.2	325.0	71.3	6.5	1/4	71.0	282.0	10.5	-	Bylund (1985); Söderlund et al. (2005)	remanence at 10 mT[a]
Nornäs i	61.42	13.21	946.8 ± 1.2	0.4	82.2	3.0	1/6	77.0	14.0	6.0	-	Piper and Smith (1980); Söderlund et al. (2005)	-
G16S05	61.4230	13.2150		Nornäs dyke, partial remagnetization and vector component contamination							-	This study	NW-SE trending (315°)
G16S06	61.4207	13.2202		Nornäs dyke, partial remagnetization and vector component contamination							-	This study	NW-SE trending (315°)
G16S07	61.2557	13.7790		142.1	58.7	2.0	1/9	-15.3	223.2	2.6	Br	This study	NW-SE trending (330°)
G16S17	61.2504	13.4103		305.5	-45.5	4.2	1/4	-8.5	240.6	4.3	-	This study	NW-SE trending (315°), same dyke as G16S18
G16S18	61.2464	13.4186		300.5	-39.8	9.4	1/5	-6.4	246.6	8.7	-	This study	NW-SE trending (315°), same dyke as G16S17
G16S17&18 comb.	-	-		302.2	-41.7	5.2	1/9	-7.0	244.6	5.0	An	This study	-
G16S24	61.1999	13.1505	~1460	110.3	30.4	6.8	1/8	-5.0	257.8	5.6	-	This study	baked Dala sandstone
G16S23	61.1992	13.1515		126.6	40.9	12.9	1/7	-4.9	240.8	12.2	Ar	This study	NW-SE trending (320°)
G16S14	61.1455	12.7273		demagnetization behavior like Nornäs dyke, partial remagnetization and vector component contamination							-	This study	NW-SE trending
G16S16	61.1118	13.8530		southern extension of Nornäs dyke, partial remagnetization and vector component contamination							-	This study	NW-SE trending (325°), width ~8 m
G16S15	61.0949	13.0151		330.7	-24.7	6.2	1/3	12.4	222.1	4.7	An	This study	NW-SE trending (325°)
G16S09	60.9265	13.1784		inconsistent directions within dyke							-	This study	NW-SE trending (305°), same dyke as G16S10
G16S37	60.9181	14.1043	947 ± 4	southern extension of Nornäs dyke, partial remagnetization and vector component contamination							-	This study	NW-SE trending (325°)

Nornäs new (G16S05,06,16&37 comb.)	-	-		307.9	-35.3	2.9	4/22	-0.8	241.7	2.6	-	This study	Mean direction calculated using great circle method
G16S10	60.8878	13.3006		inconsistent directions within dyke							-	This study	NW-SE trending (305°), same dyke as G16S09
G16S36	60.8284	14.2725		300.6	-32.0	5.9	1/8	-1.4	249.5	5.0	An	This study	NW-SE trending
G16S11	60.8077	13.5783	~1460	140.7	30.9	6.5	1/9	-14.9	223.0	2.6	-	This study	baked Öje basalt
G16S12	60.8077	13.5783	951 ± 5	142.2	36.9	6.2	1/9	3.1	228.7	5.6	Ar	This study	NW-SE trending (324°)
Andersbo	60.76	15.41		143.0	42.0	9.0	1/7	1.0	229.0	7.3	-	Bylund and Elming (1992)	-
G16S13	60.7147	13.3904		153.2	8.3	7.3	1/8	21.8	222.4	5.2	-	This study	NW-SE trending
Ejen	60.67	14.79		128.0	24.0	9.0	1/8	6.0	245.8	6.6	-	Bylund (1985)	remanence at 20 mT[a]
Falun (new)	60.59	15.58	945.7 ± 1.2	128.7	37.9	3.0	1/9	-1.7	242.3	2.6	Ar	Elming et al. (2014); Söderlund et al. (2005)	NW-SE trending (330°)
Falun (old)	60.59	15.58	945.7 ± 1.2	131.4	45.8	5.6	1/10	-6.1	237.6	5.7	-	Patchett and Bylund (1977); Söderlund et al. (2005)	remanence at 20 mT[a]
Gällsjön	60.51	14.53		136.0	48.0	12.0	1/5	18.0	241.0	8.5	-	Bylund and Elming (1992)	-
G16S40	60.3185	14.2210		106.0	67.0	8.3	1/9	-35.0	243.7	12.5	Br	This study	NW-SE trending (330°)
G16S39	60.3024	13.8662		inconsistent directions within dyke							-	This study	NW-SE trending, same dyke as G16S38
G16S38	60.3016	13.8672		inconsistent directions within dyke							-	This study	NW-SE trending, same dyke as G16S39
Årby	59.27	16.46		142.5	52.4	7.0	1/6	-7.3	227.4	8.0	-	Patchett and Bylund (1977)	remanence at 20 mT[a]
Marbystrand	58.61	16.48		127.5	31.1	3.6	1/9	3.3	246.0	3.0	-	Elming et al. (2014)	NW-SE trending (310°)
Y1	58.58	16.33	938 ± 4	311.2	-43.3	5.7	1/13	-3.4	239.0	4.0	An	Elming et al. (2014)	NE-SE trending (40°)
Y2	58.58	16.33	941 ± 6	313.3	-40.7	7.4	1/14	-0.5	238.3	7.0	An	Elming et al. (2014)	NE-SE trending (40°)
Slussen	58.2	12.2		300.9	-26.5	11.5	1/6	3.2	248.5	9.2	An	Pisarevsky and Bylund (2006)	-
Tuve	57.8	11.8	935 ± 3	122.2	53.7	3.2	2/23	-14.0	237.9	3.7	Ar	Pisarevsky and Bylund (2006); Hellström et al. (2004)	-

Small	57.8	11.8		124.5	54.6	7.4	1/3	-13.9	235.8	8.8	Ar	Pisarevsky and Bylund (2006)	-
Hjuvik	57.7	11.7		118.8	37.1	11.5	1/12	-3.3	246.9	10.3	Ar	Pisarevsky and Bylund (2006)	-
Sjunnaryd (sill)	57.7	14.8		317.1	-28.9	15.1	1/4	8.8	236.4	12.4	-	Pesonen and Klein (2014)	-
Nilstorp (sill)	57.64	14.83	966 ± 5	315.2	-27.4	9.7	1/6	9.0	238.5	7.8	-	Patchett and Bylund (1977); Söderlund et al. (2005)	remanence at 40 mT[a]
Tärnö	56.27	15.06		312.8	-41.9	4.8	1/5	0.3	237.0	4.6	-	Patchett and Bylund (1977)	remanence at 30 mT[a]
Bräkne-Hoby	56.26	15.18	948.1 ± 1.4	309.3	3.6	6.1	1/7	22.2	251.9	4.3	-	Patchett and Bylund (1977); Söderlund et al. (2005)	remanence at 40 mT[a]
Lösen-Fäjö	56.17	15.69	945.8 ± 1.0	312.6	2.6	5.4	1/6	23.3	248.9	3.8	-	Patchett and Bylund (1977); Söderlund et al. (2005)	remanence at 20 mT[a]
Väby	56.17	15.22		137.0	33.0	10.0	1/3	8.0	236.0	8.4	-	Poorter (1975)	remanence at 10 mT[a]
Karlshamn	56.15	14.86	954.2 ± 1.1	129.0	81.0	4.8	1/9	-43.2	213.5	9.1	-	Patchett and Bylund (1977); Söderlund et al. (2004a)	remanence at 30 mT[a]
Group A Mean	**-**	**-**		**128.8**	**39.6**	**6.5**	**12/116**	**-2.6**	**239.6**	**5.8**	**-**		**Averaging 12 dykes in Group An/Ar listed in this table**
Group B Mean	**-**	**-**		**127.6**	**65.4**	**9.7**	**4/36**	**-27.0**	**230.4**	**14.9**	**-**		**Averaging 4 dykes in Group Bn/Br listed in this table**

Note: Slat/Slon = site geographic latitude/longitude, Dec = declination, Inc = inclination, Plat/Plon = paleomagnetic pole latitude/longitude, N/n = number of site/sample, α_{95} = radius of 95% confidence cone of the mean direction, A_{95} = radius of 95% confidence cone of the paleomagnetic pole. [a] least scatter of data at alternating-field step used for mean vector calculation

Table 3 Paleomagnetic poles constrain the early Neoproterozoic paleogeographic reconstruction of Baltica and Laurentia.

#	Paleomagnetic Pole	Dec (°)	Inc (°)	α_{95} (°)	k	N/n	Plat (°N)	Plon (°E)	A_{95} (°)	S (°)	$\|\lambda\|$ (°)	Age (Ma)	1	2	3	4	5	6	7	Q	Reference
Baltica																					
1	Hunnedalen dykes	294.0	-75.0	6.0	115	6/69	-41.0	222.0	10.5	13.4	61.8	848 ± 27[a]; 855 ± 59[b]	1	1	1	0	1	0	1	5	Walderhaug et al. (1999)
2	Egersund-Ogna anorthosite	325.9	-80.1	4.9	73	13/69	-42.1	200.4	9.0	17.3	70.8	900[c]	1	1	1	0	0	0	1	4	Brown and McEnroe (2004)
3	Egersund anorthosite	-	-	-	-	76/-	-43.5	213.7	3.6	-	-	900[c]	0	1	1	0	0	0	1	3	Stearn and Piper (1984); Walderhaug et al. (1999)
4	Rogaland Igneous Complex	269.0	-72.0	11.0	49	5/24	-45.9	238.4	18.2	19.4	57.0	869 ± 14[a]	1	0	1	1	0	0	1	4	Walderhaug et al. (2007)
5	Bjerkreim-Sokndal intrusion	303.4	-73.5	3.7	24	66/354	-35.9	217.9	6.0	26.1	59.4	916[c]	1	1	1	0	1	0	1	5	Brown and McEnroe (2015)
6	Mean 951-935 Ma Baltica pole	308.8	-39.6	6.5	42	12/116	-2.6	239.6	5.8	10.8	22.5	951-935[d]	1	1	1	1	1	1	1	7	This study
7	971 Ma BDD dykes VGP	307.6	-65.4	14.2	68	4/36	-27.0	230.4	14.9	13.0	47.5	971 ± 7[d]	1	0	1	0	1	1	1	5	This study
8	Laanila-Ristijärvi dykes	355.5	-40.0	17.5	51	3/7	-2.1	212.2	16.4	9.0	22.8	1042 ± 50[b]	0	0	1	1	1	0	0	3	Mertanen et al. (1996)
9	Bamble Intrusion mean	-	-	-	-	-	3.0	217.0	15.0	-	-	1100-1040	0	1	1	0	0	0	0	2	Meert and Torsvik (2003)
Laurentia																					
10	Adirondack microcline gneisses	289.2	-62.8	7.6	29	14/80	-18.4	151.1	10.5	22.0	44.2	960[c]	1	1	1	0	0	1	1	5	Brown and McEnroe (2012)
11	Adirondack metamorphic anorthosites and other rocks	283.9	-67.3	7.7	28	14/68	-25.1	149.0	11.6	24.3	50.1	970[c]	1	1	1	0	0	1	1	5	Brown and McEnroe (2012)
12	Adirondack fayalite granites	297.0	-75.8	3.9	199	8/40	-28.4	132.7	6.9	10.2	63.2	990[c]	1	1	1	0	0	1	1	5	Brown and McEnroe (2012)

Note: Dec = declination, Inc = inclination, α_{95} = radius of 95% confidence cone of the mean direction, k = precision parameter, N/n = number of site/sample, Plat/Plon = paleomagnetic pole latitude/longitude, A_{95} = radius of 95% confidence cone of the paleomagnetic pole, S = angular dispersion of VGPs, $|\lambda|$ = absolute value of paleolatitude, Q = sum of quality criteria (Van der Voo, 1990). [a] Ar-Ar biotite ages, [b] Sm-Nd whole rock ages, [c] Cooling ages, [d] U-Pb baddeleyite ages.

References

Abrajevitch, A., & Van der Voo, R. (2010). Incompatible Ediacaran paleomagnetic directions suggest an equatorial geomagnetic dipole hypothesis. *Earth and Planetary Science Letters*, 293(1-2), 164-170.

Bingen, B., Nordgulen, Ø., Viola, G. (2008). A four-phase model for the Sveconorwegian orogeny, SW Scandinavia. *Norsk Geologisk Tidsskrift*, 88, 43-72.

Bingen, B., & Solli, A. (2009). Geochronology of magmatism in the Caledonian and Sveconorwegian belts of Baltica: synopsis for detrital zircon provenance studies. *Norwegian Journal of Geology*, 89, 267-290.

Bogdanova, S.V., Page, L.M., Skridlaite, G., & Taran, L.N. (2001). Proterozoic tectonothermal history in the western part of the East European Craton: $^{40}Ar/^{39}Ar$ geochronological constraints. *Tectonophysics*, 339, 39-66.

Bogdanova, S., Gorbatschev, R., Skridlaite, G., Soesoo, A., Taran, L., & Kurlovich, D. (2015). Trans-Baltic Palaeoproterozoic correlations towards the reconstruction of supercontinent Columbia/Nuna. *Precambrian Research*, 259, 5-33.

Boyden, J. A., Müller, R. D., Gurnis, M., Torsvik, T. H., Clark, J. A., Turner, M., Ivey-Law, H., Watson, R. J., & Cannon, J. S. (2011). Next-generation plate-tectonic reconstructions using GPlates. *Geoinformatics*, 9, 5-114.

Brander, L., & Söderlund, U. (2009). Mesoproterozoic (1.47–1.44 Ga) orogenic magmatism in Fennoscandia; Baddeleyite U–Pb dating of a suite of massif-type anorthosite in S. Sweden. *International Journal of Earth Science (Geologische Rundschau)*, 98, 499-516.

Brown, L. L., & McEnroe, S. A. (2004). Palaeomagnetism of the Egersund-Ogna

anorthosite, Rogaland, Norway, and the position of Fennoscandia in the Late Proterozoic. *Geophysical Journal International*, 158(2), 479-488.

Brown, L. L., & McEnroe, S. A. (2012). Paleomagnetism and magnetic mineralogy of Grenville metamorphic and igneous rocks, Adirondack Highlands, USA. *Precambrian Research*, 212, 57-74.

Brown, L. L., & McEnroe, S. A. (2015). 916 Ma pole for southwestern Baltica: Palaeomagnetism of the Bjerkreim-Sokndal layered intrusion, Rogaland igneous complex, southern Norway. *Geophysical Journal International*, 203(1), 567-587.

Buchan, K. L., & Ernst, R. E. (2016). Giant circumferential dyke swarms on Earth: Possible analogues of coronae on Venus and similar features on Mars. *Acta Geologica Sinica (English Edition)*, 90(sup.1): 186-187.

Buchan, K. L., & Ernst, R. E. (2018). A giant circumferential dyke swarm associated with the High Arctic Large Igneous Province (HALIP). *Gondwana Research*, 58, 39-57.

Butler, R. F. (1992). Paleomagnetism: magnetic domains to geologic terranes (Vol. 319). Boston: Blackwell Scientific Publications.Bylund, G. (1985). Palaeomagnetism of middle Proterozoic basic intrusives in central Sweden and the Fennoscandian apparent polar wander path. *Precambrian Research*, 28(3-4), 283-310.

Bylund, G., & Elming, S. Å. (1992). The Dala dolerites, central Sweden, and their palaeomagnetic signature. *GFF*, 114(1), 143-153.

Cawood, P. A., & Pisarevsky, S. A. (2006). Was Baltica right-way-up or upside-down in the Neoproterozoic? *Journal of the Geological Society*, 163(5), 753-759.

Christoffel, C., Connelly, J.N., Åhäll, K.-I. (1999) Timing and characterization of recurrent pre-Sveconorwegian metamorphism and deformation in the Varberg-Halmstad region

of SW Sweden. *Precambrian Research*, 98, 173-195.

Dalziel, I. W. (1997). Neoproterozoic-Paleozoic geography and tectonics: Review, hypothesis, environmental speculation. *Geological Society of America Bulletin*, 109(1), 16-42.

Day, R., Fuller, M., & Schmidt, V. A. (1977). Hysteresis properties of titanomagnetites: Grain-size and compositional dependence. *Physics of the Earth and Planetary Interiors*, 13(4), 260-267.

Denyszyn, S. W., Davis, D. W., & Halls, H. C. (2009). Paleomagnetism and U-Pb geochronology of the Clarence Head dykes, Arctic Canada: Orthogonal emplacement of mafic dykes in a large igneous province. *Canadian Journal of Earth Sciences*, 46(3), 155-167.

Dunlop, D. J. (2002). Theory and application of the Day plot (Mrs/Ms versus Hcr/Hc) 1. Theoretical curves and tests using titanomagnetite data. *Journal of Geophysical Research: Solid Earth*, 107(B3).

Elming, S. Å., Pesonen, L. J., Leino, M. A. H., Khramov, A. N., Mikhailova, N. P., Krasnova, A. F., Merlanen, S., Bylund, G., & Terho, M. (1993). The drift of the Fennoscandian and Ukrainian shields during the Precambrian: A palaeomagnetic analysis. *Tectonophysics*, 223(3-4), 177-198.

Elming, S. Å., Pisarevsky, S. A., Layer, P., & Bylund, G. (2014). A palaeomagnetic and $^{40}Ar/^{39}Ar$ study of mafic dykes in southern Sweden: A new Early Neoproterozoic key-pole for the Baltic Shield and implications for Sveconorwegian and Grenville loops. *Precambrian Research*, 244, 192-206.

Ernst, R.E., Buchan, K.L. (1998). Arcuate dyke swarms associated with mantle plumes on

Earth: Implications for Venusian coronae. Lunar and Planetary Science Conference #29, Houston, Texas, Abstract #1021.

Ernst, R. E., Desnoyers, D. W., Head, J. W., & Grosfils, E. B. (2003). Graben-fissure systems in Guinevere Planitia and Beta Regio (264°-312°E, 24°-60°N), Venus, and implications for regional stratigraphy and mantle plumes. *Icarus*, 164(2), 282-316.

Evans, D. A. D. (2009). The palaeomagnetically viable, long-lived and all-inclusive Rodinia supercontinent reconstruction. *Geological Society, London, Special Publications*, 327(1), 371-404.

Gaál, G., & Gorbatschev, R. (1987). An outline of the Precambrian evolution of the Baltic Shield. *Precambrian Research*, 35, 15-52.

Gower, C.F., Kamo, S., & Krogh, T.E. (2008). Indentor tectonism in the eastern Grenville Province. *Precambrian Research*, 167, 201-212.

Hellström, F. A., Johansson, Å., & Larson, S. Å. (2004). Age and emplacement of late Sveconorwegian monzogabbroic dykes, SW Sweden. *Precambrian Research*, 128(1), 39-55.

Hrouda, F. (1982). Magnetic anisotropy of rocks and its application in geology and geophysics. *Surveys in Geophysics*, 5(1), 37-82.

Hyodo, H., & Dunlop, D. J. (1993). Effect of anisotropy on the paleomagnetic contact test for a Grenville dike. *Journal of Geophysical Research: Solid Earth*, 98(B5), 7997-8017.

Jaffey, A. H., Flynn, K. F., Glendenin, L. E., Bentley, W. T., & Essling, A. M. (1971). Precision measurement of half-lives and specific activities of ^{235}U and ^{238}U. *Physical Review C*, 4(5), 1889-1906.

Johansson, L., & Johansson, Å. (1990). Isotope geochemistry and age relationships of mafic intrusions along the Protogine Zone, southern Sweden. *Precambrian Research*, 48(4), 395-414.

Jones, C. H. (2002). User-driven integrated software lives: "Paleomag" paleomagnetics analysis on the Macintosh. *Computers & Geosciences*, 28(10), 1145-1151.

Kirschvink, J. L. (1980). The least-squares line and plane and the analysis of palaeomagnetic data. *Geophysical Journal International*, 62(3), 699-718.

Kirschvink, J. L., Kopp, R. E., Raub, T. D., Baumgartner, C. T., & Holt, J. W. (2008). Rapid, precise, and high sensitivity acquisition of paleomagnetic and rock magnetic data: Development of a low noise automatic sample changing system for superconducting rock magnetometers. *Geochemistry, Geophysics, Geosystems*, 9(5).

Knight, M. D., & Walker, G. P. (1988). Magma flow directions in dikes of the Koolau Complex, Oahu, determined from magnetic fabric studies. *Journal of Geophysical Research: Solid Earth*, 93(B5), 4301-4319.

Tauxe, L. (2005). Inclination flattening and the geocentric axial dipole hypothesis. *Earth and Planetary Science Letters*, 233(3-4), 247-261.

Mäkitie, H., Data, G., Isabirye, E., Mänttäri, I., Huhma, H., Klausen, M. B., Pakkanen, L., & Virransalo, P. (2014). Petrology, geochronology and emplacement model of the giant 1.37 Ga arcuate Lake Victoria Dyke Swarm on the margin of a large igneous province in eastern Africa. *Journal of African Earth Sciences*, 97, 273-296.

Meert, J. G., & Torsvik, T. H. (2003). The making and unmaking of a supercontinent: Rodinia revisited. *Tectonophysics*, 375(1-4), 261-288.

Mertanen, S., Pesonen, L. J., & Huhma, H. (1996). Palaeomagnetism and Sm-Nd ages of

the Neoproterozoic diabase dykes in Laanila and Kautokeino, northern Fennoscandia. *Geological Society, London, Special Publications*, 112(1), 331-358.

McFadden, P. L., & McElhinny, M. W. (1988). The combined analysis of remagnetization circles and direct observations in palaeomagnetism. *Earth and Planetary Science Letters*, 87(1-2), 161-172.

McFadden, P. L., & McElhinny, M. W. (1990). Classification of the reversal test in palaeomagnetism. *Geophysical Journal International*, 103(3), 725-729.

Möller, C., Andersson, A., Lundqvist, I., Hellström, F. (2007) Linking deformation, migmatite formation and zircon U-Pb geochronology in polymetamorphic orthogneisses, Sveconorwegian Province, Sweden. *Journal of Metamorphic Geology*, 25, 727-750.

Muxworthy, A. R., & McClelland, E. (2000). Review of the low-temperature magnetic properties of magnetite from a rock magnetic perspective. *Geophysical Journal International*, 140(1), 101-114.

Patchett, P. J., & Bylund, G. (1977). Age of Grenville belt magnetisation: Rb-Sr and palaeomagnetic evidence from Swedish dolerites. *Earth and Planetary Science Letters*, 35(1), 92-104.

Pesonen, L. J., & Klein, R. (2013). Paleomagnetism of some Proterozoic sediments and diabases, South Sweden. Abstract in XXVI Geofysiikan Päivät 2013, 93-96.

Pesonen, L. J., Mertanen, S., & Veikkolainen, T. (2012). Paleo-Mesoproterozoic supercontinents – A paleomagnetic view. *Geophysica*, 48(1-2), 5-47.

Piper, J. D., & Smith, R. L. (1980). Palaeomagnetism of the Jotnian lavas and sediments and post-Jotnian dolerites of central Scandinavia. *GFF*, 102(2), 67-81.

Pisarevsky, S. A., Wingate, M. T., Powell, C. M., Johnson, S., & Evans, D. A. (2003). Models of Rodinia assembly and fragmentation. *Geological Society, London, Special Publications*, 206(1), 35-55.

Pisarevsky, S. A., & Bylund, G. (2006). Palaeomagnetism of 935 Ma mafic dykes in southern Sweden and implications for the Sveconorwegian Loop. *Geophysical Journal International*, 166(3), 1095-1104.

Poorter, R. P. E. (1975). Palaeomagnetism of Precambrian rocks from southeast Norway and south Sweden. *Physics of the Earth and Planetary Interiors*, 10(1), 74-87.

Li, Z. X., Bogdanova, S. V., Collins, A. S., Davidson, A., De Waele, B., Ernst, R. E., Fitzsimons, I. C. W., Fuck, R. A., Gladkochub, D. P., Jacobs, J. & Karlstrom, K. E. (2008). Assembly, configuration, and break-up history of Rodinia: A synthesis. *Precambrian Research*, 160(1), 179-210.

Ludwig, K. R. (2003). User's manual for isoplot 3.00, a geochronological toolkit for microsoft excel. *Berkeley Geochronl. Cent. Spec. Publ.*, 4, 25-32.

Lundmark, A. M., & Lamminen, J. (2016). The provenance and setting of the Mesoproterozoic Dala Sandstone, western Sweden, and paleogeographic implications for southwestern Fennoscandia. *Precambrian Research*, 275, 197-208.

Ripa, M., Mellqvist, C., Ahl, M., Andersson, D., Bastani, M., Delin, H., Kübler, L., Nyston, P., Persson, L. & Thelander, T. (2012). Bedrock map Western part of the county Dalarna, scale 1:250 000. Sveriges Geologiska Undersökning K 382.

Rochette, P., Jackson, M., & Aubourg, C. (1992). Rock magnetism and the interpretation of anisotropy of magnetic susceptibility. *Reviews of Geophysics*, 30(3), 209-226.

Rose, I., & Buffett, B. (2017). Scaling rates of true polar wander in convecting planets and

moons. *Physics of the Earth and Planetary Interiors*, 273, 1-10.

Slagstad, T., Roberts, N. M., Marker, M., Røhr, T. S., & Schiellerup, H. (2013). A non-collisional, accretionary Sveconorwegian orogen. *Terra Nova*, 25(1), 30-37.

Söderlund, U., & Johansson, L. (2002). A simple way to extract baddeleyite (ZrO_2). *Geochemistry, Geophysics, Geosystems*, 3(2).

Söderlund, U., Möller, C., Andersson, J., Johansson, L., & Whitehouse, M. (2002) Zircon geochronology in polymetamorphic gneisses in the Sveconorwegian orogen, SW Sweden: ion microprobe evidence for 1.46-1.42 and 0.98-0.96 Ga reworking. *Precambrian Research*, 113, 193-225.

Söderlund, U., Patchett, P. J., Vervoort, J. D., & Isachsen, C. E. (2004a). The ^{176}Lu decay constant determined by Lu-Hf and U-Pb isotope systematics of Precambrian mafic intrusions. *Earth and Planetary Science Letters*, 219(3), 311-324.

Söderlund, P., Söderlund, U., Möller, C., Gorbatschev, R., & Rodhe, A. (2004b). Petrology and ion microprobe U-Pb chronology applied to a metabasic intrusion in southern Sweden: A study on zircon formation during metamorphism and deformation. *Tectonics*, 23(5).

Söderlund, U., Isachsen, C. E., Bylund, G., Heaman, L. M., Patchett, P. J., Vervoort, J. D., & Andersson, U. B. (2005). U-Pb baddeleyite ages and Hf, Nd isotope chemistry constraining repeated mafic magmatism in the Fennoscandian Shield from 1.6 to 0.9 Ga. *Contributions to Mineralogy and Petrology*, 150(2), 174-194.

Söderlund, U., Elming, S. Å., Ernst, R. E., & Schissel, D. (2006). The central Scandinavian dolerite Group-Protracted hotspot activity or back-arc magmatism? Constraints from U-Pb baddeleyite geochronology and Hf isotopic data. *Precambrian Research*, 150(3),

136-152.

Solyom, Z., Lindqvist, J. E., & Johansson, I. (1992). The geochemistry, genesis, and geotectonic setting of Proterozoic mafic dyke swarms in southern and central Sweden. *GFF*, 114(1), 47-65.

Squyres, S. W., Janes, D. M., Baer, G., Bindschadler, D. L., Schubert, G., Sharpton, V. L., & Stofan, E. R. (1992). The morphology and evolution of coronae on Venus. *Journal of Geophysical Research: Planets*, 97(E8), 13611-13634.

Stacey, J. T., & Kramers, J. D. (1975). Approximation of terrestrial lead isotope evolution by a two-stage model. *Earth and Planetary Science Letters*, 26(2), 207-221.

Stearn, J. E. F., & Piper, J. D. A. (1984). Palaeomagnetism of the Sveconorwegian mobile belt of the Fennoscandian Shield. *Precambrian Research*, 23(3-4), 201-246.

Stofan, E. R., & Head, J. W. (1990). Coronae of Mnemosyne Regio: Morphology and origin. *Icarus*, 83(1), 216-243.

Van der Voo, R. (1990). The reliability of paleomagnetic data. *Tectonophysics*, 184(1), 1-9.

Veikkolainen, T., & Pesonen, L. J. (2014). Palaeosecular variation, field reversals and the stability of the geodynamo in the Precambrian. *Geophysical Journal International*, 199(3), 1515-1526.

Veikkolainen, T. H., Biggin, A. J., Pesonen, L. J., Evans, D. A., & Jarboe, N. A. (2017). Advancing Precambrian palaeomagnetism with the PALEOMAGIA and PINT ($_{QPI}$) databases. *Scientific data*, 4, 170068.

Wahlgren, C. H., Cruden, A. R., & Stephens, M. B. (1994). Kinematics of a major fan-like structure in the eastern part of the Sveconorwegian orogen, Baltic Shield, south-central Sweden. *Precambrian Research*, 70(1-2), 67-91.

Walderhaug, H. J., Torsvik, T. H., Eide, E. A., Sundvoll, B., & Bingen, B. (1999). Geochronology and palaeomagnetism of the Hunnedalen dykes, SW Norway: Implications for the Sveconorwegian apparent polar wander loop. *Earth and Planetary Science Letters*, 169(1), 71-83.

Walderhaug, H. J., Torsvik, T. H., & Halvorsen, E. (2007). The Egersund dykes (SW Norway): A robust early Ediacaran (Vendian) palaeomagnetic pole from Baltica. *Geophysical Journal International*, 168(3), 935-948.

Weil, A. B., Geissman, J. W., & Ashby, J. M. (2006). A new paleomagnetic pole for the Neoproterozoic Uinta Mountain Supergroup, central Rocky Mountain states, USA. *Precambrian Research*, 147(3), 234-259.

Wen, B., Evans, D. A., & Li, Y. X. (2017). Neoproterozoic paleogeography of the Tarim Block: An extended or alternative "missing-link" model for Rodinia? *Earth and Planetary Science Letters*, 458, 92-106.

Wen, B., Evans, D. A., Wang, C., Li, Y. X., & Jing, X. (2018). A positive test for the Greater Tarim Block at the heart of Rodinia: Mega-dextral suturing of supercontinent assembly. *Geology*, 46(8): 687-690.

Zijderveld, J.D.A. (1967). AC demagnetization of rocks: analysis of results. *Methods in paleomagnetism* 3, 254.

Chapter 2

Paleomagnetism and rock magnetism of the ca. 1.87 Ga Pearson Formation, Northwest Territories, Canada: A test of vertical-axis rotation within the Great Slave basin [1]

Zheng Gong [a], XinXin Xu [a], David A. D. Evans [a], Paul F. Hoffman [b,c], Ross N. Mitchell [d], Wouter Bleeker [e]

[a] Department of Geology and Geophysics, Yale University, 210 Whitney Avenue, New Haven CT 06511, USA

[b] Department of Earth and Planetary Sciences, Harvard University, 20 Oxford Street, Cambridge MA 02138, USA

[c] School of Earth and Ocean Sciences, University of Victoria, PO Box 1700, Victoria, BC V8W 2Y2, Canada

[d] Earth Dynamics Research Group, The Institute for Geoscience Research (TIGeR), Department of Applied Geology, Curtin University, GPO Box U1987, WA 6845, Australia

[e] Geological Survey of Canada, 601 Booth Street, Ottawa ON, K1S 0E8, Canada

---

[1] Chapter 2 published in Gong, Z., Xu, X., Evans, D. A. D., Hoffman, P. F., Mitchell, R. N., & Bleeker, W. (2018). Paleomagnetism and rock magnetism of the ca. 1.87 Ga Pearson Formation, Northwest Territories, Canada: A test of vertical-axis rotation within the Great Slave basin. *Precambrian Research*, v. 305, pp. 295-309.

Abstract

A geometrically quantitative plate-kinematic model, based on paleomagnetism, for the initial assembly of Laurentia has taken form in the past few decades. Within this framework, there remains but one problematic interval of data predominantly from the Slave craton, which is the 1.96-1.87 Ga Coronation apparent polar wander path (APWP). The Coronation APWP shows large (~110°) back-and-forth oscillations that are difficult to explain in terms of plate motion. Nonetheless, poles from the Coronation APWP have been incorporated in various paleogeographic reconstructions of Laurentia and the supercontinent Nuna, pointing to the importance of testing its veracity. In this study, we conducted a detailed paleomagnetic and rock magnetic study of the ca. 1.87 Ga Pearson Formation, East Arm of Great Slave Lake, Northwest Territories, Canada. Our results show that Pearson Formation yields a characteristic remanent magnetization carried by single-domain or small pseudo-single-domain magnetite. The age of the magnetization is constrained to be older than Paleoproterozoic deformation and is interpreted as primary. Paleomagnetic declinations reveal a one-to-one correlation with local structural attitudes, indicating that some small blocks in the fold belt likely experienced significant (~60°) vertical-axis rotations, presumably related to large dextral displacements along the McDonald Fault system. Alternative explanations, such as true polar wander or a non-dipole magnetic field, are considered less parsimonious for the data presented here. It is suspected that some existing Christie Bay Group poles (the Stark and Tochatwi Formations), which were sampled in areas with anomalous structural attitudes and differ from time-equivalent poles obtained from areas of Slave craton far from major transcurrent faults, may similarly suffer

from vertical-axis rotation. We suggest further study before using possibly rotated Christie Bay Group poles for paleogeographic reconstructions.

1. Introduction

Laurentia owes its existence to the amalgamation of six Archean cratons in early Proterozoic time (2.0-1.7 Ga; Hoffman, 1988a, 2014). The pre- and syn-collisional kinematic histories of these cratons are crucial for testing the current reconstruction models of Laurentia, and in a larger perspective, the assembly of the supercontinent Nuna. Apparent polar wander paths (APWPs) of these Archean cratons have been constructed and compared in an attempt to quantify changes of their relative orientations and positions during the amalgamation (Mitchell et al., 2014; Buchan et al., 2016; Kilian et al., 2017), but controversies remain owing to the sparsity of well-defined paleomagnetic poles.

The Slave craton, one of the key components of Laurentia, plays an important role in the amalgamation of Laurentia by its collision with the Rae craton at 1.97 Ga and the Hottah terrane at 1.88 Ga (Fig. 1a; Hoffman, 1988a, 2014; Bowring and Grotzinger, 1992). The APWP of the Slave craton in the critical 1.96-1.87 Ga interval was constructed mainly based on studies in the 1970's, and was interpreted as a long loop, termed the "Coronation loop" (McGlynn and Irving, 1978). Since then, more paleomagnetic poles of 1.96-1.87 Ga age have been obtained, which collectively show a series of back-and-forth oscillations along a large arc (>110°; Fig. 2, Table 1). In this work, we use Coronation APWP to refer to the oscillatory paleomagnetic poles of the Slave craton at 1.96-1.87 Ga. If the Coronation

APWP represents the actual paleogeographic evolution of the Slave craton in Paleoproterozoic time, then the implied motions are unusual in their oscillatory style.

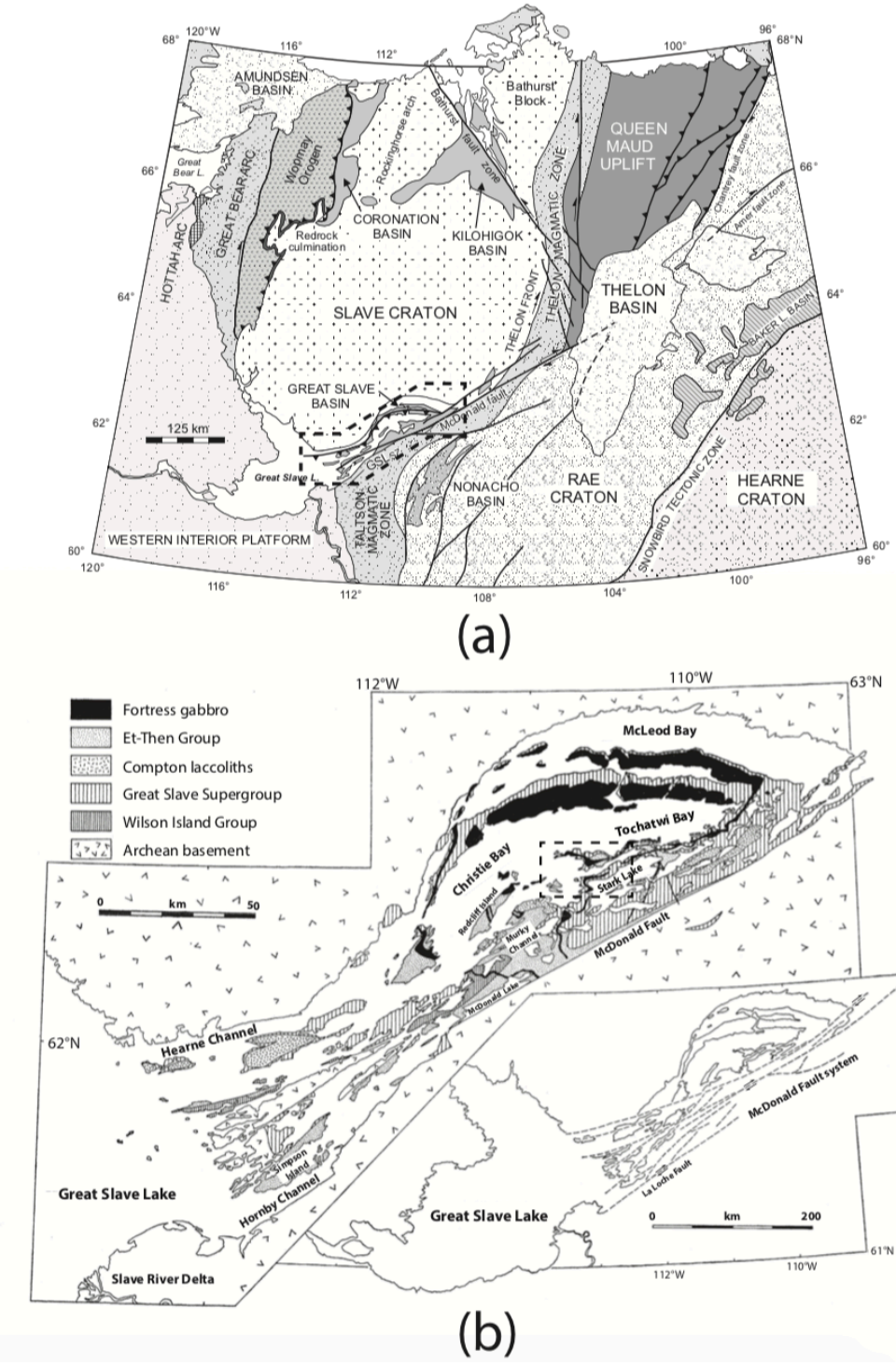

Figure 1 (a) Tectonic map of the Slave craton and environs (Hoffman, 1989; Helmstaedt, 2009). Dashed box indicates the area depicted in Fig. 1b. (b) Geologic map of the East Arm of Great Slave Lake (Hoffman, 1973). Dashed box indicates the area shown in Fig. 5.

Hypotheses other than plate motion have been invoked to explain the Coronation APWP. One hypothesis attributes the Coronation APWP to local vertical-axis rotation of the sampling areas, which was initially proposed by Bingham and Evans (1976) and then further developed by Irving et al. (2004). They suspected that some sampling areas in the Great Slave and Kilohigok basins may have experienced vertical-axis rotations due to the shearing produced by the conjugate McDonald and Bathurst Fault systems, respectively, as commonly observed in strike-slip tectonic settings (e.g., Kamerling and Luyendyk, 1979; Hornafius et al., 1986). Therefore, the Coronation APWP could be a result of these local rotations (Irving et al., 2004). Mitchell et al. (2010) applied trans-cratonic structural corrections on individual Coronation poles and argued that these poles were affected by at most minor amounts (~12°) of vertical-axis rotation. Instead, Mitchell et al. (2010) suggested that the majority of variance among Coronation poles could result from true polar wander, whereby the entire solid Earth rotates with respect to its spin axis in order to adjust to the evolving mantle mass heterogeneities.

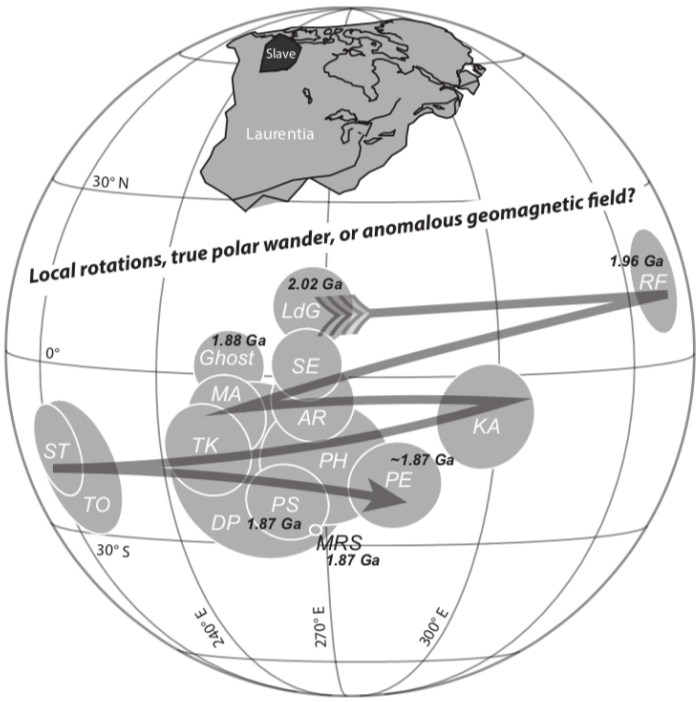

Figure 2 Stereographic projection of the Coronation APWP. Paleomagnetic poles are summarized in Table 1. In ascending stratigraphic order: LdG, Lac de Gras dykes; RF, Rifle Formation; Ghost, Ghost dykes; MA, Mara Formation; AR, Akaitcho River Formation; SE, Seton Formation; PH, Peacock Hills Formation; KA, Kahochella Group; DP, Douglas Peninsular Formation; ST, Stark Formation; TO, Tochatwi Formation; TK, Takiyuak Formation; PS, Peninsular sill; MRS, Mara River sills; PE, Pearson Formation.

Definitively testing the vertical-axis rotation hypothesis for the Coronation APWP requires adequate consideration of structural complexities on local scales and on a case-by-case basis. We approach this test by conducting a detailed paleomagnetic and rock magnetic study of the ca. 1.87 Ga Pearson Formation (basalt) in the Great Slave basin, East Arm of Great Slave Lake, Northwest Territories, Canada. We sampled the basal Pearson Formation from areas with different structural attitudes, where the Pearson basalts conformably

overlie the Portage Inlet Formation (evaporitic siltstone). Therefore, Pearson samples from different areas should be broadly similar in age because of their comparable stratigraphic levels within a lateral distance of ~20 km. If the local structural anomalies do result from rotations within the right-lateral McDonald Fault system, the paleomagnetic directions gleaned from these areas should display clockwise rotations in paleomagnetic declination.

2. Geologic setting and sampling

Early Proterozoic supracrustal rocks in the Slave craton are mainly preserved in three basins: the Coronation basin in the northwest, the Kilohigok basin in the northeast, and the Great Slave basin in the south (Fig. 1a; Hoffman, 1973). The Great Slave Supergroup is more than 12-km thick and consists of weakly metamorphosed sedimentary and volcanic rocks. It represents the depositional history of the Great Slave basin at 2.1-1.8 Ga, and is subdivided into five stratigraphic units; from lowermost to uppermost these are the Union Island, Sosan, Kahochella, Pethei and Christie Bay Groups (Stockwell, 1936; Hoffman, 1968). The regional structure of the Great Slave basin is dominated by a doubly-plunging, NNE-trending synclinorium centered on Christie Bay. The synclinorium contains a system of NW-directed, thin- and thick-skinned thrust sheets (nappes) of large displacement. The southern limb of the synclinorium exposes the entire thrust stack, while only the Christie Bay Group is allochthonous on the northern limb due to a frontal thrust ramp. Thrusting predated emplacement of the Compton Intrusive Suite (Hoffman et al., 1977; Hoffman, 1988b), a chain of laccoliths of intermediate composition extending nearly the entire length of the basin (Fig. 1b). The laccoliths are folded within the regional synclinorium, but thrusting and folding were both likely close in age to that of laccolith emplacement, which

is best estimated as 1868.46 ± 0.76 Ma based on a preliminary restudy of sample VS 79-10 (Bowring et al., 1984) by S. A. Bowring (pers. comm., 2013). The southern limb of the synclinorium, including the thrust system and the Compton laccoliths, are cut by a parallel system of brittle right-slip vertical faults, the McDonald Fault system (Fig. 1). The fault system accommodates an estimated 65-80 km of right-lateral slip (Thomas et al., 1976; Hoffman et al., 1977; Hoffman, 1981) and has a sinistral conjugate counterpart in the NW-trending Bathurst Fault system (Gibb, 1978; Fig. 1). On a more local scale, the McDonald Fault system is segmented, and the two most prominent segments, the Laloche and McDonald Faults, have a left-stepping relationship (Fig. 1b). Many right-slip (i.e., dextral strike-slip) fault systems have right-stepping segments that are linked by transtensional ("pull-apart") basins (Fig. 3a), aptly named "rhombochasms" by Carey (1958). The left-stepping Laloche-McDonald fault segments are linked by transfer faults that have oblique reverse-slip (Fig. 3b). Upthrusted basement blocks (e.g., Simpson Islands-Hornby Channel area, Fig. 1b) are flanked by steeply dipping footwall monoclines of Paleoproterozoic sedimentary strata, creating a "positive flower structure" as observed in Cenozoic transpression zones (Lowell, 1972; Wilcox et al., 1973). The difference in structural behavior, one producing a sediment sink and the other a sediment source, relates to the stress field around the fault tip. The left side of a dextral fault tip is in compression, while the right side of the fault tip is in tension (Segall and Pollard, 1980).

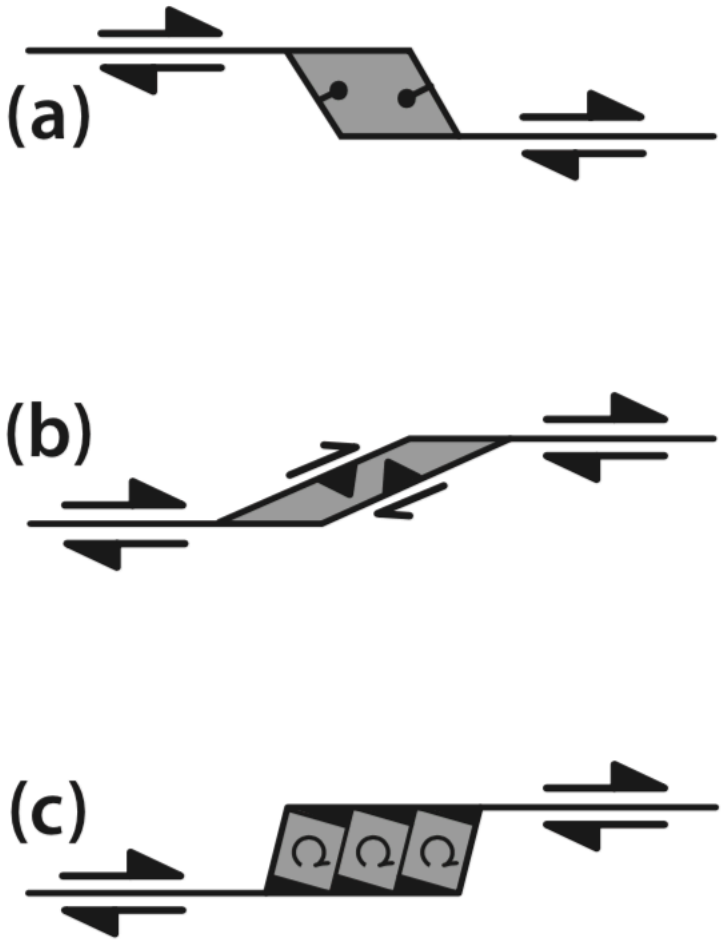

Figure 3 Styles of structural linkage in segmented dextral strike-slip faults. (a) Right-stepping right-slip faults linked by a pull-apart basin (shaded) or rhombochasm (Carey, 1958; Segall and Pollard, 1980). Ornaments identify the hanging-walls of normal faults. (b) Left-stepping right-slip faults linked by a positive flower structure (shaded; Wilcox et al., 1973). Barbs identify the hanging-walls of oblique reverse faults. (c) Left-stepping right-slip faults linked by a zone of rotated crustal blocks (Kim et al., 2004). Both the blocks

(shaded) and their bounding antithetic left-slip faults have rotated clockwise. Block rotation may be augmented by simple-shear rotation of strain axes within the transfer zone as a whole. In addition, individual block rotations will not be quantitatively self-limiting if the blocks become rounded through wear, potentially accounting for rotations > 15°.

Some left-stepping dextral fault systems (Fig. 3c) have overlapping fault segments linked by zones where small blocks have been rotated clockwise, along with their bounding antithetic left-slip faults (Kim et al., 2004). The strain field between the fault segments is similar to that of "flower structures", but limited exclusively to the horizontal plane. One of the best-documented cases of clockwise rotation in such a setting is the Transverse Ranges left-step on the San Andreas Fault in southern California (Hornafius et al., 1986).

Oblique "*en echelon* folds" (Wilcox et al., 1973) of northeasterly trend and gentle plunge are widely observed along the McDonald Fault system. They are most easily observed in the Et-Then Group, an assemblage of syn-kinematic alluvial fanglomerate and sandstone (Stockwell, 1932; Hoffman, 1969; Ritts and Grotzinger, 1994), which unconformably overlies the Great Slave Supergroup and postdates thrusting, laccolith emplacement and folding of the regional syncline. These *en echelon* folds manifest a resolved component of dextral transpression in the fault system, consistent with its wholescale rotation (see text below). The plunging folds create the structural relief that exposes the architecture of the thrust stack, and controls its expression on a geological map (Hoffman, 1988b).

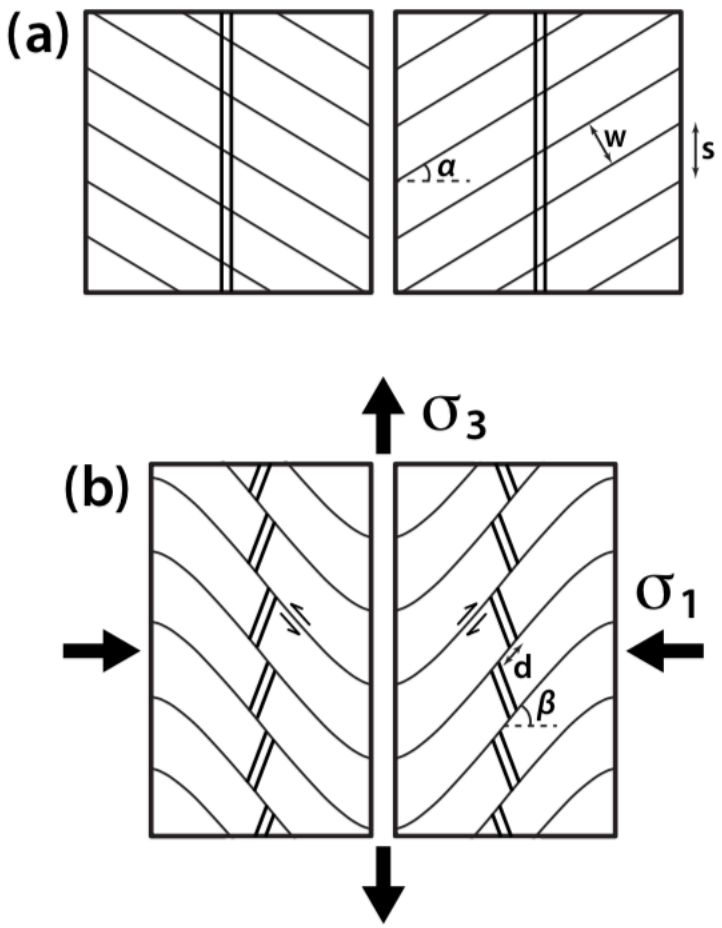

$$s = \frac{w}{\cos \alpha}, \quad \frac{d}{s} = \frac{\sin(\beta - \alpha)}{\cos \beta}, \quad \frac{d}{w} = \frac{\sin(\beta - \alpha)}{\cos \alpha \cdot \cos \beta}$$

(1) (2) (3)

Figure 4 Kinematics of conjugate transcurrent faulting (modified after Freund, 1970, 1974). Sinistral (left) and dextral (right) fault domains. (a) Initial condition showing faults (solid lines) with failure angles (α) ~30° relative to the direction of maximum compressive stress (σ_1). Spacing between faults (s) defines fault-block width (w). Passive marker indicated by double line. (b) Condition after 15% shortening. Strain is accommodated by

strike-slip displacement (d), proportional to the width and degree of rotation (β - α) of the fault-blocks toward the stretching direction (σ_3) (equations 2 and 3). Note clockwise and counterclockwise rotations of the passive marker (double lines) in sinistral and dextral fault domains, respectively. Fault-block curvature is just one possible means of accommodating loss of displacement toward the fault tips. Splay faulting (not shown) is another.

The conjugate McDonald and Bathurst Fault systems are kinematically homologous with a pervasive system of smaller-scale conjugate transcurrent faults in the Wopmay orogen (Cook, 2011; Hildebrand, 2011). The conjugate fault system in the Wopmay orogen postdates the youngest plutons of the Great Bear magmatic arc (Fig. 1a), which are dated around 1.84 Ga (Bowring, 1985; Hildebrand et al., 2010), and predates the 1.74 Ga Cleaver dykes (Hildebrand, 1985; Irving et al., 2004). The conjugate system accommodated east-west shortening by north-south lengthening (Fig. 4), implying the existence of a free face (active subduction zone) to the north or south. The strain is attributed to terminal collision in the Wopmay orogen (Hoffman, 1980; Hildebrand et al., 1987; Cook, 2011). Structural homology and permissive chronology underlie the conjecture (Hoffman, 1980, 1988b) that conjugate transcurrent faulting in the Wopmay orogen is cogenetic with the Bathurst-McDonald Fault systems far to the east. This conjecture remains untested because the age of the Bathurst and McDonald Fault displacements are too weakly constrained.

Conjugate transcurrent fault systems (Fig. 4) have been analyzed in analog models and Cenozoic examples (Cloos, 1955; Freund, 1970, 1974). Regional bulk strain is

accommodated on brittle faults by fault-block rotations (Fig. 4b). Conjugate faults have original failure angles ~30° with respect to the maximum shortening direction (σ_1), which is close to east-west in the Wopmay and Bathurst-McDonald examples. Those faults rotated toward the stretching direction (north-south, σ_3) as strain accumulated: dextral faults rotated counterclockwise and sinistral faults clockwise (Fig. 4b). In the foreland of the Wopmay orogen, Calderian folds and thrusts that predate strike-slip faulting (equivalent to the double lines in Fig. 4) trend north-south in areas where strike-slip faults are absent. These same structures were rotated clockwise or counterclockwise equivalently in domains where strike-slip faulting occurs (Hoffman, 1994). This demonstrates a regional pure shear (irrotational strain) regime (Fig. 4b), despite a strong prevalence in Wopmay orogen of dextral over sinistral fault domains.

The angle between the Bathurst and Macdonald Fault trends is close to 84°, implying that this angle widened by ~24° assuming initial failure angles of ~30° for each fault. This implies that the fault systems have each rotated by an average of 12°, the Bathurst in a clockwise direction and the McDonald counterclockwise (Mitchell et al., 2010). Such rotations apply to the fault systems as a whole. They do not necessarily describe rotations of small blocks within the fault zones (Fig. 3c; Kim et al., 2004), except in the case of the Wopmay orogen where the conjugate fault kinematics appear to be self-similar at all scales (Tirrul, 1992; Hoffman, 1994). As the Bathurst and McDonald Faults rotated toward the σ_3 (north-south) direction, the normal-stress component on the fault planes increased (Fig. 4b). This resulted in the development of transpressional structures such as *en echelon* folds (Wilcox et al., 1973). It also limited the amount of rotation that could be achieved, because

block rotation renders the fault planes progressively less favorable for strike-slip displacement (Freund, 1970, 1974).

The Pearson Formation is the uppermost member of the Christie Bay Group (Fig. 5), and experienced the early phases of deformation as described above. It is characterized by basalt flows and occurs stratigraphically between the conformably underlying Portage Inlet Formation (Christie Bay Group) and the unconformably overlying Et-Then Group. Columnar joints and (rarely) pillow structures have been observed in the field (Stockwell, 1932; Barnes, 1951). The Pearson Formation is provisionally correlated with the 1871 ± 1 Ma Peninsular sill in the Coronation basin (M. Hamilton in Buchan et al., 2010) and the 1870 ± 1 Ma Mara River sills in the Kilohigok basin (Davis et al., 2004). Such a correlation would imply that the Pearson lavas are a few million years older than the Compton laccoliths, a reasonable supposition but untestable as the two are nowhere in contact. The Pearson Formation is limited in preservation to the central part of the Christie Bay syncline (Fig. 5), where it reaches a maximum thickness of 168 m (Barnes, 1953). The lavas are amygdaloidal or vesicular; plagioclase (albite) is saussuritized and pyroxene is replaced by actinolite or chlorite (McGlynn and Irving, 1978). Opaque minerals in the basalts are dominated by magnetite, with minor amounts of maghemite and pyrite. The maximum burial temperature of the Pearson Formation is about 250-350°C, which is inferred from prehnite-pumpellyite facies metamorphism (McGlynn and Irving, 1978).

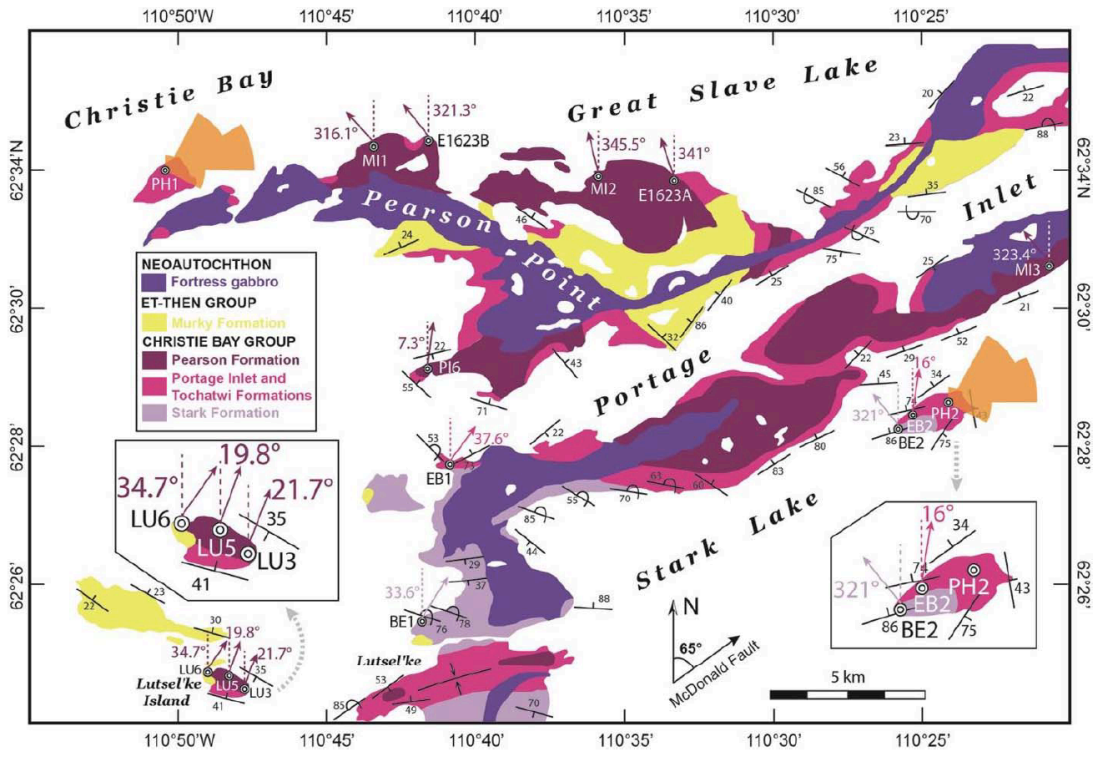

Figure 5 Geologic map of part of the East Arm of Great Slave Lake (modified after Hoffman, 1988b). Inset table is the stratigraphic column. Bedding strikes are shown with numbers indicating the degree of tilting (dip > 20° only). Pearson Point strata are shallowly dipping. Arrows are paleomagnetic remanence declinations after tilt-correction from: the Pearson Formation (sites LU3, LU5, LU6, PI6, E1623A, and E1623B are from this study and sections MI1, MI2, MI3 are from McGlynn and Irving, 1978), the Stark Formation (section BE1 and site BE2 of Bingham and Evans, 1976), and the Tochatwi Formation (section EB1 and site EB2 from Evans and Bingham, 1976). Section declinations represent averages of several sites. Rose diagrams are paleocurrent azimuths of the Tochatwi Formation (sections PH1 and PH2 from Hoffman, 1969). Black arrow shows the dominant trending direction of the McDonald Fault system.

Previous paleomagnetic study of the Pearson Formation includes samples collected from Pearson Point and northern shoreline of the Stark Lake (sections MI1, MI2, MI3 in Fig. 5), where the Pearson Formation is gently folded (dip < 20°) about NE-trending axes, consistent with the large-scale structure of the Great Slave basin (McGlynn and Irving, 1978). However, no information regarding the stratigraphic positions of those previous samples is available. For comparison with the results of McGlynn and Irving (1978), we sampled two sites at northern Pearson Point (E1623A and E1623B; Fig. 5) from the basal Pearson Formation in direct contact with the underlying Portage Inlet Formation.

To test the vertical-axis rotation hypothesis for published paleomagnetic data from the Christie Bay Group, we sampled the basal Pearson Formation in areas where the structures deviate from the typical NE trend. One site (PI6) is at the mouth of Portage Inlet and three sites (LU3, LU5, LU6) are on Lutsel'ke Island (Fig. 5). Lutsel'ke Island samples were collected from opposing limbs of a syncline for paleomagnetic fold test. Paleomagnetic samples were oriented in the field using a Brunton compass and were further checked with a sun compass whenever possible. Measured magnetic deviations (~17°E) were found to be consistent with those calculated from the International Geomagnetic Reference Field (IGRF) model. Oriented samples were trimmed to a uniform size (2.5 cm in diameter, 1.2 cm in length) for laboratory measurements. Rock chips were prepared for rock magnetic analyses.

3. Magnetic measurements

Rock magnetism was studied on representative Pearson samples from each site. In order to identify magnetic mineralogy by Curie/Néel temperature, the bulk magnetic susceptibility was measured during both heating and cooling between 25°C and 700°C in an argon gas environment with an AGICO Kappabridge KLY-4S susceptibility meter and a CS3 high temperature furnace apparatus. Additionally, magnetic parameters, including coercivity (Hc), coercivity of remanence (Hcr), saturation magnetization (Ms) and saturation remanence (Mr), were determined by hysteresis loop measurements, which were acquired from -0.5 T to 0.5 T at steps of 4 mT using a Princeton Measurements Corporation MicroMag 2900 alternating gradient magnetometer (AGM) at the Yale University Archaeomagnetism Laboratory. Paramagnetic slope correction was applied for all hysteresis loops.

Demagnetization of the Pearson samples was conducted in a magnetostatically-shielded room (ambient field intensity < 300 nT) at the Yale University Paleomagnetism Laboratory. After the measurement of natural remanent magnetization (NRM), samples were submerged in liquid nitrogen (~77 K) in a shielded cylinder for ≥ 30 minutes in order to remove the remanence carried by larger magnetic grains, following Muxworthy and McClelland (2000). Then samples were thermally demagnetized, progressively from 100°C to 580°C in about 20 steps in a nitrogen gas environment using an ASC Scientific TD-48 thermal demagnetizer. Remanences were measured by a 2G Enterprises DC-SQUID magnetometer with an automated sampling-changing vacuum system (Kirschvink et al., 2008). Paleomagnetic data were plotted using vector-endpoint diagrams (Zijderveld, 1967) in PaleoMag X (Jones, 2002). Principal component analysis (PCA) was used to

determine the remanence components of each sample (Kirschvink, 1980). Fisher statistics were used to calculate mean paleomagnetic directions in Stereonet (Cardozo and Allmendinger, 2013). Paleomagnetic poles were calculated following Butler (1992) and were plotted in GPlates (Boyden et al., 2011).

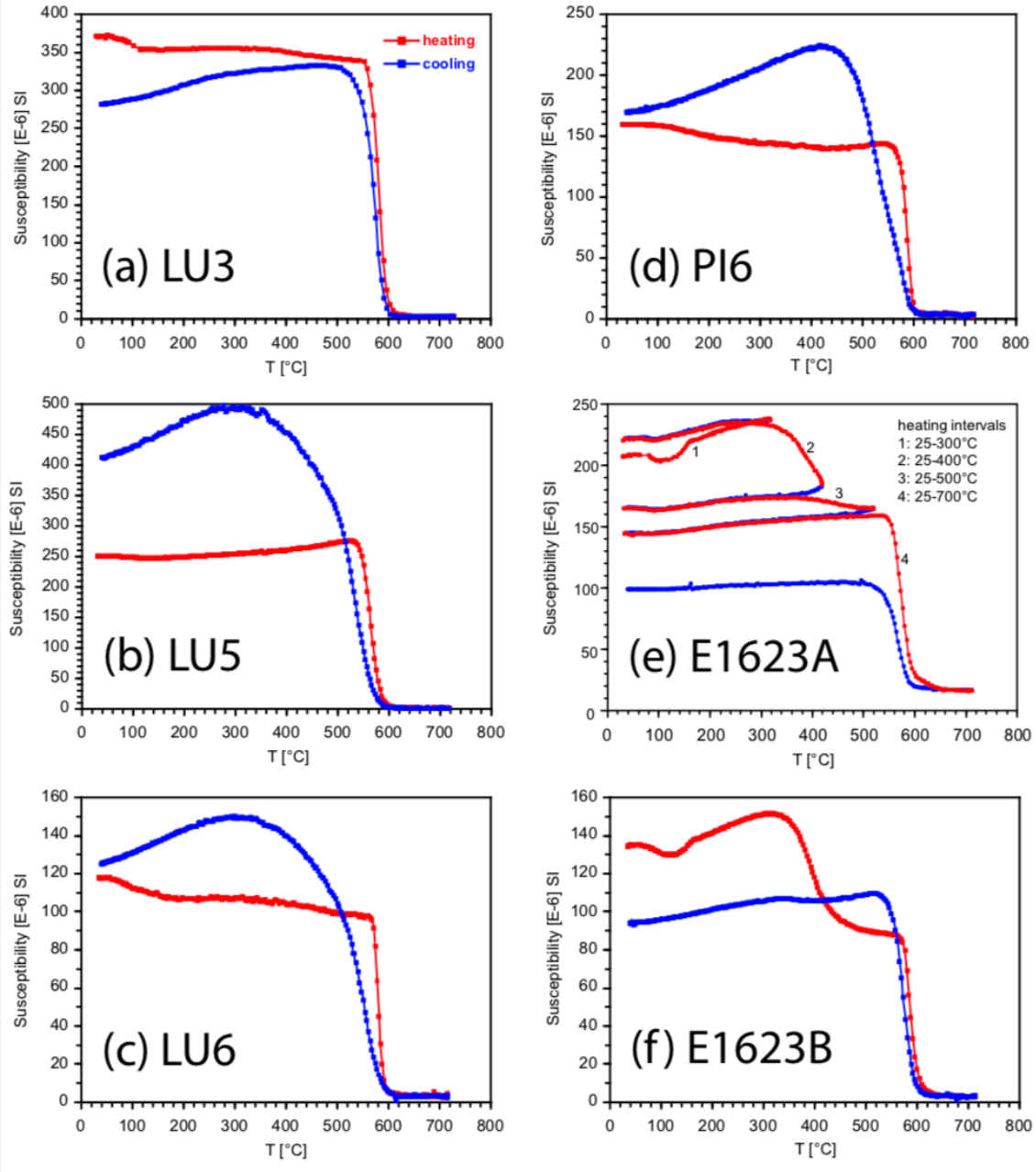

Figure 6 Thermomagnetic susceptibility experiment of the Pearson Formation. Red and blue lines represent heating and cooling curves, respectively.

4. Results

4.1 Magnetic mineralogy

Thermomagnetic susceptibility curves of representative Pearson samples from all six sites are characterized by abrupt loss of bulk magnetic susceptibility at 580-590°C during heating (Fig. 6), supporting the presence of magnetite (Curie temperature 585°C). Most thermomagnetic susceptibility curves are not reversible. The difference between heating and cooling curves is possibly due to magnetic phase transitions that occurred during thermal treatments, although the argon gas environment should have subdued chemical reactions. Different from other sites, Pearson Point samples (sites E1623A and E1623B) show three distinct susceptibility reductions at ~100°C, ~350°C and ~580°C, which are close to the Curie/Néel temperatures of goethite, pyrrhotite and magnetite, respectively (Fig. 6e-f). The cooling curves of Pearson Point samples are much lower than the heating curves, indicating significant loss of ferromagnetic composition. In order to determine at what temperature did the magnetic phase transitions take place, we heated Pearson Point samples in multiple temperature intervals, specifically at 25-300°C, 25-400°C, 25-500°C and 25-700°C. The major decrease of magnetic susceptibility occurred at 300-400°C and 500-600°C, with a moderate loss at 400-500°C. However, the complicated pattern of magnetic mineralogical change was not observed in thermal demagnetization of any Pearson Point samples (Fig. 9e-f). Thus, it is safe to regard magnetite as the dominant carrier of remanence for all Pearson samples (see discussion below).

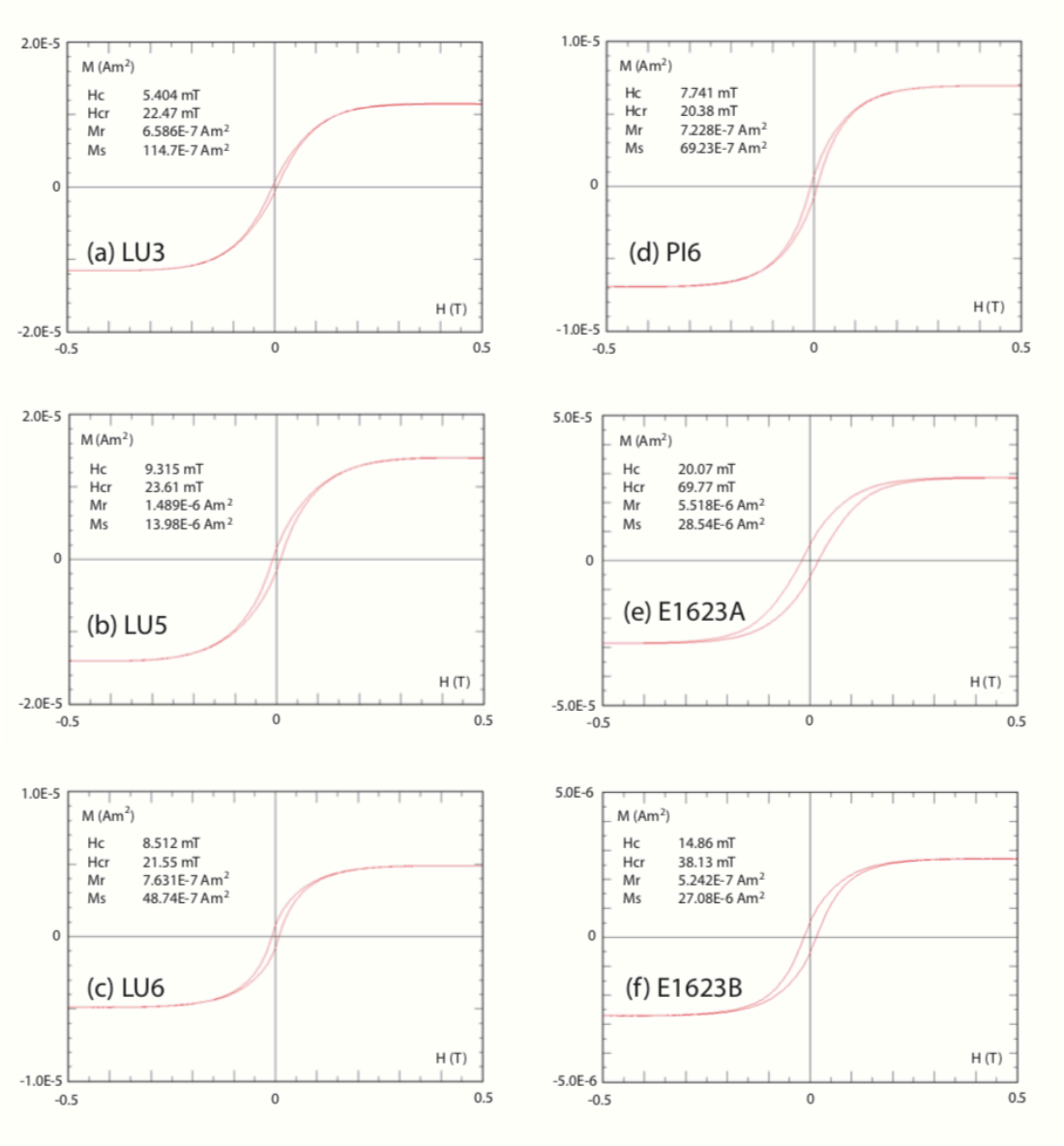

Figure 7 Hysteresis loops of the Pearson Formation after paramagnetic slope correction.

Hysteresis loops of the Pearson samples show that the magnetization is saturated between 0.2 T and 0.3 T, and the coercivity of remanence is less than 70 mT, with a typical value of 30 mT (Fig. 7). The Mr/Ms and Hcr/Hc ratios were plotted to study magnetic grain size distribution (Day et al., 1977). All Pearson samples fall into pseudo-single domain (PSD) range in the Day plot (Fig. 8). The morphology of the hysteresis loop also agrees with the

behavior of PSD grains (Tauxe, 1998). Based on the theoretical experiments of Dunlop (2002), the PSD signature results from the mixing of single domain (SD) and multidomain (MD) grains. Inferred from the Day plot, the Pearson samples contain about 20-40% of SD grains, except for site LU3, which has less (~10%) SD grain contribution (Fig. 8).

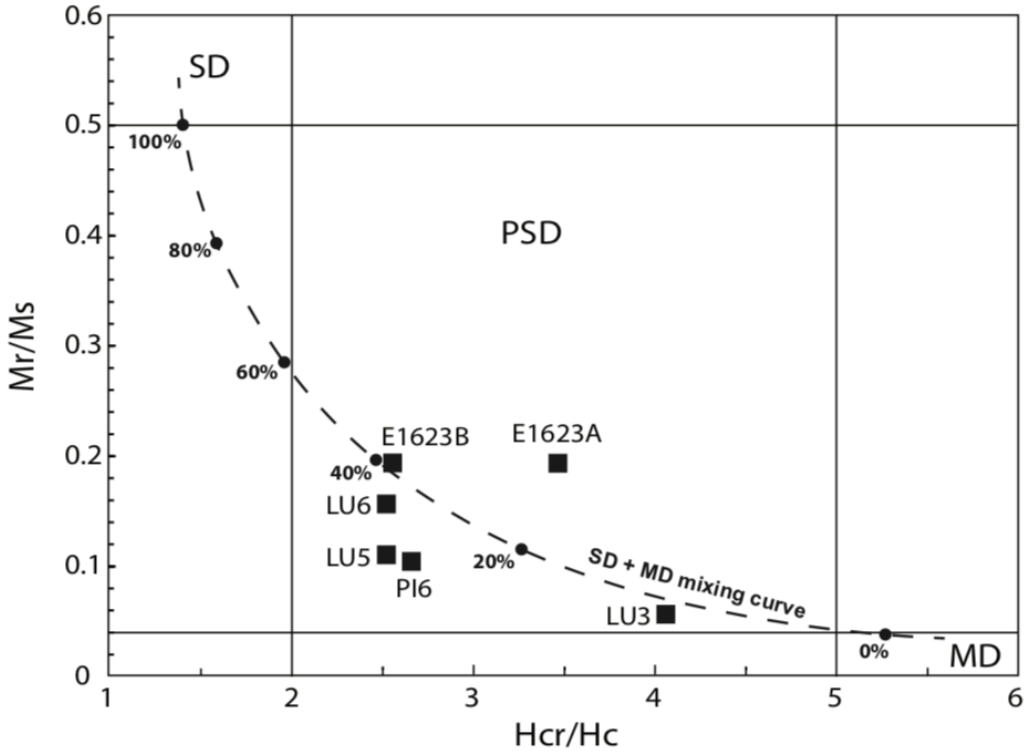

Figure 8 Day plot (Day et al., 1977) of the Pearson Formation. Dashed line represents the theoretical mixing curve for MD grains at different percentages (black dots) with SD magnetite (Dunlop, 2002). The SD, PSD, and MD regions are from Dunlop (2002).

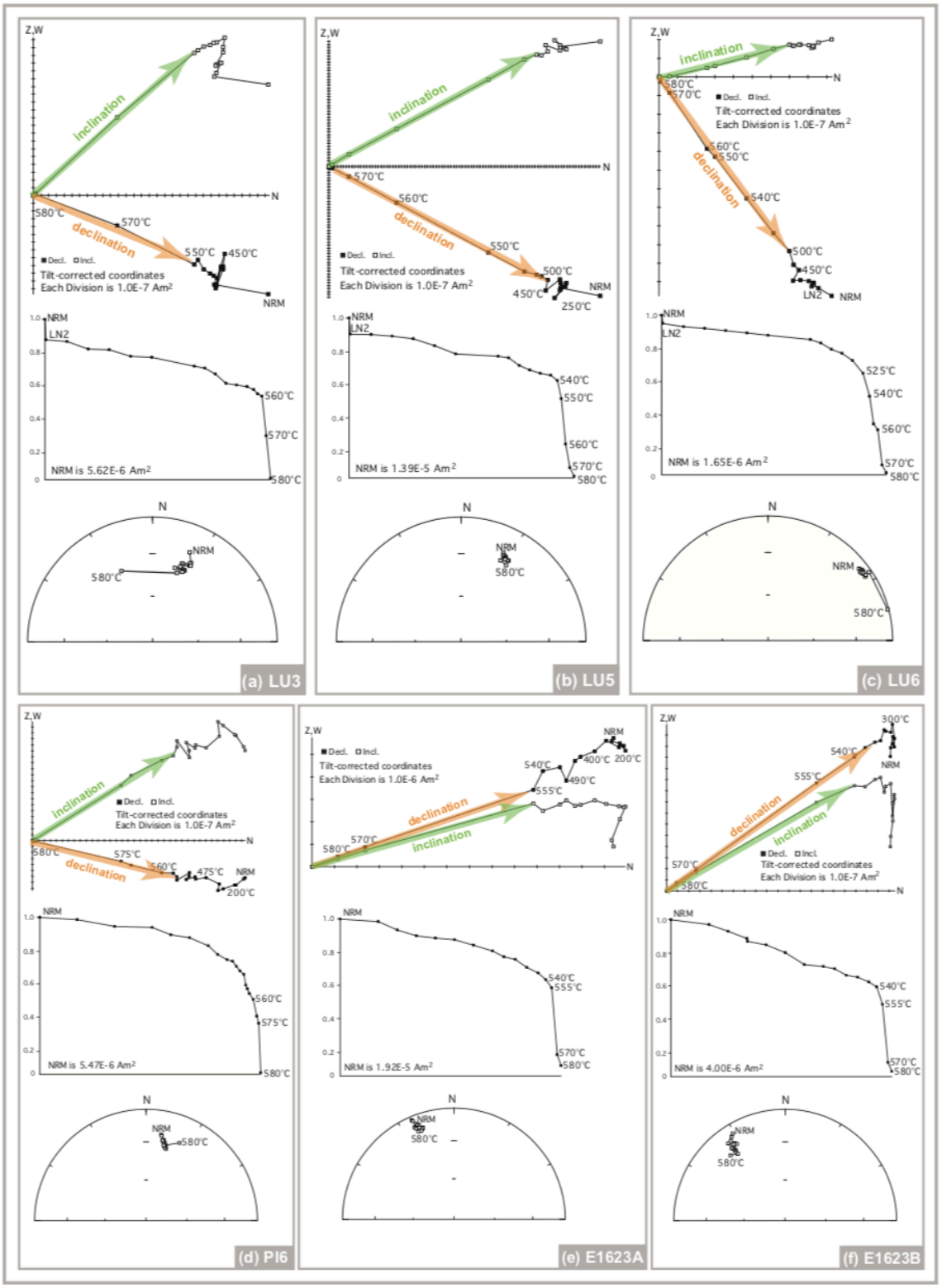

Figure 9 Representative thermal demagnetization of the Pearson Formation. Typical vector-endpoint diagrams (Zijderveld, 1967), remanence intensity (J/J_0) plots, and equal-

area stereonet plots are shown for each site. Vectors determined with least-squares analysis of magnetization components (Kirschvink, 1980) are plotted with orange and green arrows representing paleomagnetic declinations and inclinations, respectively.

4.2 Paleomagnetic results

Nearly all Pearson samples carry single magnetization components decaying towards the origin on vector-endpoint diagrams (Fig. 9), which are defined as their characteristic remanent magnetizations (ChRMs). The unblocking temperatures of the ChRMs are at 540-580°C, with square-shouldered pattern on thermal demagnetization curves (Fig. 9). Viscous overprints carried by multidomain grains were adequately removed by either liquid nitrogen bath or low temperature heating.

4.2.1 Lutsel'ke Island

Three sites (LU3, LU5, LU6 in Fig. 5) collected from the syncline on Lutsel'ke Island provide an opportunity for paleomagnetic fold test to determine the age of remanence acquisition (Fig. 10a). Before any tilt correction, site means are very distinct. ChRMs from sites LU3 and LU5 are directed upwards to the northeast and the ChRM from site LU6 is directed downwards to the south (Fig. 10b). A paleomagnetic fold test (Enkin, 2003) was performed, and the largest precision parameter (k) is achieved at 110-115% unfolding, indicating a better clustering after tilt correction (Fig. 10c-d). The in-situ and tilt-corrected site means and their corresponding virtual geomagnetic poles (VGPs) are shown in Figs. 10 and 12, respectively.

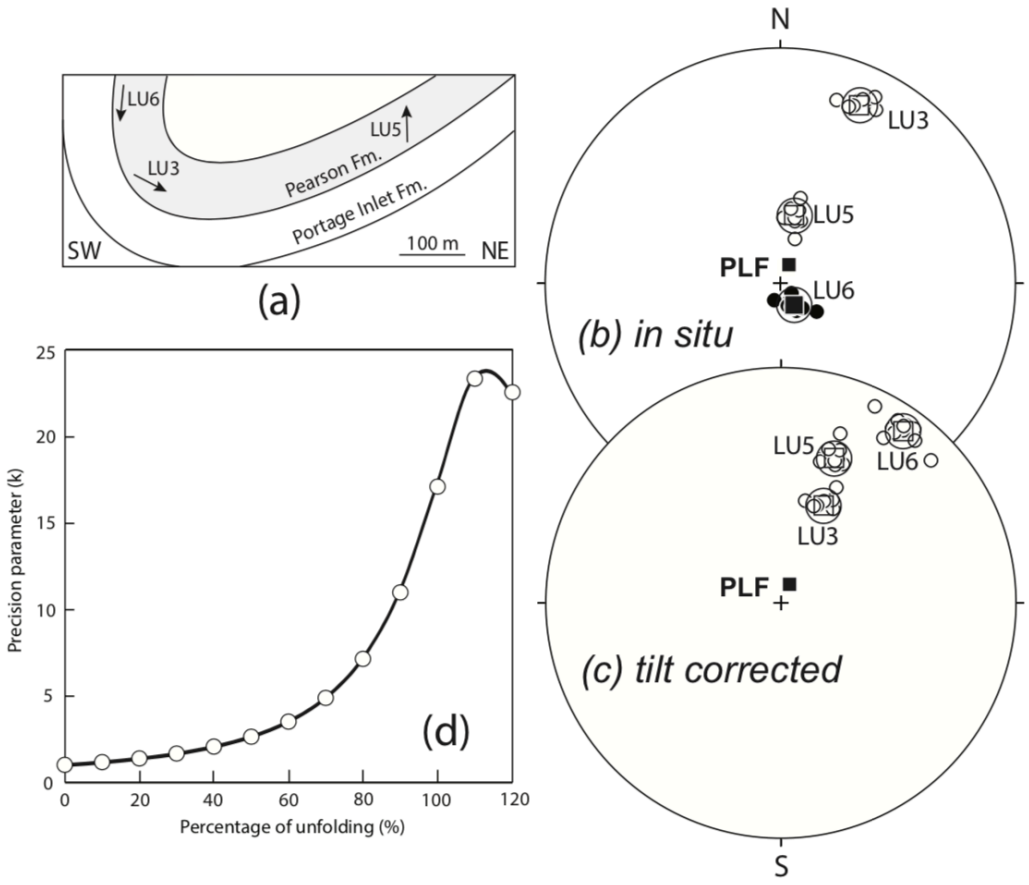

Figure 10 (a) Schematic illustration of the paleomagnetic fold test conducted on Lutsel'ke Island with site location and stratigraphic relations indicated. Black arrows show site-mean inclinations before tilt correction. Equal-area stereonets of site means (b) before tilt correction and (c) after 100% tilt correction. Mean directions are shown with 95% confidence cones. Open (filled) circles are in upper (lower) hemisphere. Present-local field (PLF) direction is represented by the square. (d) Stepwise unfolding (Enkin, 2003) shows that the maximum precision parameter (k) is achieved at 110-115% unfolding.

4.2.2 Mouth of Portage Inlet

Site PI6 (Fig. 5) was collected at the entrance to Portage Inlet, which gives an in-situ site mean of Dec_G = 11.1°, Inc_G = -26.7° (α_{95} = 10.3°, k = 35.7; Fig. 11a). The tilt-corrected

site mean is Dec_S = 7.3°, Inc_S = -25.1° (α_{95} = 10.3°, k = 35.7; Fig. 11b), and the corresponding VGP is located at 14.1°S, 242.0°E (A_{95} = 8.1°, Fig. 12).

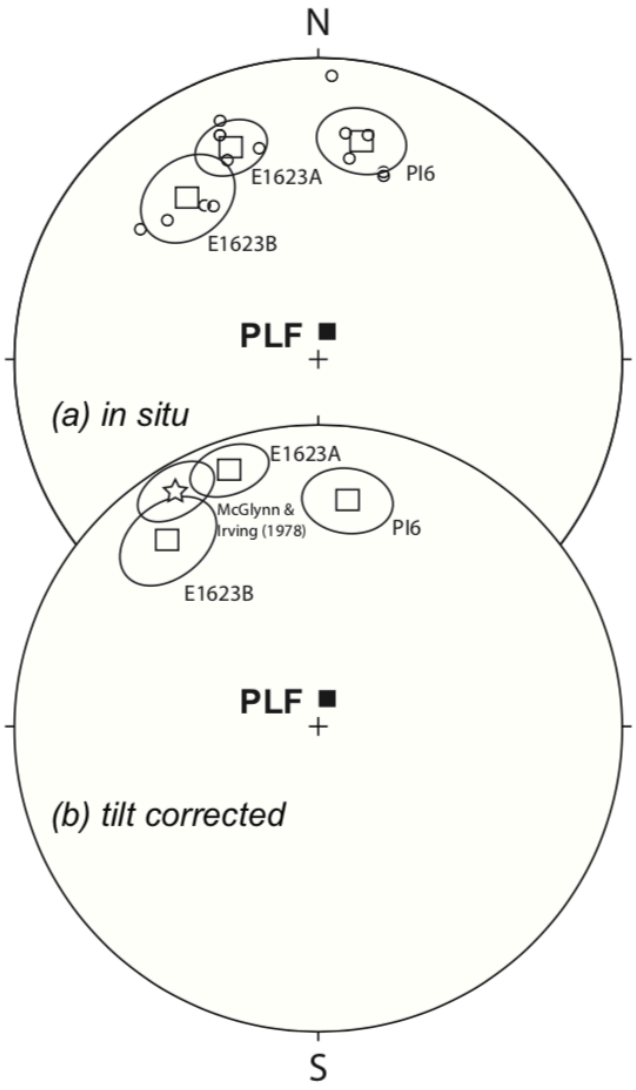

Figure 11 Equal-area stereonets of site means from two sites at Pearson Point and one site at the mouth of Portage Inlet (a) before tilt correction and (b) after tilt correction. Mean directions are shown with 95% confidence cones. Open circles are in upper hemisphere. Present-local field (PLF) direction is represented by the yellow square. Star represents the previous result of McGlynn and Irving (1978).

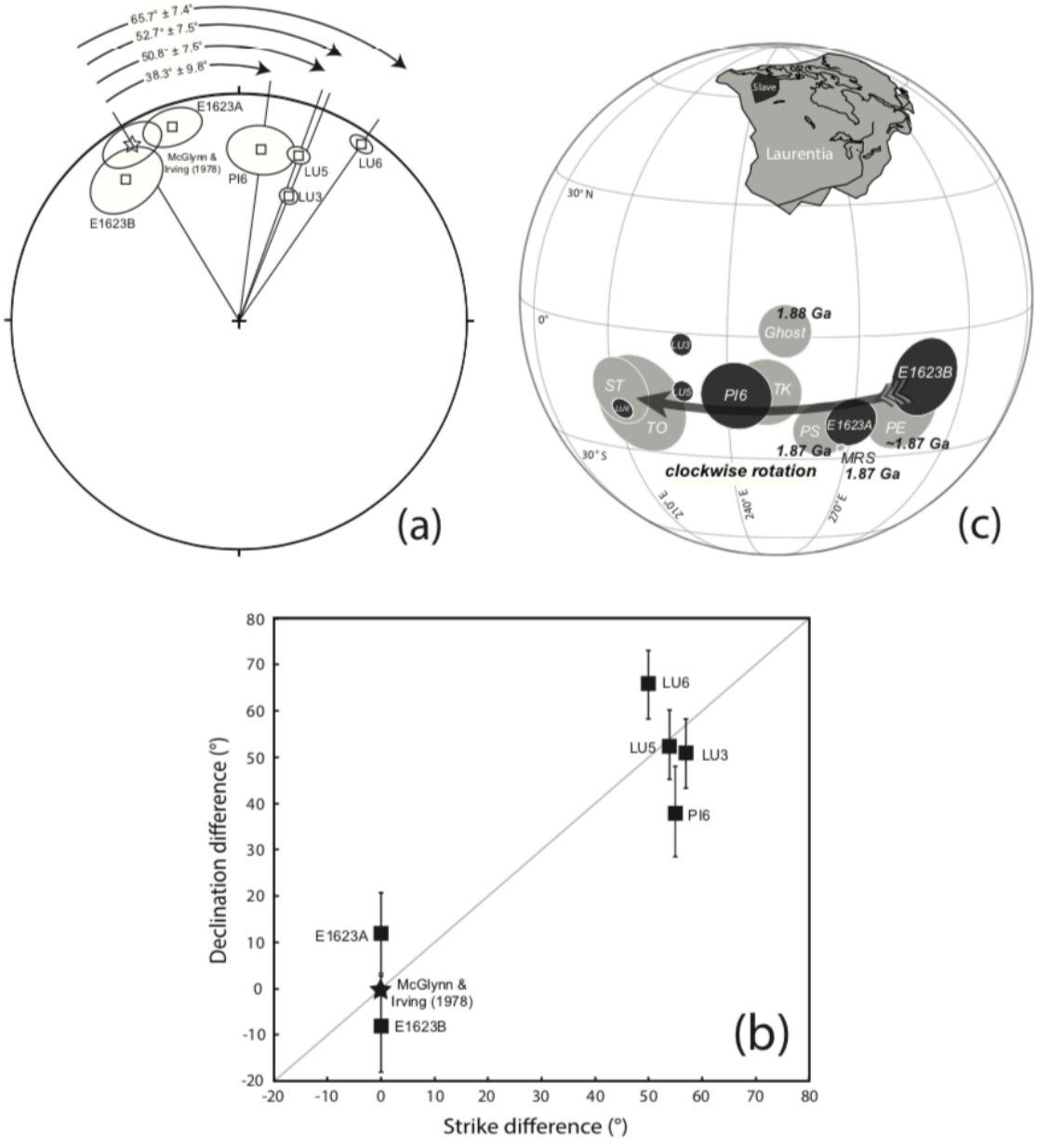

Figure 12 (a) Difference of the Pearson paleomagnetic declination between sites with respect to the result of McGlynn and Irving (1978) as a reference. Clockwise rotations and 95% confidence limits (R ± ΔR) are calculated following Butler (1992). (b) Paleomagnetic declination deviations are plotted against tectonic strike deviations. The reference declination used to calculate paleomagnetic deviations is that of McGlynn and Irving

(1978). The reference strike line used to calculate tectonic deviations is the average trend of the McDonald Fault. Grey line of unit slope is expected if declination deviation is entirely due to vertical-axis rotation. (c) Stereographic projection of Christie Bay Group and correlative paleomagnetic poles (abbreviations as in Figure 2), the 1885 Ma Ghost dyke pole (Buchan et al., 2016), and our new site-mean VGPs for the Pearson Formation. Arrow indicates the sense of inferred localized rotation of the Pearson Formation VGPs.

4.2.3 Pearson Point

Previous paleomagnetic study of the Pearson Formation was conducted at Pearson Point (sections MI1 and MI2 in Fig. 5), as well as areas on northern shoreline of Stark Lake (section MI3 in Fig. 5; McGlynn and Irving, 1978), which provides a tilt-corrected mean direction of Dec_S = 329°, Inc_S = -8° (α_{95} = 10°; Fig. 11b) and a corresponding paleomagnetic pole at 19°S, 283°E (A_{95} = 9°; Fig. 12). We collected another two sites (E1623A and E1623B) from the basal Pearson Formation at Pearson Point (Fig. 5), broadly the same area as McGlynn and Irving (1978). The site means of these two sites, after tilt correction, fall close to the 95% confidence cone of the previous mean direction (Fig. 11). The slight difference could be explained by paleosecular variation or the uncertainties generated in sampling and/or measurements.

All paleomagnetic results of the Pearson Formation are summarized in Table 2. It is noteworthy that the tilt-corrected site means of six sites show prominent differences in paleomagnetic declination, but not significant differences in paleomagnetic inclination. In

general, the declinations of Lutsel'ke Island and Portage Inlet samples are directed to the northeast, while declinations of Pearson Point samples are directed to the northwest.

5. Discussion

5.1 Remanence carrier and age of remanence acquisition

The dominant magnetic phase in Portage Inlet (PI6) and Lutsel'ke Island (LU3, LU5 and LU6) samples is magnetite, which is supported by the Curie temperature (580-590°C) determined in the thermomagnetic susceptibility experiments (Fig. 6a-d). In contrast, Pearson Point (E1623A and E1623B) samples may contain multiple magnetic phases since several different Curie/Néel temperatures have been identified on thermomagnetic susceptibility curves (Fig. 6e-f). Prominent decreases of bulk magnetic susceptibility at ~100°C, ~350°C and ~580°C on heating curves indicate the presence of goethite, pyrrhotite and magnetite, respectively. Previous mineralogical study of the Pearson samples shows the presence of maghemite and pyrite (McGlynn and Irving, 1978). Except for paramagnetic pyrite, other magnetic minerals are ferromagnetic and could be potential remanence carriers.

Results from thermal demagnetization show that all Pearson samples yield a single magnetization component that is defined as the ChRM. The unblocking temperature of the ChRMs of the Pearson samples is at 540-580°C, close to the Curie temperature of magnetite (Fig. 9). No other unblocking temperature was observed corresponding to the Curie/Néel temperatures determined in thermomagnetic susceptibility experiments. Hence,

it is important to point out that none of goethite, pyrrhotite or maghemite, if they exist, produce any significant contribution to the ChRMs of the Pearson samples.

The difference between the Curie temperature and the unblocking temperature of the magnetite in the Pearson samples likely originates from the grain size, instead of high titanium content. Larger grains, especially MD grains, have lower unblocking temperatures and yield less stability compared to SD grains (Butler, 1992). The presence of MD/PSD grains is indicated by the hysteresis loop patterns and the Day plot (Figs. 7 and 8), but the remanence contributed by MD grains should be adequately removed by liquid nitrogen bath or thermal demagnetization at low temperatures. Therefore, the ChRMs of Pearson samples are carried by SD or small PSD magnetite grains, of which the remanences have significant temporal stability.

The square-shouldered pattern exhibited at the unblocking temperature is observed in thermal demagnetization curves (Fig. 9), which suggests a thermoremanent magnetization. Additionally, there is no evidence for chemical remagnetization. Authigenic magnetite produced by chemical alterations normally shows a gradual decay of remanence intensity during thermal demagnetization. Influences of lightning (isothermal remanent magnetization) are also unlikely since the NRM intensities of Pearson samples are of typical values (10^{-5}-10^{-6} Am^2) for basalts. Besides, the overprint yielded by lightning would also show a gradual decrease in remanence intensity as temperature increases, so the square-shouldered pattern at high temperatures (nearly 580°C) should not be expected. The in-situ ChRMs of the Pearson samples are notably distinct from the present-local field (PLF)

direction (Figs. 10 and 11). The most likely tectonomagmatic events that may have had the potential to remagnetize the strata in the Great Slave basin is the Coronation (or more broadly, Trans-Hudson) orogenesis at ca. 1750 Ma and intrusion of the Mackenzie large igneous province at ca. 1270 Ma (Irving et al., 1972; Evans and Bingham, 1976; Evans et al., 1980; Reid et al., 1981). Neither of those well-defined directions is observed in the Pearson samples. Most importantly, the age of remanence acquisition is constrained by the fold test of Lutsel'ke Island samples. The site means of Lutsel'ke Island samples achieve best grouping at 110-115% unfolding, slightly over 100% (Fig. 10), which is perhaps attributable to paleosecular variation, unrecognized primary dips of the volcanic strata, uncertainties in bedding measurements (bedding of site LU6 was measured on glacial-polished surfaces of pillow basalts, which might be less accurate), or other possible minor sources of systematic error. Thus, the fold test is regarded as positive, confirming a pre-folding origin of the remanence. Since folding does not penetrate the overlying Et-Then Group (Barnes, 1951), with an age of ca. 1780 Ma estimated by stratigraphic correlation (Mitchell et al., 2010), the ChRM of the Pearson Formation was likely acquired during the initial cooling of the basalts and represents a primary thermoremanent magnetization.

5.2 Variations in the Pearson Formation magnetization directions

Tilt-corrected paleomagnetic results from the Pearson samples collected here yield several discordant directions, and correspondingly, several isolated VGPs (Fig. 12). We note that the discordance of the paleomagnetic directions is largely due to the differences in declination, with relatively small variations in inclination. To explain the discordant

paleomagnetic data, we first test the vertical-axis rotation hypothesis, and then discuss the plausibility of other possible explanations.

5.2.1 Vertical-axis rotation

Because the sense of the McDonald Fault is right-lateral (Fig. 1), localized vertical-axis rotations in the proximity to the fault are expected to be clockwise (Kim et al., 2004). In the Great Slave basin, the predominant structural trends are NNE to NE, parallel to the regional syncline and to the McDonald Fault system with varying degrees of obliquity (e.g., transfer faults, flower structures and *en echelon* folds). Northeastward-dipping strata are common in the Et-then Group (e.g., between McDonald Lake and Murky Channel, Fig. 1b), but dips are generally modest (<40°) as they relate to gently northeastward-plunging *en echelon* folds. Locally, however, steeply-dipping panels of the Pearson Formation and even tight upright folds strike northwest, at odds with regional structural trends. Two such areas are Lutsel'ke Island and the mouth of Portage Inlet (Fig. 5). If related to clockwise block rotation, the rotations would have to be large (~60°) to account for the aberrant structural trends.

To evaluate the vertical-axis block rotation hypothesis (Fig. 3c), a paleomagnetic reference direction is needed to calculate the declination difference between areas. We chose the previous remanence direction of McGlynn and Irving (1978) as a reference because of its relative tectonic stability, as well as its agreement with paleomagnetic results of presumably contemporaneous Peninsular sill (Irving and McGlynn, 1979) and Mara River sills (Evans and Hoye, 1981; Fig. 12) obtained from other regions of Slave craton. If

interpreted in this manner, declination anomalies of the Pearson paleomagnetic declinations show 38.3° ± 9.8° clockwise rotation of site PI6 at the mouth of Portage Inlet; and 52.7° ± 7.5°, 50.8° ± 7.5° and 65.7° ± 7.4° clockwise rotations of sites LU3, LU5 and LU6 on Lutsel'ke Island, respectively (Fig. 12a; Table 2). We compared the differences of the structural attitudes with the differences of the paleomagnetic declinations. The rotation of paleomagnetic declination as a function of bedding strike is illustrated in Fig. 12b. Within uncertainties, there is a direct one-to-one correlation between paleomagnetic declinations and deviations of local strike from the McDonald Fault. Hence, the Pearson data are consistent with significant, localized vertical-axis rotation of small blocks in the Great Slave basin.

5.2.2 True polar wander

Earth is a quasi-rigid, self-gravitating planet, which spins with respect to its maximum inertial axis (Gold, 1955). True polar wander (TPW) is excited due to changes in Earth's mass distribution. Studies show that TPW occurs at the velocity of < 1°/Myr (< 11 cm/yr) since late Cretaceous (e.g., Steinberger et al., 2017). But it is suggested that if the Earth's maximum and intermediate moments of inertia are nearly equal, inertial interchange can quickly take place due to the relative waxing and waning of two principal inertial axes (Evans, 1998). Inertial interchange true polar wander (IITPW) could produce rapid back-and-forth rotations of the entire solid Earth around the stable minimum inertial axis in order to realign the new maximum moment of inertia with the spin axis (Raub et al., 2007). The rate of any TPW event is controlled by the viscosity of the mantle, as the planet must deform through its rotational bulge (Tsai and Stevenson, 2007; Creveling et al., 2012; Rose

and Buffett, 2017). Geodynamic models show that, theoretically, the rate of TPW could be as fast as ~6° per Myr (Spada et al., 1992; Rose and Buffett, 2017). Mitchell et al. (2010) suggest that the Coronation APWP could be a product of multiple IITPW events when the Slave craton was located close to Earth's minimum inertial axis. However, fast, rate-limited IITPW appears not to be fast enough to explain the ~60° difference observed within broadly coeval Pearson VGPs. Even if we assume that IITPW were faster in Paleoproterozoic time due to a hotter and less viscous mantle (Tsai and Stevenson, 2007), at least ~3 Myr would be required to accommodate the ~60° difference. However, the maximum thickness of the Pearson basalt is only 168 m (Barnes, 1953) and the samples were collected at broadly similar stratigraphic levels within ~20 km lateral distance from each other. Thus, it is considered unlikely that the age difference between the Pearson VGPs is on the order of several million years. The Pearson sites collected here therefore do not support IITPW because the implausibly high rates of motion are implied.

5.2.3 Paleosecular variation or non-GAD field

Fast cooling of the Pearson basalts is suggested by pillow lavas and columnar joints observed in the field, implying that each of the Pearson VGPs records a snapshot of the ancient magnetic field. Secular variation of the geodynamo, seemingly stochastic change of both field direction and intensity on short time scales (1-100 kyr; Cox and Doell, 1964), is thus probably not adequately averaged-out at the site (VGP) level. Studies of the recent magnetic field show that paleosecular variation rarely exceeds 30° in direction (Verosub, 1988). Paleosecular variation is thus unlikely to be the cause of the ~60° difference in Pearson declinations. A time-averaged non-GAD field ca. 1.9 Ga is another potential

explanation for the Pearson data. In such a model, it can be hypothesized that during magnetic reversals, the dipole field could migrate away from the polar region and could shortly stabilize at a specific location before moving to the opposite polar region (Hoffman, 1991). This kind of non-GAD model has been used to interpret incompatible paleomagnetic directions observed in Laurentia, Baltica and Gondwana in Ediacaran time (Abrajevitch and Van der Voo, 2010, Halls et al., 2015). But it is important to point out that neither the non-GAD field nor the paleosecular variation hypotheses is expected to produce the one-to-one correlation between the declinations and bedding strikes of the Pearson samples.

5.3. Implications for the Coronation APWP

The new results from the Pearson Formation shed light on the Coronation APWP. It is noted that the paleomagnetic poles obtained from the Stark and Tochatwi Formations of the Christie Bay Group lie substantially west of the majority of the Coronation poles (Fig. 2). Furthermore, the paleomagnetic poles obtained from Lutsel'ke Island samples lie close to the Stark and Tochatwi poles (Fig. 12c), raising the question of whether blocks containing Stark and Tochatwi sites have undergone local clockwise rotations as well. Previous paleomagnetic studies of the Stark and Tochatwi Formations (Bingham and Evans, 1976; Evans and Bingham, 1976) sampled steeply-dipping (overturned) northeast-facing panels (sections BE1 and EB1 in Fig. 5; no folds in these panels) that are similar in structural attitude to Lutsel'ke Island and the mouth of Portage Inlet.

The Stark and Tochatwi Formations are stratigraphically correlated (Hoffman, 1969; Mitchell et al., 2010) with the Takiyuak Formation in the Coronation basin, where an age

of 1882.5 ± 1 Ma on a tuff from the underlying Fontano Formation (Bowring and Grotzinger, 1992) constrains the maximum age of the Takiyuak Formation. Another approximately contemporaneous rock unit in the Slave craton is the 1885 Ma Ghost dykes of the Yellowknife region. Both the Takiyuak and the Ghost poles are broadly consistent with the majority of the Coronation poles (Irving and McGlynn, 1979; Buchan et al., 2016; Fig. 12). The Ghost dykes were sampled in an area where conjugate transcurrent faults are absent and the Takiyuak Formation is in a domain of dextral faults whose azimuths imply little rotation (Fig. 4b). Mitchell et al. (2010) argued that the paleocurrent azimuths of the Tochatwi Formation agree with the basin-scale structure, so that the Tochatwi pole should not be affected by local rotations. The analysis by Mitchell et al. (2010) is useful for assessing the structural corrections applied to a majority of the paleomagnetic poles obtained from the various basins marginal to Slave craton, and their model of modest (~12°) relative rotations does align well three groups of time-equivalent poles on that large spatial scale. However, the same rotations applied by Mitchell et al. (2010) are notably insufficient to align the Stark and Tochatwi poles with that of the broadly coeval Takiyuak Formation (their Figure 6c). Assessment of the Stark and Tochatwi poles demands finer-scale analysis.

Paleocurrent data of the Tochatwi Formation (Hoffman, 1969) were collected from northwesternmost Pearson Point (section PH1 in Fig. 5) and an island in Stark Lake (section PH2 in Fig. 5), both of which have normal McDonald-parallel or sub-horizontal structural attitudes and show no evidence for paleomagnetic rotations. In fact, the Stark (site EB2 in Fig. 5) and Tochatwi (site BE2 in Fig. 5) Formations were also sampled from the island in Stark Lake, and each of them has one site with a possibly primary direction.

The Stark direction agrees with the vertical-axis rotation model (Evans and Bingham, 1976), but the Tochatwi direction does not, as it might be affected by remagnetization (Bingham and Evans, 1976). Due to inadequate number of samples analyzed from areas with normal structural attitudes, the conclusion regarding whether the Stark and Tochatwi poles result from localized vertical-axis rotation in the Great Slave basin remains inconclusive. Previous Stark and Tochatwi poles need to be tested with new data from areas where structural evidence for local block rotations is absent.

The eastern end of the Coronation APWP is defined by the paleomagnetic pole from the Rifle Formation in the Kilohigok basin (Evans and Hoye, 1981; Fig. 2), subsequently dated at 1963 ± 6 Ma (Bowring and Grotzinger, 1992). Irving et al. (2004) suggest that the Rifle pole was also affected by counterclockwise rotation due to motions on the left-lateral Bathurst Fault in the Kilohigok basin. Assessing the veracity of the aberrant Rifle Formation pole requires further testing.

6. Concluding remarks

Reliable paleomagnetic poles from the Slave craton are critical in paleogeographic reconstruction of Laurentia and the supercontinent Nuna. In this study, we tested one component of the Coronation APWP, which contains multiple Slave poles between 1.96-1.87 Ga, with a detailed paleomagnetic and rock magnetic study of the ca. 1.87 Ga Pearson Formation. Results show that the magnetization of the Pearson Formation is carried by SD or small PSD magnetite grains. A positive fold test demonstrates that the Pearson remanence predates the folding of Paleoproterozoic age, supporting that magnetite grains

faithfully recorded the ambient magnetic field direction during cooling after basalt lava emplacement. Comparing the structural attitudes and paleomagnetic declinations of the Pearson Formation from different sampling areas supports the conclusion that small blocks in the Great Slave basin experienced large degrees (~60°) of vertical-axis rotation related to dextral slip on the McDonald Fault system, calling the veracity of some of the other Coronation poles into question. Further evaluation of local structural complexities indicates that the previous paleomagnetic results from the Stark and the Tochatwi Formations might also be affected by vertical-axis rotation at a local scale. Although our localized result from the Pearson Formation does not preclude alternative explanations for other portions of the Coronation APWP (e.g., oscillatory true polar wander), it does confirm that paleomagnetic studies in the circum-Slave region need to be alerted to the potential for local vertical-axis rotations (Bingham and Evans, 1976; Irving et al., 2004; Mitchell et al., 2010).

Acknowledgements

We thank Sergei Pisarevsky and two anonymous reviewers for constructive comments on the manuscript. We thank Mark Brandon for discussions; Eric Bellefroid, Stephen Victor and Bin Wen for field and laboratory assistance. We thank the community of Lutsel'ke for endorsement of this study.

Table 1 Summarized paleomagnetic poles of the Coronation APWP.

Basin	Group	Formation	Abbreviation	Age (Ma)	Age reference	Plat (°N)	Plon (°E)	A_{95} (°)	N	Paleomagnetic reference	Local rotation*
Kilohigok		Mara River sills	MRS	1870 ± 1	Davis et al. (2004)	-27	268	0	1	Evans and Hoye (1981)	unlikely
Kilohigok	Wolverine	Peacock Hills	PH	1882 ± 4	correlation by Mitchell et al. (2010)	-15	270	11	15	Evans and Hoye (1981)	unlikely
Kilohigok	Bear Creek	Mara	MA	1885 ± 5	correlation by Mitchell et al. (2010)	-7	253	7	28	Evans and Hoye (1981)	unlikely
Kilohigok	Bear Creek	Rifle	RF	1963 ± 6	Bowring and Grotzinger (1992)	14	341	9	22	Evans and Hoye (1981)	possible
Coronation		Peninsular sill	PS	1871 ± 1	M. Hamilton in Buchan et al. (2010)	-22	263	7	7	Irving and McGlynn (1979)	unlikely
Coronation		Takiyuak	TK	ca. 1885-1870	correlation by Mitchell et al. (2010)	-13	249	8	17	Irving and McGlynn (1979)	unlikely
Great Slave	Christie Bay	Pearson (A)	PE	ca. 1870	correlation by Mitchell et al. (2010)	-19	283	9	12	McGlynn and Irving (1978)	unlikely
Great Slave	Christie Bay	Tochatwi	TO	ca. 1885-1870	correlation by Mitchell et al. (2010)	-18	216	12	8	Evans and Bingham (1976)	likely
Great Slave	Christie Bay	Stark	ST	ca. 1885-1870	correlation by Mitchell et al. (2010)	-15	212	7	39	Bingham and Irving (1976)	likely
Great Slave	Pethei	Douglas Peninsula	DP	ca. 1885-1870	correlation by Mitchell et al. (2010)	-17	258	16	6	Irving and McGlynn (1979)	unlikely
Great Slave	Kahochella	(K)	KA	1882 ± 4	correlation by Mitchell et al. (2010)	-7	298	9	18	Reid et al. (1981)	unlikely
Great Slave	Kahochella	Seton (C)	SE	1885 ± 5	correlation by Mitchell et al. (2010)	2	267	6	19	Irving and McGlynn (1979)	unlikely
Great Slave	Sosan	Akaitcho River	AR	1885 ± 5	correlation by Mitchell et al. (2010)	-4	268	7	35	Evans et al. (1980)	unlikely
		Ghost dykes	Ghost	1887-1884	Buchan et al. (2016)	2	254	6	23	Buchan et al. (2016)	unlikely
		Lac de Gras dykes	LdG	2029-2023	Buchan et al. (2009)	12	268	7	10	Buchan et al. (2009)	unlikely

*Notes: Plat = pole latitude, Plon = pole longitude, A_{95} = radius of 95% confidence cone of the pole, N = number of sites. Paleomagnetic poles are listed using values from original papers. * Mitchell et al. (2010) present a model of 12° rotations based on trans-cratonic structural analyses (not applied here).*

Table 2 Summarized paleomagnetic results of the Pearson Formation.

		GPS location		Bedding		In-situ site mean			Tilt-corrected site mean			VGP			Rotation		
Site	n	Latitude	Longitude	Strike (°)	Dip (°)	Dec_G (°)	Inc_G (°)	α_{95} (°)	Dec_S (°)	Inc_S (°)	α_{95} (°)	Plat (°N)	Plon (°E)	A_{95} (°)	Structural attitude (°)	Strike difference (°)	Dec difference (R ± ΔR)
LU3	8	62°24'36.10"N	110°48'26.50"W	299	31	23.4	-9.9	2.8	21.7	-40.7	2.8	-2.6	229.3	2.6	119 [1]	54	52.7 ± 7.5
LU5	10	62°24'57.60"N	110°48'54.00"W	122	35	10.9	-57.6	3.2	19.8	-23.9	3.2	-13.5	229.3	2.5	122 [1]	57	50.8 ± 7.5
LU6	12	62°24'58.70"N	110°49'39.60"W	295	103	149.2	78.4	2.9	34.7	-6.3	2.8	-19.3	212.1	2.0	115 [1]	50	65.7 ± 7.4
PI6	6	62°29'30.00"N	110°42'36.00"W	21	8	11.1	-26.7	10.3	7.3	-25.1	10.3	-14.1	242.0	8.1	120 [2]	55	38.3 ± 9.8
E1623A	4	62°32'20.76"N	110°33'50.40"W	104	17	337.8	-24.8	8.4	341.0	-10.8	8.4	-20.5	269.7	6.0	65 [3]	0	12.0 ± 8.7
E1623B	5	62°32'56.04"N	110°42'24.84"W	51	10	321.3	-31.5	12.0	321.3	-21.5	12.0	-10.5	287.9	9.2	65 [3]	0	-7.7 ± 10.4

Notes:

n = number of samples, Dec = declination, Inc = inclination, α_{95} = radius of 95% confidence cone, Plat = pole latitude, Plon = pole longitude, A_{95} = radius of 95% confidence cone of the pole

[1] structural attitude based on the measured site bedding

[2] structural attitudes based on average strike of underlying Portage Inlet Formation across a small fault; Pearson lava dips too gently for the rotation analysis

[3] tectonically stable areas with dips too shallow for the rotation analysis; reference strike set to match trend of the McDonald Fault because of similar paleomagnetic results between Pearson Point and eastern sampling areas of McGlynn and Irving (1978)

References

Abrajevitch, A., & Van der Voo, R. (2010). Incompatible Ediacaran paleomagnetic directions suggest an equatorial geomagnetic dipole hypothesis. *Earth and Planetary Science Letters*, 293(1), 164-170.

Barnes, F. Q. (1951). Snowdrift map-area, NWT. *Geological Survey of Canada Paper*, 51-6.

Barnes, F. Q. (1953). The Snowdrift and McLean Bay map-areas, Great Slave Lake, Northwest Territories. Ph.D. thesis, Geology Department, University of Toronto.

Bingham, D. K., & Evans, M. E. (1976). Paleomagnetism of the Great Slave Supergroup, Northwest Territories, Canada: the Stark Formation. *Canadian Journal of Earth Sciences*, 13(4), 563-578.

Bowring, S. A. (1985). U-Pb zircon geochronology of early Proterozoic Wopmay orogen, N.W.T., Canada: an example of rapid crustal evolution. Ph.D. thesis, University of Kansas, Lawrence, 148 p.

Bowring, S. A., & Grotzinger, J. P. (1992). Implications of new chronostratigraphy for tectonic evolution of Wopmay Orogen, Northwest Canadian Shield. *American Journal of Science*, 292(1), 1-20.

Bowring, S. A., Van Schmus, W. R., & Hoffman, P. F. (1984). U-Pb zircon ages from Athapuscow aulacogen, East Arm of Great Slave Lake, N.W.T., Canada. *Canadian Journal of Earth Sciences*, 21, 1315-1324.

Boyden, J. A., Müller, R. D., Gurnis, M., Torsvik, T. H., Clark, J. A., Turner, M., ... & Cannon, J. S. (2011). Next-generation plate-tectonic reconstructions using GPlates. *Geoinformatics* 9, 5-114.

Buchan, K. L., LeCheminant, A. N., & van Breemen, O. (2009). Paleomagnetism and U-Pb geochronology of the Lac de Gras diabase dyke swarm, Slave Province, Canada: implications for relative drift of Slave and Superior provinces in the Paleoproterozoic. *Canadian Journal of Earth Sciences*, 46(5), 361-379.

Buchan, K.L., Ernst, R.E., Bleeker, W., Davis, W.J., Villeneuve, M., van Breemen, O., Hamilton, M.A., Söderlund, U., 2010. Proterozoic Magmatic Events of the Slave Craton, Wopmay Orogen and Environs. Geological Survey of Canada, Open File 5989, CD-ROM, poster and 25 pp. report.

Buchan, K. L., Mitchell, R. N., Bleeker, W., Hamilton, M. A., & LeCheminant, A. N. (2016). Paleomagnetism of ca. 2.13-2.11 Ga Indin and ca. 1.885 Ga Ghost dyke swarms of the Slave craton: Implications for the Slave craton APW path and relative drift of Slave, Superior and Siberian cratons in the Paleoproterozoic. *Precambrian Research*, 275, 151-175.

Butler, R. F. (1992). Paleomagnetism: Magnetic domains to geologic terranes. Blackwell Scientific, 238 pp.

Cardozo, N., & Allmendinger, R. W. (2013). Spherical projections with OSXStereonet. *Computers & Geosciences*, 51, 193-205.

Carey, S. W. (1958). The tectonic approach to continental drift. In Carey, S. W., ed., Continental Drift: A Symposium. Geology Department, University of Tasmania, Hobart, 177-355.

Cloos, E. (1955). Experimental analysis of fracture patterns. *Geological Society of America Bulletin*, 66, 241-256.

Cook, F.A. (2011). Multiple arc development in the Palaeoproterozoic Wopmay orogen, northwest Canada. In Brown, D. & Ryan, P. D., eds, Arc-Continent Collision. Springer-Verlag, Heidelberg, 403-427.

Cox, A., & Doell, R. R. (1964). Long period variations of the geomagnetic field. *Bulletin of the Seismological Society of America*, 54(6B), 2243-2270.

Creveling, J. R., Mitrovica, J. X., Chan, N. H., Latychev, K., & Matsuyama, I. (2012). Mechanisms for oscillatory true polar wander. *Nature*, 491(7423), 244.

Davis, W. J., Bleeker, W., Hulbert, L., & Jackson, V. (2004). New geochronological results from the Slave Province Minerals and Geoscience Compilation and Synthesis Project. In Geological Science of Canada Northern Resources Program: Yellowknife Geoscience Forum (Abstracts of Talks and Posters), p. 20.

Day, R., Fuller, M., & Schmidt, V. A. (1977). Hysteresis properties of titanomagnetites: grain-size and compositional dependence. *Physics of the Earth and Planetary Interiors*, 13(4), 260-267.

Dunlop, D. J. (2002). Theory and application of the Day plot (Mrs/Ms versus Hcr/Hc) 1. Theoretical curves and tests using titanomagnetite data. *Journal of Geophysical Research: Solid Earth*, 107(B3).

Enkin, R. J. (2003). The direction-correction tilt test: an all-purpose tilt/fold test for paleomagnetic studies. *Earth and Planetary Science Letters*, 212, 151-166.

Evans, D. A. (1998). True polar wander, a supercontinental legacy. *Earth and Planetary Science Letters*, 157(1-2), 1-8.

Evans, M. E., Hoye, G. S., & Bingham, D. K. (1980). The paleomagnetism of the Great Slave supergroup: the Akaitcho River formation. *Canadian Journal of Earth Sciences*, 17(10), 1389-1395.

Evans, M. E., & Bingham, D. K. (1976). Paleomagnetism of the Great Slave Supergroup, Northwest Territories, Canada: the Tochatwi Formation. *Canadian Journal of Earth Sciences*, 13(4), 555-562.

Evans, M. E., & Hoye, G. S. (1981). Paleomagnetic results from the lower Proterozoic rocks of Great Slave Lake and Bathurst inlet areas, Northwest Territories. Proterozoic Basins of Canada: Geological Survey of Canada Paper, 81-10.

Freund, R. (1970). Rotation of strike-slip faults in Sistan, southeast Iran. *Journal of Geology*, 78, 188-200.

Freund, R. (1974). Kinematics of transform and transcurrent faults. *Tectonophysics*, 21, 93-134.

Gibb, R. A. (1978). Slave-Churchill collision tectonics. *Nature*, 271, 50-52.

Gold, T. (1955). Instability of the Earth's axis of rotation. *Nature*, 175(4456), 526-529.

Halls, H. C., Lovette, A., Hamilton, M., & Söderlund, U. (2015). A paleomagnetic and U-Pb geochronology study of the western end of the Grenville dyke swarm: Rapid changes in paleomagnetic field direction at ca. 585 Ma related to polarity reversals? *Precambrian Research*, 257, 137-166.

Helmstaedt, H. (2009). Crust-mantle coupling revisited: the Archean Slave craton, NWT, Canada. *Lithos*, 112, 1055-1068.

Hildebrand, R. S. (1985). Geology, Rainy Lake-White Eagle Falls area, District of Mackenzie. Geological Survey of Canada, Map 1546A, 1: 50,000 scale map.

Hildebrand, R. S. (1987). Tectono-magmatic evolution of the 1.9-Ga Great Bear magmatic zone, Wopmay orogen, northwestern Canada. *Journal of Volcanology and Geothermal Research*, 32, 99-118.

Hildebrand, R. S., Hoffman, P. F., Housh, T., & Bowring, S. A. (2010). The nature of volcano-plutonic relations and the shapes of epizonal plutons of continental arcs as revealed in the Great Bear magmatic zone, northwestern Canada. *Geosphere* 6, 1-28.

Hildebrand, R. S. (2011). Geological synthesis: northern Wopmay orogen/Coppermine homocline, Northwest Territories-Nunavut. Geological Survey of Canada, Open File 6390, 1: 500,000 scale map.

Hoffman, K. A. (1991). Long-lived transitional states of the geomagnetic field and the two dynamo families. *Nature*, 354(6351), 273-277.

Hoffman, P. F. (1968). Stratigraphy of the lower Proterozoic (Aphebian), Great Slave Supergroup, east arm of Great Slave Lake, District of Mackenzie. Geological Survey of Canada, Paper 68-42, 93 p.

Hoffman, P. (1969). Proterozoic paleocurrents and depositional history of the East Arm fold belt, Great Slave Lake, Northwest Territories. *Canadian Journal of Earth Sciences*, 6(3), 441-462.

Hoffman, P. (1973). Evolution of an early Proterozoic continental margin: the Coronation geosyncline and associated aulacogens of the northwestern Canadian shield. *Philosophical Transactions of the Royal Society of London A: Mathematical, Physical and Engineering Sciences*, 273(1235), 547-581.

Hoffman, P. F., Bell, I. R., Hildebrand, R. S., & Thorstad, L. (1977). Geology of the Athapuscow aulacogen, east arm of Great Slave Lake, District of Mackenzie. In Report of Activities, Part A, Geological Survey of Canada, Paper 77-1A, 117-129.

Hoffman, P. F. (1980). Wopmay orogen: a Wilson cycle of Early Proterozoic age in the northwest of the Canadian Shield. In Strangway, D. W., ed., The Continental Crust and Its Mineral Resources, *Geological Association of Canada, Special Publication* 20, 523-549.

Hoffman, P. F. (1981). Autopsy of Athapuscow Aulacogen: a failed arm affected by three collisions. In Campbel, F. H. A., ed. Proterozoic Basins of Canada. Geological Survey of Canada, Paper 81-10, 97-102.

Hoffman, P. F. (1988a). United plates of America, the birth of a craton: Early Proterozoic assembly and growth of Laurentia. *Annual Review of Earth and Planetary Sciences*, 16(1), 543-603.

Hoffman, P. F. (1988b). Geology and tectonics, East Arm of Great Slave Lake, Northwest Territories. Geological Survey of Canada, Map 1628A, scale 1: 250,000 and 1: 500,000.

Hoffman, P. F. (1989). Precambrian geology and tectonic history of North America. *The Geology of North America*, 447-512.

Hoffman, P. F. (1994). Geology, northern externides of Wopmay orogen, District of Mackenzie. Geological Survey of Canada, Open File 3251, 1: 250,000-scale map.

Hoffman, P. F. (2014). The origin of Laurentia: Rae craton as the backstop for proto-Laurentian amalgamation by slab suction. *Geoscience Canada*, 41, 313-320.

Hornafius, J. S., Luyendyk, B. P., Terres, R. R., & Kamerling, M. J. (1986). Timing and extent of Neogene tectonic rotation in the western Transverse Ranges, California. *Geological Society of America Bulletin*, 97(12), 1476-1487.

Irving, E., Park, J. K., & McGlynn, J. C. (1972). Paleomagnetism of the Et-Then Group and Mackenzie Diabase in the Great Slave Lake Area. *Canadian Journal of Earth Sciences*, 9, 744-755.

Irving, E., & McGlynn, J. C. (1979). Palaeomagnetism in the Coronation Geosyncline and arrangement of continents in the middle Proterozoic. *Geophysical Journal International*, 58(2), 309-336.

Irving, E., Baker, J., Hamilton, M., & Wynne, P. J. (2004). Early Proterozoic geomagnetic field in western Laurentia: implications for paleolatitudes, local rotations and stratigraphy. *Precambrian Research*, 129(3), 251-270.

Jones, C. H. (2002). User-driven integrated software lives: "Paleomag" paleomagnetics analysis on the Macintosh. *Computers & Geosciences*, 28(10), 1145-1151.

Kamerling, M. J., & Luyendyk, B. P. (1979). Tectonic rotations of the Santa Monica Mountains region, western Transverse Ranges, California, suggested by paleomagnetic vectors. *Geological Society of America Bulletin*, 90(4), 331-337.

Kilian, T. M., Chamberlain, K. R., Evans, D. A., Bleeker, W., & Cousens, B. L. (2016). Wyoming on the run-Toward final Paleoproterozoic assembly of Laurentia. *Geology*, 44(10), 863-866.

Kim Y. S., Peacock, D. C. P., & Sanderson, D. J. (2004). Fault damage zones. *Journal of Structural Geology*, 26, 503-517.

Kirschvink, J. L. (1980). The least-squares line and plane and the analysis of palaeomagnetic data. *Geophysical Journal International*, 62(3), 699-718.

Kirschvink, J. L., Kopp, R. E., Raub, T. D., Baumgartner, C. T., & Holt, J. W. (2008). Rapid, precise, and high-sensitivity acquisition of paleomagnetic and rock-magnetic data: Development of a low-noise automatic sample changing system for superconducting rock magnetometers. *Geochemistry, Geophysics, Geosystems*, 9(5).

Lowell, J. D. (1972). Spitsbergen Tertiary Orogenic Belt and the Spitsbergen Fracture Zone. *Geological Society of America Bulletin*, 83, 3091-3102.

McGlynn, J. C., & Irving, E. (1978). Multicomponent magnetization of the Pearson Formation (Great Slave Supergroup, NWT) and the Coronation loop. *Canadian Journal of Earth Sciences*, 15(4), 642-654.

Mitchell, R. N., Hoffman, P. F., & Evans, D. A. (2010). Coronation loop resurrected: Oscillatory apparent polar wander of Orosirian (2.05-1.8 Ga) paleomagnetic poles from Slave craton. *Precambrian Research*, 179(1), 121-134.

Mitchell, R. N., Bleeker, W., Van Breemen, O., LeCheminant, T. N., Peng, P., Nilsson, M. K., & Evans, D. A. (2014). Plate tectonics before 2.0 Ga: Evidence from paleomagnetism of cratons within supercontinent Nuna. *American Journal of Science*, 314(4), 878-894.

Muxworthy, A. R., & McClelland, E. (2000). Review of the low-temperature magnetic properties of magnetite from a rock magnetic perspective. *Geophysical Journal International*, 140(1), 101-114.

Raub, T. D., Kirschvink, J. L., & Evans, D. A. D. (2007). True polar wander: Linking deep and shallow geodynamics to hydro-and biospheric hypotheses. *Treatise on Geophysics*, 5, 565-589.

Reid, A. B., McMurry, E. W., & Evans, M. E. (1981). Paleomagnetism of the Great Slave Supergroup, Northwest Territories, Canada: multicomponent magnetization of the Kahochella Group. *Canadian Journal of Earth Sciences*, 18(3), 574-583.

Ritts, B. D., & Grotzinger, J. P. (1994). Depositional facies and detrital composition of the Paleoproterozoic Et-then Group, N.W.T., Canada: sedimentary response to intracratonic indentation. *Canadian Journal of Earth Sciences*, 31, 1763-1778.

Rose, I., & Buffett, B. (2017). Scaling rates of true polar wander in convecting planets and moons. *Physics of the Earth and Planetary Interiors*, 273, 1-10.

Segall, P., & Pollard, D. D. (1980). Mechanics of discontinuous faults. *Journal of Geophysical Research*, 85(B8), 4337-4350.

Spada, G., Ricard, Y., & Sabadini, R. (1992). Excitation of true polar wander by subduction. *Nature*, 360(6403), 452-454.

Steinberger, B., Seidel, M. L., & Torsvik, T. H. (2017). Limited true polar wander as evidence that Earth's nonhydrostatic shape is persistently triaxial. *Geophysical Research Letters*, 44(2), 827-834.

Stockwell, C. H. (1932). Great Slave Lake-Coppermine River area, Northwest Territories. *Geological Survey of Canada, Annual Reports*, Part C, 37-63.

Stockwell, C. H. (1936). Eastern portion of Great Slave Lake, District of Mackenzie, Northwest Territories. Geological Survey of Canada, Maps 377A and 378A (with descriptive notes).

Tirrul, R. (1992) Geology and structural restoration of the east-central part of Asiak thrust-fold belt, Wopmay orogen, Northwest Territories. Geological Survey of Canada, Map 1654A, 2 sheets, 1: 50,000 scale.

Tauxe, L. (1998). Paleomagnetic principles and practice. Modern approaches in geophysics. Kluwer Academic Publishers.

Thomas, M. D., Gibb, R. A., & Quince, J. R. (1976). New evidence from offset aeromagnetic anomalies for transcurrent faulting associated with the Bathurst and McDonald faults, Northwest Territories. *Canadian Journal of Earth Sciences*, 13, 1244-1250.

Tsai, V. C., & Stevenson, D. J. (2007). Theoretical constraints on true polar wander. *Journal of Geophysical Research: Solid Earth*, 112(B5).

Verosub, K. L. (1988). Geomagnetic secular variation and the dating of Quaternary sediments. *Geological Society of America Special Papers*, 227, 123-138.

Wilcox, R. E., Harding, T. P., & Seely, D. R. (1973). Basic wrench tectonics. *American Association of Petroleum Geologists Bulletin*, 57, 74-96.

Zijderveld, J. D. A. (1967). AC demagnetization of rocks: analysis of results. *Methods in paleomagnetism*, 3, 254.

Chapter 3

Paleomagnetic survey of the Goulburn Supergroup, Kilohigok Basin, Nunavut, Canada: Toward an understanding of the Orosirian apparent polar wander path of the Slave craton[1]

Zheng Gong [a], David A. D. Evans [a]

[a] Department of Earth and Planetary Sciences, Yale University, 210 Whitney Avenue, New Haven, CT 06511, USA

---

[1] Chapter 3 prepared to be published in Gong, Z. & Evans, D. A. D. (in review). Paleomagnetic survey of the Goulburn Supergroup, Kilohigok Basin, Nunavut, Canada: Toward an understanding of the Orosirian apparent polar wander path of the Slave craton. *Precambrian Research*.

Abstract

Well-constrained apparent polar wander paths (APWPs) are crucial for paleogeographic reconstructions. Although igneous rocks (e.g., mafic dyke swarms) are good paleomagnetic recorders and could also be precisely dated by U-Pb geochronology, their episodic nature sometimes lead to large gaps in the constructed APWPs. Sedimentary rocks usually provide a nearly continuous record of geological history, which could fill in the gaps in the APWPs that are solely constructed by igneous rocks. A good example would be the Orosirian APWP of the Slave craton, a major piece in the late Archean supercraton Sclavia and in the initial assembly of Laurentia. Paleopoles from two mafic dyke swarms would appear to indicate that the Slave craton only experienced slight movements between 2.02 Ga and 1.88 Ga. However, paleomagnetic data from the three circum-Slave basins (Great Slave, Coronation, and Kilohigok Basins) show large (~110°), back-and-forth swings at 1.96-1.87 Ga, known as the Coronation loops. The Coronation loops, taken at face value, would imply rapid and substantial spin motions of the Slave craton, which is at odds with modern plate tectonics. Alternatively, the Coronation loops have been interpreted as a product of basin-scale rotations, localized vertical-axis rotations, or inertial interchange true polar wander (IITPW). One way to differentiate these models is to take advantage of the remarkably correlated stratigraphy in three circum-Slave basins and see if consistent paleomagnetic directions can be reproduced on a cratonic scale. In this study, we collected ~300 samples from nine formations from the Goulburn Supergroup of the Kilohigok Basin, in shallowly dipping autochthonous sections east of the Bathurst Fault. Thermomagnetic susceptibility and anisotropy of magnetic susceptibility experiments constrain the magnetic mineralogy of these samples. An inverse baked-contact test also shows that the Burnside

River Formation magnetic remanence is older than the ca. 1270 Ma Mackenzie dyke swarm. After stepwise thermal demagnetization and removal of younger overprints, the characteristic remanent magnetizations of the samples were successfully isolated and are interpreted as primary based on: the rock magnetic results, the presence of antipodal directions, as well as the positive inverse baked-contact test. We provide seven new reconnaissance-level paleopoles of the Slave craton, namely from the Kenyon, Hackett, Rifle, Beechey, Link, Kuuvik, and Brown Sound Formations of the Goulburn Supergroup. Our results and the compiled Orosirian paleomagnetic data of the Slave craton suggest that although basin-scale rotation or local vertical-axis rotation in fault zones are able to explain some of the disagreements among time-correlative paleopoles, they could not account for the large declination variation within the homoclinal sections in individual basins. Notably, our results from the ~1963 Ma Rifle Formation show a progressive change in declination through the stratigraphy, which cannot result from either basin-scale or local vertical-axis rotations. Instead, IITPW could be the potential cause for the Coronation loops, and could also explain some aberrant paleomagnetic data observed globally during the Orosirian time. Therefore, IITPW is thus far the most parsimonious model for regional- and global-scale Orosirian paleomagnetic discrepancies.

1. Introduction

Establishing a detailed apparent polar wander path (APWP) for a tectonic plate is key to reconstruct its paleogeography. Buchan et al. (1994, 2000) proposed the concept of key paleomagnetic poles as "anchors" to APWPs, and advocated paleomagnetic studies on mafic intrusions since they are reliable magnetic recorders and can be precisely dated, thus

most likely providing reliable paleopoles. Despite their great utility in paleomagnetism, mafic intrusions are episodic and irregular events, therefore, APWPs constructed solely based on mafic intrusions often bear large gaps. Alternatively, sedimentary rocks give nearly continuous records, so they can complement and enhance the valuable information provided by mafic intrusions (Kodama, 2012).

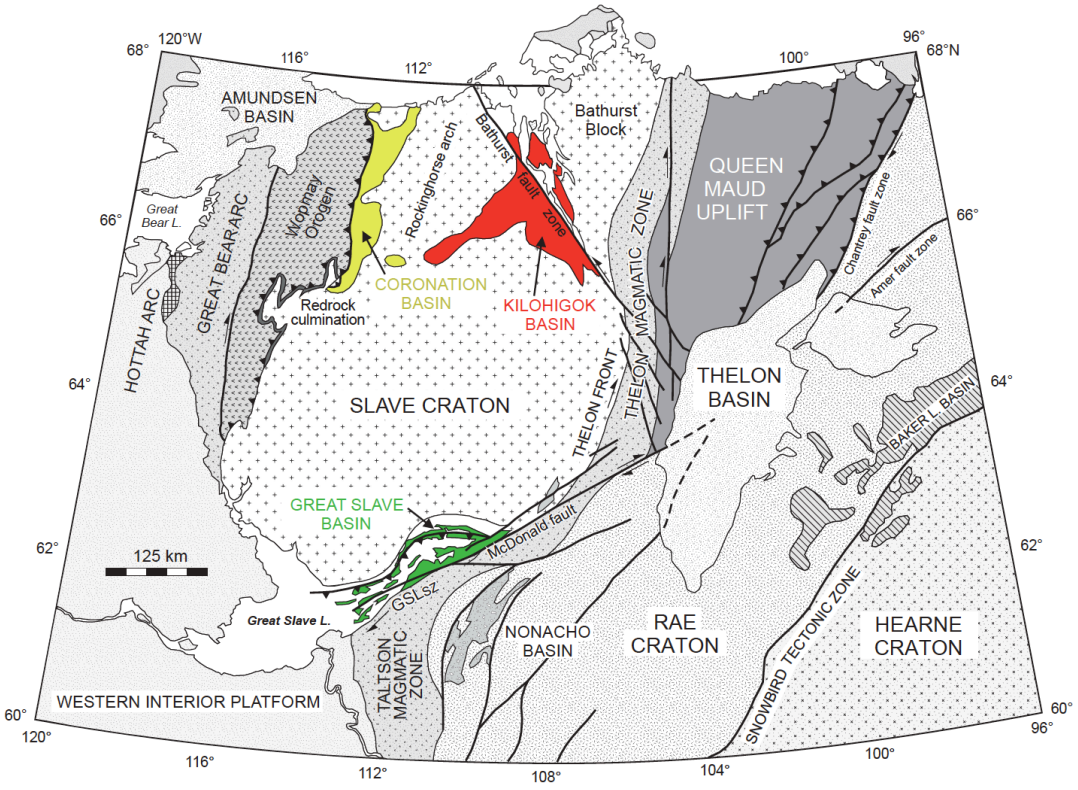

Figure 1 Geological map of the Slave craton (modified from Hoffman, 1989; Helmstaedt, 2009). Three circum-Slave basins are marked with colors: Kilohigok Basin in red, Coronation Basin in yellow, Great Slave Basin in green.

Paleomagnetic studies of the Slave craton, northwest Laurentia (Fig. 1) during Orosirian time provide a great example of the power of the sedimentary records in delineating a high-resolution APWP. A detailed Orosirian APWP of the Slave craton is useful because it

marks a transitional period when the Slave craton rifted from the Sclavia supercraton (Bleeker, 2003; French and Heaman, 2010) and eventually collided with other blocks to build Laurentia (Hoffman, 1988). If using only the paleopoles from trans-Slave mafic intrusions (i.e., the Lac de Gras and Ghost dyke swarms; Buchan et al., 2009, 2016), the length of Orosirian APWP of the Slave craton is short (Fig. 2), which would appear to indicate minimal plate motions within ~140-million-years. However, paleopoles from the successions in the three Paleoproterozoic circum-Slave basins (i.e., Kilohigok, Great Slave, and Coronation Basins; Fig. 1) show a back-and-forth swinging pattern (Fig. 2), known as the Coronation loops (McGlynn and Irving, 1978), in radical contrast with the fragmentary (though reliable) dyke swarm dataset.

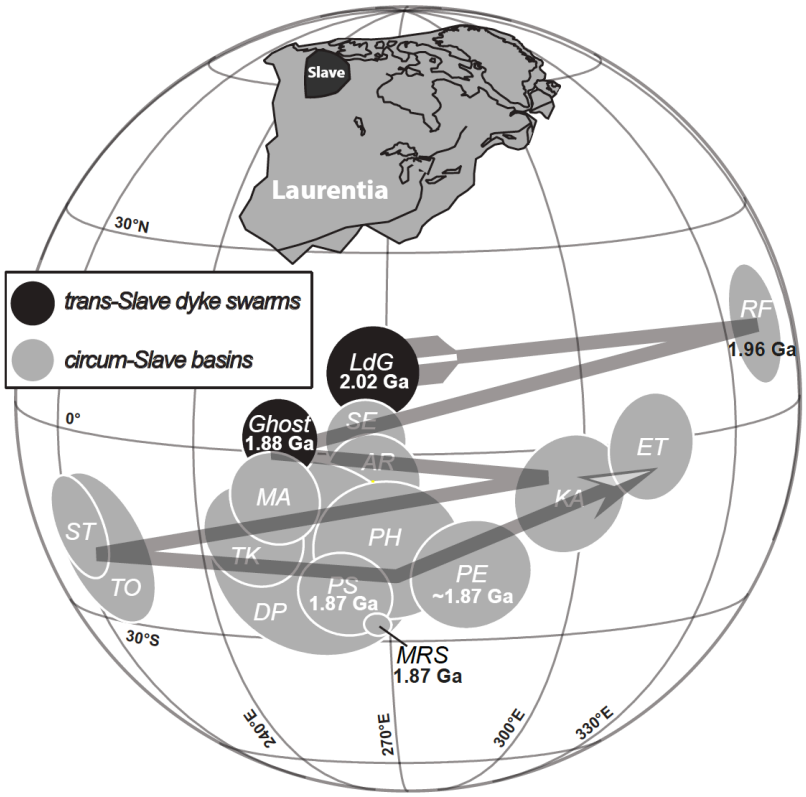

Figure 2 Orosirian paleopoles of the Slave craton define the Coronation loops. Arrow points towards the younging direction of the Coronation loops. Paleopoles in black are

from trans-Slave mafic dyke swarms and poles in grey are from circum-Slave basins. Paleopole positions and abbreviations are listed in Table 4.

Taken at face value, the Coronation loops would indicate fast back-and-forth spinning motions of the Slave craton that are not easily accommodated by our current understanding of plate tectonics. Competing models have been proposed to explain the Coronation loops. For example, Mitchell et al. (2018) argued that the swinging pattern of the Coronation loops could be produced by inertial interchange true polar wander (IITPW); while other workers suggested that a few paleopoles in the Coronation loops come from small blocks within the McDonald fault zone, with localized vertical-axis rotations (Bingham and Evans, 1976; Irving et al., 2004; Gong et al., 2018). One way to test these different models is to take advantage of the remarkably well correlated stratigraphy in three circum-Slave basins (Fraser and Tremblay, 1969; Fig. 3) and see if consistent paleomagnetic directions can be reproduced on a cratonic scale.

Here, we present a paleomagnetic survey of nearly the entire stratigraphy of the Goulburn Supergroup in the Kilohigok Basin, Nunavut, Canada. Comparing our results with time-correlative paleopoles from the Great Slave and Coronation Basins, we discuss the potential factors contributing to the complexities of the Coronation loops in order to facilitate refinement and understanding of the Orosirian APWP of the Slave craton.

2. Geological background

Slave craton is one of the well-preserved Archean crustal blocks located in the Canadian Shield (Fig. 1; Bleeker, 2003). The basement rocks of the Slave craton are composed of the 4.02-2.9 Ga Central Slave Basement Complex, the overlying 2.9-2.8 Ga Central Slave Cover Group, the 2.8-2.6 Ga volcano-sedimentary package of the Yellowknife Supergroup, and a suite of 2.61-2.58 Ga tonalitic-granitic intrusions (Isachsen and Bowring, 1994; Bleeker, 2002). The basement was crosscut by numerous trans-cratonic mafic dyke swarms, including the ~2.23 Ga Malley swarm, the ~2.19 Ga Dogrib swarm, the ~2.11 Ga Indin swarm, the ~2.07 Ga Lac de Gras swarm, the ~1.88 Ga Ghost swarm, the ~1.74 Ga Cleaver swarm, the ~1.27 Ga Mackenzie swarm, and the ~720 Ma Franklin swarm (summarized in Buchan et al., 2010). These dyke swarms are thought to be related to different rifting stages of the Slave craton over several supercontinental cycles (Buchan et al., 2010). In the cratonic margin, three Paleoproterozoic basins sit unconformably above the Archean basement. Specifically, these circum-Slave basins are the Coronation Basin in the west, the Kilohigok Basin in the east, and the Great Slave Basin in the south (Fig. 1; Hoffman, 1973). The unmetamorphosed successions of the three basins are remarkably correlatable, with stratigraphic thicknesses up to 10 km (Fig. 3). The correlation was first made by Fraser and Tremblay (1969), and was greatly improved by the U-Pb geochronological work of Bowring et al. (1984), Bowring and Grotzinger (1992), Hoffman et al. (2011), Sheen et al. (2019), and others. These basins mark the transitional period of the Slave craton between its separation from the Sclavia supercraton and the collision with the Rae craton along the Thelon-Taltson orogenic belt during the assembly of Laurentia (Fig. 1; Bleeker, 2003; French and Heaman, 2010; Hoffman, 1988, 1989). The collision with the Hottah terrane during the ~1.9 Ga Wopmay orogen is associated with the development of the conjugate

McDonald-Bathurst fault systems that displace the strata in the Great Slave and Kilohigok Basins (Hoffman, 1980).

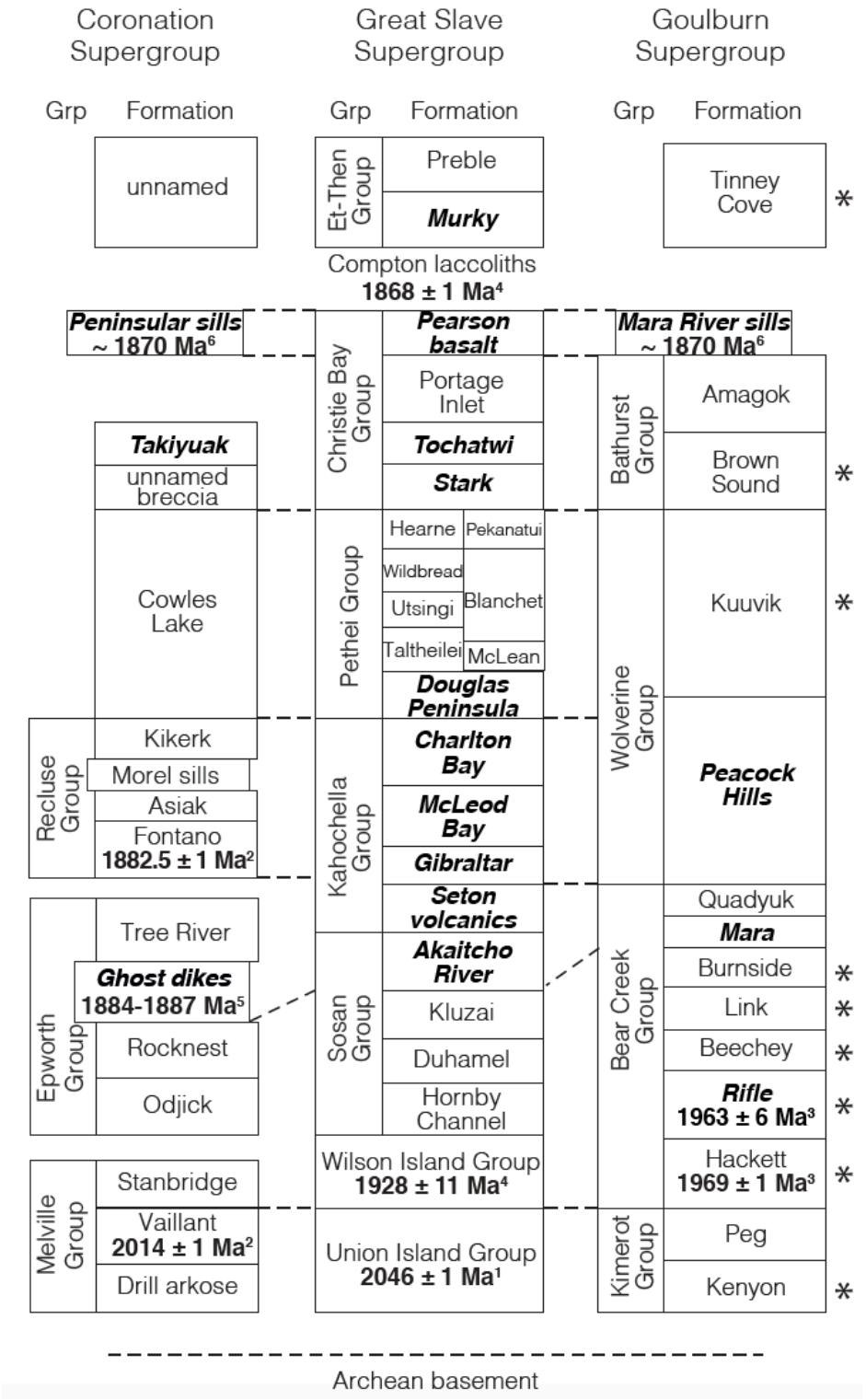

Figure 3 Stratigraphic correlation of circum-Slave basins (Fraser and Tremblay, 1969; Bowring and Grotzinger, 1992; Mitchell et al., 2010). Formations with fold and italic fonts are those of which the paleomagnetic results were reported. Asterisks mark the formations sampled by this study. Age references: [1]Sheen et al. (2019); [2]Hoffman et al. (2011); [3]Bowring and Grotzinger (1992); [4]Bowring et al. (1984); [5]Buchan et al. (2016); [6]Buchan et al. (2010).

The Kilohigok Basin was proposed as a failed rift system by Hoffman (1973). But that model has been challenged and now it is generally accepted that the Kilohigok Basin is syn-collisional transtensional basin related to Slave-Rae amalgamation (McCormick and Grotzinger, 1992, 1993). Detailed mapping and stratigraphic nomenclature were conducted by Fraser and Tremblay (1969) and Campbell and Cecile (1975, 1976), and revised by Grotzinger et al. (1987). The Goulburn Supergroup of the Kilohigok Basin is subdivided into four groups, namely the Kimerot, Bear Creek, Wolverine, and Bathurst Groups in an ascending order (Figs. 3, 4; Grotzinger et al., 1987). The Kimerot Group consists of the Kenyon Formation (quartzite) and the Peg Formation (carbonate) in a passive margin environment (Figs. 3, 4; McCormick and Grotzinger, 1992). The Bear Creek Group is made of red sandstones and red siltstones of the Hackett, Rifle, Beechey, Link, Burnside, and Mara Formations, and stromatolitic dolomites of the Quadyuk Formation in the foredeep environment (Figs. 3, 4; Campbell and Cecile, 1975; McCormick and Grotzinger, 1992). The Hackett and Rifle Formations are dated by zircons from the interbedded volcanic ash layers to be 1969 ± 1 Ma and 1963 ± 6 Ma, respectively (Fig. 3; Bowring and Grotzinger, 1992). The Wolverine Group contains the Peacock Hills Formation (red siltstone) and the

Kuuvik Formation (stromatolitic dolomite), and the Bathurst Group includes the Brown Sound Formation (red sandstone) and the Amagok Formation (red arkose), which are intruded by the ~1870 Ma Mara River sills (Figs. 3, 4; Campbell and Cecile, 1975; McCormick and Grotzinger, 1992; Buchan et al., 2010). The Tinney Cove Formation (conglomerate, arkose) has an angular unconformable contact with the underlying successions (Figs. 3, 4).

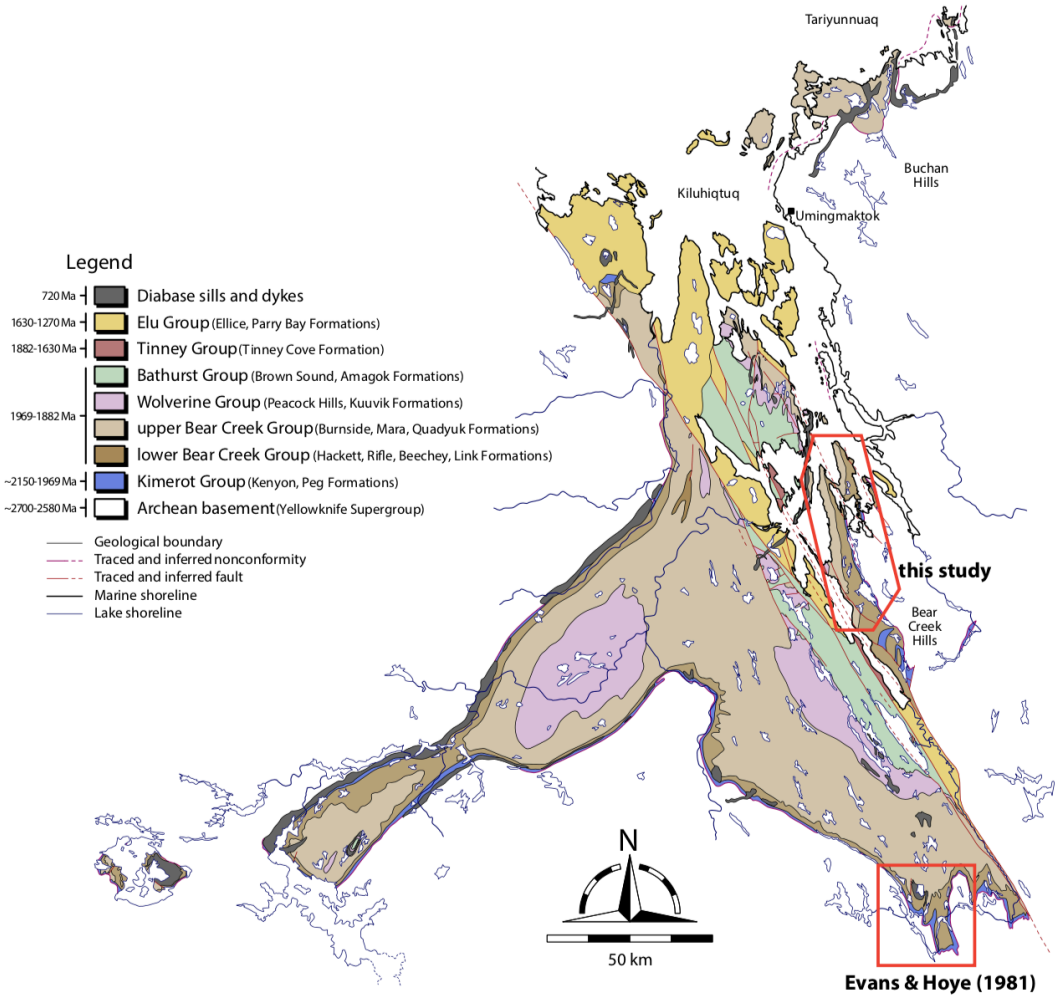

Figure 4 Geological map of the Kilohigok Basin (modified from Campbell and Cecile, 1976; Ielpi et al., 2017). Red polygons show the sampling areas of Evans and Hoye (1981) and this study.

Previous paleomagnetic studies on the three circum-Slave basins was conducted mainly in the 1970s and 1980s, and the results are summarized in Table 4. The Great Slave Basin received most of the paleomagnetic attention while the Coronation and Kilohigok Basins are understudied. Paleomagnetic data from the Akaitcho River Formation, Seton volcanics, Kahochella Group, Douglas Peninsula, Stark, and Tochatwi Formations, as well as the Pearson basalt are reported in a number of studies (Table 4; Bingham and Evans, 1976; Evans and Bingham; 1976; McGlynn and Irving, 1978; Irving and McGlynn, 1979; Evans, 1980; Reid et al., 1981; Gong et al., 2018). Only one paper was published regarding the paleomagnetism of the Kilohigok Basin, in which the data from the Rifle, Mara, Peacock Hills Formations, as well as the Mara River sills were reported (Table 4; Fig. 4; Evans and Hoye, 1981). Similarly, only the Takiyuak Formation and the Peninsular sills in the Coronation Basin were studied paleomagnetically by Irving and McGlynn (1979). However, the paleomagnetic data from the three circum-Slave basins collectively determine a large and back-and-forth swinging APWP, known as the Coronation loops of which the origin has been debated (Bingham and Evans, 1976; Irving et al., 2004; Mitchell et al., 2010; Gong et al., 2018). Within the cratonic interior, contemporaneous mafic intrusions such as the 2.02 Ga Lac de Gras dykes and the 1.88 Ga Ghost dykes were also studied paleomagnetically by Buchan et al. (2009, 2016).

3. Sampling and methods

Field sampling was guided by the geological map of Campbell and Cecile (1976). The targeted rock units are complementary to the study of Evans and Hoye (1981). Sampling

locations are marked in Figs. 4, 5. Section/site names are provided in the parentheses below. In the Gordon Bay area, we sampled, in an ascending order, the Kenyon Formation (GB1), two sections of the Hackett Formation (GB2, GB3), two sections of the Rifle Formation (GB4, GB5), and the Beechey Formation (GB6). Upsection, the Link Formation was collected from two limbs of an anticline (BC1, BC2) in southern Bear Creek Hills. One site (BC3) was sampled in a conglomerate layer a few decameters above Site BC2. Then, the Burnside Formation was sampled in two sites (MP1, MP2) in northern Bear Creek Hills. The overlying Kuuvik (KV1) and Brown Sound (BS1, BS2) Formations were sampled on a small island north of the Bathurst Inlet Lodge (Fig. 5). A northwest-trending, 12-m-wide doleritic dyke together with its host rock Brown Sound Formation was sampled for an inverse baked-contact test (BS3). Finally, the Tinney Cove Formation (TC2) and an intraformational conglomerate layer (TC1) were sampled above an angular unconformity that overlies the older strata. Details about the GPS locations, stratigraphic thicknesses, structural attitudes, and lithology of the measured sections are summarized in Table 1.

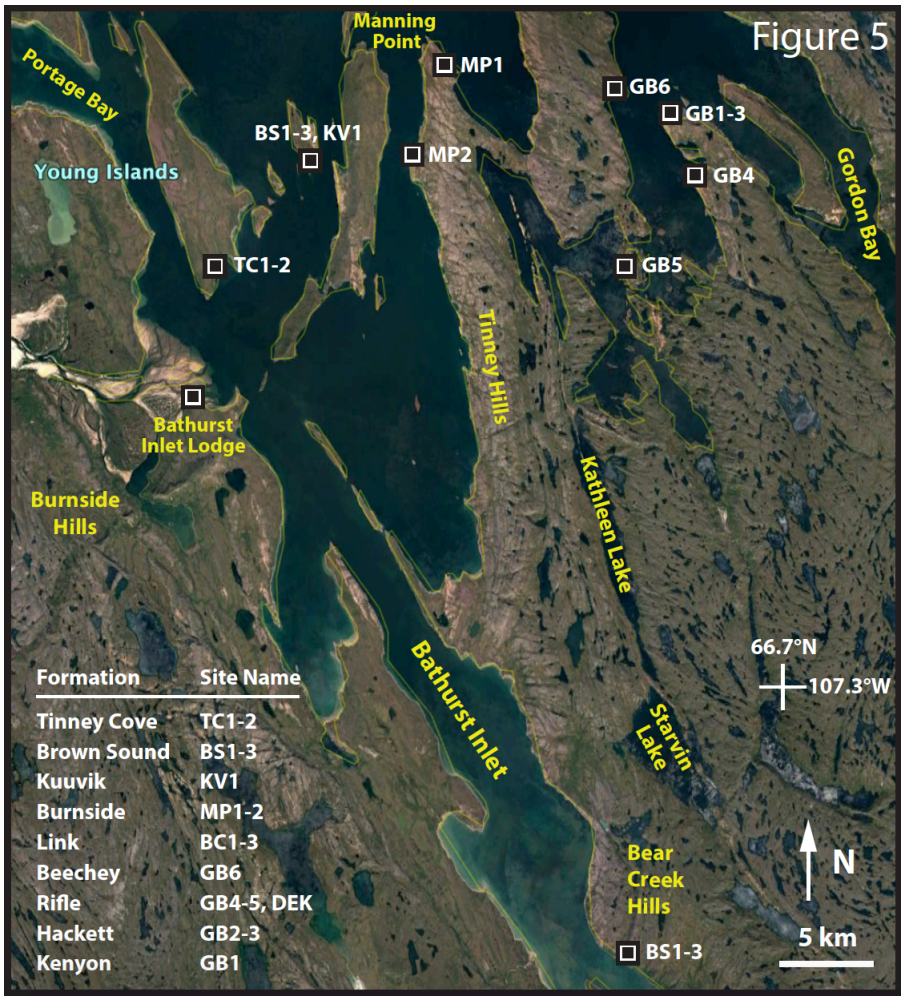

Figure 5 Sampling locations of this study with Google Earth™ satellite image as background.

A gasoline-powered portable drill was used in sample collection. Both the magnetic and sun compass were used to orient the drill cores and correct local declination deflections. The anisotropy of magnetic susceptibility (AMS) of the samples was measured. Powders were made from rock chips and were subjected to thermomagnetic susceptibility (K-T) analysis in an argon-gas environment. AMS and K-T analyses utilized an AGICO Kappabridge KLY-4S susceptibility meter coupled with a CS3 temperature control unit. In the magnetostatically shielded Yale Paleomagnetic Facility (ambient field <300 nT),

stepwise thermal demagnetization was performed in an ASC Scientific TD-48 thermal demagnetizer in a nitrogen gas environment. The remanent magnetizations were determined by a 2G Enterprises cryogenic DC-SQuID magnetometer coupled with an automated sample-delivering system (Kirschvink et al., 2008). Data were plotted on vector-endpoint diagrams (Zijderveld, 1967) and the characteristic remanent magnetizations (ChRMs) were analyzed by least-squares lines (Kirschvink, 1980) combined with planar fits when necessary (McFadden and McElhinny, 1988) in PaleoMag X software (Jones, 2002). Paleogeographic reconstructions were performed in GPlates software (Müller et al., 2018). The carbon and oxygen isotopic signatures of the Kuuvik carbonates were studied using a Thermo Scientific MAT-253 mass spectrometer coupled with a KIEL IV carbonate device at Yale Analytical and Stable Isotope Center.

4. Results

AMS data, in general, reflect a depositional fabric of the studied sedimentary rocks (Fig. 6). The mean bulk susceptibility falls in typical range of the siliciclastic rocks. The degree of anisotropy (P_j) of each site is typically lower than 1.035, except for the Beechey Formation (GB6), which is 1.09 (Table 2). The shape of the AMS ellipsoid could be assessed by the shape parameter T (Jelinek, 1981). Most AMS ellipsoids have a positive T value, indicating an oblate fabric (Table 2). Specifically, sites from the Bear Creek Group are usually characterized by steep K_3 axes and almost flat K_1 and K_2 axes (Fig. 6). The girdles defined by K_1 and K_2 axes are parallel/subparallel to the bedding planes and K_3 axes are perpendicular to the bedding planes, which is a typical depositional fabric. Although the T values of Hackett (GB3) and Link (BC1) Formations are slightly negative

(Table 2), the AMS fabrics show clear depositional signatures. Brown Sound Formation, both the baked (BS3) and unbaked sites (BS2), shows typical depositional fabric (Fig. 6). The AMS pattern of Kenyon Formation (GB1) is different, with steep K_1 axis and flat K_2 and K_3 axes (Fig. 6). The AMS patterns of Brown Sound Formation (BS1) and Kuuvik Formation (KV1) are also inconsistent with the depositional fabric (Fig. 6). The AMS pattern of Mackenzie dyke (BS3) is oblate with flat K_3 axis and vertical girdle plane defined by K_1 and K_2 axes, and accurately reflects the NW trending of the dyke (Fig. 6).

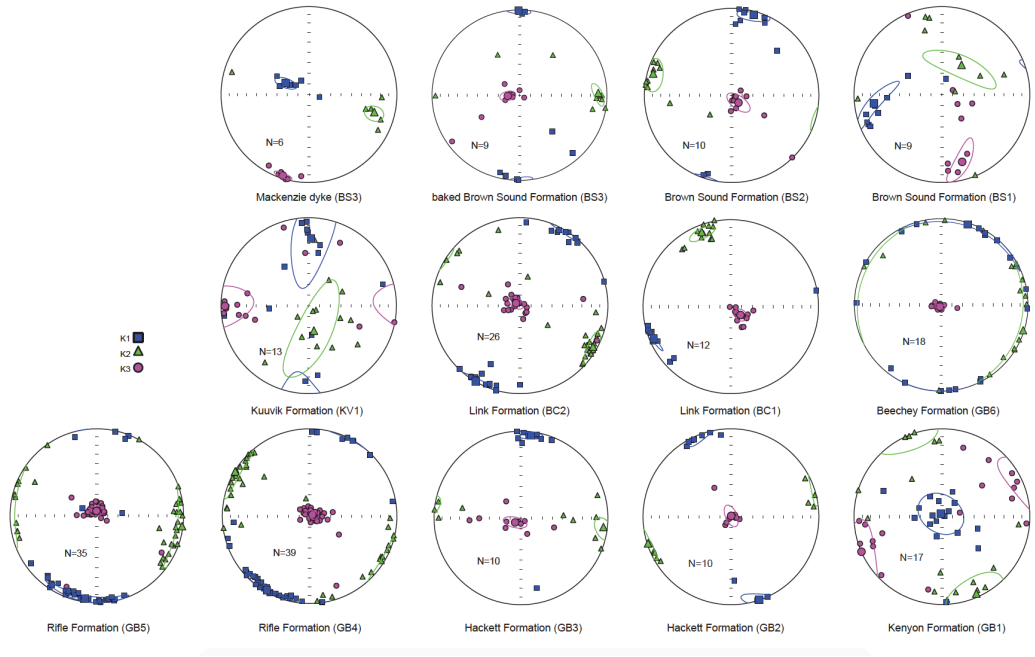

Figure 6. Representative anisotropy of magnetic susceptibility (AMS) data, shown in tilt-corrected coordinates for all sedimentary sites. Squares, triangles, and circles show the K_1, K_2, and K_3 axes of AMS ellipsoids, respectively. Mean K_1, K_2, and K_3 axes are also shown with their corresponding confidence ellipses.

For all samples from redbed units, the K-T curves show two-step decrease of magnetic susceptibility during heating, one at 520-600°C and the other at 650-680°C (Fig. 7). The

Kuuvik Formation is composed of carbonates, and its K-T curve only shows a one-step drop at ~500-580°C (Fig. 7). During the cooling, susceptibility increase significantly (note the scale difference between heating and cooling curves). The susceptibility increases occurs at ~580°C and 300-350°C (Fig. 7). For Mackenzie dyke samples, the heating curve shows a single drop of magnetic susceptibility between 550°C and 580°C, and the susceptibility decreases during cooling (Fig. 7).

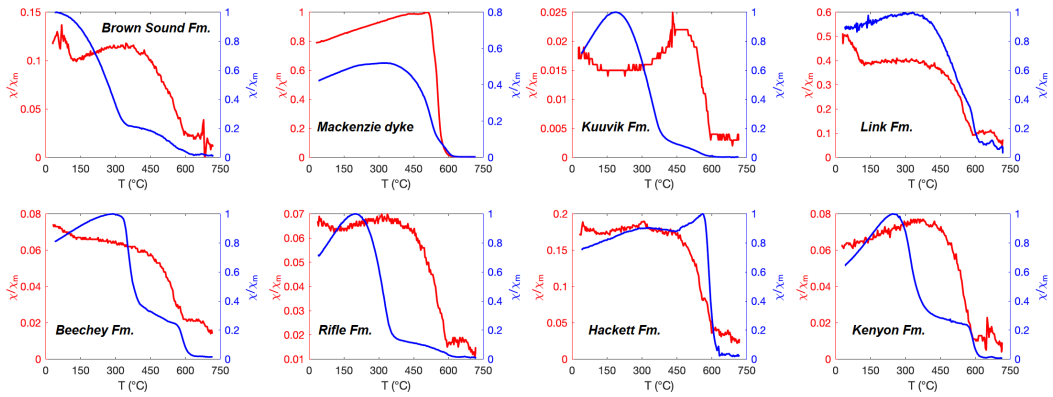

Figure 7 Results of thermomagnetic susceptibility (K-T) analyses. Analyses were conducted in an argon gas environment. Susceptibility values are normalized by the maximum for each sample. Heating and cooling curves are represented by red and blue colors, respectively. Note that scales for heating and cooling curves are different.

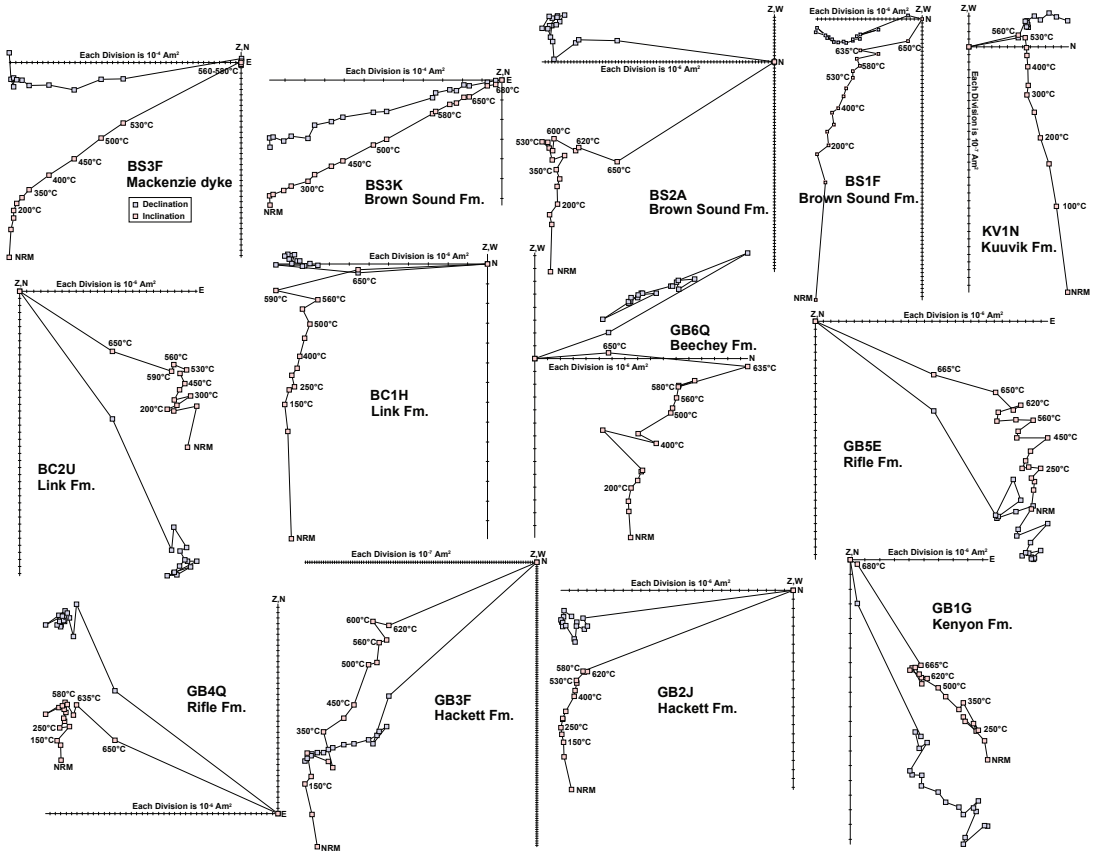

Figure 8 Results of thermal demagnetization are shown by the Zijderveld diagrams of representative samples.

Thermal demagnetization results of the redbeds show that the majority samples carry two components. The low-to-medium-temperature component (thereafter LTC-MTC) is typically isolated between natural remanent magnetization (NRM) and 350-580°C (Fig. 8), which is characterized by a steep inclination, close to the present-day local field direction (i.e. IGRF model) or the Coronation overprint direction (Irving et al., 2004). After the removal of the LTC-MTC, a high-temperature component (HTC) could be obtained between 580°C and 650-665°C, which has a shallow inclination. The HTCs are antipodal, with N-up/NW-up and S-down/SE-down directions (Fig. 8), which are interpreted as the

ChRMs of the samples. The ChRMs of the Kuuvik carbonates reside at 500-560°C (Fig. 8). The ChRMs of Mackenzie dyke samples were isolated between 350-580°C, and the Brown Sound samples that were baked by the Mackenzie dyke yield the same ChRMs as the dyke (Fig. 8). Tinney Cove and Burnside River Formations did not yield stable and consistent directions. We calculated the site mean directions using Fisher statistics, corrected bedding attitudes, and plotted them using stereonet projection (Fig. 9). Results of parallel sections of the Hackett, Rifle, Link, and Brown Sound Formations were combined during the mean direction calculations. Corresponding paleopoles were also calculated. Detailed paleomagnetic directions are summarized in Table 3.

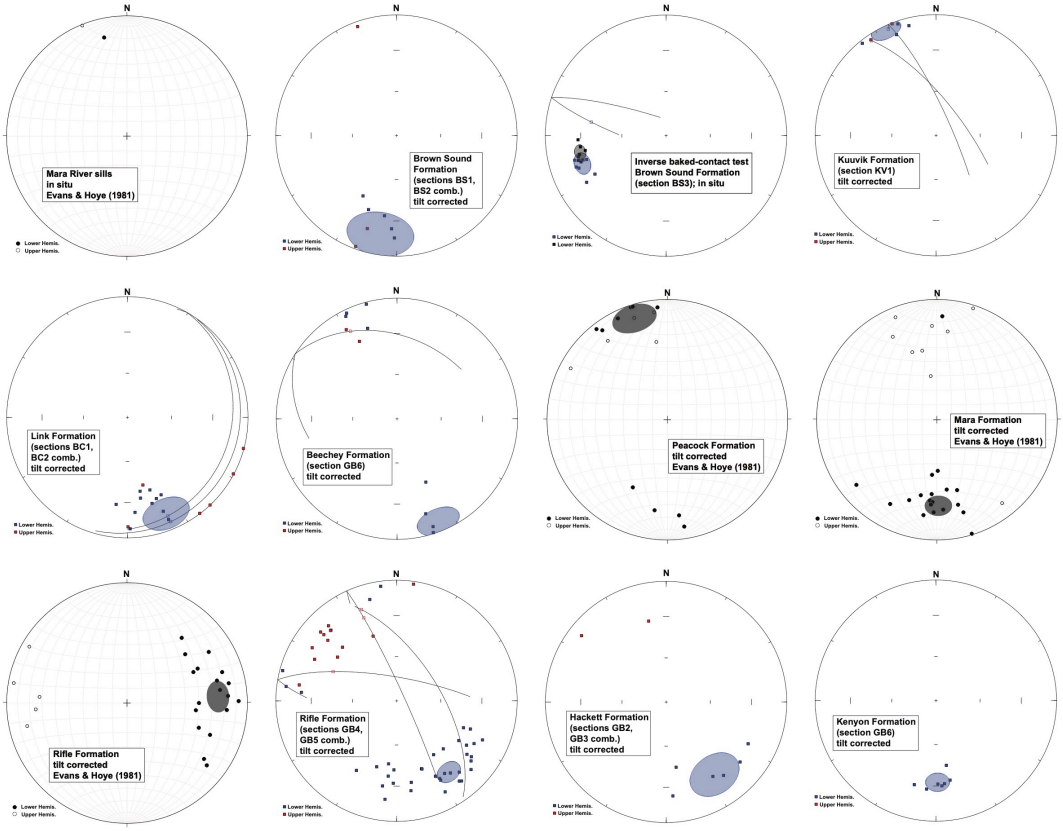

Figure 9 Site-mean directions of the Goulburn Supergroup. Mean directions and the corresponding 95% confidence cone are shown by the ovals. Squares and dots are least-squares line fits; curves are great-circle fits.

We conducted reversal tests following McFadden and McElhinny (1990) for the formations that show antipodal directions. Specifically, the antipodal polarities of the Hackett Formation (GB2, GB3 combined) have an angle difference of 6.1°, which is within a critical angle (95% confidence level) of 39.4°. Although the reversal test is passed with a classification of indeterminate, since the NW polarity only has two data points (Fig. 9), the Hackett Formation should be only regarded as appearance of antipodal directions within sites. For the Rifle Formation (GB4, GB5 combined), the angle difference between the antipodal polarities is 24.0°, which is larger than the critical angle of 14.6° at 95% confidence level. Therefore, Rifle Formation does not pass the reversal test. For the Beechey Formation (GB6), the angle difference between the antipodal polarities is 15.6°, which falls within the critical angle of 23.5° at 95% confidence level. Thus, the Beechey Formation passes the reversal test with a classification of indeterminate. Since the Brown Sound Formation (BS1, BS2 combined) has only one data point in the NW polarity (Fig. 9), we did not perform a reversal test but instead only marked this formation as appearance of antipodal directions.

$\delta^{13}C$ values of the Kuuvik stromatolites are around 0.8-1.2‰ and are stable across the sampled 1.5-m-long section (Fig. 10). $\delta^{18}O$ values range from -15‰ to -13‰ (Fig. 10). It is noticed that lower $\delta^{13}C$ values correspond with lower $\delta^{18}O$ values, and the lowest $\delta^{18}O$

values are from the top 0.25-m layer of the stromatolites which show orange color (Fig. 10).

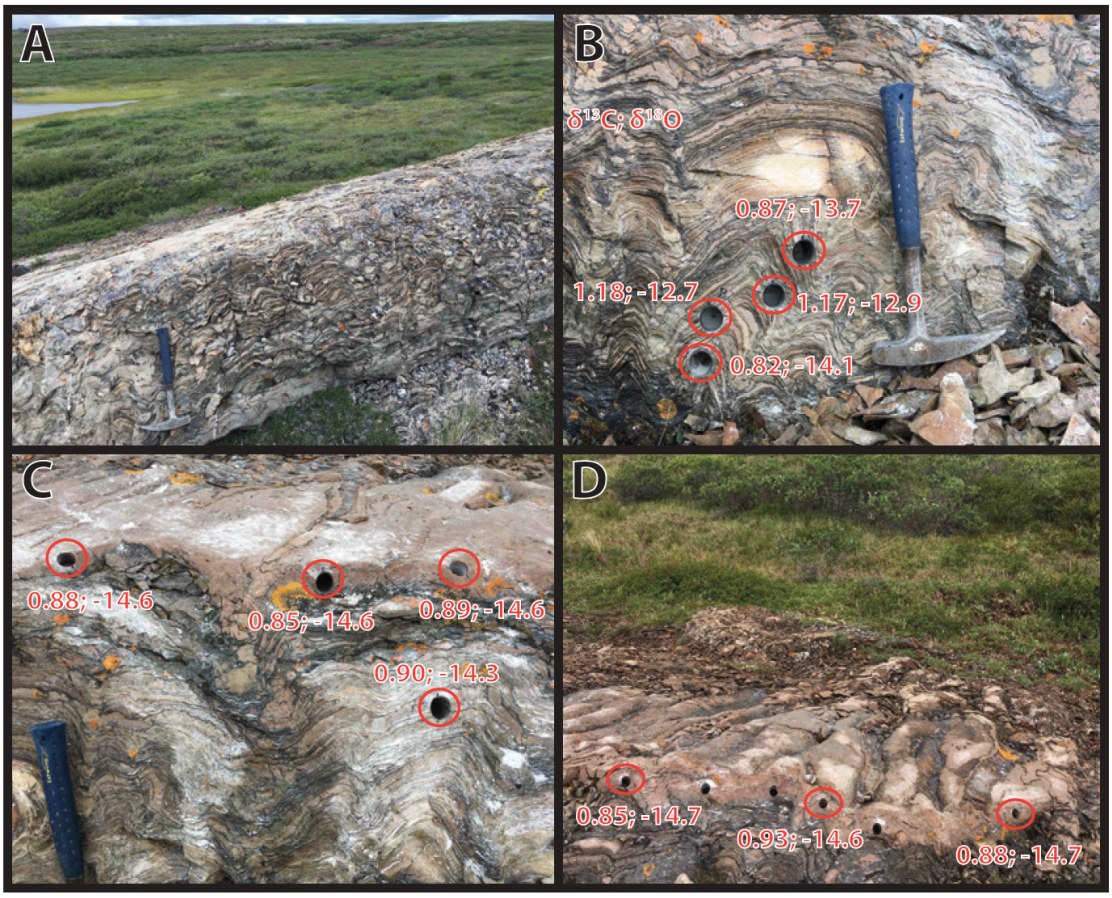

Figure 10. (A) Overview of the Kuuvik stromatolites. (B-D) Location of drilled samples, with their $\delta^{13}C$ and $\delta^{18}O$ values in permil.

5. Discussion

5.1 Rock magnetism, paleomagnetism, and $\delta^{13}C$-$\delta^{18}O$ isotopes

Rock magnetic experiments including the K-T experiments and the sample behaviors during the thermal demagnetization indicate that for Mackenzie dyke and Kuuvik carbonate samples, the ChRMs are carried by magnetite (Figs. 7, 8), and for redbed samples from other formations in the Goulburn Supergroup that we studied, the ChRMs are carried

by both magnetite and hematite (Figs. 7, 8). The low degree of anisotropy and the depositional AMS fabric shown by the majority of redbed sites as well as the primary AMS fabric shown by the Mackenzie dyke site suggest that the samples have experienced no or minimal deformation or alteration (Table 2; Fig. 6). The non-depositional fabric shown by the Kenyon Formation is probably due to the compression and recrystallization processes during the formation of the quartzite (Borradaile and Jackson, 2004). The non-depositional fabric shown by the Kuuvik Formation possibly reflects the "teepee" structure of the stromatolites (Figs. 6, 10). $\delta^{13}C$ values of the Kuuvik Formation are comparable to those obtained from the Pethei Group in the Great Slave Basin (Whittaker et al., 1998; Hotinski et al., 2004), and consistent with typical Paleoproterozoic values (Cramer and Jarvis, 2020). Therefore, we interpret that the carbon isotopes reflect primary values. $\delta^{18}O$ values of the Kuuvik Formation are low and likely affected by meteoric diagenesis which is commonly observed in ancient carbonates (Banner and Hanson, 1990). Results of the thermal demagnetization shows that the LTC-MTCs of the samples are successfully removed (Fig. 8). Plus, the inverse baked contact test is positive, and the antipodal directions were observed in multiple sites (Fig. 9). Overall, we interpret that the ChRMs of the samples were acquired during the rock deposition or dyke intrusion, and remain primary since then.

5.2 Paleopole comparisons among the circum-Slave basins, and the complexities of the Coronation loops

Adding the paleopoles obtained by this study, the Coronation loops seem to become even more complicated than before (Fig. 11), and more loops are required to connect the APWP. The prominent feature that all Orosirian paleopoles are distributed along a girdle that is

~90° away from the Slave craton still persists (Fig. 11). It is difficult to explain the Coronation loops by modern plate tectonic style since the frequent back-and-forth spinning of the Slave craton is quite unusual and the required speed is too rapid. Below, we compare the paleopoles from the correlative units from the circum-Slave basins, and discuss the possible factors that could contribute to the complexities of the Coronation loops.

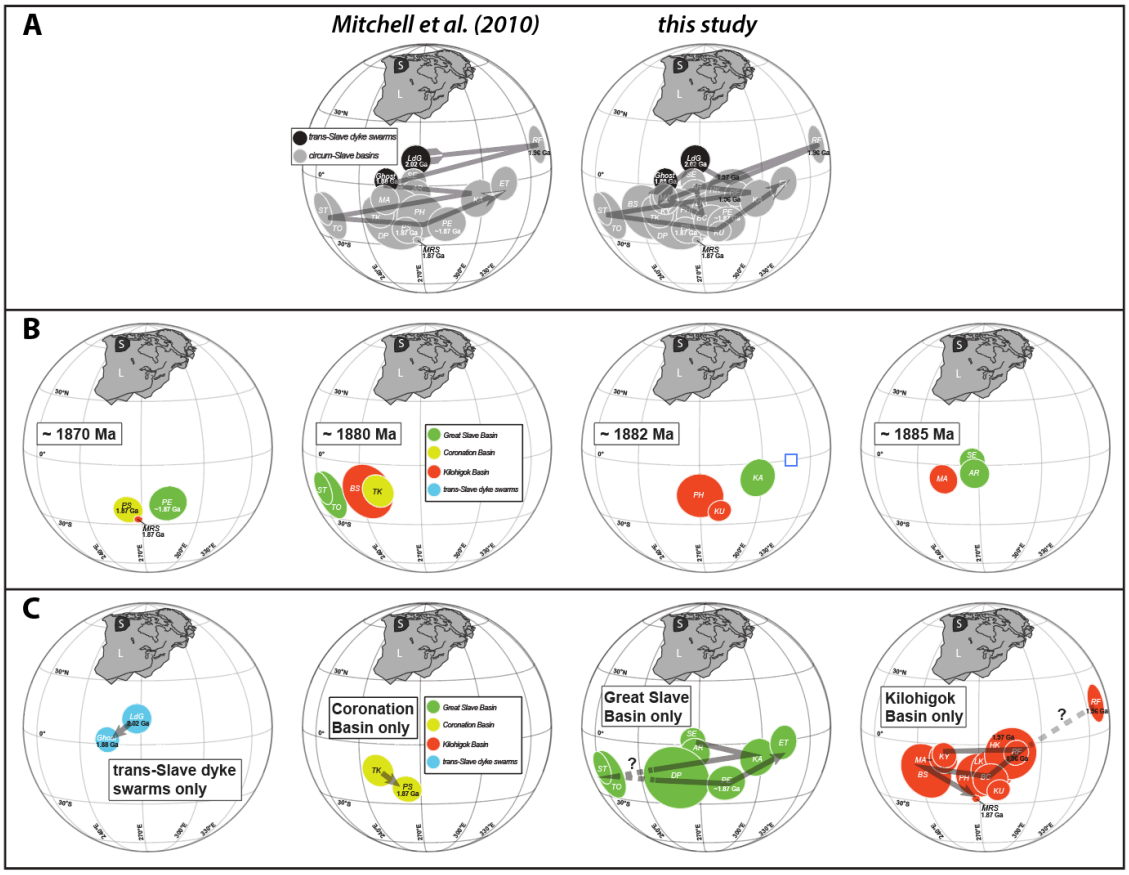

Figure 11. (A) Coronation loops before and after adding the new results of this study. (B) Comparisons of the correlative paleopoles from the three circum-Slave basins. (C) Orosirian paleopoles from the trans-Slave mafic dyke swarms, and from each circum-Slave basin. To avoid potential circularity of our discussion, no regional local rotations (i.e., Mitchell et al., 2010; Gong et al., 2018) were applied to paleopoles in this figure. L =

Laurentia, S = Slave. Question marks and the dashed lines indicate that poles from the Rifle (RF), Stark (ST,) and Tochatwi (TO) Formations are considered likely unreliable.

Firstly, influences from the secular variation of the geomagnetic field and a non-geocentric-axial-dipole (GAD) field scenario should be neglectable. It is possible that the paleopoles obtained from the ~1870 Ma Pearson basalt, Mara River sills and Peninsular sills have not adequately averaged out the secular variation (Irving and McGlynn, 1979; Evans and Hoye, 1981; Gong et al., 2018). However, these units do not signify the paleopole spread on the Coronation loops (Fig. 11). For poles from redbeds, given their typically low sedimentation rates, secular variations should be averaged out. Besides, the presence of antipodal directions indicate that the geomagnetic field should not be that different from a GAD geometry.

Apart from the outstanding differences in the declinations of these Orosirian paleopoles, it is noticeable that the inclinations of trans-Slave dyke swarms are steeper (~15°) than those from the sedimentary units (Fig. 11). The slight inclination differences could be explained by small age differences or little latitudinal plate movements. However, the inclination difference is also very likely due to the inclination shallowing effect on sedimentary rocks (Kodama, 2012). Until now, no study has tried to correct for the inclination shallowing effect on the Orosirian paleomagnetic data of the Slave craton. There are two commonly used correction methods: one is the E/I method developed by Tauxe and Kent (2004), and the other is the anisotropy-based method advocated by Kodama (2012). The E/I method of Tauxe and Kent (2004) is straightforward and easy to employ, but it requires large dataset

(usually >100 sites and >20 samples per site) to achieve a reasonable representation of the secular variation distribution pattern (Tauxe and Kent, 2004). Orosirian paleopoles from the Slave craton suffer from low number of samples (summarized by Gong et al., 2018), making it inappropriate to use the E/I method. The anisotropy-based method of Kodama (2012) usually requires extensive measurements of remanence anisotropy or redepositional experiments. These measurements need specific laboratory setups and techniques, which are not always available in typical paleomagnetic labs. Nonetheless, it should be pointed out that the Slave craton was at low latitudes during Orosirian time, where the inclination shallowing effect is not severe compared to the mid-latitudes (King, 1955). Therefore, even without the correction, it should not be a big concern, and these poles should still be useful for paleogeographic reconstructions, especially given that there are contemporaneous igneous paleopoles available to gauge the amount of inclination shallowing effect (Fig. 11).

Mitchell et al. (2010) noticed that the angle between the conjugated McDonald-Bathurst faults is 84°, which is 24° larger than the prediction based on the Coulomb theory (Anderson, 1951). Therefore, Mitchell et al. (2010) suggested that the conjugate McDonald-Bathurst faults experienced 24° outward rotation due to the far field compressional force of the Wopmay Orogen in the west (Fig. 1). To restore the outward rotation back, Mitchell et al. (2010) applied 12° counterclockwise (CCW) rotation for poles from the Kilohigok Basin and 12° clockwise (CW) rotation for poles from the Great Slave Basin. These basin-scale rotations would bring some correlative poles from the three circum-Slave basins closer. For example, the Peacock Hill and Kuuvik poles from the Kilohigok Basin are ~30° away from the Kahochella pole from the Great Slave Basin (Fig.

11; Table 4). These poles would fall on top of each other after the rotation (Fig. 11; also see Fig. 6 in Mitchell et al., 2010). Also, the ~1870 Ma Mara River sill, Pearson basalt, and Peninsular sill poles are closer after rotation (see Fig. 6 in Mitchell et al., 2010). However, after the rotation of Mitchell et al. (2010), the Stark and Tochatwi poles become even more distant from the correlative Brown Sound and Takiyuak poles (Fig. 11; also see Fig. 6 in Mitchell et al., 2010), meaning their difference may not be resolved by the basin-scale rotation.

Bingham and Evans (1976) and Irving et al. (2004) proposed that the shearing of the McDonald and Bathurst faults could cause the localized vertical-axis rotation of small blocks, which could influence some poles in the Coronation loops. Gong et al. (2018) directly tested this idea by sampling the ~1870 Ma Pearson basalt from areas with different structural attitudes from the Great Slave Basin. Gong et al. (2018) found a strong correlation between bedding strike and declination, which support the existence of local-scale vertical-axis rotation in the Great Slave Basin. The amount of rotation could be substantial, up to 65° (Gong et al., 2018). Since the sense of the McDonald fault is dextral (Fig. 1), the block needs to be rotated CCW in order to restore the vertical-axis rotation. Gong et al. (2018) suggested that the Stark and Tochatwi poles could result from this local-scale vertical-axis rotation, which, if restored ~30° CCW, could shift the poles eastward and align them with the correlative Brown Sound and Takiyuak poles (Fig. 11; Table 4). We need to point out that the vertical-axis rotation occurs locally and should be carefully examined on a case-by-case basis. The Rifle pole of Evans and Hoye (1981) lies far away to the east, and could be potentially explained by local vertical-axis rotation by proximity

to the sinistral Bathurst fault. However, according to the geological map of Campbell and Cecile (1976), the sampling sites of the Rifle Formation in Evans and Hoye (1981) are structurally coherent and no major fault zones are observed, unlike the complicated McDonald fault system in the Great Slave Basin (Figs. 1, 4). In addition, large declination change is also seen within the homoclinal sections of the Rifle Formation (GB4, GB5) in our study, which will be discussed below.

Another explanation for the Coronation loops is the IITPW model proposed by Mitchell et al. (2010). During IITPW events, small mass anomalies would cause the Earth's maximum and intermediate inertia axes to interchange, which manifests as the wholesale rotation of the silicate Earth along the minimum inertia axis (Evans, 1998). If Slave craton was located close to Earth's minimum inertia axis during the Orosirian time, the IITPW events would lead to substantial spin motions of the Slave craton, manifesting as substantial declination variations in paleomagnetic directions. The IITPW model could be supported by our new results from the ~1963 Ma Rifle Formation. We observed large (~60°) declination variations from two parallel and homoclinal Rifle sections (Fig. 9). When we consider the antipodal directions entirely in the SE polarity for the sake of comparison, they show a continuous and progressive declination change with respect to the stratigraphy (Fig. 12). This feature is best presented by Section GB5; data from Section GB4 are a little noisier but also shows a similar trend (Fig. 12). Small differences in the parallel sections could result from the difference in the sedimentation rates given that these sections are close to the flexural arch (Figs. 4, 5). The Rifle results from the study of Evans and Hoye (1981) also show large declination variations, but unfortunately there is no information regarding

the stratigraphic level of their samples, thus a similar analysis cannot be conducted. But the mean directions between our Rifle results and those of Evans and Hoye (1981) are quite different (Fig. 11; Table 4). It could be that the stratigraphic levels of our samples are consistently different from those of Evans and Hoye (1981). We suggest a resampling of Evans and Hoye (1981)'s sections as well as new sampling of the Rifle Formation from the much thicker sections in the Tinney Hills area (Grotzinger et al., 1989) to capture the declination changes of the Rifle Formation more completely (Figs. 4, 5). Before such proposed final verification, data from the Rifle Formation might be taken with caution and not used in paleogeographic reconstructions (e.g., Lubnina et al., 2017).

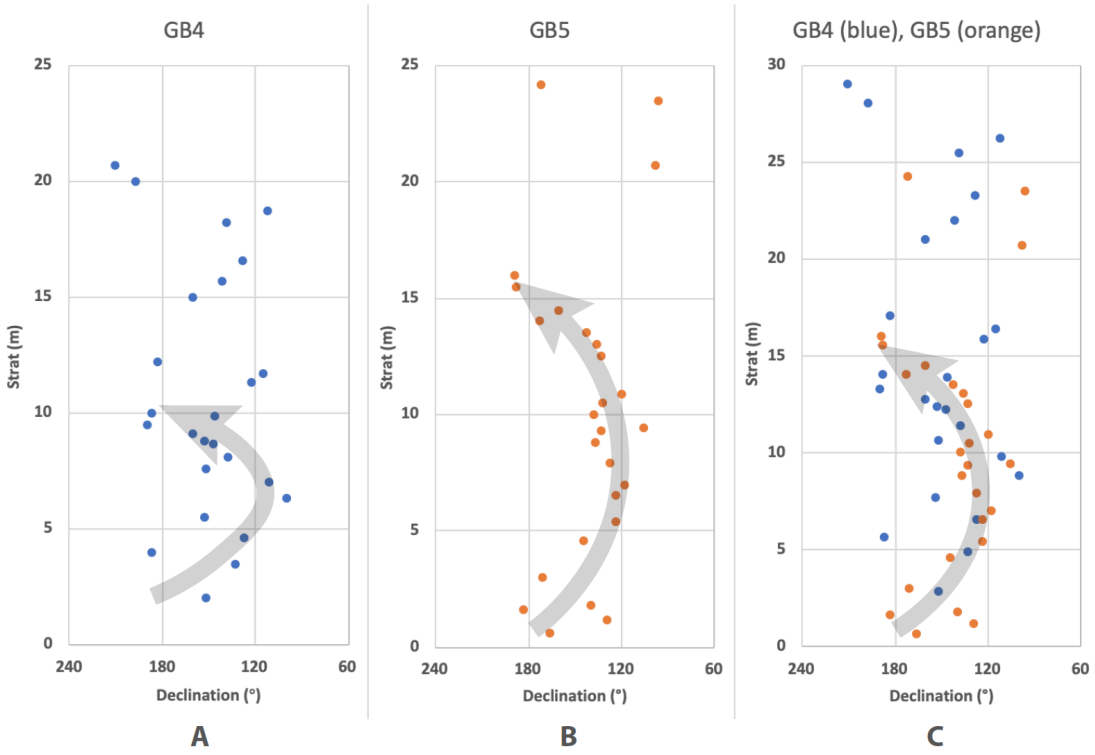

Figure 12 Declination variations against stratigraphy of the Rifle Formation. Declinations were flipped to one polarity. Grey arrows highlight the large and consistent declination variations. (A) Sections GB4. (B) Section GB5. (C) Comparison between two sections.

Section GB4 was stretched with a factor of 1.4 to match Section GB5. Since both sections could be correlated at the bottom and top lithologically, the stretch factor reflects the slight difference in local sedimentation rates.

Nevertheless, even if the Rifle pole is excluded, and to be more conservative, if the Stark and Tochatwi poles are excluded as well (Gong et al., 2018), the Coronation loops still have an arc length of more than 60°. Antonio et al. (2017) compiled the Orosirian paleomagnetic data globally and noticed that poles from Superior craton, India, Kalahari, Amazonia, and others also show a girdle distribution. Antonio et al. (2017, 2021) propose that global IITPW events at ~1880-1860 Ma are so far the best way to explain the Orosirian paleomagnetic data from multiple cratons. Since IITPW should be a global event, predictions can be made for future tests. For example, the plates located near to the minimum inertia axis should have changes predominately in their orientation, while the plates far away from the minimum inertia axis should have great changes in their paleolatitudes, and experience profound transient sea level changes associated with the IITPW (Mound et al., 1999).

All in all, the Coronation loops and the Orosirian paleomagnetic data of the Slave craton are complicated. We suggest this level of complexity may be caused by a combination factors, for example basin-scale rotation, localized vertical-axis rotation in fault zones, as well as IITPW; and IITPW could likely be the predominant factor for creating the Coronation loops.

6. Summary and future work

(1) By paleomagnetic and rock magnetic survey of the Goulburn Supergroup of the Kilohigok Basin, we provide a new suite of Orosirian paleopoles for the Slave craton (Tables 3, 4), largely complementing the previous work of Evans and Hoye (1981).

(2) With the addition of our new results, paleopoles from the three circum-Slave basins could be better compared to facilitate the understanding of the rapid back-and-forth swinging pattern of the Coronation loops.

(3) By a careful examination of the possible causes, we suggest that the complexity of the Coronation loops could result from a combination of factors, for example basin-scale rotation, localized vertical-axis rotation in fault zones, and IITPW. While regional and local rotations could affect a few poles, we suspect that IITPW likely controls the overall pattern of the Coronation loops. IITPW is also able to explain the aberrant paleomagnetic directions observed globally, including Superior craton, India, Kalahari, and Amazonia (Mitchell et al., 2010; Antonio et al., 2017).

(4) Specifically, the Rifle Formation shows progressive changes in declination with respect to stratigraphy in two parallel and homoclinal sections, which bolsters the IITPW interpretation of the Coronation loops. However, the Rifle Formation we studied yields a mean paleomagnetic direction substantially different from the previous results of Evans and Hoye (1981). To understand this discrepancy, it is necessary to resample the sections of Evans and Hoye (1981) to place their data in stratigraphic context, as well as sampling

the thicker sections in the Tinney Hills area to better characterize declination changes within the Rifle Formation.

(5) Compared with the Great Slave and Kilohigok Basins, the Coronation Basin in the west is apparently undersampled. Only two poles from the Takiyuak Formation and Peninsular sills are available, and there are no paleomagnetic data from older successions of the Coronation Supergroup. Therefore, the Coronation Basin can be the focus for future studies. Also, the chronostratigraphy and correlation of the circum-Slave basins need to be better constrained by additional geochronological studies.

Acknowledgments

We thank Alessandro Ielpi and Holly Steenkamp for their help in field logistics, and Page Burt, Colin Fraser, and the First Nations community of the Bathurst Inlet for field assistance. Nunavut Research Institute, Nunavut Impact Review Board, and Nunavut Water Board are acknowledged for granting research permission. Brad Erkkila is thanked for carbon and oxygen isotope measurements. Ross Mitchell is thanked for discussion on Slave geology and for help with crafting Figure 3. Z. Gong acknowledges supports from the GSA Graduate Research Grant and GSA Geophysics Division Student Research Award, and D. Evans acknowledges support from Yale University.

Table 1 Summary of the sample information of this study. Bedding strikes were measured following the right-hand rule (RHR). Slat/Slon = site latitude/longitude, N = number of samples.

Group	Formation	Section/Site	Slat (°N)	Slon (°W)	Section thickness (m)	N	Mean Strike/Dip (true north)	Lithology
	Tinney Cove	TC2	66.9114	107.9996	2.0	12	147°/47°	red siltstone
		TC1	66.9047	108.0023	–	24	140°/36°	conglomerate
	Mara River sills	Studied by Evans and Hoye (1981)						
Bathurst	Amagok	Not yet sampled						
	Brown Sound	BS3	66.9565	107.8884	–	15	164°/42°	doleritic dyke/baked red siltstone
		BS2	66.9553	107.8833	29.0	10	163°/73°	red siltstone
		BS1	66.9627	107.8858	11.5	9	138°/36°	red siltstone
Wolverine	Kuuvik	KV1	66.9613	107.8817	1.5	14	159°/21°	stromatolitic dolomite
	Peacock Hill	Studied by Evans and Hoye (1981)						
Bear Creek	Quadyuk	Not yet sampled						
	Mara	Studied by Evans and Hoye (1981)						
	Burnside	MP2	66.9631	107.7598	–	19	175°/26°	conglomerate
		MP1	67.0069	107.7146	11.0	11	149°/25°	red siltstone
	Link	BC3	66.5600	107.4744	–	16	194°/37°	conglomerate
		BC2	66.5599	107.4714	34.0	26	177°/24°	red siltstone
		BC1	66.5544	107.4602	2.0	12	100°/25°	red siltstone
	Beechey	GB6	66.9912	107.5057	15.5	18	132°/14°	red siltstone
	Rifle	GB5	66.9056	107.4939	24.5	35	151°/13°	maroon mudstone
		GB4	66.9524	107.4028	22.0	39	122°/13°	maroon mudstone
	Hackett	GB3	66.9812	107.4485	4.5	10	140°/27°	purple-brown mudstone
		GB2	66.9824	107.4396	3.5	10	175°/12°	red mudstone
Kimerot	Peg	Not yet sampled						
	Kenyon	GB1	66.9819	107.4269	22.0	17	173°/22°	quartzite

Table 2 Results of anisotropy of magnetic susceptibility (AMS). N = number of samples, K_m = mean magnetic susceptibility, stdev = standard deviation, L = lineation, F = foliation, P_j = degree of anisotropy, T = Jelinek shape parameter.

Formation	Section	N	K_m (SI)	K_m stdev	L	F	P_j	T
Tinney Cove	TC2	12	5.06E-05	1.64E-05	1.009	1.017	1.027	0.327
Brown Sound	BS2	10	3.41E-04	1.98E-05	1.012	1.013	1.026	0.017
Link	BC2	26	3.83E-04	8.84E-05	1.013	1.021	1.035	0.175
	BC1	12	3.76E-04	3.19E-05	1.015	1.014	1.030	-0.057
Beechey	GB6	18	3.73E-04	4.35E-05	1.003	1.075	1.090	0.914
Rifle	GB5	35	2.33E-04	3.24E-05	1.004	1.024	1.030	0.614
	GB4	39	2.56E-04	2.58E-05	1.010	1.020	1.030	0.295
Hackett	GB3	10	1.79E-04	2.74E-05	1.007	1.006	1.013	-0.066
	GB2	10	2.98E-05	2.33E-05	1.009	1.024	1.035	0.422
Kenyon	GB1	17	8.80E-05	3.42E-05	1.007	1.006	1.013	-0.124

Table 3 Summary of paleomagnetic results. Abbreviations: comb. = combined, Slat/Slon = site latitude/longitude, n = number of samples used in calculating mean directions, N = number of samples subjected to thermal demagnetization and measured, Dec_g/Inc_g = mean declination/inclination in geographic coordinates, Dec_s/Inc_s = mean declination/inclination in stratigraphic coordinates, α_{95} = radius of 95% confidence cone of the mean direction, k = precision parameter, Plat/Plon = paleopole latitude/longitude, A_{95} = radius of 95% confidence cone of the paleomagnetic pole (geometric mean of virtual geomagnetic pole's elliptical semi-axes dp, dm).

Formation	Section	Slat (°N)	Slon (°W)	n/N	Dec_g (°)	Inc_g (°)	α_{95} (°)	Dec_s (°)	Inc_s (°)	α_{95} (°)	k	Plat (°N)	Plon (°E)	A_{95} (°)
Brown Sound	BS1, BS2 comb.	66.96	107.89	8/19	164.8	24.2	18.3	189.3	17.2	18.3	10.1	-14.0	242.6	13.6
Kuuvik	KV1	66.96	107.88	8/14	337.1	10.4	7.7	334.6	3.8	7.7	52.7	-22.6	279.8	5.5
Link	BC1, BC2 comb.	66.55	107.46	19/38	152.3	17.7	11.7	158.1	14.4	12.9	7.7	-14.5	275.0	9.5
Beechey	GB6	66.99	107.51	11/18	155.9	12.3	11.0	158.0	8.6	11.3	17.3	-17.1	275.4	8.1
Rifle	GB4, GB5 comb.	66.95	107.40	54/74	137.7	26.7	7.5	143.8	27.6	7.3	8.0	-4.2	287.5	5.9
Hackett	GB2, GB3 comb.	66.98	107.44	8/20	140.1	20.3	16.3	146.3	27.8	15.3	14.1	-4.7	285.1	12.4
Kenyon	GB1	66.98	107.43	7/17	164.7	29.7	8.0	178.9	32.7	7.1	73.2	-5.3	253.6	6.0

Table 4 Orosirian paleopoles for Slave craton. Plat/Plon = paleopole latitude/longitude, A_{95} = radius of 95% confidence cone of the paleomagnetic pole. Fm. = Formation, Grp. = Group, correl. = stratigraphic correlation. Note the directional difference of the Rifle Formation between this study and Evans and Hoye (1981)' study (italicized).

Rock unit	Abbrevia-tion	Age (Ma)	Plat (°N)	Plon (°E)	A_{95}	Paleomagnetic references	Geochronological references
Mafic dyke swarms							
Ghost dykes	Ghost	1887-1884	2.0	254.0	6.0	Buchan et al. (2016)	Buchan et al. (2016)
Lac de Gras dykes	LdG	2027-2023	12.0	268.0	7.0	Buchan et al. (2009)	Buchan et al. (2009)
Coronation Basin							
Peninsular sills	PS	1871 ± 1	-22.0	263.0	7.0	Irving and McGlynn (1979)	Buchan et al. (2010)
Takiyuak Fm.	TK	~1885-1870	-13.0	249.0	8.0	Irving and McGlynn (1979)	correl. by Michell et al. (2010)
Great Slave Basin							
Et-Then Grp.	ET	~1780	-1.0	312.0	8.0	Irving et al. (1972)	correl. by Michell et al. (2010)
Pearson basalt (A)	PE	~1870	-19.0	283.0	9.0	McGlynn and Irving (1978)	correl. by Michell et al. (2010)
Tochatwi Fm.	TO	1885-1870	-18.0	216.0	12.0	Evans and Bingham (1976)	correl. by Michell et al. (2010)
Stark Fm.	ST	1885-1870	-15.0	212.0	8.0	Bingham and Evans (1976)	correl. by Michell et al. (2010)
Douglas Peninsula Fm.	DP	1885-1870	-17.0	258.0	16.0	Irving and McGlynn (1979)	correl. by Michell et al. (2010)
Kahochella (K) Grp.	KA	1882 ± 4	-7.0	298.0	9.0	Reid et al. (1981)	correl. by Michell et al. (2010)
Seton (C) volcanics	SE	1885 ± 5	2.0	267.0	6.0	Irving and McGlynn (1979)	correl. by Michell et al. (2010)
Akaitcho River Fm.	AR	1885 ± 5	-4.0	268.0	7.0	Evans et al. (1980)	correl. by Michell et al. (2010)
Kilohigok Basin							
Mara River sills	MRS	1870 ± 1	-27.0	268.0	0.0	Evans and Hoye (1981)	Buchan et al. (2010)

Brown Sound Fm.	BS	1885-1870	-14.0	242.6	13.6	this study	correl. by Michell et al. (2010)
Kuuvik Fm.	KU	1885-1870	-22.6	279.8	5.5	this study	correl. by Michell et al. (2010)
Peacock Hills Fm.	PH	1882 ± 4	-15.0	270.0	11.0	Evans and Hoye (1981)	correl. by Michell et al. (2010)
Mara Fm.	MA	1885 ± 5	-7.0	253.0	7.0	Evans and Hoye (1981)	correl. by Michell et al. (2010)
Link Fm.	LK		-14.5	275.0	9.5	this study	
Beechey Fm.	BC		-17.1	275.4	8.1	this study	
Rifle Fm.	*RF*	*1963 ± 6*	*14.0*	*341.0*	*9.0*	*Evans and Hoye (1981)*	*Bowring and Grotzinger (1992)*
Rifle Fm.	RF	1963 ± 6	-4.2	287.5	5.9	this study	Bowring and Grotzinger (1992)
Hackett Fm.	HK	1969 ± 1	-4.7	285.1	12.4	this study	Bowring and Grotzinger (1992)
Kenyon Fm.	KY		-5.3	253.6	6.0	this study	

References

Anderson, E. M. (1951). The dynamics of faulting and dyke formation with applications to Britain. Oliver and Boyd. White Plains, NY, 206 pp.

Antonio, P. Y. J., D'Agrella-Filho, M. S., Trindade, R. I., Nedelec, A., de Oliveira, D. C., da Silva, F. F., ... & Lana, C. (2017). Turmoil before the boring billion: paleomagnetism of the 1880–1860 Ma Uatumã event in the Amazonian craton. *Gondwana Research*, 49, 106-129.

Antonio, P. Y. J., D'Agrella-Filho, M. S., Nédélec, A., Poujol, M., Sanchez, C., Dantas, E. L., Dall'Agnol, R., Teixeira, M. F. B., Proietti, A., Martínez Dopico, C. I., Oliveira, D. C., Silva, F. F., Marangoanha, B., & Trindade, R. I. F. (2021). New constraints for paleogeographic reconstructions at ca. 1.88 Ga from geochronology and paleomagnetism of the Carajás dyke swarm (eastern Amazonia). *Precambrian Research*, 353, 106039.

Banner, J. L., & Hanson, G. N. (1990). Calculation of simultaneous isotopic and trace element variations during water-rock interaction with applications to carbonate diagenesis. *Geochimica et Cosmochimica Acta*, 54(11), 3123-3137.

Bingham, D. K., & Evans, M. E. (1976). Paleomagnetism of the Great Slave Supergroup, Northwest Territories, Canada: the Stark Formation. *Canadian Journal of Earth Sciences*, 13(4), 563-578.

Bleeker, W. (2002). Archaean tectonics: a review, with illustrations from the Slave craton. *Geological Society, London, Special Publications*, 199(1), 151-181.

Bleeker, W. (2003). The late Archean record: a puzzle in ca. 35 pieces. *Lithos*, 71(2-4), 99-134.

Borradaile, G. J., & Jackson, M. (2004). Anisotropy of magnetic susceptibility (AMS): magnetic petrofabrics of deformed rocks. *Geological Society, London, Special Publications*, 238(1), 299-360.

Bowring, S. A., Schmus, W. V., & Hoffman, P. F. (1984). U–Pb zircon ages from Athapuscow aulacogen, east arm of Great Slave Lake, NWT, Canada. *Canadian Journal of Earth Sciences*, 21(11), 1315-1324.

Bowring, S. A., & Grotzinger, J. P. (1992). Implications of new chronostratigraphy for tectonic evolution of Wopmay Orogen, Northwest Canadian Shield. *American Journal of Science*, 292(1), 1-20.

Buchan, K. L., Mortensen, J. K., & Card, K. D. (1994). Integrated paleomagnetic and U-Pb geochronologic studies of mafic intrusions in the southern Canadian Shield: Implications for the early Proterozoic polar wander path. *Precambrian Research*, 69(1-4), 1-10.

Buchan, K. L., Mertanen, S., Park, R. G., Pesonen, L. J., Elming, S. Å., Abrahamsen, N., & Bylund, G. (2000). Comparing the drift of Laurentia and Baltica in the Proterozoic: the importance of key palaeomagnetic poles. *Tectonophysics*, 319(3), 167-198.

Buchan, K. L., LeCheminant, A. N., & van Breemen, O. (2009). Paleomagnetism and U-Pb geochronology of the Lac de Gras diabase dyke swarm, Slave Province, Canada: implications for relative drift of Slave and Superior provinces in the Paleoproterozoic. *Canadian Journal of Earth Sciences*, 46(5), 361-379.

Buchan, K. L., Ernst, R. E., Bleeker, W., Davis, W. J., Villeneuve, M., van Breemen, O., Hamilton, M. A., & Söderlund, U. (2010). Proterozoic Magmatic Events of the Slave

Craton, Wopmay Orogen and Environs. Geological Survey of Canada, Open File 5989, CD-ROM, 1 poster and 25 p. report.

Buchan, K. L. (2013). Key paleomagnetic poles and their use in Proterozoic continent and supercontinent reconstructions: A review. *Precambrian Research*, 238, 93-110.

Buchan, K. L., Mitchell, R. N., Bleeker, W., Hamilton, M. A., & LeCheminant, A. N. (2016). Paleomagnetism of ca. 2.13-2.11 Ga Indin and ca. 1.885 Ga Ghost dyke swarms of the Slave craton: Implications for the Slave craton APW path and relative drift of Slave, Superior and Siberian cratons in the Paleoproterozoic. *Precambrian Research*, 275, 151-175.

Campbell, F. H. A., & Cecile, M. P. (1975). Report on the geology of the Kilohigok Basin. Goulburn Group, Bathurst Inlet: NWT Geological Survey of Canada, Paper, 75-1.

Campbell, F. H. A., & Cecile, M. P. (1976) Geology of the Kilohigok Basin, Bathurst Inlet, N.W.T. Geological Survey of Canada, Open File 332, 1:500 000 Scale Map.

Cramer, B. D., & Jarvis, I. (2020). Carbon Isotope Stratigraphy. In Geologic Time Scale 2020 (pp. 309-343). Elsevier.

Davis, W. J., Bleeker, W., Hulbert, L., & Jackson, V. (2004). New geochronological results from the Slave Province Minerals and Geoscience Compilation and Synthesis Project. In Geological Science of Canada Northern Resources Program: Yellowknife Geoscience Forum (Abstracts of Talks and Posters), p. 20.

Evans, M. E., & Bingham, D. K. (1976). Paleomagnetism of the Great Slave Supergroup, Northwest Territories, Canada: the Tochatwi Formation. *Canadian Journal of Earth Sciences*, 13(4), 555-562.

Evans, M. E., Hoye, G. S., & Bingham, D. K. (1980). The paleomagnetism of the Great Slave supergroup: the Akaitcho River formation. *Canadian Journal of Earth Sciences*, 17(10), 1389-1395.

Evans, M. E., & Hoye, G. S. (1981). Paleomagnetic results from the lower Proterozoic rocks of Great Slave Lake and Bathurst inlet areas, Northwest Territories. Proterozoic Basins of Canada: Geological Survey of Canada Paper, 81-10, 191-202.

Evans, D. A. (1998). True polar wander, a supercontinental legacy. *Earth and Planetary Science Letters*, 157(1-2), 1-8.

Fraser, J. A., & Tremblay, L. P. (1969). Correlation of Proterozoic strata in the northwestern Canadian Shield. *Canadian Journal of Earth Sciences*, 6(1), 1-9.

French, J. E., & Heaman, L. M. (2010). Precise U–Pb dating of Paleoproterozoic mafic dyke swarms of the Dharwar craton, India: implications for the existence of the Neoarchean supercraton Sclavia. *Precambrian Research*, 183(3), 416-441.

Gong, Z., Xu, X., Evans, D. A., Hoffman, P. F., Mitchell, R. N., & Bleeker, W. (2018). Paleomagnetism and rock magnetism of the ca. 1.87 Ga Pearson Formation, Northwest Territories, Canada: A test of vertical-axis rotation within the Great Slave basin. *Precambrian Research*, 305, 295-309.

Grotzinger, J. P., McCormick, D. S., & Pelechaty, S. M. (1987). Progress report on the stratigraphy, sedimentology and significance of the Kimerot and Bear Creek groups, Kilohigok Basin, District of Mackenzie. Geological Survey of Canada, 87(1A), 219-238.

Grotzinger, J. P., Adams, R. D., McCormick, D. S., & Myrow, P. (1989). Sequence stratigraphy, correlations between Wopmay Orogen and Kilohigok Basin, and further

investigations of the Bear Creek Group (Goulburn Supergroup), District of Mackenzie, N.W.T. In: Current Research, Part C, Geological Survey of Canada, Paper 89-1C, 107-119.

Helmstaedt, H. (2009). Crust-mantle coupling revisited: the Archean Slave craton, NWT, Canada. *Lithos*, 112, 1055-1068.

Hoffman, P. F. (1980). Geology and tectonics, East Arm of Great Slave Lake, District of Mackenzie, Geological Survey of Canada Map 1625A, pp. Scales 1:250,000 (geology) and 1:500,000 (tectonics).

Hoffman, P. F. (1988). United plates of America, the birth of a craton: Early Proterozoic assembly and growth of Laurentia. *Annual Review of Earth and Planetary Sciences*, 16(1), 543-603.

Hoffman, P. F. (1989). Precambrian geology and tectonic history of North America. *The Geology of North America*, 447-512.

Hoffman, P. F., Bowring, S. A., Buchwaldt, R., & Hildebrand, R. S. (2011). Birthdate for the Coronation paleocean: age of initial rifting in Wopmay orogen, Canada. *Canadian Journal of Earth Sciences*, 48(2), 281-293.

Hotinski, R. M., Kump, L. R., & Arthur, M. A. (2004). The effectiveness of the Paleoproterozoic biological pump: A $\delta^{13}C$ gradient from platform carbonates of the Pethei Group (Great Slave Lake Supergroup, NWT). *Geological Society of America Bulletin*, 116(5-6), 539-554.

Ielpi, A., Michel, S., Greenman, J. W., & Lebeau, L. E. (2017). Stratigraphy, gamma-ray spectrometry and uranium prospectivity of the Kilohigok paleosol, Bear Creek Hills, western Nunavut. *Summary of Activities*, 37-48.

Irving, E., Park, J. K., & McGlynn, J. C. (1972). Paleomagnetism of the Et-Then Group and Mackenzie Diabase in the Great Slave Lake Area. *Canadian Journal of Earth Sciences*, 9, 744-755.

Irving, E., & McGlynn, J. C. (1979). Palaeomagnetism in the Coronation Geosyncline and arrangement of continents in the middle Proterozoic. *Geophysical Journal International*, 58(2), 309-336.

Irving, E., Baker, J., Hamilton, M., & Wynne, P. J. (2004). Early Proterozoic geomagnetic field in western Laurentia: implications for paleolatitudes, local rotations and stratigraphy. *Precambrian Research*, 129(3), 251-270.

Isachsen, C. E., & Bowring, S. A. (1994). Evolution of the Slave craton. *Geology*, 22(10), 917-920.

Jelinek, V. (1981). Characterization of the magnetic fabric of rocks. *Tectonophysics*, 79(3-4), T63-T67.

Jones, C. H. (2002). User-driven integrated software lives: "Paleomag" paleomagnetics analysis on the Macintosh. *Computers & Geosciences*, 28(10), 1145-1151.

King, R. F. (1955). The remanent magnetism of artificially deposited sediments. Geophysical Supplements to the Monthly Notices of the Royal Astronomical Society, 7(3), 115-134.

Kirschvink, J. L. (1980). The least-squares line and plane and the analysis of palaeomagnetic data. *Geophysical Journal International*, 62(3), 699-718.

Kirschvink, J. L., Kopp, R. E., Raub, T. D., Baumgartner, C. T., & Holt, J. W. (2008). Rapid, precise, and high-sensitivity acquisition of paleomagnetic and rock-magnetic

data: Development of a low-noise automatic sample changing system for superconducting rock magnetometers. *Geochemistry, Geophysics, Geosystems*, 9(5).

Kodama, K. P. (2012). Paleomagnetism of sedimentary rocks: Process and interpretation. John Wiley & Sons.

Lubnina, N. V., Pisarevsky, S. A., Stepanova, A. V., Bogdanova, S. V., & Sokolov, S. J. (2017). Fennoscandia before Nuna/Columbia: Paleomagnetism of 1.98–1.96 Ga mafic rocks of the Karelian craton and paleogeographic implications. *Precambrian Research*, 292, 1-12.

McCormick, D. S., & Grotzinger, J. P. (1992). Evolution and significance of an overfilled alluvial foreland basin: Burnside Formation (1.9 Ga), Kilohigok Basin, N.W.T., Canada. *Basin Research*, 4(3-4), 253-278.

McCormick, D. S., & Grotzinger, J. P. (1993). Distinction of marine from alluvial facies in the Paleoproterozoic (1.9 Ga) Burnside Formation, Kilohigok basin, N.W.T., Canada. *Journal of Sedimentary Research*, 63(3), 398-419.

McFadden, P. L., & McElhinny, M. W. (1988). The combined analysis of remagnetization circles and direct observations in palaeomagnetism. *Earth and Planetary Science Letters*, 87(1-2), 161-172.

McFadden, P. L., & McElhinny, M. W. (1990). Classification of the reversal test in palaeomagnetism. *Geophysical Journal International*, 103(3), 725-729.

McGlynn, J. C., & Irving, E. (1978). Multicomponent magnetization of the Pearson Formation (Great Slave Supergroup, NWT) and the Coronation loop. *Canadian Journal of Earth Sciences*, 15(4), 642-654.

Mitchell, R. N., Hoffman, P. F., & Evans, D. A. (2010). Coronation loop resurrected: Oscillatory apparent polar wander of Orosirian (2.05-1.8 Ga) paleomagnetic poles from Slave craton. *Precambrian Research*, 179(1), 121-134.

Mound, J. E., Mitrovica, J. X., Evans, D. A., & Kirschvink, J. L. (1999). A sea-level test for inertial interchange true polar wander events. *Geophysical Journal International*, 136(3), F5-F10.

Müller, R. D., Cannon, J., Qin, X., Watson, R. J., Gurnis, M., Williams, S., ... & Zahirovic, S. (2018). GPlates: building a virtual Earth through deep time. *Geochemistry, Geophysics, Geosystems*, 19(7), 2243-2261.

Reid, A. B., McMurry, E. W., & Evans, M. E. (1981). Paleomagnetism of the Great Slave Supergroup, Northwest Territories, Canada: multicomponent magnetization of the Kahochella Group. *Canadian Journal of Earth Sciences*, 18(3), 574-583.

Sheen, A. I., Heaman, L. M., Kjarsgaard, B., Ootes, L., Pearson, D. G., & Creaser, R. A. (2019). Athapuscow aulacogen revisited: geochronology and geochemistry of the 2046 Ma Union Island Group mafic magmatism, East Arm of Great Slave Lake, Northwest Territories, Canada. *Precambrian Research*, 321, 85-102.

Tauxe, L., & Kent, D.V. (2004). A simplified statistical model for the geomagnetic field and the detection of shallow bias in paleomagnetic inclinations: Was the ancient magnetic field dipolar? In: Channell, J.E.T., Kent, D.V., Lowrie, W., Meert, J. (Eds.), In: Timescales of the Paleomagnetic Field, Vol. 145. American Geophysical Union, Washington, D.C, pp. 101-116.

Whittaker, S. G., Sami, T. T., Kyser, T. K., & James, N. P. (1998). Petrogenesis of 1.9 Ga limestones and dolostones and their record of Paleoproterozoic environments. *Precambrian Research*, 90(3-4), 187-202.

Zijderveld, J. D. A. (1967). AC demagnetization of rocks: analysis of results. *Methods in Paleomagnetism*, 3, 254.

Part II

Paleogeographic Reconstruction of West African Craton in Proterozoic Supercontinents

Chapter 4

Constraints on the Precambrian paleogeography of West African Craton [1]

Zheng Gong [a] and David A. D. Evans [a]

[a] Department of Earth and Planetary Sciences, Yale University, New Haven, CT 06511, USA

---

[1] Chapter 4 published in Gong, Z. & Evans, D. A. D. (2021). Constraints on the Precambrian paleogeography of West African Craton. In: Pesonen, L. J., Salminen, J. M., Evans, D. A. D., Elming, S. Å. & Veikkolainen, T. (eds.), *Ancient Supercontinents and the Paleogeography of Earth*. Elsevier, in press.

Abstract

This chapter reviews the Precambrian paleogeography of West African Craton (WAC), which is critical for understanding the plate tectonics on early Earth and the configurations of Proterozoic supercontinents. We've summarized the geological history and paleoclimate indicators of WAC, and thoroughly evaluated the available paleomagnetic data. Although we found that WAC has essentially no highly reliable paleomagnetic data of pre-Ediacaran age, ubiquitous mafic dyke swarms could be promising targets for paleomagnetism. In this context, we compiled all high-precision ages pertaining to the mafic intrusions recognized in WAC, and constructed a magmatic barcode for global comparisons. Finally, various paleogeographic reconstruction models regarding the position of WAC in supercontinents Nuna/Columbia and Rodinia were presented and discussed. Because of the lack of robust data, WAC is poorly-constrained paleogeographically in Proterozoic supercontinents. We hope this review can provide a basic introduction with regard to the paleogeography of WAC in the Precambrian and advocate future studies.

1. Introduction

Paleogeography of cratonic pieces, and their amalgamations, fragmentations and interactions, are considered to have profoundly influenced the Earth's geological, biological and environmental cycles. One end-member scenario of paleogeographic evolution is that nearly all cratons assembled together to form supercontinents. Our knowledge regarding the configurations of supercontinents has been greatly improved, owing to increasing geological evidence discovered worldwide, advances in the visualization of kinematic reconstructions, and the inventions and improvements of field

and laboratory techniques. For Precambrian time, however, due to less preserved geological records, the configurations of supercontinents and drift histories of individual cratons are still highly debated. As one of the major cratons in the area of exposure (Fig. 1A), West African Craton (WAC) is an important component for global paleogeographic reconstructions. Yet, the Precambrian paleogeography of WAC and its relationships with other cratons are very loosely constrained due to the scarcity of robust paleogeographic indicators. In this contribution, we attempt to summarize available reconstruction models pertinent to WAC, including an overview of its tectonic history for intracratonic and global comparisons, a thorough evaluation of all available paleomagnetic data, and an update of its magmatic record. We hope this review could set the stage for future studies regarding the paleogeography of WAC in Precambrian time.

2. Geology of West African Craton

WAC is bounded on all sides by Pan-African orogens (Fig. 1B) that developed during late Neoproterozoic-Cambrian time. Boundaries are as follows: the South Atlas Fault to the north of the craton, Trans-Saharan Belt to the east, Bassarides/Mauritanides to the west, and to the south a Gondwana-inherited connection to the São Luís Block and Gurupi Belt that are now located in northern Brazil (Ennih and Liégeois, 2008). Basement rocks in WAC are exposed in three regions: Man-Leo Shield in the south, Reguibat Shield in the north, and Anti-Atlas Belt at the northernmost cratonic limit (Fig. 1B). Both Man-Leo and Reguibat Shields are characterized by Archean basement in the west and Paleoproterozoic basement in the east. In the Anti-Atlas Belt of Morocco, Paleoproterozoic basement is exposed within a number of inliers, and there is no Archean basement observed. Man-Leo

and Reguibat Shields are straddled by the Taoudeni Basin, which was initiated in late Mesoproterozoic time, and was possibly associated with extension caused by continental breakup along the craton's margins (Bertrand-Sarfati et al., 1991; Rooney et al., 2010). In the north, the Tindouf Basin lies between Reguibat Shield and Anti-Atlas Belt; it consists mostly of Phanerozoic sedimentary sequences but the oldest part in the north flank of the basin could potentially be correlated with early Neoproterozoic strata in the Taoudeni Basin (Bertrand-Sarfati et al., 1991). Here, we briefly review the geology of Man-Leo and Reguibat Shields and Anti-Atlas Belt in an attempt to draw temporal and spatial comparisons across WAC.

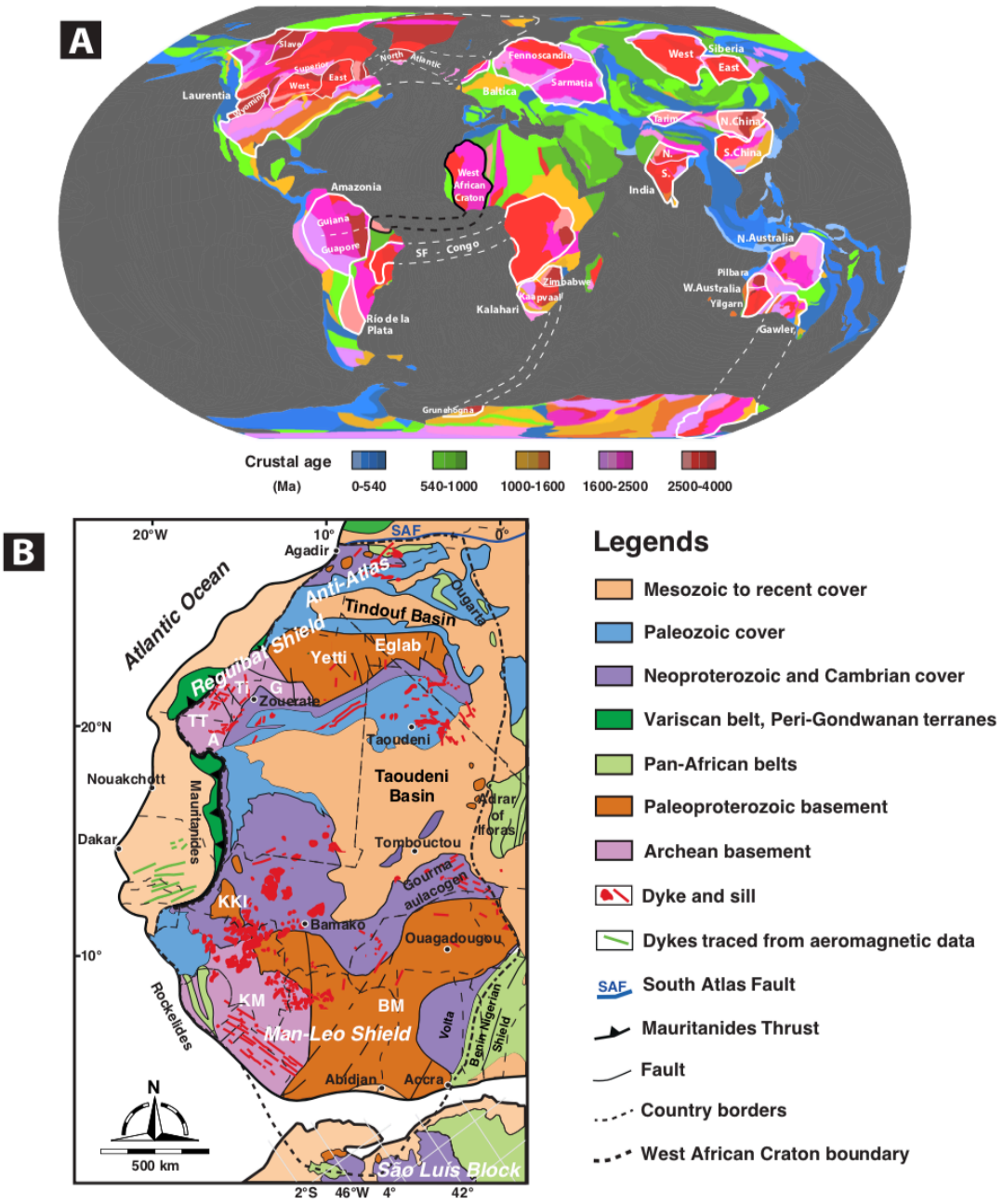

Figure 1 (A) Global age distribution of continental crust. White lines highlight major cratonic blocks. Black lines delineate the boundary of West African Craton, including the São Luís Block. SL = São Luís, SF = São Francisco. (B) Geological map of West African Craton. TT = Tasiast-Tijirit, A = Amsaga, Ti = Tiris, G = Ghallaman, KKI = Kedougou-

Kéniéba and Kayes inliers, KM = Kénéma-Man, BM = Baoulé-Mossi. Modified from Ennih and Liégeois (2008).

2.1 Man-Leo Shield

Archean basement of Man-Leo Shield, known as Kénéma-Man domain, crops out in Guinea, Sierra Leone, Liberia, and Ivory Coast (Fig. 1B). The oldest exposed rock is the 3.53 Ga granite-gneiss formation identified in Guinea (Thiéblemont et al., 2001). Afterwards, continental growth advanced through successive magmatism and accretion at 3.05–2.95 Ga (Leonian orogeny) and 2.85–2.75 Ga (Liberian orogeny) (Fig. 2). Paleoproterozoic basement (a.k.a. Birimian terranes) of Man-Leo Shield consists of Baoulé-Mossi domain mainly in Burkina Faso, Ghana, Togo, Ivory Coast, and Mali, the Kedougou-Kéniéba and Kayes inliers in Senegal, and the São Luís Block in Brazil. Paleoproterozoic basement is characterized by volcanic and siliciclastic successions of Birimian Supergroup, with numerous episodes of intrusions (Grenholm et al., 2019). Collision between Kénéma-Man and Baoulé-Mossi domains occurred at ~2.15 Ga through the Eburnean orogeny (Baratoux et al., 2011) along the Sassandra mylonite belt (Fig. 2), and was followed by syn- and post-orogenic granitic intrusions (Rocci et al., 1991). Subsequent cratonic stability was punctuated by localized mafic intrusions at 1.79–1.76 Ga, 1.57–1.52 Ga, and 0.91–0.85 Ga (Baratoux et al., 2019).

Epicratonic sedimentation began in the latest Mesoproterozoic in the Taoudeni Basin (Rooney et al., 2010), starting with the basal conglomerate to mark the erosional surface (Fig. 2). Subsequently, Char Group is dominated mostly by siliciclastic rocks with minor

carbonates and evaporites. Above Char Group is Atar Group, which is characterized by carbonates and shales. Overlying Atar Group is Assabet el Hassiane Group, which mainly consists of siliciclastic successions. Above a regional angular unconformity, a widespread layer of diamictite is (usually) correlated with the ca. 635 Ma Marinoan glaciation (Fig. 2). Atop the diamictite are the mainly siliciclastic Téniagouri and Falaise d'Atar Groups (Bertrand-Sarfati et al., 1991).

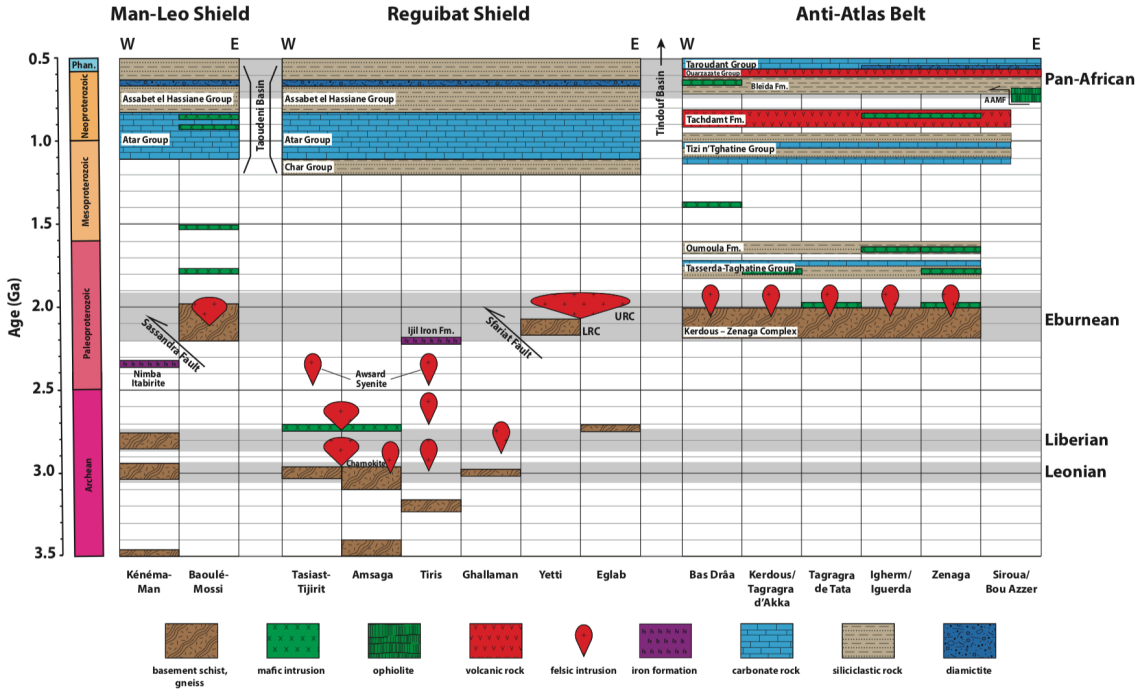

Figure 2 Time-space diagram demonstrating the spatial and tectonic relationships between the tectonostratigraphic units of West African Craton. LRC = Lower Reguibat Complex, URC = Upper Reguibat Complex, AAMF = Anti-Atlas Major Fault. Neoproterozoic dykes intruded basement rocks in Man-Leo Shield.

The ages of Taoudeni sequences are poorly constrained. Rb-Sr ages on clay minerals suggested that most if not all of the Taoudeni successions were Neoproterozoic (Clauer,

1976; Clauer et al., 1982; Clauer and Deynoux, 1987). But a recent Re-Os geochronological study from the organic-rich sediments in lower Atar Group yielded ages of 1109 ± 22 Ma and 1107 ± 12 Ma (Rooney et al., 2010), which would suggest Char and Atar Groups are ~200 Ma older than previously thought. The Mesoproterozoic ages are consistent with relatively muted $\delta^{13}C$ isotopic compositions (Kah et al., 2012). Mafic dykes, which could possibly be associated with the early-Neoproterozoic continental breakup, intruded Atar Group at 915 ± 7 Ma and 867 ± 16 Ma (Baratoux et al., 2019). The age of Assabet el Hassiane Group is suggested to be mid-Neoproterozoic because its lateral stratigraphic equivalent unit, the Aioun Group, contains a prominent Tonian (ca. 880 Ma) detrital-zircon population (Bradley et al., 2015). Above the ca. 635 Ma Marinoan-equivalent diamictite horizon, tuff beds in Téniagouri Group have been dated by U-Pb SHRIMP on zircon at ca. 610–605 Ma (see Álvaro et al., 2007).

2.2 Reguibat Shield

Archean basement of Reguibat Shield is mainly exposed in Western Sahara, northern Mauritania, and Mali, and is divided into four domains which are separated by faults: Amsaga in the southeast, Tasiast-Tijirit in the southwest, Tiris in the center, and Ghallaman in the northeast (Rocci et al., 1991; Key et al., 2008; Schofield et al., 2012) (Fig. 1B). Amsaga contains the 3.5–3.4 Ga crust (Auvray et al., 1992; Potrel et al., 1996) and is thought to represent the oldest crustal growth in the shield (Fig. 2). Later on, there was a charnockite intrusion at ~3.0 Ga, which marks the major granulite-facies metamorphic event between 3.2 Ga and 3.0 Ga (Potrel et al., 1998, Key et al., 2008). At ~2.7 Ga, granitic and gabbroic intrusions were emplaced coevally, and dykes of this age are observed with

a NE strike (Auvray et al. 1992; Potrel et al. 1998; Tait et al., 2013). Contemporaneous bimodal intrusions are also found in southern Tasiast-Tijirit across Tâçarât-Inemmaûdene Shear Zone (TISZ). In Tasiast-Tijirit, the earliest crustal materials, manifested by gneisses and granitic intrusions, are dated at ~3.0 Ga (Chardon, 1997; Key et al., 2008). Similarly-aged granite also intruded westernmost Amsaga near the TISZ (Key et al., 2008). There is a 2.46 Ga syenite in Awsard, northernmost Tasiast-Tijirit (Montero et al., 2014). In Tiris, the major intrusive events occurred at 3.0–2.9 Ga and 2.7–2.6 Ga (Schofield et al., 2012) and the younger 2.46 Ga syenitic suite is also observed (Montero et al., 2014). Massive Ijil Iron Formation is suggested to be ~2.2 Ga (Bronner and Chauvel, 1979). The Ghallaman sector is separated from Paleoproterozoic basement of Reguibat Shield by Sfariat Belt. The basement gneisses are dated at ~3.0 Ga, which was intruded by a ~2.9 Ga granite (Schofield et al., 2012). The boundary between Ghallaman and Tiris is not clearly defined due to younger sedimentary cover (Schofield et al., 2012).

Eburnean terranes occupy northeast Mauritania and southwest Algeria, exposed within the Paleoproterozoic Yetti and Eglab massifs (Fig. 1B). Yetti massif is characterized by a strongly folded 2.1 Ga volcano-sedimentary series, known as the Lower Reguibat Complex (LRC; Peucate et al., 2005) (Fig. 2). To the east, Eglab massif is mainly composed of 2.2 Ga foliated volcano-sedimentary rocks (Oued Souss series) and the younger 2.07 Ga syn- and post-orogenic felsic intrusions (Eglab and Aftout series), which are defined as Upper Reguibat Complex (URC; Peucat et al., 2005). Relict oceanic crust of ~2.7 Ga in age outcrops in west Eglab massif (Peucat et al., 2005). Paleoproterozoic basement rocks were thrust onto Archean basement of Reguibat Shield at ~2.07 Ga along the Sfariat Belt, but

only had minimal metamorphic reworking to reactivate biotite (Rocci et al., 1991). Thereafter, Reguibat Shield stabilized and cratonized, and no further history is recorded until Taoudeni deposition in the latest Mesoproterozoic (Rooney et al., 2010).

2.3 Anti-Atlas Belt

Paleoproterozoic basement rocks in Anti-Atlas Belt are located in Morocco, bounded by South Atlas Fault in the north and the Tindouf Basin in the south (Fig. 1B). The lithostratigraphic framework of Anti-Atlas Belt is well constructed by Thomas et al. (2004). Anti-Atlas Belt can be subdivided into two parts by the Anti-Atlas Major Fault (AAMF) (Fig. 2). Inliers southwest of AAMF contain ~2.2 Ga supracrustal schists, gneisses and migmatites, referred to as Kerdous-Zenaga Complex (Thomas et al., 2004). The metamorphic grade is generally lower towards the west. Younger granitic intrusions with ages around 2.05 Ga are ubiquitous in all inliers west of AAMF (Thomas et al., 2004). In Tagragra de Tata and Zenaga inliers, 2.04 Ga mafic dykes are also observed (Walsh et al., 2002; Kouyaté et al., 2013). The Kerdous-Zenaga Complex and subsequent magmatic suites are correlated with contemporaneous Eburnean events in Reguibat Shield. Following this cratonization, the next stratigraphic event indicates regional extension, as manifested by 1.75 Ga mafic dykes observed in Tagragra d'Akka, Iguerda and Zenaga inliers (Youbi et al., 2013). The Tasserda-Taghatine Group (quartzite and carbonates) and overlying Oumoula Formation (mainly quartzite) were deposited across several inliers, and that succession is cut by mafic intrusions, with ages of ca. 1.71 Ga in Igherm inlier (Ikenne et al., 2017) and ca. 1.65 Ga in Kerdous inlier (Ait Lahna et al., 2020). At ~1.41–1.38 Ga and ~0.88–0.85 Ga, mafic dykes intruded Bas Draa inlier, and Iguerda and Zenaga inliers,

respectively (Fig. 2; El Bahat et al., 2013; Söderlund et al., 2013a; Kouyaté et al., 2013), which might be associated with the breakup of supercontinents Nuna/Columbia and Rodinia, respectively. The Tizi n'Tghatine Group, which mainly consists of interbedded siliciclastics and carbonates, are suggested to be late Mesoproterozoic to early-Neoproterozoic in age (Bouougri et al., 2020; Ait Lahna et al., 2020). Extensive early-Neoproterozoic lava basalts and associated dykes (Tachdamt Formation) have been identified across several Anti-Atlas inliers (Fig. 2; Álvaro et al., 2014; Ait Lahna et al., 2020). In mid-Neoproterozoic time, obduction and arc accretion occurred along the AAMF, which involved Bou Azzer Group (ophiolites) and Saghro Group (volcanics and turbidites). The siliciclastic-dominated Bleïda Formation found in many inliers is likely mid-late Neoproterozoic in age (Bouougri et al., 2020; Ait Lahna et al., 2020). During the Pan-African orogeny, the Ouarzazate Group, which consists of thick volcano-sedimentary accumulations, extensively covered Anti-Atlas Belt (Thomas et al., 2002, 2004; Blein et al., 2014a, 2014b). Glacial deposits of ~590–580 Ma were also found in a few inliers, which could be equivalent to Gaskiers glaciation (Letsch et al., 2018). In early Cambrian time, thick carbonate rocks (Taroudant Group and correlative successions) were deposited across Anti-Atlas Belt and northern Tindouf Basin (Bertrand-Sarfati et al., 1991); these deposits include minor volcanogenic components in a likely rift setting (Pouclet et al, 2018).

Compilation of magmatic ages in Man-Leo and Reguibat Shields and Anti-Atlas Belt all show the significant 2.2–2.05 Ga peaks during Eburnean orogeny (Grenholm et al., 2019), which could indicate that the basement of WAC was formed by a series of accretion of Paleoproterozoic rocks to Archean nuclei in Man-Leo and Reguibat Shields; and shortly

afterwards, Anti-Atlas Belt was accreted to Reguibat Shield at the northern margin. The Taoudeni Basin onlaps both Man-Leo and Reguibat Shields, further demonstrating their connection before 1.1 Ga. Coeval ca. 1.76–1.75 Ga and ca. 0.88–0.85 Ga mafic magmatism in Man-Leo Shield and Anti-Atlas Belt provides additional evidence for a united WAC since the Paleoproterozoic (Fig. 2).

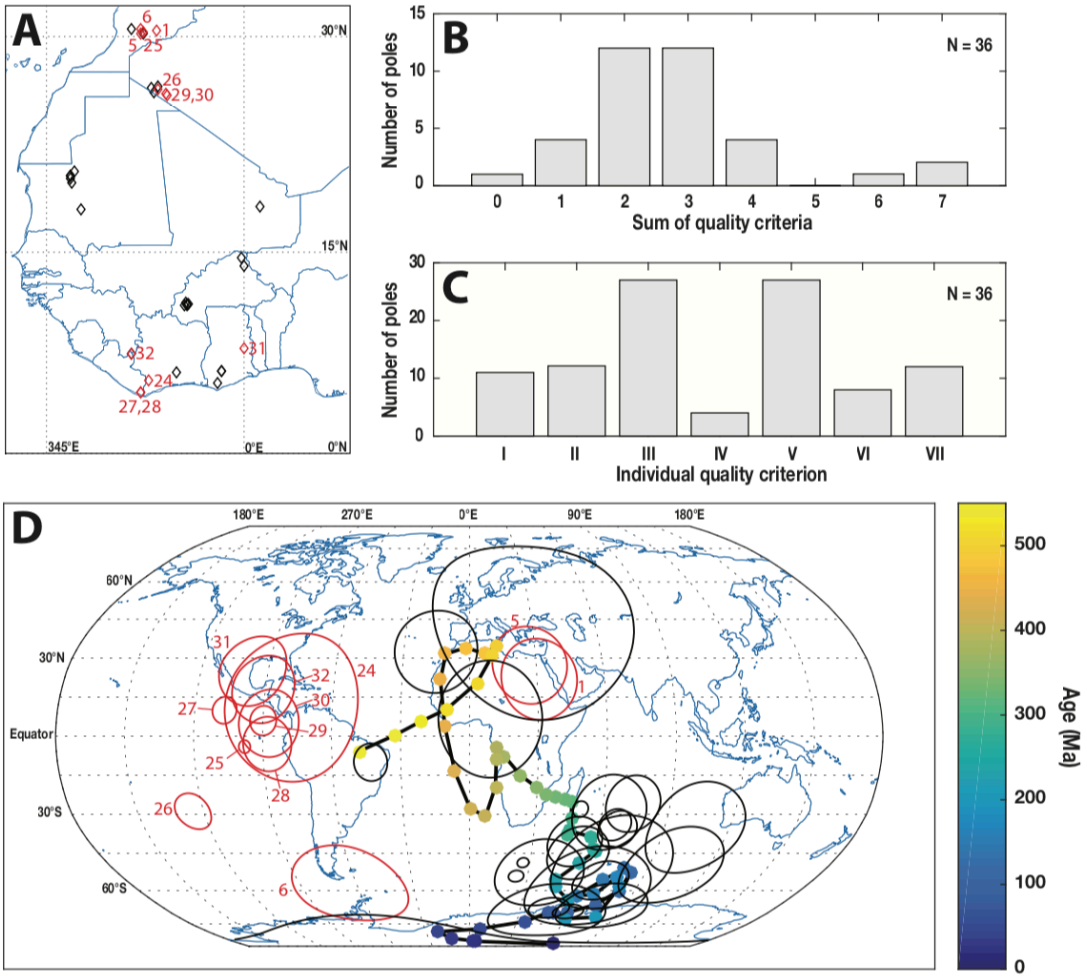

Figure 3 (A) Distribution of Precambrian paleomagnetic data in West African Craton. Black and red diamonds show paleopoles that resemble and differ from Phanerozoic poles, respectively (B) Sum of quality criteria (Van der Voo, 1990). (C) Individual quality criterion (Van der Voo, 1990). N = total number of paleopoles. (D) Projection of

paleopoles with respect to the Phanerozoic apparent polar wander path of West African Craton. Black and red poles represent the ones that overlap and non-overlap with Phanerozoic poles, respectively. The Phanerozoic running mean polar path of West African Craton is from Torsvik et al. (2012). Pole numbers refer to Table 1.

3. Review of paleomagnetic data

Here, all available paleomagnetic data from WAC are compiled on the basis of the Precambrian database PALEOMAGIA (Veikkolainen et al., 2017), the Global Paleomagnetic Database (GPMDB; Pisarevsky, 2005), and the recent Nordic Paleomagnetic Workshops (Evans et al., this issue) (Fig. 3; Table 1). We try to provide a careful evaluation of these data, as well as pointing out the directions for future paleomagnetic studies in WAC.

The attempt of paleomagnetic studies of Precambrian rocks in WAC was first made in the early 1970s, and then culminated in the late 1970s to 1980s. Specifically, in Man-Leo Shield, Piper and Lomax (1973) reported the first dataset from Paleoproterozoic mafic intrusions and a greenstone body in Ghana and Ivory Coast. Later on, Onstott et al. (1984) studied the Paleoproterozoic amphibolite in Liberia and also conducted $^{40}Ar/^{39}Ar$ dating of these rocks. A subsequent study by Onstott and Dorbor (1987) presented paleomagnetic and geochronological data from Paleoproterozoic and early Mesoproterozoic lower-amphibolite to granulite facies metamorphic rocks in a nearby area in Liberia. The most recent work in Man-Leo Shield is provided by Nomade et al. (2003), who analyzed the magnetization of mid-Paleoproterozoic granite in Ivory Coast. In Reguibat Shield, Lomax

(1975) and Sabaté and Lomax (1975) first documented the paleomagnetism of several late Paleoproterozoic and early Mesoproterozoic mafic intrusions from Yetti-Eglab region. Aïfa et al. (2001) mentioned results from 1.9–1.4 Ga dyke swarms in Eglab region, but since no data were presented in that paper, we excluded their study from Table 1. Sedimentary rocks in the Taoudeni Basin have also been studied. Results from the late-Mesoproterozoic Char and Atar Groups in Mauritania were reported in Morris and Carmichael (1978), Perrin et al. (1988) and Perrin and Prévot (1988). Younger sequences were also sampled by Kent et al. (1984) in Mauritania, and by Boudzoumou et al. (2011) in Burkina Faso, and were assigned to be Cryogenian or Ediacaran based on stratigraphic correlation. The Pan-African Adma diorite (ca. 616 Ma) in Mali was also studied paleomagnetically by Morel (1981), but technically speaking that unit lies to the east of the craton in the Hoggar Shield. In Anti-Atlas Belt, Martin et al. (1978) discussed the magnetization of Ediacaran sediments in Morocco for the first time. Recently, two new papers have been published regarding the data from Anti-Atlas Belt. Neres et al. (2016) studied several mafic intrusions in Iguerda inlier in Morocco, with two dykes dated to be 885 ± 13 Ma (Kouyaté et al., 2013) and 1746.8 ± 3.7 Ma (Youbi et al., 2013). The most recent study provided data from the Ouarzazate and Taroudant Groups in Agadir Melloul, Iguerda and Bou Azzer inliers in Morocco, for which Ediacaran volcanic deposits and lava flows were analyzed (Robert et al., 2017). In general, paleomagnetic data cover all cratonic parts in WAC (Fig. 3A). However, as of now, fewer than twenty papers have been published, with only four in this century, which makes WAC the least studied region paleomagnetically compared to other cratons.

We evaluate Precambrian paleomagnetic data in WAC following the quality criteria proposed by Van der Voo (1990) (Fig. 3B–D). The current WAC dataset faces five major problems. First and foremost is the age constraint on the rocks, as well as the age of magnetization. It is noted that the ages of the rocks in the studies published in the 1970s and 1980s usually are constrained by stratigraphic correlation, or merely by geological cross-cutting relationships. Even though some studies gave radiometric ages, these ages have issues in either the precision or the accuracy or both. Another wrinkle to this problem is that metamorphic rocks in some of these studies could have quite complicated thermal histories, therefore the age of the magnetization could be very different from the age of the rock. Second, most of the old works can only be counted as reconnaissance studies since they often applied a spotty sampling of rocks with different ages across a large area, without fully investigating a particular rock unit. For example, two-thirds of the paleopoles fail to satisfy the second criterion of Van der Voo (1990) (Fig. 3C), which means they don't have sufficient number of samples in order to yield any robust paleopole. Nearly thirty percent of the paleopoles were calculated from data containing only one paleomagnetic sampling site (Fig. 3C), which is inadequate for statistical purposes, and the secular variation of ancient geomagnetic field cannot be averaged out. The third problem concerns the demagnetization techniques. Since modern demagnetization methods and/or high-precision rock magnetometers were either not available or just becoming established four decades ago, most samples in the earliest literature were not adequately demagnetized in high temperatures or alternating fields. It is possible that data from those samples are partly contaminated by overprints to various degrees. Fortunately, this problem becomes much less relevant when dealing with more recent publications. Fourth, Precambrian WAC data

rarely have field tests to determine if the magnetization is primary. The last problem is that some older paleopoles show resemblance to younger poles, which indicates the suspicion of remagnetization. When we plotted WAC dataset against the Phanerozoic apparent polar wander path (APWP) of WAC, we found that many paleopoles overlap with the late-Paleozoic and early-Mesozoic segment of the path (Fig. 3D). A resemblance to younger poles could be just coincidental, if considering a long timescale of hundreds of million years or more (Pivarunas et al., 2018). However, we believe that the resemblances shown in the WAC dataset are likely evidence for remagnetizations. In Table 1, we can see that paleopoles similar to late-Carboniferous segment have south-seeking declinations, which should be predominant during the Kiaman reverse superchron (Torsvik et al., 2012). This remagnetization is likely related to the Hercynian/Variscan orogeny when Gondwana collided with Laurussia to build the Pangea supercontinent. Paleopoles similar to the Permian and early-Mesozoic segment have very shallow inclinations, when WAC occupied low-latitude areas (Torsvik et al., 2012). But we should point out that this remagnetization issue should not discourage future research in WAC, because some studied rocks could still preserve the primary information, which was not able to be isolated in older studies due to inadequate demagnetization and low-precision measurement.

In fact, promising data still exist in WAC dataset. Five paleopoles of Ediacaran age fulfill at least four quality criteria of Van der Voo (1990), especially the three yielded by the Ouarzazate and Taroudant volcanics (Robert et al., 2017). With a positive fold test and a positive intraformational conglomerate test, these three paleopoles are believed to be robust (Robert et al., 2017), and should contribute to a better understanding of the complexity of

Ediacaran geomagnetic field and the paleogeography of WAC. It is also noticed that there is a paleopole clustering around Gulf of Mexico-Caribbean Sea, for which the ages range from 2050 Ma to 1750 Ma (Fig. 3D). This paleopole clustering might have potential in providing a useful Orosirian pole for WAC, but awaits more paleomagnetic and geochronological investigations.

Overall, huge gaps remain in the paleomagnetic record of Precambrian rocks in WAC (Evans et al., this issue), hindering paleogeographic reconstruction in deep time. Future studies should consider all major problems in WAC dataset, by taking advantage of newly published high-precision ages (e.g., Rooney et al., 2010) and modern paleomagnetic and rock magnetic routines. We also suggest mafic dyke swarms originated from the large igneous provinces (LIPs) as research priorities since they are reliable recorders of magnetization, and can be precisely dated at the same time. The geometry of dyke swarms can be compared with coeval swarms in other cratons and restored back for reconstructing the LIPs, and at the same time the paleogeography of cratons. In addition, baked-contact tests can be conducted in paleomagnetic studies of dyke swarms. Previous studies have witnessed many successful cases of using mafic dykes to generate robust paleopoles for Precambrian APWPs (e.g., Buchan et al., 1994). The study of Neres et al. (2016), while itself insufficiently limited to a small number of sampled sites, points the way toward further research on Proterozoic mafic dykes within the Anti-Atlas Belt.

4. LIP records in West African Craton

In view of the significance of LIPs in paleogeographic studies, we summarize all precisely-dated Precambrian mafic dykes and sills in WAC (Table 2), together with the available information about their geometry and geochemistry and suggested tectonic settings. Numerous mafic intrusions (mainly dykes) are ubiquitous in WAC and show clear lineation on satellite images and strong magnetic anomalies. A recent contribution of Jessell et al. (2015) mapped mafic dykes in WAC comprehensively. This new map is mainly based on aeromagnetic data and incorporates all previous publications. It is shown that dykes densely intruded all basement rocks and old basins in WAC (Fig. 4). Areas devoid of dykes are usually covered by younger strata so there is no exposure. Varying orientations and cross-cutting relationships of dykes indicate that intrusions should have various ages. In the Anti-Atlas Belt, a total of six swarms have been dated. The oldest 2.04 Ga Tagragra de Tata swarm is defined by two ENE-striking dykes in Tagragra de Tata and Zenaga inliers (Walsh et al., 2002; Kouyaté et al., 2013). The origin of this swarm is proposed to be post-Eburnean extension because the 2.04 Ga dyke postdates all Eburnean-granite in Tagragra de Tata inlier (Walsh et al., 2002). However, Kouyaté et al. (2013) suggest that the granite and mafic dykes are the products of a bimodal magmatic suite, which could be related to the WAC-North Atlantic Craton separation at 2.04 Ga. The 1.75 Ga Tagragra d'Akka swarm has been found in at least four inliers (Tagragra d'Akka, Tafeltast-Kerdous, Zenaga, Iguerda) with a consistent NW strike (Youbi et al., 2013). A ca. 1.71 Ga sill in Igherm inlier also likely belongs to this event (Ikenne et al., 2017). Titanium/vanadium ratios of the 1.75 Ga dykes show a continental flood basalt or a mid-ocean ridge basalt signature, which indicates a rifting context (Youbi et al., 2013). The 1.65 Ga Zenaga event is named after two sills and a NE-striking dyke in Zenaga inlier (Kouyaté et al., 2013). The 1.41–

1.38 Ga Bas Drâa swarm is determined by two dated dykes in Bas Drâa inlier (El Bahat et al., 2013; Söderlund et al., 2013a). Geochemistry (Th/Yb vs. Ta/Yb, La/Sm vs. Zr/Nb) shows a within-plate volcanic zone signature (El Bahat et al., 2013). The 1.41–1.38 Ga dykes are similar in age to the breakup of the supercontinent Nuna/Columbia; therefore, they are suggested to possibly originate from a hotspot mantle source beneath WAC during rifting (El Bahat et al., 2013). The 0.88–0.85 Ga Iguerda-Taïfast swarm is based on two dated NE-striking dykes in Iguerda-Taïfast inlier (Kouyaté et al., 2013), and they could be associated with the rifting event within the supercontinent Rodinia. A 611 Ma dyke in Bas Drâa inlier is dated by El Bahat et al. (2017) and could belong to a swarm that has not been recognized to its full extent. Southward, the Reguibat Shield has the two oldest dykes thus found in WAC: the 2.73 Ga NE-striking Ahmeyim Great dyke (Tait et al., 2013) and the 2.69 Ga NW-striking Aousserd-Tichla dyke (Söderlund et al., 2013b). The relationship between these two dykes is not clear, and they might represent two separate events. Geochemical analysis points to a boninitic provenance of the 2.73 Ga Ahmeyim Great dyke, but it is suggested to be a signal of crustal contamination and the dyke is unlikely related to subduction (Tait et al., 2013). In Man-Leo Shield, Baratoux et al. (2019) recently published a series of new U-Pb baddeleyite ages of dykes that have been previously dated by K-Ar or Ar-Ar methods. In total, there are six swarms, namely the 1.79 Ga Libiri swarm, the 1.76 Ga Kédougou swarm, the 1.57 Ga Korsimoro swarm, the 1.52 Ga Essakane swarm, the 0.91 Ga Oda swarm, and the 0.85 Ga Manso swarm (Baratoux et al., 2019). Across the craton, the 1.75 Ga Tagragra d'Akka swarm in Anti-Atlas Belt and the 1.76 Ga Kédougou swarm in Man-Leo Shield could be related to the same event because of the matching ages. In addition, the 0.88–0.85 Ga Iguerda-Taïfast swarm in Anti-Atlas Belt and the 0.85 Ga

Manso swarm could also originate from a single event. With the rapid growth of geochronological data regarding the mafic intrusions in WAC, we expect more swarms to be identified and the magmatic history of WAC to be better constrained.

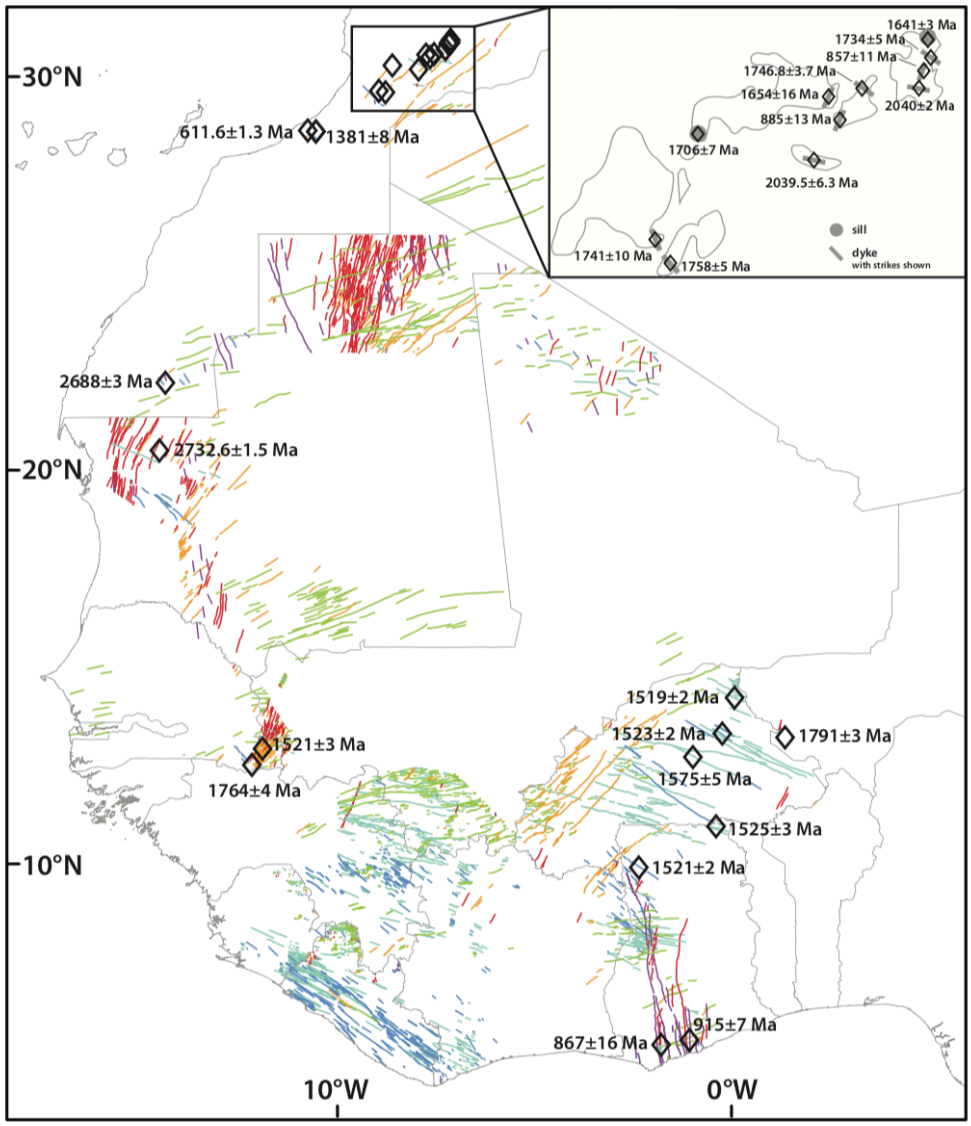

Figure 4 Mafic dyke distribution across West African Craton. Black diamonds mark the locations of the dated dykes. Modified from Jessell et al. (2015).

Magmatic barcode comparisons are made between WAC and its potential neighboring cratons in Proterozoic supercontinents, e.g., Amazonia, Baltica, Laurentia, Siberia, etc. (Fig. 5). During certain time intervals, several cratons share similar-aged magmatism. For instance, in WAC, the 2.04 Ga swarm is coeval with the Korak and Kangâmuit-MD3 swarms in North Atlantic Craton (Nilsson et al., 2013); the 1.79 Ga swarm matches the Avanavero swarm in Amazonia (Reis et al., 2013), the Xiong'er swarm in North China (Peng, 2010), the Tomashgorod swarm in Baltica (Bogdanova et al., 2013), and the Florida swarm in Río de la Plata (Teixeira et al., 2013); the 1.75 Ga swarm could be correlated with the Cleaver-Hadley Bay-Nueltin swarm in Laurentia (Ernst et al., 2013), the Espinhaço swarm in São Francisco (Danderfer et al., 2009), and the Chaya swarm in Siberia (Gladkochub et al., 2010); the 1.65 Ga swarm is comparable with the Khibelen swarm in Siberia (Gladkochub et al., 2007) and the Häme swarm in Baltica (Salminen et al., 2017); the 1.52 Ga swarm is likely associated with the Käyser swarm in Amazonia (Baratoux et al., 2019); the 1.41–1.38 Ga swarm is of the same age as the Mashak swarm in Baltica (Puchkov et al., 2013), the Chieress swarm in Siberia (Ernst et al., 2000), the Nova Lacerda swarm in Amazonia (Teixeira et al., 2016), the Kunene event in Congo (McCourt et al., 2013), and the Hart River-Salmon Arch and Midsommerso-Zig Zag Dal swarms in Laurentia (Ernst et al., 2013); the 0.88 Ga swarm may be linked with the late stage of the Dashigou swarm in North China (Peng et al., 2011); and the 0.61 Ga swarm could be connected to the early stage of the Central Iapetus Magmatic Province (CIMP) in Laurentia and Baltica (Ernst and Bell, 2010). Although it seems that penecontemporaneous swarms can be traced across several cratons, we emphasize that these temporal matches should be treated as indicative rather than diagnostic. Besides, the tectonic backgrounds of

these swarms are still debated, e.g., whether they are LIPs events during continental rifting or regional extensions. Nevertheless, paleomagnetism of these swarms can provide an independent test to constrain the relative positions between WAC and possible neighboring cratons in future studies.

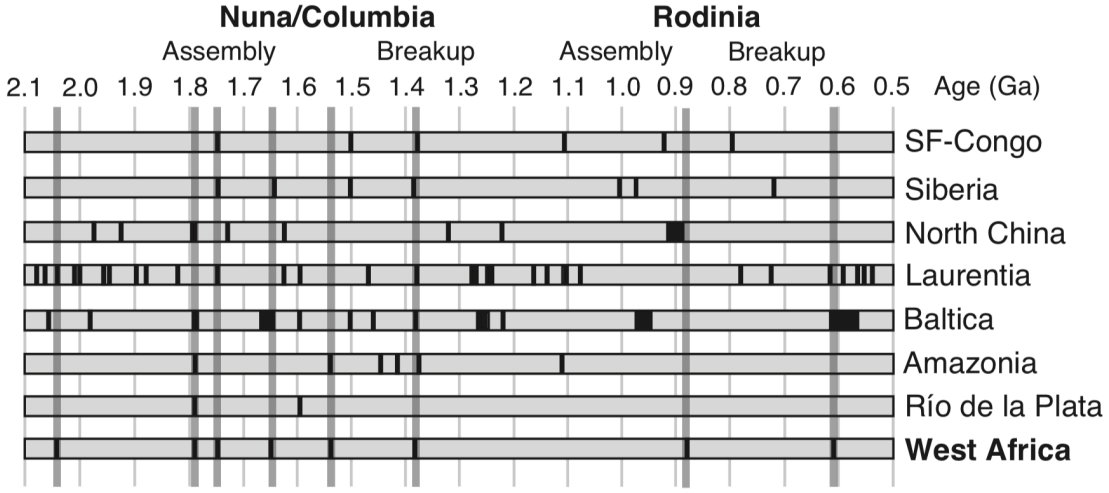

Figure 5 LIP barcodes of Proterozoic cratons. Thin lines represent single pulses and wide boxes indicate prolonged pulses for a certain event. Note potential correlations between West African Craton and other cratons are shown by shaded bars (correlation window size = 15 Myr). SF = São Francisco. Modified from Ernst et al. (2013).

5. Paleoclimate indicators

Geological records preserve information about Earth's climate in the past. Commonly used paleoclimate indicators can be subdivided into three categories: lithological, geochemical, and paleontological. Some of the indicators can be paleogeographically indicative as well. Here, we summarize available paleoclimate indicators in WAC, plotting against the reconstruction of WAC's paleolatitude based on the paleomagnetic data. It's worthwhile to mention the uncertainties of paleolatitudinal reconstructions before late Neoproterozoic

time. First, the geomagnetic polarity is not constrained, so WAC can be placed in either hemisphere. Second, because the quality of paleomagnetic data is low, the inferred paleolatitude is less robust compared to the late Neoproterozoic.

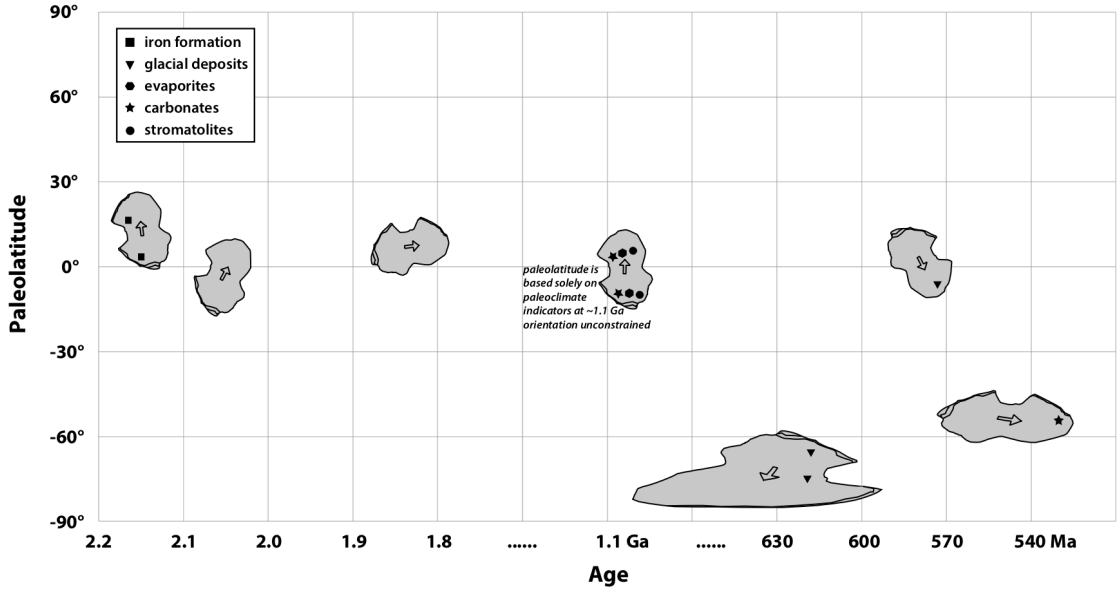

Figure 6 Paleoclimate indicators. Paleolongitude is arbitrary. Due to the magnetic polarity flexibility, West African Craton can be placed in either hemisphere before late Neoproterozoic time. Paleolatitude of West African Craton at ~1.1 Ga is constrained solely by paleoclimate indicators. Arrows point to present-day north. Note that the age scale is not linear.

Two important Paleoproterozoic iron formations are found in WAC: the ca. 2.2 Ga Ijil Group in Mauritania, Reguibat Shield (Bronner and Chauvel, 1979) and the ca. 2.3 Ga Nimba Itabirite in Liberia, Man-Leo Shield (Berge, 1974). The origin of Paleoproterozoic iron formation is highly debated, but it is suggested that the iron is either sourced from hydrothermal systems or continental inputs, and was deposited due to the enhanced oxygen availability in the ocean (Konhauser et al., 2017). During the deposition of these two iron

formations, WAC was likely located at low- to mid-latitudes (Fig. 6). In the latest Mesoproterozoic, the Char and Atar Groups of the Taoudeni Basin are characterized by carbonates, with columnar stromatolites and evaporites (Bertrand-Sarfati et al., 1991). Paleomagnetic inclinations of Char and Atar carbonates, if primary, imply a low-latitudinal position of WAC (Perrin et al., 1988), which would be consistent with the depositional environment of carbonates and evaporites. During the Ediacaran, large latitudinal shift of WAC is indicated by paleomagnetic data, which could be caused by a rapid true polar wander event (Robert et al., 2017). Marinoan-equivalent diamictites are found in the Assabet el Hassiane Group of the Taoudeni Basin (Bertrand-Sarfati et al., 1991). In addition, possible Gaskiers-equivalent diamictites are observed in the Taoudeni Basin and the Anti-Atlas Belt (Deynoux, 1985; Letsch et al., 2018; Fig. 6). In the Anti-Atlas Belt, massive carbonates were deposited in Taroudant Group (Bertrand-Sarfati et al., 1991), where Ediacara-biota have also been identified (Fig. 6; Letsch et al., 2019).

6. Precambrian paleogeography of West African Craton

Discussions regarding the Precambrian paleogeography of WAC are reviewed here, ranging from its possible positions in Atlantica supercraton, and Nuna/Columbia and Rodinia supercontinents, to the final amalgamation within Gondwana. Both paleomagnetic and geological constraints are considered in reconstructions.

6.1 Paleogeographic connection between West African Craton and Amazonia

Many paleogeographic reconstructions treat WAC and Amazonia as a long-lived conjoined entity since Paleoproterozoic time, by linking the southern margin of WAC to the Guiana

Shield of Amazonia, until they were finally separately by the opening of the Atlantic Ocean in the Mesozoic. This idea was first proposed by Onstott and Hargraves (1981), who observed a general overlapping of paleopoles from the two cratons between 2.1 Ga and 1.5 Ga. They also suggested that the lineaments of the Guri Belt (fault zone separating the Archean Imataca domain and the Paleoproterozoic Maroni-Itacaiúnas domain) in Guiana Shield and the Sassandra Belt (fault zone separating the Archean Kénéma-Man domain and the Paleoproterozoic Baoulé-Mossi domain) in Man-Leo Shield should be aligned as a piercing point (Fig. 7A) that was subsequently displaced by more than 1000 km through dextral transcurrent faulting during Pan-African orogeny (Onstott and Hargraves, 1981). This reconstruction would also align the general trends of the Paleoproterozoic Eburnean and Transamazonian orogenic belts in WAC and Amazonia, respectively.

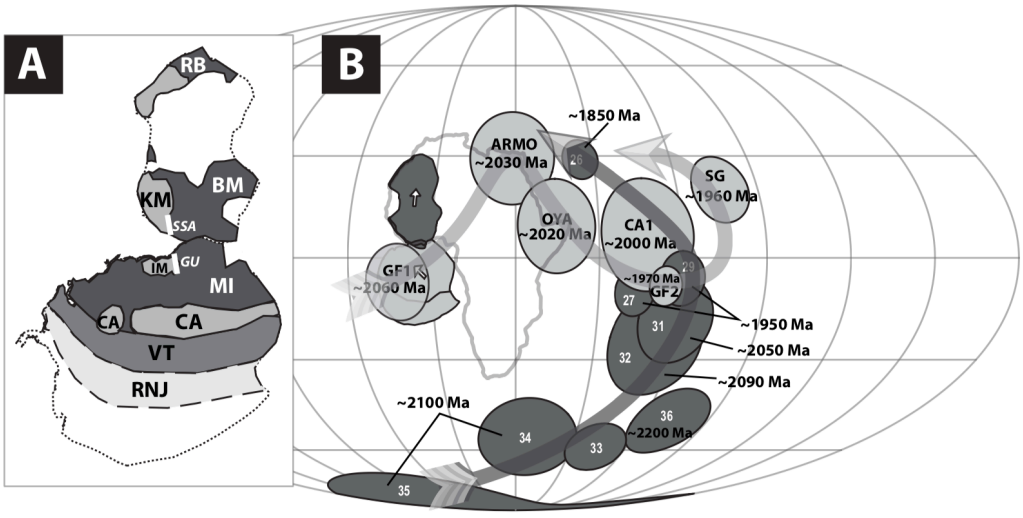

Figure 7 (A) Paleogeographic connection between West African Craton and Guiana Shield in mid-Paleoproterozoic time. RNJ = Rio Negro-Juruena domain, VT = Ventuari-Tapajós domain, CA = Central Amazonia domain, MI = Maroni-Itacaiúnas domain, IM = Imataca domain, GU = Guri Belt, BM = Baoulé-Mossi domain, KM = Kénéma-Man domain, RB =

Reguibat Shield, SSA = Sassandra Belt. Modified from Bispo-Santos et al. (2014). (B) Orosirian apparent polar wander paths of West African Craton and Amazonia in present West Africa reference frame. Euler rotation of Amazonia with respect to absolute reference: 43.3°N, 330.5°E, 71.5°. Paleopoles of West African Craton are numbered as in Table 1. Paleopoles of Amazonia are from Bispo-Santos et al. (2014). White arrows show present-day north.

Nomade et al. (2003) attempted to test this direct WAC-Amazonia connection by comparing the APWPs of both cratons, and suggested that such a connection is paleomagnetically permissive. Recently, new paleomagnetic data from Guiana Shield allows a better-defined APWP to be constructed. On that basis, Bispo-Santos et al. (2014) found that the APWPs of the two cratons begin to match around 1980-1960 Ma (Fig. 7B), and WAC and Amazonia might be linked at that time. It should be pointed out that ca. 2.0-Ga paleopoles from WAC need more rigorous reliability tests and the precision of their ages should be largely improved. Also, numerous dyke swarms observed in Man-Leo and Guiana Shields seem to indicate that continental rifting occurred several times since 1.9 Ga; if so, why would the geological and paleomagnetic datasets persist in their similarities? Nonetheless, the long-lived connection model requires further tests by developing more comprehensive younger-Proterozoic APWPs from both cratons.

6.2 West African Craton in Precambrian supercontinents

It is still highly uncertain whether there ever existed a supercontinent (a.k.a. Kenorland) or a few supercratons in the Neoarchean and the earliest Paleoproterozoic. But some ideas

have been proposed regarding the configuration of the possible supercratons (Rogers, 1996; Bleeker, 2003). Atlantica supercraton (Rogers, 1996) is proposed to be the continental landmass formed at ~2 Ga by the collision of WAC, São Francisco-Congo, Amazonia and Río de la Plata, with their relative positions being similar to those within Pangea. The geological underpinning of Atlantica supercraton is a supposedly correlative ~2 Ga fluvio-deltaic sedimentary succession across all of the constituent cratons (Ledru et al., 1994). Rogers (1996) suggested that Atlantica stayed as a coherent entity since its formation and only experienced intracratonic orogenic activities until the final destruction by the opening of Atlantic Ocean in the Mesozoic. Regardless of the existing views against the longevity of Atlantica (e.g., D'Agrella-Filho et al., 2011; Evans, 2013), its configuration is also challenged by paleomagnetic data (Rapalini et al., 2015; Franceschinis et al., 2019). For example, by matching the 2.1–1.9 Ga paleopoles of Río de la Plata, Guiana, WAC and São Francisco-Congo, Franceschinis et al. (2019) suggested that Río de la Plata should sit between Guiana and São Francisco-Congo before 2.0 Ga, and later southeast WAC collided with southeast Río de la Plata to form so called "unorthodox" Atlantica. Due to the sparsity of poles from WAC and São Francisco-Congo during that period of Earth's history, such a revision of Atlantica still needs further investigation.

Speculation on the late Paleoproterozoic-early Mesoproterozoic supercontinent Nuna/Columbia was initiated by the recognition of widespread Orosirian orogenic belts (Hoffman, 1989), and has received much recent attention. Dozens of reconstruction models have been put forward. Here we list some representative reconstruction models, limiting our discussion to the position of WAC and proposed immediate neighbors in

Nuna/Columbia. We refer readers to original publications for the details of Nuna/Columbia reconstructions. In the models of Rogers and Santosh (2002, 2009), the Atlantica supercraton idea was retained, and WAC was placed close to Amazonia and São Francisco-Congo (Fig. 8A). Zhao et al. (2002, 2004) compared the ages and general trends of 2.1–1.8 Ga orogens, and linked cratons in South America and Africa with Baltica to align the Paleoproterozoic basement rocks in these cratons (Fig. 8B). In that reconstruction, WAC faces southern Baltica so that the Archean components in Reguibat and Sarmatia can be aligned. It should be pointed out that these two models are primarily based on geological comparisons, of which the correlations would be non-unique. A more recent reconstruction of Nuna/Columbia was conducted by Zhang et al. (2012), who incorporated all available paleopoles from seven cratons and adopted the tight Laurentia-Siberia-Baltica fit proposed by Evans and Mitchell (2011) and the tight Baltica-Amazonia-WAC fit proposed by Johansson (2009) (Fig. 8C). The tight Baltica-Amazonia-West Africa fit, well-known as the SAMBA model, is supported by the similar 1.6–1.5 Ga rapakivi suites and anorthosite-mangerite-charnockite-granite (AMCG) plutons in Guiana and Fennoscandia, and also the Paleoproterozoic banded iron formations in Sarmatia, Imataca and Kénéma-Man domains of the three cratons (Johansson, 2009). The connection between WAC and Siberia in Zhang et al. (2012) seems to be possible based on the coeval LIP records at 1.75 Ga, 1.65 Ga and 1.38 Ga, but the proposed connection between WAC and India currently has little supporting evidence. Pisarevsky et al. (2014), by comparing the 1.45–1.42 Ga paleopoles from Baltica and Amazonia, questioned the reliability of the SAMBA model. Instead, they argued that Amazonia and WAC were connected in Nuna/Columbia (Fig. 8D), but were separated from Baltica by an oceanic tract wide enough to include two opposing subduction

systems (Pisarevsky et al., 2014). Bispo-Santos et al. (2008) placed North China between Baltica and Amazonia, within which Trans-North China orogen would be continuous with approximately time-equivalent orogens in Baltica (Svecofennian) and Amazonia (Ventuari-Tapajós). It is noted that despite large differences in the configurations of Nuna/Columbia in these models, WAC-Amazonia connection was commonly favored, considering the aforementioned geological and paleomagnetic evidence. However, there are models that break the WAC-Amazonia connection. For example, Chaves and Rezende (2019) suggested a radically different model, whereby North China was located between southern WAC and northeast Amazonia, in order to match the trends of coeval 1.79–1.78 Ga mafic intrusions in three cratons, and also to align the Paleoproterozoic orogenic belts in Amazonia and North China (Fig. 8E). The tight Laurentia-Siberia-Baltica fit is also disrupted and WAC is assigned to occupy the core of Nuna/Columbia (Chaves and Rezende, 2019). This model requires testing from careful, time-space comparisons of the crustal evolutions of involved cratons, and more reliable paleomagnetic data.

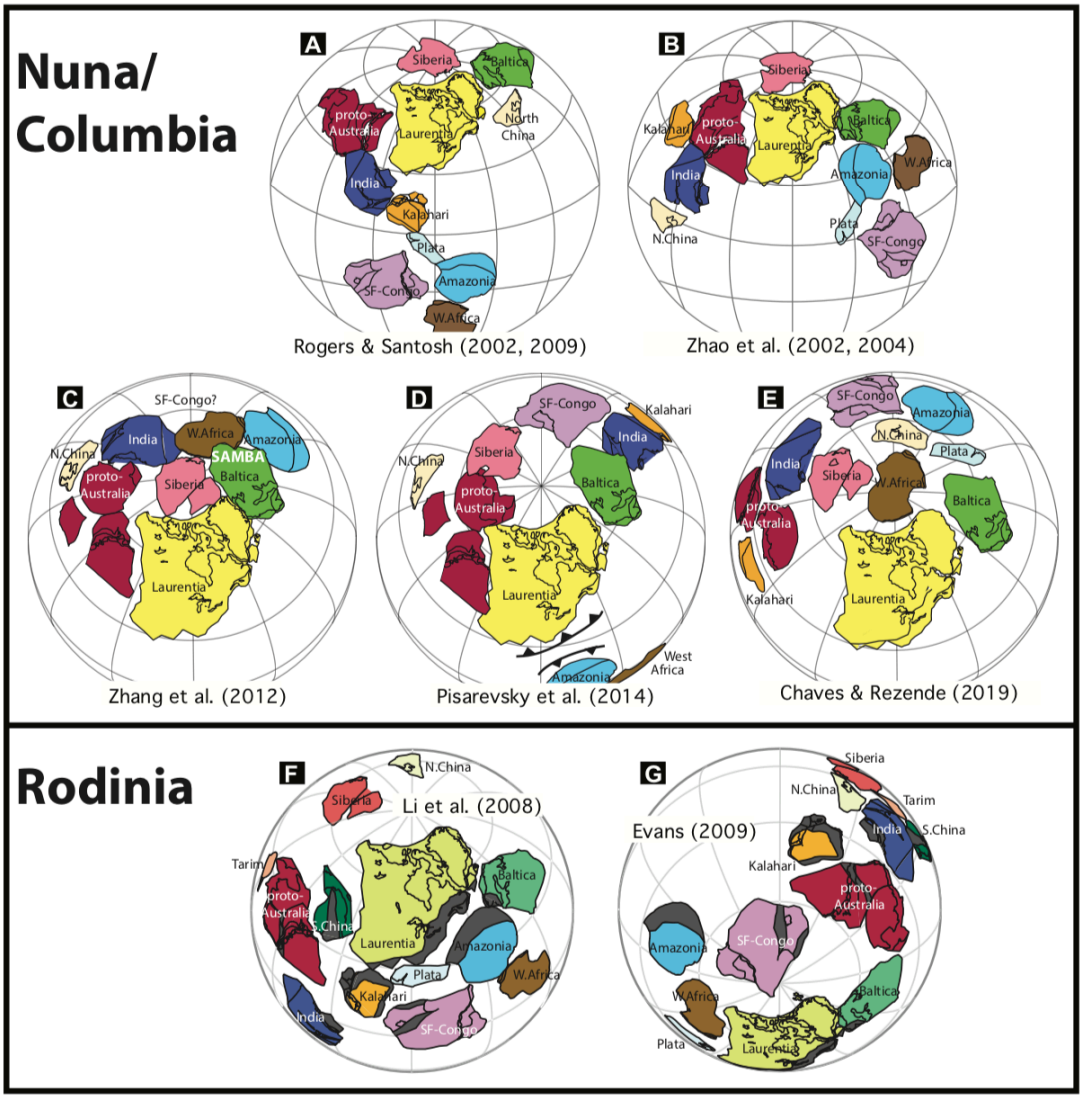

Figure 8 Various configurations of the supercontinents Nuna/Columbia and Rodinia, modified from Evans (2013). All projections are in present North American reference frame, with a common color scale to facilitate comparison and contrast. Grey areas indicate the 1.3–0.9 Ga "Grenvillian" orogens. (A) Rogers and Santosh (2002, 2009). (B) Zhao et al. (2002, 2004). (C) Zhang et al. (2012). (D) Pisarevsky et al. (2014). (E) Chaves and Rezende (2019). (F) Li et al. (2008). (G) Evans (2009).

The existence of early Neoproterozoic supercontinent Rodinia is well accepted, whilst its configuration is still highly controversial. In fact, after Li et al. (2008) published the influential and all-inclusive reconstruction of Rodinia (Fig. 8F), many new arguments have led to dissension rather than consensus (e.g., Santos et al., 2008; Evans, 2009; Fu et al., 2015; Ernst et al., 2016; Wen et al., 2018, Slagstad et al., 2019). Because of the inadequate paleomagnetic data and the lack of "Grenvillian" orogen in WAC, its position in Rodinia was largely constrained by the data from Amazonia, if the WAC-Amazonia connection was assumed to be valid. There remain many debates about whether the Grenville orogen in Laurentia and the Sunsás orogen in Amazonia should be continuous or facing each other, or even disconnected (Santos et al., 2008; D'Agrella-Filho et al., 2008; Evans, 2009, 2013). For instance, in Santos et al. (2008)'s model where Grenville and Sunsás orogens are continuous, southern WAC should be in contact with western Laurentia so that the mid-Paleoproterozoic Birimian and Wopmay orogens could be bridged. However, in Evans's (2009) reconstruction, Amazonia is separated from Laurentia, and the Sunsás orogen is considered to be accretionary instead of collisional. Evans (2009) also adopted the coupling of southern WAC and western Laurentia, but in that model northern WAC is attached to northeastern Amazonia (Fig. 8G). In this scenario, the alignment of Sassandra Belt in Man-Leo Shield and the Guri Belt in Guiana would be disrupted. Although Guri Belt could be tied in with the Sfariat Belt in Reguibat Shield, the polarity of Archean and Paleoproterozoic domains in these two shields would be twisted. The Evans (2009) model is also challenged by the need for WAC to detach from Amazonia, rotate nearly 180° and reconnect with Amazonia again in Gondwana.

After the breakup of Rodinia in the mid-Neoproterozoic, WAC experienced a series of Pan-African tectonic activities, i.e., the Bou Azzer-Siroua island arc accretion to the north, collision along the Trans-Saharan Belt to the east, tectonism within the Rokelide and Bassaride Belts to the southwest, and the Mauritanide Belt to the west (Ennih and Liégeois, 2008). WAC was welded together with other cratons to form Gondwana through these Pan-African activities. Around the Neoproterozoic-Paleozoic transition, several so-called "peri-Gondwanan" terranes (e.g., Avalonia, Cadomia, Carolina) were stripped off the margin of WAC (and/or Amazonia) and later collided with Laurentia to form Pangea (Nance et al., 2008). The opening of Atlantic Ocean in the Mesozoic separated WAC from Amazonia and brought the two cratons to their current positions.

7. Concluding remarks

Thus far, paleogeography of WAC in the Precambrian has been poorly constrained, and the scarcity of both geological and paleomagnetic data yield notable gaps in the tectonic and kinematic history of WAC and its interactions with neighboring cratons. Since paleomagnetism provides essentially the only quantitative paleogeographic constraints, future paleomagnetic studies should take advantage of ubiquitous mafic dyke swarms recognized in WAC in order to generate high-quality and well-dated paleopoles. In addition to the efforts in new data acquisition, any future reconstruction model should proceed from a kinematic point of view, that is, hypothesizing the continuous drift history of WAC rather than proposing a single snapshot at a given time of interest. Another perspective is the significance of individual cratons in helping us understand the configuration of supercontinents, and the transitional pattern from one supercontinent to another. The

ongoing discussions about how supercontinents dispersed and reassembled cyclically have inspired different geodynamic models: introversion (closure of the interior oceans), extroversion (closure of the exterior ocean), the alternation between introversion and extroversion (superocean episodes), or orthoversion (closure 90° away from the predecessor supercontinent) (Murphy and Nance, 2003; Mitchell et al., 2012; Li et al., 2019). Accurate paleogeography of poorly-constrained cratons including WAC could provide a critical test for these alternative models.

Acknowledgments

This study was funded by a U.S. National Science Foundation grant (EAR-1953549) to D. Evans. Z. Gong was supported by Yale University Graduate Student Fellowship. We thank Augusto Rapalini, Johanna Salminen, and an anonymous reviewer for constructive comments that led to an improved manuscript.

Table 1 Precambrian paleomagnetic data from West African Craton.

#	Formation (Paleopole name)	Slat (°N)	Slon (°E)	Nominal age (Ma)	Met	Rock isotopic age (Ma)	B/N	Dec (°)	Inc (°)	α_{95} (°)	k	Plat (°N)	Plon (°E)	A_{95} (°)	Reliability criteria								References	
															1	2	3	4	5	6	7	Σ	Paleomagnetism	Geochronology
1	**Djebel Boho volcanics (B2)**	**30.4**	**353.4**	**547**	**g**	**541 ± 6**	**16*/78**	**87.7**	**71.9**	**9.9**	**14.9**	**27.3**	**27.1**	**14.9**	**1**	**1**	**1**	**1**	**1**	**1**	**1**	**7**	**Robert et al. (2017)**	**Blein et al. (2014a)**
2	Iguerda mafic dykes (Cluster D4)	30.2	352.4	550	a		2/9*	45.9	-56.7	5.8	79.0	-10.0	316.8	7.2	0	0	1	0	1	0	0	2	Neres et al. (2016)	
3	Azougui Formation (I2)	20.5	346.9	550	a		4*/60	339.0	-17.3	3.1	34.0	-54.1	24.1	2.3	0	1	0	0	1	0	0	2	Perrin and Prévot (1988)	
4	Serie lie de vin sediments (M0)	30.5	351.5	557	a, s		8*/8	124.0	-1.7	20.5	8.2	-29.2	63.3	14.5	0	0	0	0	1	0	0	1	Martin et al. (1978)	
5	**Fajjoud and Tadoughast volcanics (B1)**	**30.2**	**352.2**	**562**	**g**	**556 ± 5**	**20*/99**	**93.7**	**67.0**	**10.5**	**10.7**	**21.9**	**31.0**	**15.6**	**1**	**1**	**1**	**1**	**1**	**1**	**1**	**7**	**Robert et al. (2017)**	**Blein et al. (2014b)**
6	**Adrar-n-takoucht Volcanics (C)**	**30.5**	**352.2**	**571**	**g**	**571 ± 6**	**9*/53**	**27.7**	**18.0**	**19.4**	**8.0**	**-57.6**	**295.6**	**15.7**	**1**	**0**	**1**	**1**	**1**	**1**	**1**	**6**	**Robert et al. (2017)**	**Blein et al. (2014b)**
7	Mejeria red sandstone	18.1	347.7	582	a, s		4*/17	137.1	14.4	13.2	49.0	-40.5	49.9	9.7	0	0	0	0	1	0	0	1	Kent et al. (1984)	
8	Oujeft Group (CO8+CO10)	20.0	347.0	600	a, e	595 ± 45	2/14*	127.0	23.0	4.0	89.0	-28.0	50.0	3.1	0	0	1	0	1	0	0	2	Morris and Carmichael (1978)	Clauer et al. (1982)
9	Adma diorite	18.3	1.2	616	g	616 ± 11	13*/62	317.3	78.6	9.0	22.0	32.5	344.7	15.9	1	1	1	0	1	0	0	4	Morel (1981)	per. comm. w/Ducrot, Lancelot, and Renaud
10	Tin Akof carbonates (TA)	14.0	0.0	618	a		1/7*	332.1	-0.1	16.6	14.2	-58.8	64.6	16.6	0	0	1	1	1	1	0	4	Boudzoumou et al. (2011)	
11	Tin Dioulaf cap carbonates (TD)	14.6	359.8	635	corr.		1/10*	130.5	16.2	7.0	48.5	-35.8	68.5	7.2	1	0	1	0	1	0	0	3	Boudzoumou et al. (2011)	Boudzoumou et al. (2011)
12	Guinguette sediments (G)	11.1	355.7	715	a		1/8*	322.6	-11.5	18.5	10.0	-49.1	71.7	18.8	0	0	1	0	1	0	0	2	Boudzoumou et al. (2011)	
13	Banarodougou sediments (B)	11.3	355.6	715	a		1/15*	345.0	-10.8	4.4	75.5	-67.6	46.9	4.5	0	0	1	0	1	0	0	2	Boudzoumou et al. (2011)	
14	Tiara sediments (Tr)	11.2	355.8	715	a		1/18*	343.1	-2.2	3.2	107.0	-69.2	59.1	3.2	0	0	1	0	1	0	0	2	Boudzoumou et al. (2011)	
15	Digouéra sediments (D)	11.1	355.5	715	a		1/13*	346.0	-8.6	11.9	13.0	-69.2	47.3	12.0	0	0	1	0	1	1	0	3	Boudzoumou et al. (2011)	
16	Toussiana sediments (T)	11.2	355.7	775	a	775 ± 52	1/9*	300.2	-26.1	10.1	27.0	-25.9	73.4	10.9	0	0	1	0	1	1	0	3	Boudzoumou et al. (2011)	
17	Atar group, Unit I9	20.8	347.2	1100	l	1107 ± 12, 1109 ± 22, 1105 ± 37	2/15*	125.2	-6.8	8.6	20.0	-34.0	66.9	6.1	0	0	1	0	1	1	0	3	Perrin et al. (1988)	Rooney et al. (2010)
18	Char Group (I2)	20.3	346.9	1150	s, e	998 ± 34	5*/25	336.0	37.0	11.0	36.0	-67.0	78.0	9.9	0	1	1	0	1	0	0	3	Morris and Carmichael (1978)	Clauer et al. (1982); Rooney et al. (2010)
19	Char group, Unit I2	20.5	346.9	1150	s, e	998 ± 34	4*/52	334.4	-23.6	2.5	63.0	-48.7	26.6	1.9	0	1	1	0	1	0	0	3	Perrin et al. (1988)	Clauer et al. (1982); Rooney et al. (2010)
20	Nimba-Harper metamorphic rocks (NiB)	7.5	351.5	1480	c	1450 ± 10, 1510 ± 10	4*/22	140.2	26.7	13.0	51.0	-45.0	52.8	10.4	1	0	1	0	0	1	0	3	Onstott and Dorbor (1987)	Onstott et al. (1984); Onstott and Dorbor (1987)
21	Shahra dykes	26.6	353.0	1500	s		7*/34	55.1	71.1	21.5	8.9	41.2	31.0	35.0	0	0	0	0	1	0	0	1	Sabaté and Lomax (1975)	
22	Quartz diorite	26.3	353.2	1500	s		3*/18	139.5	77.0	12.5	97.9	6.6	9.1	22.5	0	0	0	0	0	0	0	0	Sabaté and Lomax (1975)	
23	Dykes intruding Guelb el Hadid Series	26.7	353.5	1500	s		9*/53	296.6	50.6	16.0	11.3	-35.1	104.9	17.7	0	1	0	0	1	0	0	2	Sabaté and Lomax (1975)	
24	**Ivory Coast dolerite intrusions**	**5.5**	**352.8**	**1730**	**d**	**1730 ± 170**	**1/10***	**281.0**	**14.0**	**39.0**	**2.5**	**11.0**	**282.0**	**28.5**	**0**	**0**	**0**	**0**	**1**	**0**	**1**	**1**	**Piper and Lomax (1973)**	**Knopf (1967)**

25	**Iguerda mafic dyke (Cluster D1)**	**30.3**	**352.4**	**1747**	**g**	**1747 ± 4**	**1/22***	**86.7**	**4.6**	**3.5**	**81.0**	**-4.0**	**262.1**	**2.5**	**1**	**0**	**1**	**0**	**1**	**0**	**1**	**4**	**Neres et al. (2016)**	**Youbi et al. (2013)**
26	**Aftout gabbro**	**26.5**	**353.5**	**1869**	**a**	**1869 ± 50**	**5*/26**	**72.4**	**55.5**	**5.7**	**179.0**	**-28.8**	**235.1**	**6.9**	**0**	**1**	**0**	**0**	**0**	**0**	**1**	**2**	**Sabaté and Lomax (1975)**	
27	**Harper amphibolite (HaA1)**	**4.6**	**352.2**	**1950**	**e, c**	**1983 ± 34, 1964 ± 2, 1894 ± 2**	**3/11***	**274.0**	**-14.0**	**7.0**	**39.0**	**10.0**	**253.0**	**5.2**	**1**	**0**	**1**	**0**	**0**	**0**	**1**	**3**	**Onstott et al. (1984)**	**Onstott et al. (1984)**
28	**Harper amphibolite (HaA2)**	**4.6**	**352.2**	**1950**	**e, c**	**1983 ± 34, 1964 ± 2, 1894 ± 2**	**1/3***	**89.0**	**-19.0**	**14.0**	**76.0**	**-3.0**	**272.0**	**10.5**	**1**	**0**	**1**	**0**	**0**	**0**	**1**	**3**	**Onstott et al. (1984)**	**Onstott et al. (1984)**
29	**Aftout plutons (E)**	**26.2**	**354.1**	**1966**	**s**		**6*/40**	**92.8**	**-15.5**	**7.8**	**75.1**	**6.0**	**270.1**	**5.7**	**0**	**1**	**1**	**0**	**0**	**0**	**1**	**3**	**Lomax (1975)**	
30	**Aftout plutons (C)**	**26.1**	**354.2**	**1966**	**s**		**4*/24**	**90.8**	**-19.2**	**17.2**	**29.4**	**5.0**	**272.6**	**13.0**	**0**	**0**	**1**	**0**	**0**	**0**	**1**	**2**	**Lomax (1975)**	
31	**Nimba-Harper metamorphic rocks (NiA)**	**7.5**	**351.5**	**2050**	**c**	**2050 ± 6**	**6*/38**	**286.6**	**18.4**	**13.0**	**28.0**	**18.0**	**269.0**	**13.0**	**1**	**1**	**1**	**0**	**0**	**0**	**1**	**4**	**Onstott and Dorbor (1987)**	**Onstott et al. (1984); Onstott and Dorbor (1987)**
32	**Ferke batholith (IC2)**	**7.9**	**0.0**	**2094**	**j**	**2094 ± 6**	**9*/40**	**296.0**	**3.0**	**18.9**	**8.4**	**25.0**	**263.0**	**13.4**	**0**	**0**	**1**	**0**	**0**	**0**	**1**	**2**	**Nomade et al. (2003)**	**Doumbia et al. (1998)**
33	Obuasi dolerite dyke	6.2	358.3	2100	s		1/10*	328.0	-11.0	11.0	20.9	-56.0	69.0	7.9	0	0	1	0	1	0	0	2	Piper and Lomax (1973)	
34	Tarkwa dolerite intrusions	5.3	358.0	2100	s		5*/29	156.0	40.0	14.0	32.0	-53.0	36.0	13.5	0	1	1	0	1	0	0	3	Piper and Lomax (1973)	
35	Ivory Coast TTG plutons (IC1)	6.1	354.9	2100	s, a		6*24	8.4	3.7	16.1	18.3	-82.0	292.0	11.4	0	1	1	0	1	0	0	3	Nomade et al. (2003)	
36	Obuasi greenstone body	6.2	358.3	2200	g	~2200	5*/74	320.0	26.0	19.0	20.7	-50.0	102.0	15.3	1	0	0	0	1	0	0	2	Piper and Lomax (1973)	per. comm. w/P.G. Coomer

*Note: Slat/Slon = site geographic latitude/longitude, Met = magnetization age determination method following PALEOMAGIA Database (a = geological/APWP, c = $^{40}Ar/^{39}Ar$, corr. = correlation, d = K-Ar, e = Rb-Sr, g = U-Pb, j = Pb-Pb, l = Re-Os, s = stratigraphic), B/N = number of sites/samples, * = level of mean calculation, Dec = declination, Inc = inclination, Plat/Plon = paleopole latitude/longitude, α_{95} = radius of 95% confidence cone of the mean direction, k = precision parameter, A_{95} = radius of 95% confidence cone of the paleomagnetic pole. Reliability criteria follow Van der Voo (1990). Bold font highlights paleopoles that non-overlap with the Phanerozoic apparent polar wander path of West African Craton.*

Table 2 Geochronology of Precambrian mafic intrusions in West African Craton.

Location	Swarm	Latitude (°N)	Longitude (°E)	Sample name	Dyke trend	Age (Ma)	Method	References
Anti-Atlas, Tagragra de Tata	Tagragra de Tata	29.9058	352.0117	41801	N105°	2039.5 ± 6.3	SHRIMP on zircon	Walsh et al. (2002)
Anti-Atlas, Zenaga	Tagragra de Tata	30.3713	352.6913	DZ49	N100°	2040 ± 2	ID-TIMS U-Pb on zircon	Kouyaté et al. (2013)
Anti-Atlas, Tagragra d'Akka	Tagragra d'Akka	29.3728	351.1764	DAK10	N125°	1758 ± 5	ID-TIMS U-Pb on zircon	Youbi et al. (2013)
Anti-Atlas, Tafeltast-Kerdous	Tagragra d'Akka	29.4077	351.0089	AT14	N170°	1741 ± 10	ID-TIMS U-Pb on baddeleyite	Youbi et al. (2013)
Anti-Atlas, Iguerda-Taïfast	Tagragra d'Akka	30.2602	352.4015	DIGI064	N135°	1746.8 ± 3.7	ID-TIMS U-Pb on baddeleyite	Youbi et al. (2013)
Anti-Atlas, Zenaga	Tagragra d'Akka	30.5221	352.8222	DZ67	N125°	1734 ± 5	ID-TIMS U-Pb on baddeleyite	Youbi et al. (2013)
Anti-Atlas, Igherm	Tagragra d'Akka?	29.9983	351.3500	IM3	(sill)	1706 ± 7	ID-TIMS U-Pb on baddeleyite	Ikenne et al. (2017)
Anti-Atlas, Zenaga	Zenaga	30.5841	352.8218	DZ40	(sill)	1656 ± 9	ID-TIMS U-Pb on baddeleyite	Kouyaté et al. (2013)
Anti-Atlas, Zenaga	Zenaga	30.5828	352.8173	DZ36	(sill)	1641 ± 3	ID-TIMS U-Pb on baddeleyite	Kouyaté et al. (2013)
Anti-Atlas, Agadir Melloul	Zenaga	30.2460	352.1994	AMHA069	N45°	1654 ± 16	ID-TIMS U-Pb on baddeleyite	Kouyaté et al. (2013)
Anti-Atlas, Bas Drâa	Bas Drâa	28.4818	349.2164	BD21	N40°	1384 ± 6	ID-TIMS U-Pb on baddeleyite	El Bahat et al. (2013)
						1416 ± 7	LA-ICP-MS U-Pb on baddeleyite	Söderlund et al. (2013a)
Anti-Atlas, Bas Drâa	Bas Drâa	28.4603	349.4232	BD12	N135°	1381 ± 8	ID-TIMS U-Pb on baddeleyite	El Bahat et al. (2013)
Anti-Atlas, Iguerda-Taïfast	Iguerda-Taïfast	30.1905	352.3044	DAS094	N30°	885 ± 13	ID-TIMS U-Pb on zircon	Kouyaté et al. (2013)
Anti-Atlas, Zenaga	Iguerda-Taïfast	30.5065	352.7611	DZ2	N30°	857 ± 11	ID-TIMS U-Pb on baddeleyite	Kouyaté et al. (2013)
Anti-Atlas, Bas Drâa	–	28.4573	349.4225	D16	N75°	611.6 ± 1.3	$^{40}Ar/^{39}Ar$ on hornblende	El Bahat et al. (2017)
Reguibat	Ahmeyim	20.7163	345.4753	GTD-8	N30°	2732.6 ± 1.5	ID-TIMS U-Pb on baddeleyite	Tait et al. (2013)
Reguibat	Aousserd-Tichla	22.3984	345.6255	CMS-25	N125°	2688 ± 3	ID-TIMS U-Pb on baddeleyite	Söderlund et al. (2013b)
Man-Leo	Libiri	13.3980	1.2548	DO109	N5-10°	1791 ± 3	ID-TIMS U-Pb on baddeleyite	Baratoux et al. (2019)
Man-Leo	Kédougou	12.6827	347.8080	BK031	N30-40°	1764 ± 4	ID-TIMS U-Pb on baddeleyite	Baratoux et al. (2019)
Man-Leo	Korsimoro	12.8860	358.9295	DO112	N100°	1575 ± 5	ID-TIMS U-Pb on baddeleyite	Baratoux et al. (2019)
Man-Leo	Essakane	14.4271	359.9812	DO115	N130°	1519 ± 2	ID-TIMS U-Pb on baddeleyite	Baratoux et al. (2019)
Man-Leo	Essakane	11.0774	359.5137	YU14	N130°	1525 ± 3	ID-TIMS U-Pb on baddeleyite	Baratoux et al. (2019)
Man-Leo	Essakane	13.4974	359.6712	DO09	N130°	1523 ± 2	ID-TIMS U-Pb on baddeleyite	Baratoux et al. (2019)
Man-Leo	Essakane	9.9983	357.5661	BN29	N130°	1521 ± 2	ID-TIMS U-Pb on baddeleyite	Baratoux et al. (2019)
Man-Leo	Essakane (Sambarabougou)	13.1036	348.0760	BK001	N90°	1521 ± 3	ID-TIMS U-Pb on baddeleyite	Baratoux et al. (2019)
Man-Leo	Oda	5.4338	358.8423	MG-8	N70°	915 ± 7	ID-TIMS U-Pb on baddeleyite	Baratoux et al. (2019)
Man-Leo	Manso	5.3083	358.1293	GH370	N175°	867 ± 16	ID-TIMS U-Pb on baddeleyite	Baratoux et al. (2019)

References

Aïfa, T., Lefort, J.P., Drareni, A., 2001. New paleopoles at 1.4–1.9 Ga from dyke swarms of the West African Craton: paleomagnetic contribution to the accretionary phase of Rodinia. *Gondwana Research* 4(4), 559-560.

Ait Lahna, A., Youbi, N., Tassinari, C.C.G., Basei, M.A.S., Ernst, R.E., Chaib, L., Barzouk, A., Mata, J., Gärtner, A., Admou, H., Boumehdi, M.A., Söderlund, U., Bensalah, M.K., Bodinier, J-L., Maacha, L., Bekker, A., 2020. Revised stratigraphic framework for the lower Anti-Atlas supergroup based on U–Pb geochronology of magmatic and detrital zircons (Zenaga and Bou Azzer-El Graara inliers, Anti-Atlas Belt, Morocco). *Journal of African Earth Sciences* 171, 103946.

Álvaro, J.J., Macouin, M., Bauluz, B., Clausen, S., Ader, M., 2007. The Ediacaran sedimentary architecture and carbonate productivity in the Atar cliffs, Adrar, Mauritania: Palaeoenvironments, chemostratigraphy and diagenesis. *Precambrian Research* 153(3-4), 236-261.

Álvaro, J.J., Pouclet, A., Ezzouhairi, H., Soulaimani, A., Bouougri, E.H., Imaz, A.G., Fekkak, A., 2014. Early Neoproterozoic rift-related magmatism in the Anti-Atlas margin of the West African craton, Morocco. *Precambrian Research* 255, 433-442.

Auvray, B., Peucat, J.J., Potrel, A., Burg, J.P., Caruba, C., Dars, R., Lo, K., 1992. Données géochronologiques nouvelles sur l'Archéen de l'Amsaga (Dorsale Réguibat, Mauritanie). Comptes rendus de l'Académie des sciences. Série 2, Mécanique, Physique, Chimie, Sciences de l'univers, *Sciences de la Terre* 315(1), 63-70.

Baratoux, L., Metelka, V., Naba, S., Jessell, M.W., Grégoire, M., Ganne, J., 2011. Juvenile Paleoproterozoic crust evolution during the Eburnean orogeny (~ 2.2–2.0 Ga), western Burkina Faso. *Precambrian Research* 191(1-2), 18-45.

Baratoux, L., Söderlund, U., Ernst, R.E., De Roever, E., Jessell, M.W., Kamo, S., Naba, S., Perrouty, S., Metelka, V., Yatte, D., Grenholm, M., 2019. New U–Pb baddeleyite ages of mafic dyke swarms of the West African and Amazonian cratons: Implication for their configuration in supercontinents through time. In Dyke Swarms of the World: A Modern Perspective (263-314). Springer, Singapore.

Berge, J.W., 1974. Geology, geochemistry, and origin of the Nimba itabirite and associated rocks, Nimba County, Liberia. *Economic Geology* 69(1), 80-92.

Bertrand-Sarfati, J., Moussine-Pouchkine, A., Affaton, P., Trompette, R., Bellion, Y., 1991. Cover sequences of the West African craton. In the West African orogens and circum-Atlantic correlatives (Chapter 4). Springer, Berlin, Heidelberg.

Bispo-Santos, F., D'Agrella-Filho, M.S., Pacca, I.I., Janikian, L., Trindade, R.I., Elming, S.Å., Silva, J.A., Barros, M.A., Pinho, F.E., 2008. Columbia revisited: Paleomagnetic results from the 1790 Ma colider volcanics (SW Amazonian Craton, Brazil). *Precambrian Research* 164(1-2), 40-49.

Bispo-Santos, F., D'Agrella-Filho, M.S., Janikian, L., Reis, N.J., Trindade, R.I., Reis, M.A.A., 2014. Towards Columbia: Paleomagnetism of 1980–1960 Ma Surumu volcanic rocks, Northern Amazonian Craton. *Precambrian Research* 244, 123-138.

Bleeker, W., 2003. The late Archean record: a puzzle in ca. 35 pieces. Lithos 71 (2-4), 99-134.

Blein, O., Baudin, T., Chevremont, P., Soulaimani, A., Admou, H., Gasquet, P., Cocherie, A., Egal, E., Youbi, N., Razin, P., Bouabdelli, M., 2014a. Geochronological constraints on the polycyclic magmatism in the Bou Azzer-El Graara inlier (central Anti-Atlas Morocco). *Journal of African Earth Sciences* 99, 287-306.

Blein, O., Baudin, T., Soulaimani, A., Cocherie, A., Chevremont, P., Admou, H., Ouanaimi, H., Hafid, A., Razin, P., Bouabdelli, M., Roger, J., 2014b. New geochemical, geochronological and structural constraints on the Ediacaran evolution of the south Sirwa, Agadir-Melloul and Iguerda inliers, Anti-Atlas, Morocco. *Journal of African Earth Sciences* 98, 47-71.

Bogdanova, S.V., Gintov, O.B., Kurlovich, D.M., Lubnina, N.V., Nilsson, M.K., Orlyuk, M.I., Pashkevich, I.K., Shumlyanskyy, L.V., Starostenko, V.I., 2013. Late Palaeoproterozoic mafic dyking in the Ukrainian Shield of Volgo-Sarmatia caused by rotation during the assembly of supercontinent Columbia (Nuna). *Lithos* 174, 196-216.

Boudzoumou, F., Vandamme, D., Affaton, P., Gattacceca, J., 2011. Neoproterozoic paleomagnetic poles in the Taoudeni basin (West Africa). *Comptes Rendus Geoscience* 343 (4), 284-294.

Bouougri, E.H., Ait Lahna, A., Tassinari, C.C.G., Basei, M.A.S., Youbi, N., Admou, H., Saquaque, A., Boumehdi, A., Maacha, L., 2020. Time constraints on early Tonian Rifting and Cryogenian Arc terrane-continent convergence along the northern margin of the West African craton: Insights from SHRIMP and LAICP–MS zircon geochronology in the Pan-African Anti-Atlas belt (Morocco), *Gondwana Research* 85, 169-188.

Bradley, D.C., O'Sullivan, P., Cosca, M.A., Motts, H.A., Horton, J.D., Taylor, C.D., Beaudoin, G., Lee, G.K., Ramezani, J., Bradley, D.B., Jones, J.V., Bowring, S., 2015. Synthesis of geological, structural, and geochronologic data (phase V, deliverable 53). Chapter A of Taylor, C.D., ed., Second projet de renforcement institutionnel du secteur minier de la République Islamique de Mauritanie (PRISM-II): U.S. Geological Survey Open-File Report 2013-1280-A, 328p., http://dx.doi.org/10.3133/ofr20131280. [In English and French].

Bronner, G., Chauvel, J.J., 1979. Precambrian banded iron-formations of the Ijil Group (Kediat Ijil, Reguibat Shield, Mauritania). *Economic Geology* 74(1), 77-94.

Buchan, K.L., Mortensen, J.K., Card, K.D., 1994. Integrated paleomagnetic and U–Pb geochronologic studies of mafic intrusions in the southern Canadian Shield: Implications for the early Proterozoic polar wander path. *Precambrian Research* 69(1-4), 1-10.

Chardon, D., 1997. Les deformations continentals Archéennes. Examples naturels et modèlisation thermomécanique. Mémoires de Géosciences, Rennes, 76.

Chaves, A.D.O., de Rezende, C.R., 2019. Fragments of 1.79–1.75 Ga Large Igneous Provinces in reconstructing Columbia (Nuna): a Statherian supercontinent-superplume coupling? *Episodes* 42(1), 55-67.

Clauer, N., 1976. Géochimie isotopique du strontium des milieux sédimentaires. Application à la géochronologie de la couverture du craton ouest-africain (Vol. 45, No. 1). Persée-Portail des revues scientifiques en SHS.

Clauer, N., Caby, R., Jeannette, D., Trompette, R., 1982. Geochronology of sedimentary and metasedimentary Precambrian rocks of the West African craton. *Precambrian Research* 18(1-2), 53-71.

Clauer, N., Deynoux, M., 1987. New information on the probable isotopic age of the late Proterozoic glaciation in West Africa. *Precambrian Research* 37(2), 89-94.

Danderfer, A., De Waele, B., Pedreira, A.J., Nalini, H.A., 2009. New geochronological constraints on the geological evolution of Espinhaço basin within the São Francisco Craton–Brazil. *Precambrian Research* 170(1-2), 116-128.

D'Agrella-Filho, M.S., Tohver, E., Santos, J.O., Elming, S.Å., Trindade, R.I., Pacca, I.I., Geraldes, M.C., 2008. Direct dating of paleomagnetic results from Precambrian sediments in the Amazon craton: Evidence for Grenvillian emplacement of exotic crust in SE Appalachians of North America. *Earth and Planetary Science Letters* 267(1-2), 188-199.

D'Agrella-Filho, M.S., Trindade, R.I., Tohver, E., Janikian, L., Teixeira, W., Hall, C., 2011. Paleomagnetism and $^{40}Ar/^{39}Ar$ geochronology of the high-grade metamorphic rocks of the Jequié block, São Francisco Craton: Atlantica, Ur and beyond. *Precambrian Research* 185(3-4), 183-201.

Deynoux, M., 1985. Terrestrial or waterlain glacial diamictites? Three case studies from the Late Precambrian and Late Ordovician glacial drifts in West Africa. *Palaeogeography, Palaeoclimatology, Palaeoecology* 51(1-4), 97-141.

Doumbia, S., Pouclet, A., Kouamelan, A., Peucat, J.J., Vidal, M., Delor, C., 1998. Petrogenesis of juvenile-type Birimian (Paleoproterozoic) granitoids in Central Côte-

d'Ivoire, West Africa: geochemistry and geochronology. *Precambrian Research* 87(1-2), 33-63.

El Bahat, A., Ikenne, M., Söderlund, U., Cousens, B., Youbi, N., Ernst, R., Soulaimani, A., Hafid, A., 2013. U–Pb baddeleyite ages and geochemistry of dolerite dykes in the Bas Drâa Inlier of the Anti-Atlas of Morocco: newly identified 1380 Ma event in the West African Craton. *Lithos* 174, 85-98.

El Bahat, A., Ikenne, M., Cousens, B., Söderlund, U., Ernst, R., Klausen, M.B., Youbi, N., 2017. New constraints on the geochronology and Sm-Nd isotopic characteristics of Bas-Drâa mafic dykes, Anti-Atlas of Morocco. *Journal of African Earth Sciences* 127, 77-87.

Ennih, N., Liégeois, J.P., 2008. The boundaries of the West African craton, with special reference to the basement of the Moroccan metacratonic Anti-Atlas belt. *Geological Society, London, Special Publications* 297(1), 1-17.

Ernst, R.E., Buchan, K.L., Hamilton, M.A., Okrugin, A.V., Tomshin, M.D., 2000. Integrated paleomagnetism and U-Pb geochronology of mafic dikes of the eastern Anabar Shield region, Siberia: Implications for Mesoproterozoic paleolatitude of Siberia and comparison with Laurentia. *The Journal of Geology* 108(4), 381-401.

Ernst, R.E., Bell, K., 2010. Large igneous provinces (LIPs) and carbonatites. *Mineralogy and Petrology* 98(1-4), 55-76.

Ernst, R.E., Bleeker, W., Söderlund, U., Kerr, A.C., 2013. Large Igneous Provinces and supercontinents: Toward completing the plate tectonic revolution. *Lithos* 174, 1-14.

Ernst, R.E., Hamilton, M.A., Söderlund, U., Hanes, J.A., Gladkochub, D.P., Okrugin, A.V., Kolotilina, T., Mekhonoshin, A.S., Bleeker, W., LeCheminant, A.N., Buchan, K.L.,

2016. Long-lived connection between southern Siberia and northern Laurentia in the Proterozoic. *Nature Geoscience* 9(6), 464-469.

Evans, D.A.D., 2009. The palaeomagnetically viable, long-lived and all-inclusive Rodinia supercontinent reconstruction. *Geological Society, London, Special Publications* 327(1), 371-404.

Evans, D.A.D., Mitchell, R.N., 2011. Assembly and breakup of the core of Paleoproterozoic–Mesoproterozoic supercontinent Nuna. *Geology* 39(5), 443-446.

Evans, D.A.D., 2013. Reconstructing pre-Pangean supercontinents. *Geological Society of America Bulletin* 125(11-12), 1735-1751.

Evans, D.A.D., Eglington, B.M., Elming, S.-Å., Gong, Z., Li, Z.-X., McCausland, P.J., Meert, J.G., Mertanen, S., Pesonen, L.J., Pisarevsky, S.A., Pivarunas, A.F., Salminen, J.M., Swanson-Hysell, N., Torsvik, T.H., Trindade, R.I.F., Veikkolainen, T., Zhang, S., 2021. Chapter 19: An expanding list of reliable paleomagnetic poles for Precambrian tectonic reconstructions. In: Pesonen, L.J., Salminen, J.M., Evans, D.A.D., Elming, S.-Å., Veikkolainen, T. (eds.), *Ancient Supercontinents and the Paleogeography of Earth*. Elsevier, xxx-xxx.

Franceschinis, P.R., Rapalini, A.E., Bettucci, L.S., Dopico, C.M., Milanese, F.N., 2019. Paleomagnetic confirmation of the "unorthodox" configuration of Atlantica between 2.1–2.0 Ga. *Precambrian Research* 334, 105447.

Fu, X., Zhang, S., Li, H., Ding, J., Li, H., Yang, T., Wu, H., Yuan, H., Lv, J., 2015. New paleomagnetic results from the Huaibei Group and Neoproterozoic mafic sills in the North China Craton and their paleogeographic implications. *Precambrian Research* 269, 90-106.

Gladkochub, D.P., Donskaya, T.V., Mazukabzov, A.M., Stanevich, A.M., Sklyarov, E.V., Ponomarchuk, V.A., 2007. Signature of Precambrian extension events in the southern Siberian craton. *Russian Geology and Geophysics* 48(1), 17-31.

Gladkochub, D.P., Pisarevsky, S.A., Ernst, R., Donskaya, T.V., Söderlund, U., Mazukabzov, A.M., Hanes, J., 2010. Large igneous province of about 1750 Ma in the Siberian Craton. *Doklady Earth Sciences* 430(2), 168-171.

Grenholm, M., Jessell, M., Thébaud, N., 2019. A geodynamic model for the Paleoproterozoic (ca. 2.27–1.96 Ga) Birimian Orogen of the southern West African Craton–Insights into an evolving accretionary-collisional orogenic system. *Earth-Science Reviews* 192, 138-193.

Hoffman, P.F., 1989. Speculations on Laurentia's first gigayear (2.0 to 1.0 Ga). *Geology* 17(2), 135-138.

Ikenne, M., Söderlund, U., Ernst, R.E., Pin, C., Youbi, N., Hafid, A., 2017. A c. 1710 Ma mafic sill emplaced into a quartzite and calcareous series from Ighrem, Anti-Atlas–Morocco: Evidence that the Taghdout passive margin sedimentary group is nearly 1 Ga older than previously thought. *Journal of African Earth Sciences* 127, 62-76.

Jessell, M., Santoul, J., Baratoux, L., Youbi, N., Ernst, R.E., Metelka, V., Miller, J., Perrouty, S., 2015. An updated map of West African mafic dykes. *Journal of African Earth Sciences* 112, 440-450.

Johansson, Å., 2009. Baltica, Amazonia and the SAMBA connection–1000 million years of neighbourhood during the Proterozoic? *Precambrian Research* 175(1-4), 221-234.

Kah, L. C., Bartley, J. K., Teal, D. A., 2012. Chemostratigraphy of the Late Mesoproterozoic Atar Group, Taoudeni Basin, Mauritania: Muted isotopic variability, facies correlation, and global isotopic trends. *Precambrian Research* 200, 82-103.

Kent, D.V., Dia, O., Sougy, J.M.A., 1984. Paleomagnetism of Lower-Middle Devonian and Upper Proterozoic-Cambrian(?) rocks from Mejeira (Mauritania, West Africa). Geodynamics Series: Plate Reconstruction from Paleozoic Paleomagnetism 12, 99-115.

Key, R.M., Loughlin, S.C., Gillespie, M., Del Rio, M., Horstwood, M.S.A., Crowley, Q.G., Darbyshire, D.P.F., Pitfield, P.E.J., Henney, P.J., 2008. Two Mesoarchaean terranes in the Reguibat shield of NW Mauritania. *Geological Society, London, Special Publications* 297(1), 33-52.

Knopf, D., 1967. Les dolerites de Coté d'Ivoire. Soc. Dev. Min. Coté d'lvoire, Mem. 188.

Konhauser, K.O., Planavsky, N.J., Hardisty, D.S., Robbins, L.J., Warchola, T.J., Haugaard, R., Lalonde, S.V., Partin, C.A., Oonk, P.B.H., Tsikos, H., Lyons, T.W., 2017. Iron formations: A global record of Neoarchaean to Palaeoproterozoic environmental history. *Earth-Science Reviews* 172, 140-177.

Kouyaté, D., Söderlund, U., Youbi, N., Ernst, R., Hafid, A., Ikenne, M., Soulaimani, A., Bertrand, H., Chaham, K.R.K., 2013. U–Pb baddeleyite and zircon ages of 2040 Ma, 1650 Ma and 885 Ma on dolerites in the West African Craton (Anti-Atlas inliers): Possible links to break-up of Precambrian supercontinents. *Lithos* 174, 71-84.

Ledru, P., Johan, V., Milési, J.P., Tegyey, M., 1994. Markers of the last stages of the Palaeoproterozoic collision: evidence for a 2 Ga continent involving circum-South Atlantic provinces. *Precambrian Research* 69(1-4), 169-191.

Letsch, D., Large, S.J., Buechi, M.W., Winkler, W., von Quadt, A., 2018. Ediacaran glaciations of the west African Craton–Evidence from Morocco. *Precambrian Research* 310, 17-38.

Letsch, D., Large, S.J., Bernasconi, S.M., Klug, C., Blattmann, T.M., Winkler, W., von Quadt, A., 2019. Northwest Africa's Ediacaran to early Cambrian fossil record, its oldest metazoans and age constraints for the basal Taroudant Group (Morocco). *Precambrian Research* 320, 438-453.

Li, Z.X., Bogdanova, S.V., Collins, A.S., Davidson, A., De Waele, B., Ernst, R.E., Fitzsimons, I.C.W., Fuck, R.A., Gladkochub, D.P., Jacobs, J., Karlstrom, K.E., 2008. Assembly, configuration, and break-up history of Rodinia: A synthesis. *Precambrian Research* 160(1-2), 179-210.

Li, Z.X., Mitchell, R.N., Spencer, C.J., Ernst, R., Pisarevsky, S., Kirscher, U., Murphy, J.B., 2019. Decoding Earth's rhythms: modulation of supercontinent cycles by longer superocean episodes. *Precambrian Research* 323, 1-5.

Lomax, K., 1975. Palaeomagnetic studies of Proterozoic rocks in Britain and West Africa. PhD Thesis, University of Leeds, 176p.

Martin, D. L., Nairn, A. E. M., Noltimier, H. C., Petty, M. H., Schmitt, T. J., 1978. Paleozoic and Mesozoic paleomagnetic results from Morocco. *Tectonophysics* 44 (1-4), 91-114.

Nomade, S., Chen, Y., Pouclet, A., Féraud, G., Théveniaut, H., Daouda, B. Y., Rigolet, C., 2003. The Guiana and the West African shield Palaeoproterozoic grouping: new palaeomagnetic data for French Guiana and the Ivory Coast. *Geophysical Journal International* 154 (3), 677-694.

Onstott, T.C., Hargraves, R.B., 1981. Proterozoic transcurrent tectonics: palaeomagnetic evidence from Venezuela and Africa. *Nature* 289(5794), 131-136.

Onstott, T.C., Hargraves, R.B., York, D., Hall, C., 1984. Constraints on the motions of South American and African Shields during the Proterozoic: I. $^{40}Ar/^{39}Ar$ and paleomagnetic correlations between Venezuela and Liberia. *Geological Society of America Bulletin* 95(9), 1045-1054.

Onstott, T.C., Dorbor, J., 1987. $^{40}Ar/^{39}Ar$ and paleomagnetic results from Liberia and the Precambrian APW data base for the West African Shield. *Journal of African Earth Sciences* 6(4), 537-552.

Peng, P., 2010. Reconstruction and interpretation of giant mafic dyke swarms: a case study of 1.78 Ga magmatism in the North China craton. *Geological Society, London, Special Publications* 338(1), 163-178.

Peng, P., Bleeker, W., Ernst, R.E., Söderlund, U., McNicoll, V., 2011. U–Pb baddeleyite ages, distribution and geochemistry of 925 Ma mafic dykes and 900 Ma sills in the North China craton: evidence for a Neoproterozoic mantle plume. *Lithos* 127(1-2), 210-221.

Perrin, M., Prévot, M., 1988. Uncertainties about the Proterozoic and Paleozoic polar wander path of the West African craton and Gondwana: evidence for successive remagnetization events. *Earth and Planetary Science Letters* 88(3-4), 337-347.

Perrin, M., Elston, D.P., Moussine-Pouchkine, A., 1988. Paleomagnetism of Proterozoic and Cambrian strata, Adrar de Mauritanie, cratonic West Africa. *Journal of Geophysical Research: Solid Earth* 93(B3), 2159-2178.

Peucat, J.J., Capdevila, R., Drareni, A., Mahdjoub, Y., Kahoui, M., 2005. The Eglab massif in the West African Craton (Algeria), an original segment of the Eburnean orogenic belt: petrology, geochemistry and geochronology. *Precambrian Research* 136(3-4), 309-352.

Piper, J.D.A., Lomax, K., 1973. Palaeomagnetism of Precambrian Birrimian and Tarkwaian rocks of West Africa. *Geophysical Journal International* 34(4), 435-450.

Pisarevsky, S., 2005. New edition of the global paleomagnetic database. Eos, Transactions American Geophysical Union 86(17), 170.

Pisarevsky, S.A., Elming, S.Å., Pesonen, L.J., Li, Z.X., 2014. Mesoproterozoic paleogeography: supercontinent and beyond. *Precambrian Research* 244, 207-225.

Pivarunas, A.F., Meert, J.G., Miller, S.R., 2018. Assessing the intersection/remagnetization puzzle with synthetic apparent polar wander paths. *Geophysical Journal International* 214(2), 1164-1172.

Potrel, A., Peucat, J. J., Fanning, C. M., 1998. Archean crustal evolution of the West African Craton: example of the Amsaga Area (Reguibat Rise). U-Pb and Sm-Nd evidence for crustal growth and recycling. *Precambrian Research* 90 (3-4), 107-117.

Potrel, A., Peucat, J. J., Fanning, C. M., Auvray, B., Burg, J. P., Caruba, C., 1996. 3.5 Ga old terranes in the West African craton, Mauritania. *Journal of the Geological Society* 153 (4), 507-510.

Pouclet, A., El Hadi, H., Álvaro, J.J., Bardintzeff, J.M., Benharref, M., Fekkak, A., 2018. Review of the Cambrian volcanic activity in Morocco: geochemical fingerprints and geotectonic implications for the rifting of West Gondwana. *International Journal of Earth Sciences* 107(6), 2101-2123.

Puchkov, V.N., Bogdanova, S.V., Ernst, R.E., Kozlov, V.I., Krasnobaev, A.A., Söderlund, U., Wingate, M.T., Postnikov, A.V., Sergeeva, N.D., 2013. The ca. 1380 Ma Mashak igneous event of the Southern Urals. *Lithos* 174, 109-124.

McCourt, S., Armstrong, R.A., Jelsma, H., Mapeo, R.B.M., 2013. New U–Pb SHRIMP ages from the Lubango region, SW Angola: insights into the Palaeoproterozoic evolution of the Angolan Shield, southern Congo Craton, Africa. *Journal of the Geological Society* 170(2), 353-363.

Mitchell, R.N., Kilian, T.M., Evans, D.A.D., 2012. Supercontinent cycles and the calculation of absolute palaeolongitude in deep time. *Nature* 482(7384), 208-211.

Montero, P., Haissen, F., El Archi, A., Rjimati, E., Bea, F., 2014. Timing of Archean crust formation and cratonization in the Awsard-Tichla zone of the NW Reguibat Rise, West African Craton: A SHRIMP, Nd–Sr isotopes, and geochemical reconnaissance study. *Precambrian Research* 242, 112-137.

Morel, P., 1981. Palaeomagnetism of a Pan-African diorite: A Late Precambrian pole for western Africa. *Geophysical Journal International* 65(2), 493-503.

Morris, W.A., Carmichael, C.M., 1978. Paleomagnetism of some late Precambrian and lower Paleozoic sediments from L'Adrar de Mauritanie, West Africa. *Canadian Journal of Earth Sciences* 15(2), 253-262.

Murphy, J.B., Nance, R.D., 2003. Do supercontinents introvert or extrovert? Sm-Nd isotope evidence. *Geology* 31(10), 873-876.

Nance, R.D., Murphy, J.B., Strachan, R.A., Keppie, J.D., Gutiérrez-Alonso, G., Fernández-Suárez, J., Quesada, C., Linnemann, U., D'lemos, R., Pisarevsky, S.A., 2008. Neoproterozoic-early Palaeozoic tectonostratigraphy and palaeogeography of the peri-

Gondwanan terranes: Amazonian v. West African connections. *Geological Society, London, Special Publications* 297(1), 345-383.

Neres, M., Silva, P.F., Ikenne, M., Martins, S., Hafid, A., Mata, J., Almeida, F., Youbi, N., Boumehdi, M.A., 2016. Evidences for multiple remagnetization of Proterozoic dykes from Iguerda inlier (Anti-Atlas Belt, Southern Morocco). *Studia Geophysica et Geodaetica* 60(4), 700-730.

Nilsson, M.K.M., Klausen, M.B., Söderlund, U., Ernst, R.E., 2013. Precise U–Pb ages and geochemistry of Palaeoproterozoic mafic dykes from southern West Greenland: linking the North Atlantic and the Dharwar cratons. *Lithos* 174, 255-270.

Rapalini, A.E., Bettucci, L.S., Badgen, E., Vásquez, C.A., 2015. Paleomagnetic study on mid-Paleoproterozoic rocks from the Rio de la Plata craton: Implications for Atlantica. *Gondwana Research* 27(4), 1534-1549.

Reis, N.J., Teixeira, W., Hamilton, M.A., Bispo-Santos, F., Almeida, M.E., D'Agrella-Filho, M.S., 2013. Avanavero mafic magmatism, a late Paleoproterozoic LIP in the Guiana Shield, Amazonian Craton: U–Pb ID–TIMS baddeleyite, geochemical and paleomagnetic evidence. *Lithos* 174, 175-195.

Robert, B., Besse, J., Blein, O., Greff-Lefftz, M., Baudin, T., Lopes, F., Meslouh, S., Belbadaoui, M., 2017. Constraints on the Ediacaran inertial interchange true polar wander hypothesis: A new paleomagnetic study in Morocco (West African Craton). *Precambrian Research* 295, 90-116.

Rocci, G., Bronner, G., Deschamps, M., 1991. Crystalline basement of the West African craton. In the West African orogens and circum-Atlantic correlatives (Chapter 3). Springer, Berlin, Heidelberg.

Rogers, J.J., 1996. A history of continents in the past three billion years. *The Journal of Geology* 104(1), 91-107.

Rogers, J.J., Santosh, M., 2002. Configuration of Columbia, a Mesoproterozoic supercontinent. *Gondwana Research* 5(1), 5-22.

Rogers, J.J., Santosh, M., 2009. Tectonics and surface effects of the supercontinent Columbia. *Gondwana Research* 15(3-4), 373-380.

Rooney, A.D., Selby, D., Houzay, J.P., Renne, P.R., 2010. Re–Os geochronology of a Mesoproterozoic sedimentary succession, Taoudeni basin, Mauritania: Implications for basin-wide correlations and Re–Os organic-rich sediments systematics. *Earth and Planetary Science Letters* 289(3-4), 486-496.

Salminen, J., Klein, R., Veikkolainen, T., Mertanen, S., Mänttäri, I., 2017. Mesoproterozoic geomagnetic reversal asymmetry in light of new paleomagnetic and geochronological data for the Häme dyke swarm, Finland: Implications for the Nuna supercontinent. *Precambrian Research* 288, 1-22.

Santos, J.O.S., Rizzotto, G.J., Potter, P.E., McNaughton, N.J., Matos, R.S., Hartmann, L.A., Chemale Jr, F., Quadros, M.E.S., 2008. Age and autochthonous evolution of the Sunsás Orogen in West Amazon Craton based on mapping and U–Pb geochronology. *Precambrian Research* 165(3-4), 120-152.

Schofield, D.I., Horstwood, M.S.A., Pitfield, P.E.J., Gillespie, M., Darbyshire, F., O'Connor, E.A., Abdouloye, T.B., 2012. U–Pb dating and Sm–Nd isotopic analysis of granitic rocks from the Tiris Complex: New constaints on key events in the evolution of the Reguibat Shield, Mauritania. *Precambrian Research* 204, 1-11.

Tait, J., Straathof, G., Söderlund, U., Ernst, R.E., Key, R., Jowitt, S.M., Lo, K., Dahmada, M.E.M., N'Diaye, O., 2013. The Ahmeyim great dyke of Mauritania: a newly dated Archaean intrusion. *Lithos* 174, 323-332.

Teixeira, W., D'Agrella-Filho, M.S., Hamilton, M.A., Ernst, R.E., Girardi, V.A., Mazzucchelli, M., Bettencourt, J.S., 2013. U–Pb (ID-TIMS) baddeleyite ages and paleomagnetism of 1.79 and 1.59 Ga tholeiitic dyke swarms, and position of the Rio de la Plata Craton within the Columbia supercontinent. *Lithos* 174, 157-174.

Teixeira, W., Ernst, R.E., Hamilton, M.A., Lima, G., Ruiz, A.S., Geraldes, M.C., 2016. Widespread ca. 1.4 Ga intraplate magmatism and tectonics in a growing Amazonia. *GFF* 138(1), 241-254.

Thiéblemont, D., Delor, C., Cocherie, A., Lafon, J.M., Goujou, J.C., Baldé, A., Bah, M., Sané, H., Fanning, C.M., 2001. A 3.5 Ga granite–gneiss basement in Guinea: further evidence for early Archean accretion within the West African Craton. *Precambrian Research* 108(3-4), 179-194.

Thomas, R.J., Chevallier, L.P., Gresse, P.G., Harmer, R.E., Eglington, B.M., Armstrong, R.A., De Beer, C.H., Martini, J.E.J., De Kock, G.S., Macey, P.H., Ingram, B.A., 2002. Precambrian evolution of the Sirwa window, Anti-Atlas orogen, Morocco. *Precambrian Research* 118(1-2), 1-57.

Thomas, R.J., Fekkak, A., Ennih, N., Errami, E., Loughlin, S.C., Gresse, P.G., Chevallier, L.P., Liégeois, J.P., 2004. A new lithostratigraphic framework for the Anti-Atlas Orogen, Morocco. *Journal of African Earth Sciences* 39(3-5), 217-226.

Torsvik, T.H., Van der Voo, R., Preeden, U., Mac Niocaill, C., Steinberger, B., Doubrovine, P.V., Van Hinsbergen, D.J., Domeier, M., Gaina, C., Tohver, E., Meert, J.G., 2012.

Phanerozoic polar wander, palaeogeography and dynamics. *Earth-Science Reviews* 114(3-4), 325-368.

Sabaté, P., Lomax, K., 1975. Données stratigraphiques et paléomagnétiques de la région Yetti-Eglab (Sahara occidental algérien). *Bulletin de B.R.G.M.* 4, 292-311.

Söderlund, U., Ibanez-Mejia, M., El Bahat, A., Ernst, R.E., Ikenne, M., Soulaimani, A., Youbi, N., Cousens, B., Hafid, A., 2013a. Reply to Comment on "U–Pb baddeleyite ages and geochemistry of dolerite dykes in the Bas-Drâa inlier of the Anti-Atlas of Morocco: Newly identified 1380 Ma event in the West African Craton" by André Michard and Dominique Gasquet. *Lithos* 174, 101-108.

Söderlund U., Ernst R.E., Youbi N., Rjimati, E.C., Zemmouri, A., 2013b. A major Archean (2688 Ma) dyke swarm discovered in the western Reguibat Shield, West African craton, Morocco. Unpublished Report #A131. Consortium Project for Reconstruction of Supercontinents Back to 2.7 Ga Using the Large Igneous Province (LIP) Record (www. supercontinent.org), CAMIRO (Canadian Mining Industry Research Organization) and Ernst Geosciences, 1-6.

Slagstad, T., Kulakov, E., Kirkland, C.L., Roberts, N.M., Ganerød, M., 2019. Breaking the Grenville–Sveconorwegian link in Rodinia reconstructions. *Terra Nova* 31, 430-437.

Van der Voo, R., 1990. The reliability of paleomagnetic data. *Tectonophysics* 184(1), 1-9.

Veikkolainen, T.H., Biggin, A.J., Pesonen, L.J., Evans, D.A.D., Jarboe, N.A., 2017. Advancing Precambrian palaeomagnetism with the PALEOMAGIA and PINT (QPI) databases. *Scientific Data* 4, 170068.

Walsh, G.J., Aleinikoff, J.N., Benziane, F., Yazidi, A., Armstrong, T.R., 2002. U–Pb zircon geochronology of the Paleoproterozoic Tagragra de Tata inlier and its Neoproterozoic cover, western Anti-Atlas, Morocco. *Precambrian Research* 117(1-2), 1-20.

Wen, B., Evans, D.A.D., Wang, C., Li, Y.X., Jing, X., 2018. A positive test for the Greater Tarim Block at the heart of Rodinia: Mega-dextral suturing of supercontinent assembly. *Geology* 46(8), 687-690.

Youbi, N., Kouyaté, D., Söderlund, U., Ernst, R.E., Soulaimani, A., Hafid, A., Ikenne, M., El Bahat, A., Bertrand, H., Chaham, K.R., Abbou, M.B., 2013. The 1750 Ma magmatic event of the west African craton (Anti-Atlas, Morocco). *Precambrian Research* 236, 106-123.

Zhang, S., Li, Z.X., Evans, D.A.D., Wu, H., Li, H., Dong, J., 2012. Pre-Rodinia supercontinent Nuna shaping up: a global synthesis with new paleomagnetic results from North China. *Earth and Planetary Science Letters* 353, 145-155.

Zhao, G., Cawood, P.A., Wilde, S.A., Sun, M., 2002. Review of global 2.1–1.8 Ga orogens: implications for a pre-Rodinia supercontinent. *Earth-Science Reviews* 59(1-4), 125-162.

Zhao, G., Sun, M., Wilde, S.A., Li, S., 2004. A Paleo-Mesoproterozoic supercontinent: assembly, growth and breakup. *Earth-Science Reviews* 67(1-2), 91-123.

Chapter 5

Reorienting the West African Craton in Paleoproterozoic-Mesoproterozoic Supercontinent Nuna [1]

Zheng Gong [a], David A.D. Evans [a], Nasrrddine Youbi [b,c], Abdelhak Ait Lahna [b], Ulf Söderlund [d,e], Malika Ait Malek [b], Bin Wen [a], Xianqing Jing [a], Jikai Ding [a], Moulay A. Boumehdi [b], Richard E. Ernst [c,f]

[a] Department of Earth and Planetary Sciences, Yale University, New Haven, CT 06511, USA

[b] Department of Geology, Cadi Ayyad University, Marrakech, P.O. Box 2390, Morocco

[c] Faculty of Geology and Geography, Tomsk State University, Tomsk 634050, Russia

[d] Department of Geology, Lund University, Lund SE-223 62, Sweden

[e] The Swedish Museum of Natural History, Stockholm SE-114 18, Sweden

[f] Department of Earth Science, Carleton University, Ottawa, ON K1S 5B6, Canada

---

[1] Chapter 5 published in Gong, Z., Evans, D. A. D., Youbi, N., Ait Lahna, A., Söderlund, U., Ait Malek, M., Wen, B., Jing, X. Q., Ding, J. K., Boumehdi, M. & Ernst, R. E. (2021). Reorienting the West African Craton in Paleoproterozoic-Mesoproterozoic supercontinent Nuna. *Geology*, v. 49, in press.

Abstract

The location of the West African Craton (WAC) has been poorly constrained in the Paleoproterozoic-Mesoproterozoic supercontinent Nuna (also known as Columbia). Previous Nuna reconstruction models suggested that WAC was connected to Amazonia in a way similar to their relative position in Gondwana. By an integrated paleomagnetic and geochronological study of the Proterozoic mafic dikes in the Anti-Atlas Belt, Morocco, we provide two reliable paleomagnetic poles to test this connection. Incorporating our new poles with quality-filtered poles from the neighboring cratons of WAC, we propose an inverted WAC-Amazonia connection, with northern WAC attached to northeastern Amazonia, as well as a refined configuration of Nuna. Global large igneous province records also conform to our new reconstruction. The inverted WAC-Amazonia connection suggests a substantial change in their relative orientation from Nuna to Gondwana, providing an additional example of large-magnitude cumulative azimuthal rotations between adjacent continental blocks over supercontinental cycles.

1. Introduction

The assembly and dispersal of the Paleoproterozoic-Mesoproterozoic supercontinent Nuna (also known as Columbia) are possibly the earliest manifestation of Earth's supercontinent cycle, which has profoundly influenced Earth's geosphere, biosphere, and atmosphere (Nance et al., 2014). In the past two decades, numerous attempts have been made to reconstruct Nuna, mainly tectono-stratigraphically and paleomagnetically (Evans, 2013). Though still debated, the broad configuration of Nuna is gradually shaping up: a central kernel of Laurentia and Baltica (Gower et al., 1990; Evans and Pisarevsky, 2008), Siberia

either closely or more distally adjacent to northern Laurentia (Evans and Mitchell, 2011; Pisarevsky et al., 2014; Ernst et al., 2016), and proto-Australia near western Laurentia (Payne et al., 2009; Kirscher et al., 2021). However, the positions of the remaining building blocks have great uncertainties, which makes the configuration of Nuna and its transition to the successor supercontinent Rodinia unclear.

West African Craton (WAC, including the São Luís Block in Brazil) is one of the least constrained cratonic pieces of Nuna. Previous Nuna models usually consider an "upright" connection between WAC and Amazonia, with southern WAC attached to northeastern Amazonia, similar to their relationship in Gondwana (Onstott and Hargraves, 1981; Nomade et al., 2003; D'Agrella-Filho et al., 2016). This "upright" connection is presumed to be long-lived, with little change from Paleoproterozoic to Jurassic (Onstott and Hargraves, 1981). With this "upright" connection model being accepted, as well as the lack of reliable pre-Ediacaran paleomagnetic data, WAC is essentially a "puppet" of Amazonia, where its paleogeography in Nuna is entirely determined by data from Amazonia. For example, Johansson (2009) and Zhang et al. (2012) place Baltica, Amazonia, and WAC in juxtaposition to each other along the northeastern margin of Laurentia, known as the "SAMBA" model. Pisarevsky et al. (2014) place WAC and Amazonia off the Grenville margin of Laurentia, where the two cratons are separated from Nuna by oceans and subduction zones, yet the "upright" WAC-Amazonia relationship is maintained. Due to the large gap in pre-Ediacaran paleomagnetic data from WAC, both the "upright" connection between WAC and Amazonia and the position of WAC in Nuna await further tests.

We present an integrated paleomagnetic and geochronological study of two Proterozoic mafic dike swarms in the Anti-Atlas Belt, Morocco (Fig. 1), which provides direct constraints on the paleogeography of WAC. Combined with time-correlative, quality-filtered paleomagnetic poles, and the global large igneous province (LIP) records from other major bounding cratons, we propose a new connection between WAC and Amazonia, and a refined configuration of Nuna.

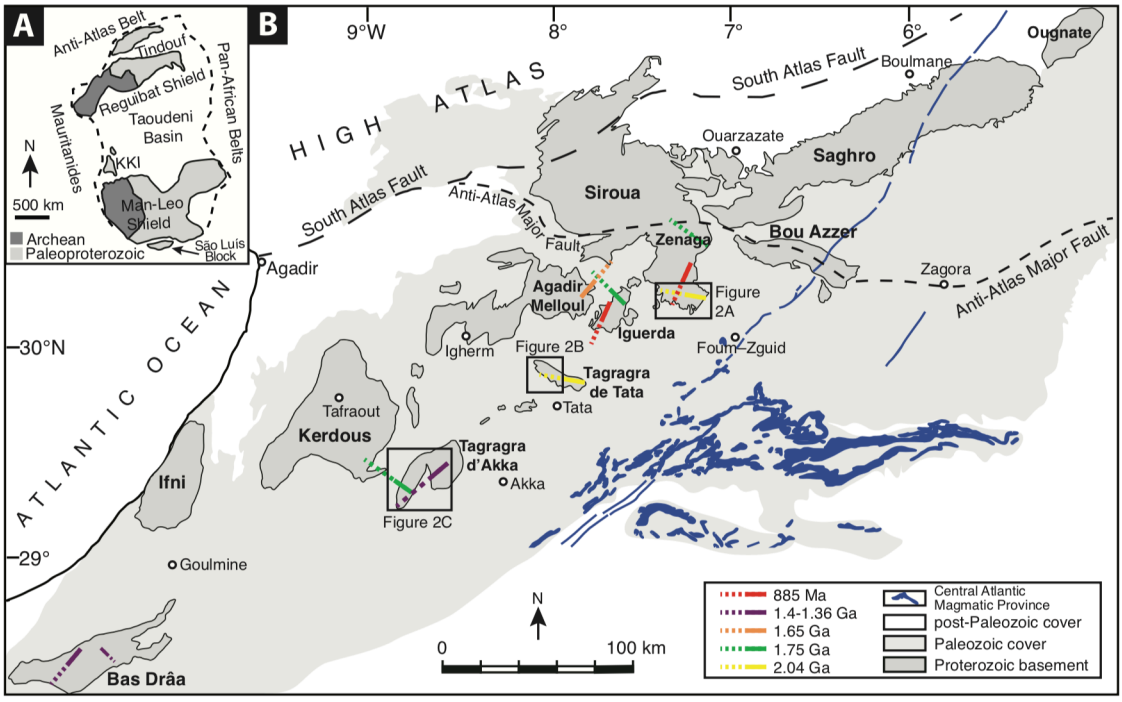

Figure 1 (A) Geological map of the basement rocks in the West African Craton. KKI = Kédougou-Kéniéba and Kayes inliers. The dashed line delineates the cratonic boundary. (B) Geological overview of the mafic dike swarms in the Anti-Atlas Belt, Morocco. Boxes indicate the studied inliers.

2. Mafic dike swarms in the Anti-Atlas Belt

The Anti-Atlas Belt is an 800-km long NE-SW trending anticlinorium that marks the northernmost boundary of WAC (Fig. 1). Paleoproterozoic basement is exposed in ~10 inliers that are enveloped by sedimentary cover since the latest Ediacaran (Maloof et al., 2005). Numerous mafic dikes cross-cut the basement, retaining near-verticality in all directions. These dikes, if precisely dated, are ideal targets for paleomagnetic studies to test various reconstruction models. Recent geochronological work has proposed at least five swarms in the Anti-Atlas Belt, specifically: the E-W striking 2.04 Ga swarm, the NW-SE striking 1.75 Ga swarm, the NE-SW striking 1.65 Ga swarm, the NE-SW striking 1.4-1.36 Ga swarm, and the NNE-SSW striking 885 Ma swarm (Fig. 1; Walsh et al., 2002; El Bahat et al., 2013; Kouyaté et al., 2013; Söderlund et al., 2013; Youbi et al., 2013). The dikes show consistent ages and strikes across the Anti-Atlas inliers (Fig. 1). Contemporaneous dikes have also been recognized in the Man-Leo Shield in southern WAC, such as the NE-SW striking 1.76 Ga Kédougou swarm and the N-S striking 867 Ma Manso swarm (Baratoux et al., 2019), which demonstrates the structural integrity of WAC on a cratonic scale (Gong and Evans, 2021).

3. New Proterozoic paleomagnetic poles

We collected samples from nine dikes of the E-W striking 2.04 Ga swarm from two regions, the Zenaga and Tagragra de Tata inliers (Figs. 2A and 2B). Field and laboratory methods are provided in the Appendix. Two dikes have been precisely dated, one in the Zenaga inlier (dike G18M48) at 2040 ± 2 Ma (ID-TIMS baddeleyite age; Kouyaté et al., 2013) and one in the Tagragra de Tata inlier (dike G19M33) at 2040 ± 6 Ma (SHRIMP zircon age; Walsh et al., 2002). Stable characteristic remanent magnetizations (ChRMs) are isolated

typically from 535-580°C, consistently showing northwest-up and southeast-down directions (Fig. 2D). Although lacking explicit field tests on the age of magnetization, the reliability of these ChRMs is supported by demagnetization results, antipodal directions, and rock magnetic experiments (Supplemental Material). Combining the virtual geomagnetic poles (VGPs) calculated from the nine site-mean directions yielded a 2.04 Ga pole at -22.3°N, 49.6°E (A_{95} = 7.1°, K = 53.3) for WAC.

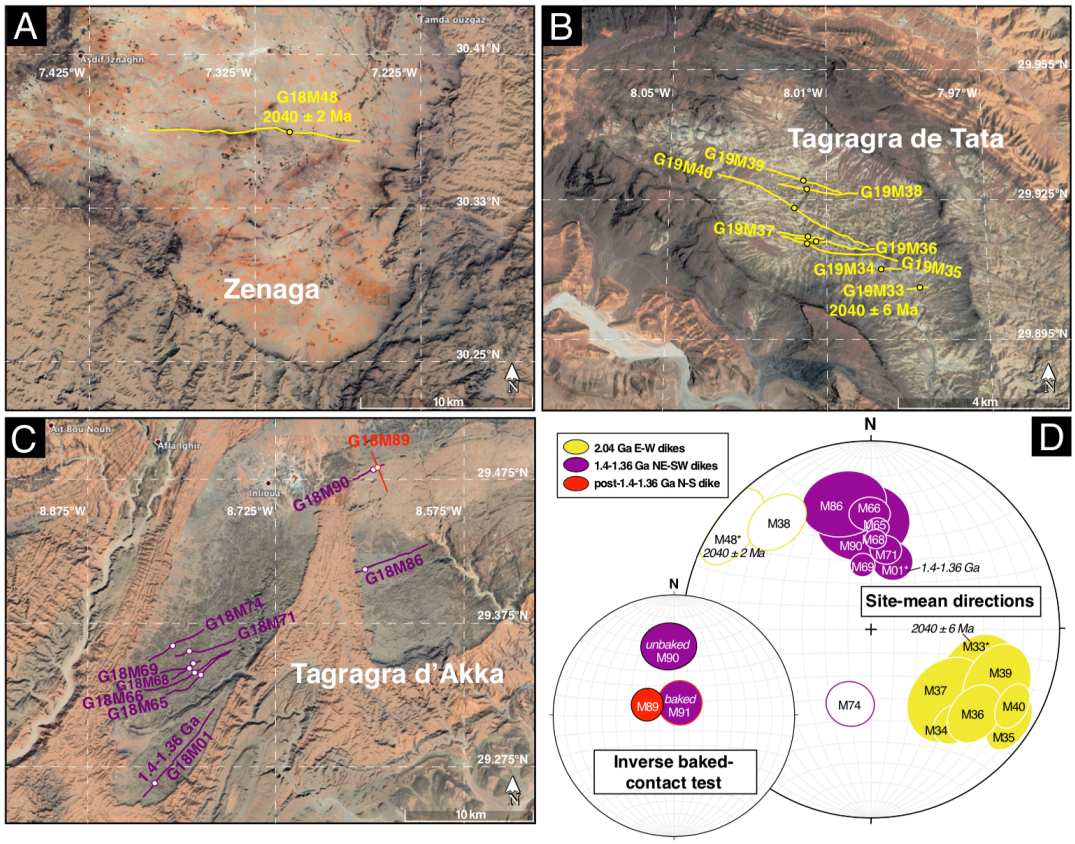

Figure 2 Site locality maps of (A) Zenaga, (B) Tagragra de Tata, and (C) Tagragra d'Akka inliers (Anti-Atlas Belt, Morocco) with Google Earth™ satellite images as the background. (D) Stereographic projection of site-mean directions of the 2.04 Ga dikes (yellow) and the 1.4-1.36 Ga dikes (purple), and the results of the inverse baked-contact test. Dated dikes are marked by asterisks.

In the Tagragra d'Akka inlier, nine sub-parallel NE-SW striking dikes were sampled (Fig. 2C). Results of the ID-TIMS baddeleyite geochronology on one dike (G18M01) show that its age should be 1.4-1.36 Ga (Supplemental Material). Dikes with predominantly NE-SW strikes have also been observed in the Bas Drâa inlier ~180 km southwest of the Tagragra d'Akka inlier (Fig. 1), which are dated to 1.4-1.38 Ga (Söderlund et al., 2013). We suggest that these NE-SW striking dikes across the Anti-Atlas Belt should belong to the same swarm, and the dikes in the Tagragra d'Akka inlier could represent the late-stage pulse of this magmatic episode. Thermal demagnetization reveals stable ChRMs from 350-580°C, which are characterized by antipodal, north-down and south-up directions (Fig. 2D). One dike (G18M90) is cross-cut by a younger N-S striking dike (G18M89) which although itself undated is very likely Precambrian because it does not penetrate the Ediacaran-Cambrian sedimentary cover of the Anti-Atlas Belt. In the immediate baked-contact zone, remanences of the older dike with consistent magnetic mineralogy (Fig. S5) are deflected into near-parallelism with those of the younger dike (Fig. 2D), suggestive of a positive inverse baked-contact test and hence a Precambrian age of remanence for the Tagragra d'Akka NE-SW swarm. From the VGPs of the nine dikes, we obtained a 1.4-1.36 Ga pole at 87.4°N, 44.7°E (A_{95} = 7.8°, K = 44.1) for WAC.

4. An inverted WAC-Amazonia connection

Incorporating our new 2.04 Ga and 1.4-1.36 Ga paleomagnetic poles with a 1.75 Ga VGP obtained from a 1747 ± 4 Ma mafic dike in the Iguerda inlier of the Anti-Atlas Belt (Neres et al., 2016), we can test the connection between WAC and Amazonia. Previous "upright"

models were generated by aligning the Sassandra shear zone in the Man-Leo Shield with the Guri shear zone in the Guiana Shield (Onstott and Hargraves, 1981), and were supported by 2.1-2.0 Ga paleomagnetic data (ibid., Nomade et al., 2003; D'Agrella-Filho et al., 2016). More recently, Chardon et al. (2020) proposed that the Brobo and the Pisco-Jurua shear zones from the two cratons should be continuous, and to align these shear zones they rotated Amazonia ~40° anticlockwise as compared to the reconstruction of Onstott and Hargraves (1981). In the model of Chardon et al. (2020), WAC is still connected to Amazonia in an "upright" sense, and this connection could be accommodated by the ca. 2.0 Ga paleomagnetic data (Antonio et al., 2021).

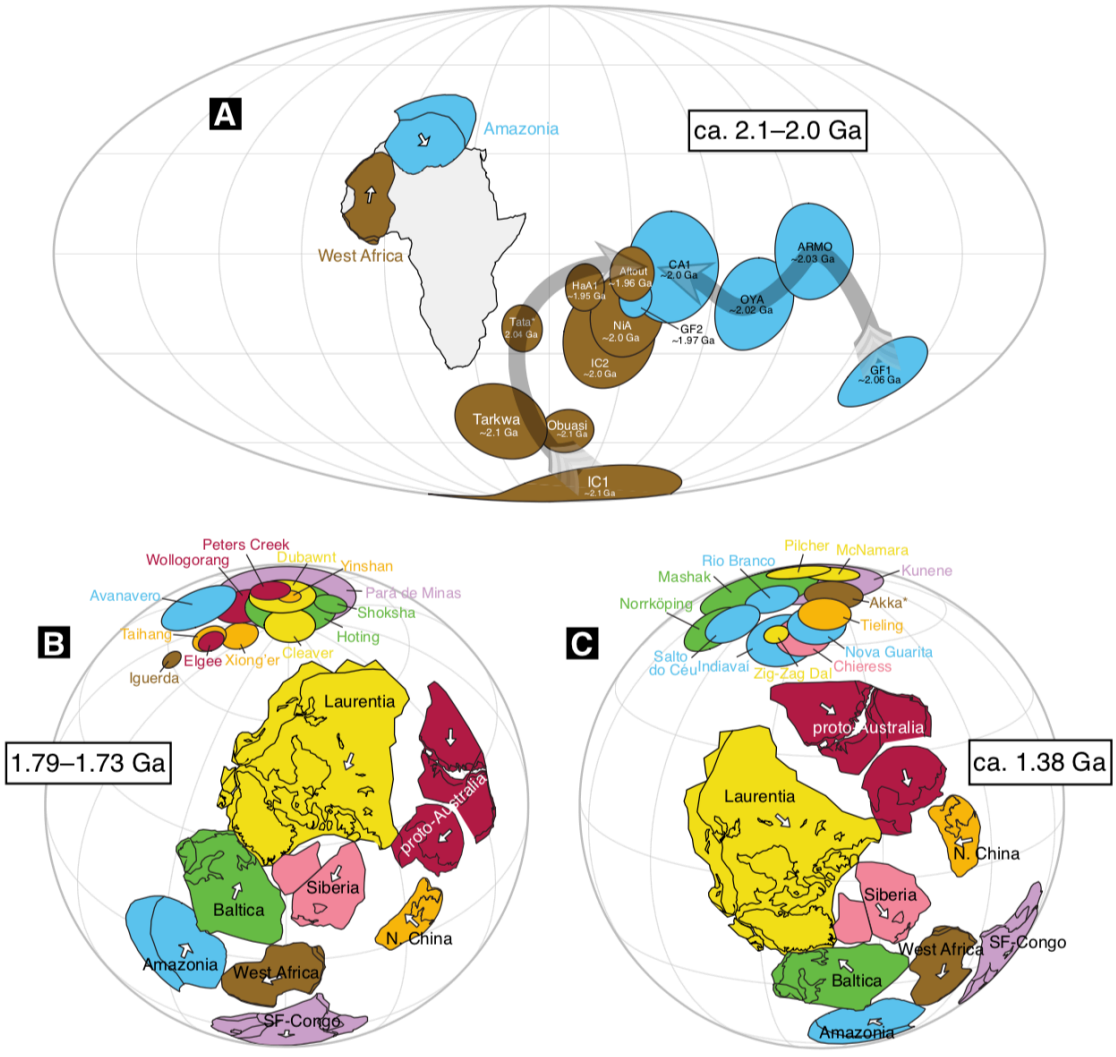

Figure 3 (A) Paleogeographic evolution between West African Craton and Amazonia at 2.1-2.0 Ga. Reconstruction is in present West Africa reference frame, with the outline of Africa shown as the background. The shaded arrows show the younging direction of the apparent polar wander paths. Paleogeographic reconstruction of Nuna at (B) 1.79-1.73 Ga and (C) ca. 1.38 Ga. The white arrows indicate the present-day north direction of the cratons. The selected paleomagnetic poles of each craton (with their abbreviations) are listed in Table S3, of which the colors match those of the cratons. The poles marked by asterisks are from this study. Table S4 lists Euler rotation parameters. SF = São Francisco.

Post-2.0 Ga paleomagnetic data can test whether these "upright"-style models can permissibly persist in Nuna. We examined various Nuna reconstruction models that adopt an "upright"-style connection of WAC and Amazonia (Zhang et al., 2012; D'Agrella-Filho, 2016, 2020; Chardon et al., 2020). None of these models simultaneously match the 1.75 Ga VGP and our 1.4-1.36 Ga pole from WAC with the coeval poles from other cratons (Fig. S8). In particular, in these "upright"-style models, a disagreement is shown between our 1.4-1.36 Ga pole and its time-equivalents from other cratons (Fig. S8). Only breaking the connection between WAC and Amazonia can accommodate our 1.4-1.36 Ga pole in an "upright"-style model (Fig. S8), but then the compatible basement ages and LIP records of these two cratons become unsatisfyingly disjointed.

Alternatively, we consider the opposite polarity of all pre-Ediacaran paleomagnetic poles from WAC, and propose an inverted WAC-Amazonia connection, with northern WAC attached to northeastern Amazonia. In this new model, the apparent polar wander paths

(APWPs) of the two cratons still support a cratonic convergence at 2.1-2.0 Ga (Fig. 3A). More importantly, correlative poles from Amazonia and other cratons agree well with the 1.75 Ga VGP and our new 1.4-1.36 Ga pole from WAC, considering the slight age differences and the uncertainties of the poles themselves (Figs. 3B and 3C). This inverted connection of WAC and Amazonia would negate the shear zone alignments that were proposed as piercing points by Onstott and Hargraves (1981) and Chardon et al. (2020). However, shear zones of 2.1-1.8 Ga age are commonly observed features (Zhao et al., 2002), which makes them less powerful as precise correlation tools. Our inverted model still permits the continuity of Eburnean orogens of WAC with Transamazonian orogens in Amazonia. Specifically, the 2.2-2.0 Ga Anti-Atlas Belt and the Yetti-Eglab massifs in the Reguibat Shield of WAC continue into the 2.2-1.95 Ga Maroni-Itacaiunas Province in Amazonia. In addition, the 2.2-2.05 Ga volcano-sedimentary sequences in Baoulé-Mossi domain and São Luís Block of WAC and the Guiana Shield of Amazonia can still be correlated along an accretionary belt as suggested by Klein et al. (2020) but in a more general sense (Fig. 3A). The subsequent cratonization following the WAC-Amazonia assembly is compatibly reflected by the broadly overlapping 2.0-1.95 Ga poles from the two cratons, with only insignificant APWP distances through late Paleoproterozoic time (Fig. 3A; Gong and Evans, 2021).

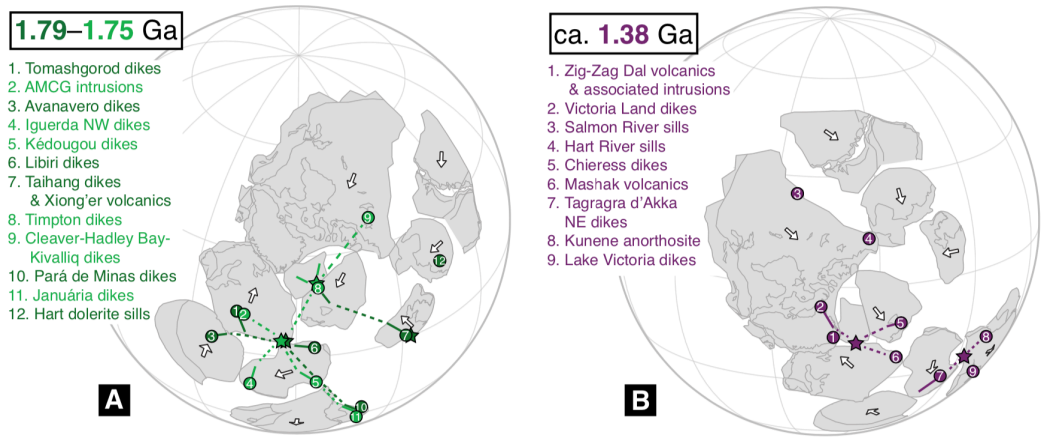

Figure 4 Global LIP records at (A) 1.79-1.75 Ga and (B) ca. 1.38 Ga in Nuna. The solid line segments show the trends of the dike swarms. The dashed lines are potential linkages of the LIPs. The stars indicate proposed plume centers. The white arrows show the present-day north direction for cratons. See Table S5 for bibliographic references for the LIPs. AMCG = anorthosite-mangerite-charnockite-granite.

5. Refined Nuna configuration

Combining our inverted WAC-Amazonia connection with newly published paleomagnetic results from other cratons, we propose a refined configuration of Nuna (Fig. 3). In our reconstruction, Laurentia and Baltica are located in the core of Nuna, with northern Europe connected to eastern Greenland (Gower et al., 1990; Evans and Pisarevsky, 2008). Pisarevsky et al. (2014) suggested that Siberia should be distal to northern Laurentia, which is paleomagnetically permissive. However, we prefer a tight fit between Siberia and Laurentia as suggested by the paleomagnetic study of Evans and Mitchell (2011), which is also supported by their closely matched Proterozoic magmatic records (Ernst et al., 2016). Proto-Australia is located near southwestern Laurentia at ca. 1.8 Ga, then becomes separated from Laurentia by a small ocean, and finally joins Nuna at ca. 1.65 Ga

(Pisarevsky et al., 2014; Kirscher et al., 2019). North China Craton is attached to proto-Australia and off the western margin of Siberia (Kirscher et al., 2021). Unlike Pisarevsky et al. (2014)'s model, we place northwest Amazonia close to southwest Baltica based on the shared histories of long-lived accretions (Johansson, 2009). Additionally, the São Francisco (SF)-Congo Craton, constrained by the new 1.79 Ga Pará de Minas pole from SF (D'Agrella-Filho et al., 2020), juxtaposes with present-day western WAC (Fig. 3). The magmatic barcode of WAC when compared with the barcodes of its bounding cratons shows time-correlative LIP records (Gong and Evans, 2021). With our new reconstruction, these LIPs and their geometries are placed in paleogeographic context. Collectively, LIPs show broad radiating patterns that could indicate potential plume centers near the eastern margin of Baltica around 1.79-1.75 Ga (Fig. 4A), and the northern margin of Baltica and southern margin of SF-Congo at ca. 1.38 Ga (Fig. 4B). The former LIP events would have occurred during the assembly phase of Nuna, whereas the latter should have accompanied the early stages of the supercontinent's fragmentation (Kirscher et al., 2021).

6. Reconstruction implications

Our inverted WAC-Amazonia connection in Nuna, compared to their configuration in Gondwana, indicates large (~180°) relative rotation between these two cratons. Large-scale azimuthal rotations of tectonic blocks are commonplace features of oroclines, where ribbon-like fragments of active continental margins can buckle isoclinally in map view (e.g., Şengör et al., 1993). In contrast, within larger tectonic plates, equidimensional continental blocks from the past few hundred million years have experienced more muted amounts of relative azimuthal rotation, with motions described by distally located Euler

stage poles that give rise to long and quasi-linear seafloor spreading ridges (Vérard et al., 2012). There are exceptions to this general rule, however, leaving aside the more controversial pre-Jurassic ~180° rotational restoration of Malvinas/Falkland microplate to Africa (Martin, 2007). For instance, the Siberian craton rotated nearly 180° relative to Baltica between Ediacaran and Permian time (Şengör et al., 1993) and a similar amount relative to Laurentia during the Rodinia-Pangea supercontinental transition (Merdith et al., 2021). As another example, Amazonia rotated ~180° relative to Laurentia prior to Rodinia assembly, regardless of which pre-Rodinia paleomagnetic polarity option one adopts (D'Agrella-Filho et al., 2016). The relative orientation of North China Craton and Australia also changed by ~180° between their likely Nuna configuration (Kirscher et al., 2021) and early Paleozoic time (Zhao et al., 2021). Although a global model of prescribed Mesoproterozoic-Neoproterozoic plate motions is not yet available, our proposal for the nearly 180° relative rotation between WAC and Amazonia over supercontinental cycles provides an additional instance of this intriguing kinematic style. The dynamics of such large-scale changes in relative orientations are likely related to successive intervals of divergence, convergence, and transform motion accompanying the series of ancient global plate reorganizations (e.g., Müller et al., 2016).

Acknowledgments

Financial support is acknowledged from a U.S. NSF grant (EAR-1953549) to D. Evans, a Swedish Middle East & North Africa (MENA) grant to U. Söderlund, N. Youbi, and R. Ernst, a Russian Mega-Grant (14.Y26.31.0012) to R. Ernst and N. Youbi, and the LIPs–Industry Consortium Project led by R. Ernst (with industry support matched by a Canadian

NSERC grant CRDPJ523131-17). Comments from S. Pisarevsky, R. Mitchell, U. Kirscher, and an anonymous reviewer helped to improve the manuscript.

REFERENCES CITED

Antonio, P.Y.J., D'Agrella-Filho, M.S., Nedelec, A., Poujol, M., Sanchez, C., Dantas, E.L., Dall'Agnol, R., Teixeira, M.F.B., Proietti, A., Dopico, C.M., and Oliveira, D.C., 2021, New constraints for paleogeographic reconstructions at ca. 1.88 Ga from geochronology and paleomagnetism of the Carajás dyke swarm (eastern Amazonia): Precambrian Research, v. 353, p. 106039. https://doi.org/10.1016/j.precamres.2020.106039.

Baratoux, L., Söderlund, U., Ernst, R.E., De Roever, E., Jessell, M.W., Kamo, S., Naba, S., Perrouty, S., Metelka, V., Yatte, D., and Grenholm, M., 2019, New U–Pb baddeleyite ages of mafic dyke swarms of the West African and Amazonian cratons: Implication for their configuration in supercontinents through time, *in* Srivastava, R.K., Ernst, R.E., and Peng, P., eds., Dyke Swarms of the World: A Modern Perspective, p. 263-314. https://doi.org/10.1007/978-981-13-1666-1_7.

Chardon, D., Bamba, O., and Traoré, K., 2020, Eburnean deformation pattern of Burkina Faso and the tectonic significance of shear zones in the West African craton: BSGF-Earth Sciences Bulletin, v. 191, 2, p. 1-18. https://doi.org/10.1051/bsgf/2020001.

D'Agrella-Filho, M.S., Bispo-Santos, F., Trindade, R.I.F., and Antonio, P.Y.J., 2016, Paleomagnetism of the Amazonian Craton and its role in paleocontinents: Brazilian Journal of Geology, v. 46(2), p. 275-299. https://doi.org/10.1590/2317-4889201620160055.

D'Agrella-Filho, M.S., Teixeira, W., da Trindade, R.I., Patroni, O.A., and Prieto, R.F., 2020, Paleomagnetism of 1.79 Ga Pará de Minas mafic dykes: Testing a São

Francisco/Congo-North China-Rio de la Plata connection in Columbia: Precambrian Research, v. 338, p. 105584. https://doi.org/10.1016/j.precamres.2019.105584.

El Bahat, A., Ikenne, M., Söderlund, U., Cousens, B., Youbi, N., Ernst, R., Soulaimani, A., and Hafid, A., 2013, U–Pb baddeleyite ages and geochemistry of dolerite dykes in the Bas Drâa Inlier of the Anti-Atlas of Morocco: newly identified 1380 Ma event in the West African Craton: Lithos, v. 174, p. 85-98. https://doi.org/10.1016/j.lithos.2012.07.022.

Ernst, R.E., Hamilton, M.A., Söderlund, U., Hanes, J.A., Gladkochub, D.P., Okrugin, A.V., Kolotilina, T., Mekhonoshin, A.S., Bleeker, W., LeCheminant, A.N., and Buchan, K.L., 2016, Long-lived connection between southern Siberia and northern Laurentia in the Proterozoic: Nature Geoscience, v. 9(6), p. 464-469. https://doi.org/10.1038/ngeo2700.

Evans, D.A.D., and Pisarevsky, S.A., 2008, Plate tectonics on early Earth? Weighing the paleomagnetic evidence, *in* Condie, K.C., and Pease, V., eds., When did plate tectonics begin on planet Earth: The Geological Society of America Special Paper, v. 440, p. 249-263. https://doi.org/10.1130/2008.2440(12).

Evans, D.A.D., and Mitchell, R.N., 2011, Assembly and breakup of the core of Paleoproterozoic–Mesoproterozoic supercontinent Nuna: Geology, v. 39(5), p. 443-446. https://doi.org/10.1130/G31654.1.

Evans, D.A.D., 2013, Reconstructing pre-Pangean supercontinents: Geological Society of America Bulletin, v. 125(11-12), p. 1735-1751. https://doi.org/10.1130/B30950.1.

Gong, Z., and Evans, D.A.D., 2021, Constraints on the Precambrian paleogeography of West African Craton, *in* Pesonen, L.J., Evans, D.A.D., Elming, S.Å., Salminen, J.M., and Veikkolainen, T., eds., Ancient Supercontinents and the Paleogeography of Earth. p. XXX.

Gower, C.F., Ryan, A.B., and Rivers, T., 1990, Mid-Proterozoic Laurentia-Baltica: An overview of its geological evolution and a summary of the contributions made by this volume, *in* Gower, C.F., Rivers, T., and Ryan, A.B., eds., Mid-Proterozoic Laurentia-Baltica: Geological Association of Canada Special Paper, v. 38, p. 1-20. ISBN: 978-0-919216-45-7.

Johansson, Å., 2009, Baltica, Amazonia and the SAMBA connection—1000 million years of neighbourhood during the Proterozoic?: Precambrian Research, v. 175(1-4), p. 221-234. https://doi.org/10.1016/j.precamres.2009.09.011.

Kirscher, U., Liu, Y., Li, Z.X., Mitchell, R.N., Pisarevsky, S.A., Denyszyn, S.W., and Nordsvan, A., 2019, Paleomagnetism of the Hart Dolerite (Kimberley, Western Australia)–A two-stage assembly of the supercontinent Nuna?: Precambrian Research, v. 329, p. 170-181. https://doi.org/10.1016/j.precamres.2018.12.026.

Kirscher, U., Mitchell, R.N., Liu, Y., Nordsvan, A.R., Cox, G.M., Pisarevsky, S.A., Wang, C., Wu, L., Murphy, J.B., and Li, Z.X., 2021, Paleomagnetic constraints on the duration of the Australia-Laurentia connection in the core of the Nuna supercontinent: Geology, v. 49(2), p. 174-179. https://doi.org/10.1130/G47823.1.

Klein, E.L., Rodrigues, J.B., Lopes, E.C., de Oliveira, R.G., Souza-Gaia, S.M., and de Oliveira, L.B.T., 2020, Age, provenance and tectonic setting of metasedimentary sequences of the Gurupi Belt and São Luís cratonic fragment, northern Brazil:

Broadening the understanding of the Proterozoic-Early Cambrian tectonic evolution: Precambrian Research, v. 351, p. 105950. https://doi.org/10.1016/j.precamres.2020.105950.

Kouyaté, D., Söderlund, U., Youbi, N., Ernst, R., Hafid, A., Ikenne, M., Soulaimani, A., Bertrand, H., and Chaham, K.R.K., 2013, U–Pb baddeleyite and zircon ages of 2040 Ma, 1650 Ma and 885 Ma on dolerites in the West African Craton (Anti-Atlas inliers): Possible links to break-up of Precambrian supercontinents: Lithos, v. 174, p. 71-84. https://doi.org/10.1016/j.lithos.2012.04.028.

Maloof, A.C., Schrag, D.P., Crowley, J.L., and Bowring, S.A., 2005, An expanded record of Early Cambrian carbon cycling from the Anti-Atlas Margin, Morocco: Canadian Journal of Earth Sciences, v. 42(12), p. 2195-2216. https://doi.org/10.1139/e05-062.

Martin, A.K., 2007, Gondwana breakup via double-saloon-door rifting and seafloor spreading in a backarc basin during subduction rollback: Tectonophysics, v. 445(3-4), p. 245-272. https://doi.org/10.1016/j.tecto.2007.08.011.

Merdith, A.S., Williams, S.E., Collins, A.S., Tetley, M.G., Mulder, J.A., Blades, M.L., Young, A., Armistead, S.E., Cannon, J., Zahirovic, S., and Müller, R.D., 2021, Extending full-plate tectonic models into deep time: Linking the Neoproterozoic and the Phanerozoic: Earth-Science Reviews, v. 214, p. 103477. https://doi.org/10.1016/j.earscirev.2020.103477.

Müller, R.D., Seton, M., Zahirovic, S., Williams, S.E., Matthews, K.J., Wright, N.M., Shephard, G.E., Maloney, K.T., Barnett-Moore, N., Hosseinpour, M., and Bower, D.J., 2016, Ocean basin evolution and global-scale plate reorganization events since Pangea

breakup: Annual Review of Earth and Planetary Sciences, v. 44, p. 107-138. https://doi.org/10.1146/annurev-earth-060115-012211.

Nance, R.D., Murphy, J.B., and Santosh, M., 2014, The supercontinent cycle: A retrospective essay: Gondwana Research, v. 25(1), p. 4-29. https://doi.org/10.1016/j.gr.2012.12.026.

Neres, M., Silva, P.F., Ikenne, M., Martins, S., Hafid, A., Mata, J., Almeida, F., Youbi, N., and Boumehdi, M.A., 2016, Evidences for multiple remagnetization of Proterozoic dykes from Iguerda inlier (Anti-Atlas Belt, Southern Morocco): Studia Geophysica et Geodaetica, v. 60(4), p. 700-730. https://doi.org/10.1007/s11200-014-0178-x.

Nomade, S., Chen, Y., Pouclet, A., Féraud, G., Théveniaut, H., Daouda, B.Y., Vidal, M., and Rigolet, C., 2003, The Guiana and the West African shield Palaeoproterozoic grouping: New palaeomagnetic data for French Guiana and the Ivory Coast: Geophysical Journal International, v. 154(3), p. 677-694. https://doi.org/10.1046/j.1365-246X.2003.01972.x.

Onstott, T.C., and Hargraves, R.B., 1981, Proterozoic transcurrent tectonics: Palaeomagnetic evidence from Venezuela and Africa: Nature, v. 289(5794), p. 131-136. https://doi.org/10.1038/289131a0.

Payne, J.L., Hand, M., Barovich, K.M., Reid, A., and Evans, D.A.D., 2009, Correlations and reconstruction models for the 2500-1500 Ma evolution of the Mawson Continent: Geological Society, London, Special Publications, v. 323(1), p. 319-355. https://doi.org/10.1144/SP323.16.

Pisarevsky, S.A., Elming, S.Å., Pesonen, L.J., and Li, Z.X., 2014, Mesoproterozoic paleogeography: Supercontinent and beyond: Precambrian Research, v. 244, p. 207-225. https://doi.org/10.1016/j.precamres.2013.05.014.

Şengör, A.M.C., Natal'In, B.A., and Burtman, V.S., 1993, Evolution of the Altaid tectonic collage and Palaeozoic crustal growth in Eurasia: Nature, v. 364(6435), p. 299-307. https://doi.org/10.1038/364299a0.

Söderlund, U., Ibanez-Mejia, M., El Bahat, A., Ernst, R.E., Ikenne, M., Soulaimani, A., Youbi, N., Cousens, B., and Hafid, A., 2013, Reply to Comment on "U–Pb baddeleyite ages and geochemistry of dolerite dykes in the Bas-Drâa inlier of the Anti-Atlas of Morocco: Newly identified 1380 Ma event in the West African Craton" by André Michard and Dominique Gasquet: Lithos, v. 174, p. 101-108. https://doi.org/10.1016/j.lithos.2013.04.003.

Verard, C., Hochard, C., and Stampfli, G., 2012, Non-random distribution of euler poles: is plate tectonics subject to rotational effects? Terra Nova, v. 24(6), p. 467-476. https://doi.org/10.1111/j.1365-3121.2012.01085.x.

Walsh, G.J., Aleinikoff, J.N., Benziane, F., Yazidi, A., and Armstrong, T.R., 2002. U–Pb zircon geochronology of the Paleoproterozoic Tagragra de Tata inlier and its Neoproterozoic cover, western Anti-Atlas, Morocco: Precambrian Research, v. 117(1-2), p. 1-20. https://doi.org/10.1016/S0301-9268(02)00044-X.

Youbi, N., Kouyaté, D., Söderlund, U., Ernst, R.E., Soulaimani, A., Hafid, A., Ikenne, M., El Bahat, A., Bertrand, H., Chaham, K.R., and Abbou, M.B., 2013, The 1750 Ma magmatic event of the west African craton (Anti-Atlas, Morocco): Precambrian Research, v. 236, p. 106-123. https://doi.org/10.1016/j.precamres.2013.07.003.

Zhang, S., Li, Z.X., Evans, D.A.D., Wu, H., Li, H., and Dong, J., 2012, Pre-Rodinia supercontinent Nuna shaping up: A global synthesis with new paleomagnetic results from North China: Earth and Planetary Science Letters, v. 353, p. 145-155. https://doi.org/10.1016/j.epsl.2012.07.034.

Zhao, G., Cawood, P.A., Wilde, S.A., and Sun, M., 2002, Review of global 2.1–1.8 Ga orogens: implications for a pre-Rodinia supercontinent: Earth-Science Reviews, v. 59(1-4), p. 125-162. https://doi.org/10.1016/S0012-8252(02)00073-9.

Zhao, H., Zhang, S., Zhu, M., Ding, J., Li, H., Yang, T., and Wu, H., 2021, Paleomagnetic insights into the Cambrian biogeographic conundrum: Did the North China craton link Laurentia and East Gondwana?: Geology, v. 49(4), p. 372-376. https://doi.org/10.1130/G47932.1.

Appendix I (for Chapter 5)

Reorienting the West African Craton in Paleoproterozoic-Mesoproterozoic Supercontinent Nuna

Zheng Gong [a], David A.D. Evans [a], Nasrrddine Youbi [b,c], Abdelhak Ait Lahna [b], Ulf Söderlund [d,e], Malika Ait Malek [b], Bin Wen [a], Xianqing Jing [a], Jikai Ding [a], Moulay A. Boumehdi [b], Richard E. Ernst [c,f]

[a] Department of Earth and Planetary Sciences, Yale University, New Haven, CT 06511, USA

[b] Department of Geology, Cadi Ayyad University, Marrakech, P.O. Box 2390, Morocco

[c] Faculty of Geology and Geography, Tomsk State University, Tomsk 634050, Russia

[d] Department of Geology, Lund University, Lund SE-223 62, Sweden

[e] The Swedish Museum of Natural History, Stockholm SE-114 18, Sweden

[f] Department of Earth Science, Carleton University, Ottawa, ON K1S 5B6, Canada

This file includes:

Supplementary text

Figures S1 to S8

Tables S1 to S5

References cited

Supplementary text

1. Geological background and sampling

The basement rocks in the West African Craton (WAC) consist of the Man-Leo Shield in the south, the Reguibat Shield in the north, and the Anti-Atlas Belt in the craton's northernmost margin (Figure 1). Significant crust forming events (Eburnean-Birimian orogeny) took place around 2.2-2.0 Ga (Baratoux et al., 2011; Schofield et al., 2016; Grenholm et al., 2019; McFarlane et al., 2019), during which the three blocks became the coherent WAC with linkage beneath the intervening Taoudeni and Tindouf sedimentary basins (Cahen et al., 1984). The Man-Leo and Reguibat Shields are composed of Archean rocks in the west and Paleoproterozoic rocks in the east. In the Anti-Atlas Belt, a total of ten inliers with Paleoproterozoic basement rocks lie to the south of the Anti-Atlas Major Fault. During the Hercynian orogeny in the late Paleozoic, regional folding was developed in the Anti-Atlas Belt that uplifted these inliers (Michard et al., 2008). Later erosion and weathering unroofed the sedimentary cover and exposed the basement. Due to the Hercynian event, the degree of metamorphism is stronger in the southwest, but only attained lower greenschist grade at its maximum, and attenuates towards the northeast of the Anti-Atlas Belt (Ruiz et al., 2008). The low grade of metamorphism permits retention of primary magnetization because the peak temperatures are well below the unblocking temperature of magnetite or low-Ti magnetite, which are considered as the main carriers of the remanent magnetization of mafic rocks. Margins of the inliers are gently tilted, as indicated by the Ediacaran-Paleozoic sedimentary cover nonconformably overlying the Proterozoic inliers, which bear the brunt of Hercynian thin-skinned deformation that leaves

the basement largely intact (Soulaimani and Burkhard, 2008). Interior parts of the inliers preserve cross-cutting sets of dikes that have retained verticality in all directions, demonstrating the structural integrity of the Anti-Atlas Belt. Paleomagnetic sampling was conducted using a portable, gasoline-powered drill. Usually 8-10 rock cores were collected from each dike. Cores were oriented by a Brunton magnetic compass and a solar compass was also used to correct for local geomagnetic variations. The strikes of the dikes were measured locally by a Brunton compass and the long-distance trends were traced on the Google Earth™ satellite images. Geochronological samples were collected from the central, coarsest-grained part of the mafic dikes. Please see Table S2 for the detailed locations of the dike samples.

2. ID-TIMS U-Pb Geochronology

2.1 Method

Preparation work for the geochronology of the dike G18M01 was carried out at the Department of Geology, Lund University, Sweden. After removing the weathered surfaces, about 0.5 kg sample was cut into small pieces and then crushed for baddeleyite separation. Using the Wilfley water-shaking table technique developed by Söderlund and Johansson (2002), a number of baddeleyite grains were successfully separated. A total of eight, dark-brownish color baddeleyite grains were picked out for further isotopic analysis due to their lack of alteration. We grouped the baddeleyite grains into 4 analyses, with each analysis containing 1-3 grains (Table S1). Baddeleyite grains were transferred to Teflon capsules and then repeatedly washed using 3 M HNO_3, including a hot acid bath for 30 minutes. Afterwards, we added 10 droplets of HF-HNO_3 (10:1) and 1 droplet of the ^{205}Pb-$^{233-236}U$

tracer solution to each capsule. To completely dissolve the baddeleyite grains, capsules were put in a high-pressure, high-temperature (~190°C) oven for 72 hours. Subsequently, we evaporated the samples on a 100°C hotplate and re-dissolved them in 10 droplets of 3.1 M HCl and 1 droplet of 0.25 M H_3PO_4. The U and Pb fractions were loaded on outgassed Re-filaments together with 2 μL silica gel. In the Laboratory of Isotope Geology at the Swedish Museum of Natural History in Stockholm, Sweden, we performed the analysis using a Finnigan Triton thermal ionization mass spectrometer (TIMS). U and Pb isotope intensities were measured in dynamic (peak-switching) mode using an ETP-SEM detector equipped with an RPQ filter. Filament temperatures for U and Pb isotope measurements are > 1300°C and 1200-1230°C, respectively. Data were processed in Excel Add-In program "Isoplot 3.75" developed by Ludwig (2012). Decay constants for ^{238}U and ^{235}U follow Jaffey et al. (1971). Initial Pb isotope compositions were corrected based on the Stacey and Kramers (1975) global terrestrial Pb evolution model. Isotope ratios and ages are reported in details with 2σ errors in Table S1. The U-Pb concordia diagram is shown in Figure S1A.

2.2 Results

The four fractions of dike G18M01 are moderately discordant (4-10%) with $^{207}Pb/^{206}Pb$ dates ranging between 1356 Ma and 1371 Ma (Table S1). The upper intercept is 1359 ± 6 Ma (2σ, mean square weighted deviates [MSWD] = 1.8), if the lower intercept is set to be 0 ± 100 Ma (Figure S1A). If the 1359 ± 6 Ma date is interpreted as the crystallization age of the dike G18M01, it is slightly younger than the 1.41-1.38 Ga dike swarm in the Bas Drâa inlier (El Bahat et al., 2013; Söderlund et al., 2013). The discordance of the individual

fractions could alternatively result from the Neoproterozoic Pan-African or late Paleozoic Hercynian events that caused partial loss of Pb and, sometimes, replacement of baddeleyite to polycrystalline zircon (Söderlund et al., 2013). In fact, the LA-ICPMS dating of the dike BD21 from the Bas Drâa inlier yielded an older, more concordant date of 1416 ± 7 Ma compared to the TIMS date of 1384 ± 6 Ma (Figure S1B; Söderlund et al., 2013). Forcing the lower intercept to be Pan-African or Hercynian-aged does yield an older date for the dike G18M01 (Figure S1A). For example, if the lower intercept is set to 300 ± 50 Ma, the upper intercept is 1380 ± 19 Ma, and if the lower intercept is set to 600 ± 50 Ma, the upper intercept is 1420 ± 49 Ma (Figure S1A). The paleomagnetic data from some samples do show a Hercynian-age overprint, which may justify the choice of a ~300 Ma age as the lower intercept. Nevertheless, to be conservative, we suggest that the age of the dike G18M01, and its parallel dikes in the Tagragra d'Akka inlier, should be 1.4-1.36 Ga, and plausibly belong to a slightly younger magmatic pulse than the 1.4-1.38 Ga swarm in the Bas Drâa inlier.

3. Paleomagnetism

3.1 Method

Paleomagnetic analysis was performed at Yale Paleomagnetic Facility with an ambient magnetic field weaker than 300 nT. Oriented cores with a diameter of 2.54 cm and a length of 1.0 cm were prepared for demagnetization following the protocol of the RAPID (Rock and Paleomagnetism Instrument Development) paleomagnetic system (http://rapid.gps.caltech.edu/). To demagnetize the remanent magnetization carried by multi-domain magnetite (Muxworthy and McClelland, 2000), we bathed the

paleomagnetic cores using liquid nitrogen (~77 K) in a magnetically shielded container. Then, routine stepwise thermal demagnetization was carried out using an ASC Scientific TD-48SC thermal demagnetizer with a nitrogen gas interior environment. Temperature increments are ~50°C in the beginning and narrow to 5-10°C towards the unblocking temperatures of the samples, which yields a total of 15-20 demagnetizing steps. Alternating-field (AF) demagnetization was also conducted on sister samples of each dike by a Molspin tumbler AF demagnetizer. Remanent magnetization was measured by a 2G Enterprises cryogenic DC-SQuID magnetometer coupled with an automated sample-changing device (Kirschvink et al., 2008). Data analysis benefits from the Paleomag X program developed by Jones (2002). Linear principal component analysis (Kirschvink, 1980), and to a less extent great circle analysis (McFadden and McElhinny, 1988), was used to determine the characteristic remanent magnetization (ChRM) on vector-endpoint diagrams (Zijderveld, 1967). Fisher spherical statistics was used to calculate the mean directions on site level (Fisher, 1953).

3.2 Results

3.2.1 The 2.04 Ga E-W dikes

Most dikes exhibit two, and a few dikes carry three, components of remanent magnetization (Figure S2). The low-temperature component is isolated normally between natural remanent magnetization (NRM) and 200°C, which is probably a viscous overprint in the recent geomagnetic field (Figures S2, S4). The intermediate-temperature component, which is observed in some dikes between 300°C and 500°C (e.g., dike G19M33; Figure S2), shows a direction similar to the one reported from the Cambrian cover sequence Lie

de Vin Formation in the Anti-Atlas Belt (Kirschvink et al., 1980). Compared to the apparent polar wander path of West African Craton (Torsvik et al., 2012), the intermediate-temperature component should be Late Paleozoic and is likely associated with the Hercynian tectono-thermal event. The high-temperature component, which is isolated mostly between 535°C and 580°C, is interpreted as the ChRM of each sample. The remanences of the samples become unstable after 580°C. Results from the AF demagnetization is consistent with those of the thermal demagnetization (Figure S2). According to the unblocking temperature and the results from magnetic susceptibility versus temperature experiments, the ChRM should reside in magnetite or titanomagnetite with very low Ti content. The ChRMs are southeast and moderately down or northwest and shallowly up (Figure S2). These antipodal directions do not pass the reversal test of McFadden and McElhinny (1990), which could be simply due to the low number of northwest-directed sites. When we flip one polarity, these antipodal directions overlap within uncertainties. We suggest that the ChRM is primary because: (1) the consistency of the ChRM from the same-age E-W striking dikes from two Anti-Atlas inliers ~80 km away from each other; (2) the presence of antipodal directions; (3) the isolation of Hercynian overprint at temperatures lower than the unblocking temperature of the ChRM; (4) the similarity to the ~2 Ga paleomagnetic results from the Man-Leo and the Reguibat Shields (Piper and Lomax, 1973; Lomax, 1975; Onstott et al., 1984; Onstott and Dorbor, 1987; Nomade et al, 2003). For paleomagnetic pole calculation, we first used the site-mean directions to get the virtual geomagnetic pole (VGP) for each site/dike (Table S2). Then, the VGPs were averaged to yield a paleomagnetic pole. From a total of 9 E-W dikes we studied, we obtained a pole of Plat = -22.3°N, Plon = 49.6°E (A_{95} = 7.1°, K = 53.3) for the

2.04 Ga E-W dikes. Detailed data regarding site-mean directions and paleomagnetic poles are listed in Tables S2 and S3.

3.2.2 The 1.4-1.36 Ga NE-SW dikes

Nearly all dikes show two components of remanent magnetization (Figure S3). The low-temperature component, in general, is isolated below 200-300°C (Figure S3). This low-temperature component is probably acquired viscously in the recent geomagnetic field or randomly distributed (Figure S4). The high-temperature component, which exhibits a clear decay-to-origin demagnetization line between 350°C and 580°C on the Zijderveld diagrams, is determined as the ChRM of these dike samples. Results from the thermal demagnetization are reproducible in the AF demagnetization (Figure S3). Based on unblocking temperatures and rock-magnetic characteristics, the ChRMs are likely carried by magnetite or low-Ti titanomagnetite. The ChRMs are north and down or south and up, with a direction in each sample notably distinct from the low-temperature component (Figure S3). We conducted an inverse baked-contact test to constrain the age of the ChRMs of the 1.4-1.36 Ga dikes. The N-S, younger dike (G18M89) we sampled intersects the dike G18M90 (Figure S5). We also sampled the baked zone (G18M91) of the older dike G18M90, which is within 2.2 m of the west margin of dike G18M89. Thermal demagnetization results show that the baked G18M91 site has the same remanent magnetizations as the younger dike G18M89 (Figure S5), demonstrating that the ChRMs of the 1.4-1.36 Ga dikes are older than the emplacement of the younger dike G18M89. Although we do not know the exactly age of the younger dike G18M89, it is at least Precambrian and older than the cover sequence starting from the latest Ediacaran (Maloof

et al., 2005; Letsch et al., 2019). Therefore, the reliability of the 1.4-1.36 Ga dikes' ChRM is strongly supported by the positive inverse baked-contact test, as well as the presence of antipodal directions. Thermo-susceptibility experiments also support that the 1.4-1.36 Ga dike was baked by the younger dike. The ~1-m wide contact aureole zone is clearly shown by the different magnetic mineralogy of the samples inside versus outside the aureole zone (Figure 5S). For example, inside the aureole zone, the sample G18M91C was affected by contact metamorphism and has a different magnetic mineralogy compared with the unbaked sample G18M90, of which the remanence is also unable to yield a stable direction during demagnetization. While outside the aureole zone, the baked samples G18M91D and G18M91H have a similar magnetic mineralogy as the unbaked sample G18M90, but carry steep-inclination directions the same as the younger dike (Figure S5), which supports the inverse baked-contact test. We carried out the reversal test of McFadden and McElhinny (1990), the angle between two antipodal directions is 12.25°, smaller than the critical angle of 24.87°. Thus, the reversal test is positive but inconclusive due to the large value of the critical angle. The paleomagnetic pole we got from nine 1.4-1.36 Ga NE-SW dikes is Plat = 87.4°N, Plon = 44.7°E (A_{95} = 7.8°, K = 44.1). Please see Table S2 for site-mean directions.

4. Rock magnetism

4.1 Method

Rock magnetic experiments were also conducted at Yale Paleomagnetic Facility. Anisotropy of magnetic susceptibility (AMS) analysis was performed using an AGICO Kappabridge KLY-4S susceptibility meter. AMS sample size is 2.54 cm in diameter and 2.2 cm in length. AMS data were processed in the AGICO Anisoft42 software. Magnetic

susceptibility versus temperature experiments were carried out and the temperature was controlled by a CS3 AGICO high-temperature furnace apparatus that is attached to the Kappabridge. About 1 g powders were prepared for each sample. A total of ~200 measurements were obtained from each sample during heating and cooling in air or argon gas environment through the temperature range of 35-715°C. Magnetic susceptibility as a function of temperature was plotted by the AGICO Cureval8 software.

4.2 Results

AMS data show that the degree of anisotropy (P_j) of Moroccan dikes in our study is in general below 10%, which is comparable to the typical value for igneous rocks (Hrouda, 1982). The magnetic fabric of most dikes is characterized by an oblate ellipsoid, with the maximum (K_1) and intermediate (K_2) axes defining a vertical or sub-vertical flattening/foliation plane with the minimum (K_3) axis perpendicular to it (Figure S6). The orientation of the K_1-K_2 plane mimics the strike of the dikes that was measured either in the field or on Google Earth™ satellite images. Therefore, the oblate magnetic fabric likely has resulted from the intrusion of the dikes, and the orientation of the dike intrusion is also preserved in the fabric. In summary, both the low P_j values and the primary magnetic fabric suggest that the dikes we studied have not experienced significant deformation, hence, likely retain primary magnetization. Magnetic susceptibility versus temperature experiments show that the susceptibility value becomes higher during cooling (Figure S7), which indicates magnetic mineralogy changes. During heating, the susceptibility value declines substantially from 580-600°C, suggesting magnetite is the main magnetic component in the dike samples. It is noticed that around 300°C there is a susceptibility

hump and between 600°C and 700°C the susceptibility value still has a slight decrease (Figure S7). It is possible that there is a small amount of maghemite in the dike samples, which converts to hematite during heating (Gehring et al., 2009). Overall, magnetic susceptibility versus temperature results suggest that magnetite is the main carrier of the remanent magnetization.

5. Paleogeographic reconstruction

GPlates software was used in the paleogeographic reconstruction (Müller et al., 2008). Paleomagnetic poles and Euler poles used in the reconstruction are listed in Tables S3 and S4, respectively.

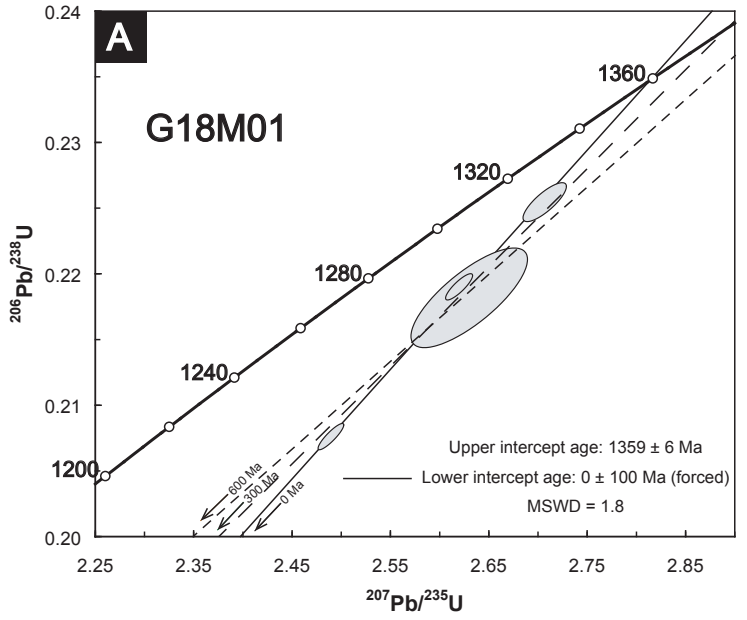

Upper intercept age: 1380 ± 19 Ma
— — — Lower intercept age: 300 ± 50 Ma (Hercynian)
MSWD = 10.3

Upper intercept age: 1420 ± 49 Ma
– – – – – – Lower intercept age: 600 ± 50 Ma (Pan-African)
MSWD = 37

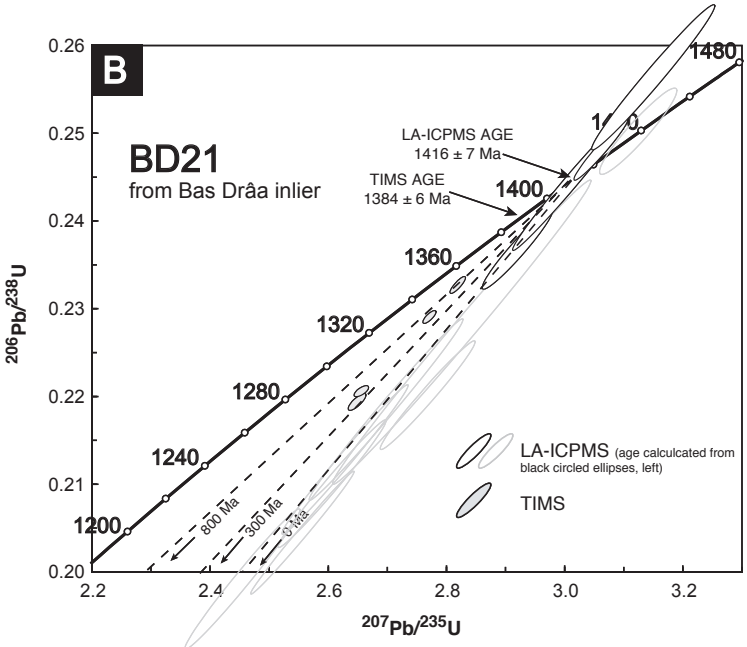

Figure S1 Concordia diagrams of the dike G18M01 from the Tagragra d'Akka inlier (A) and the dike BD21 from the Bas Drâa inlier (B). Dike BD21 data is from Söderlund et al. (2013).

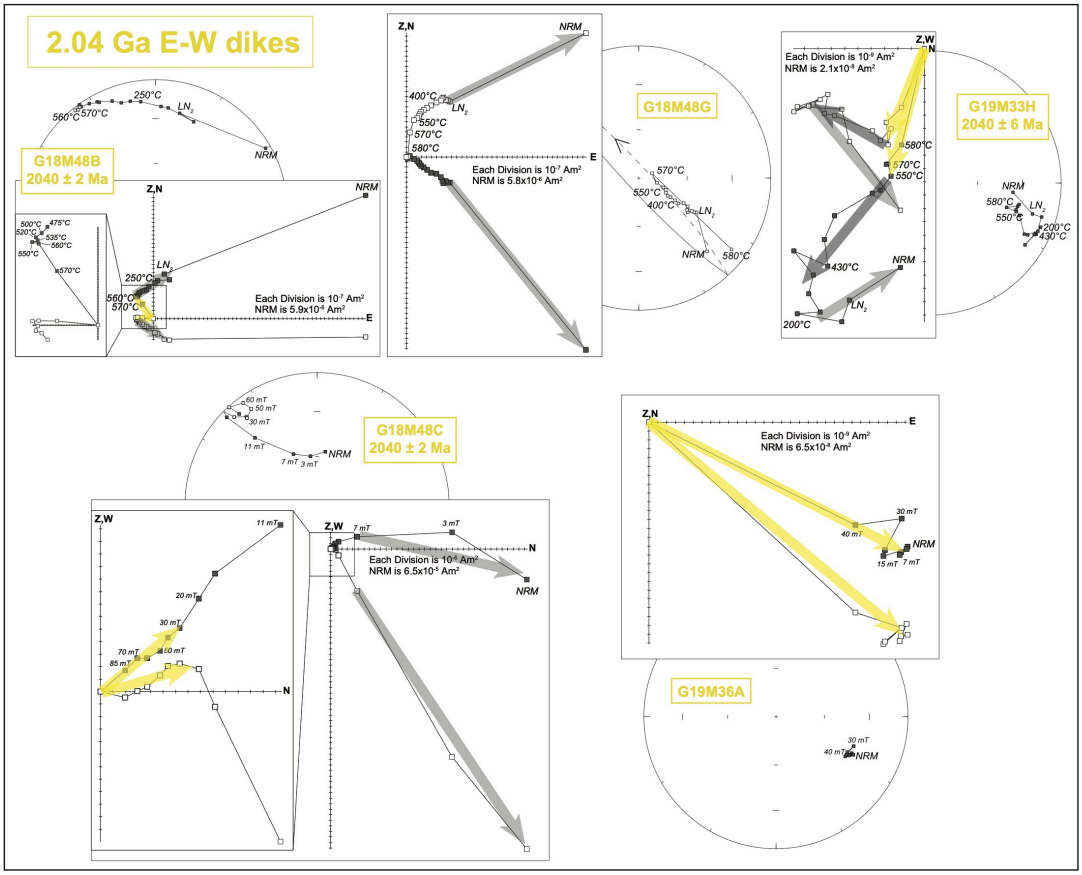

Figure S2 Zijderveld diagrams and Stereographic projection of the thermal and alternating-field demagnetization results of representative samples from the 2.04 Ga E-W dikes. The yellow arrows are the characteristic remanent magnetization of each sample, whereas dark and light grey arrows indicate the intermediate- and low-temperature, secondary magnetizations. The size of samples is 2.54 cm in diameter and 1.0 cm in length following the protocol of the RAPID paleomagnetic system (http://rapid.gps.caltech.edu/), which yields a volume of 5 cm^3.

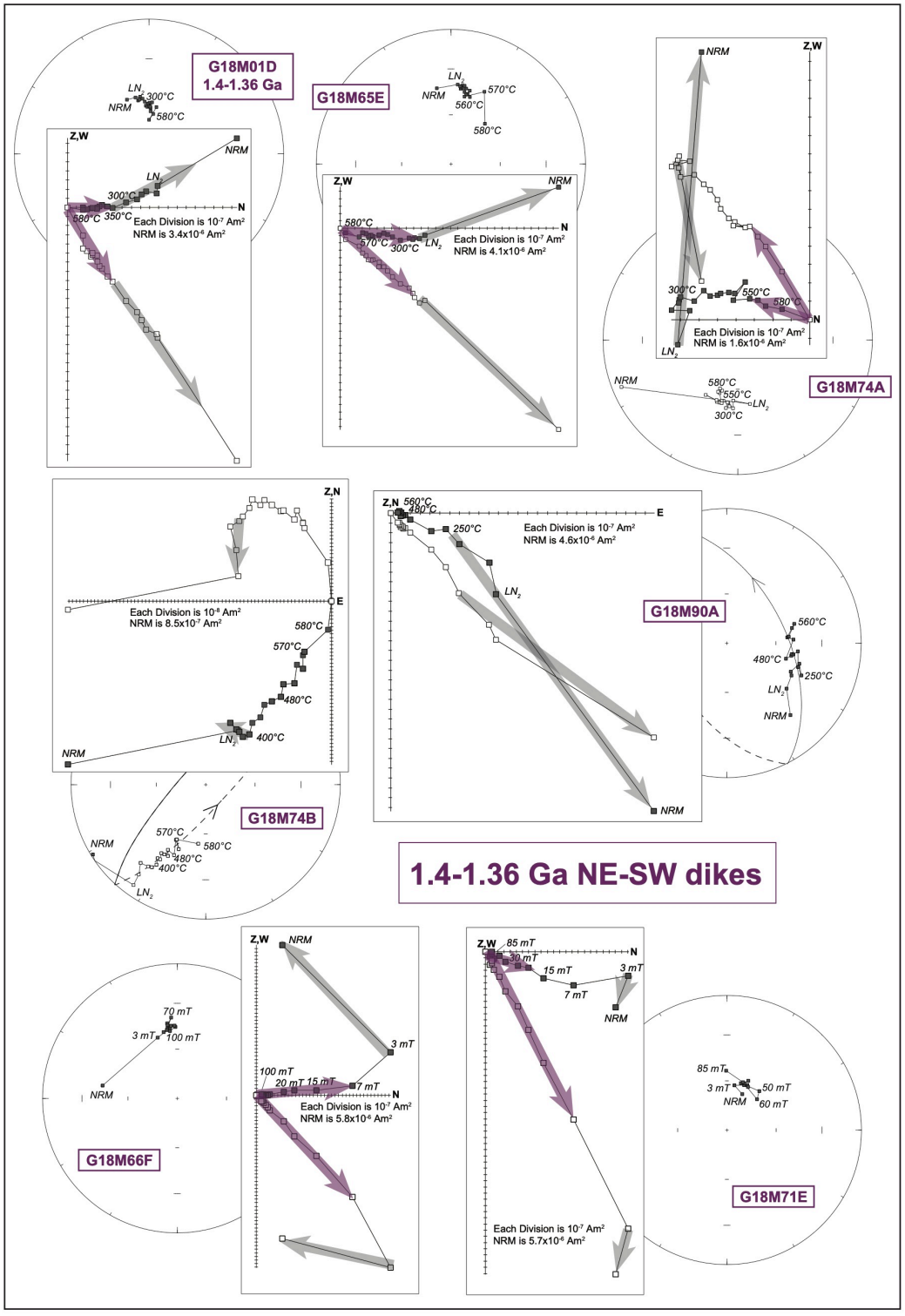

Figure S3 Zijderveld diagrams and Stereographic projection of the thermal and alternating-field demagnetization results of representative samples from the 1.4-1.36 Ga

NE-SW dikes. The purple arrows are the characteristic remanent magnetization of each sample, whereas light grey arrows indicate the low-temperature, secondary magnetizations. The size of samples is 2.54 cm in diameter and 1.0 cm in length following the protocol of the RAPID paleomagnetic system (http://rapid.gps.caltech.edu/), which yields a volume of 5 cm^3.

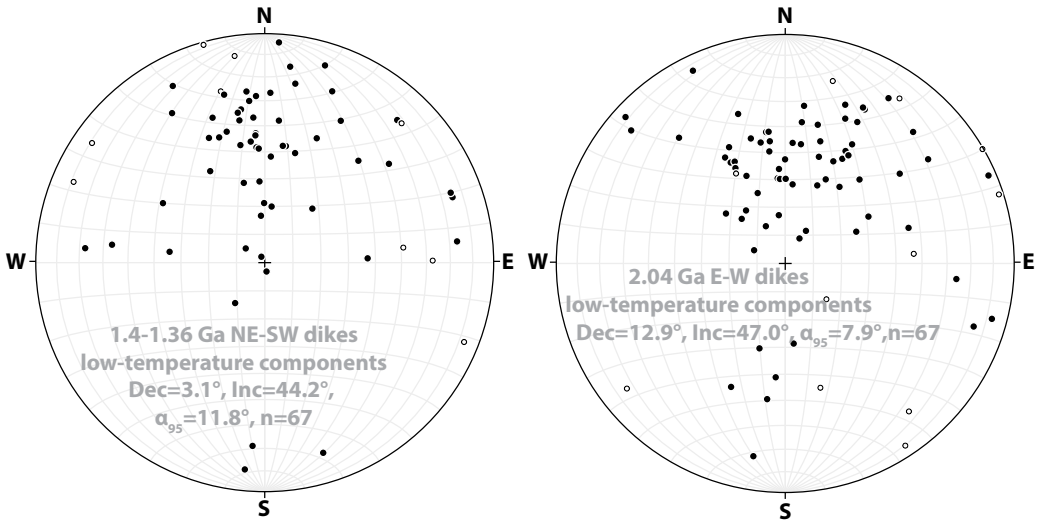

Figure S4 Stereographic projections of the low-temperature components of the 1.4-1.36 Ga NE-SW dikes (left), and the 2.04 Ga E-W dikes (right).

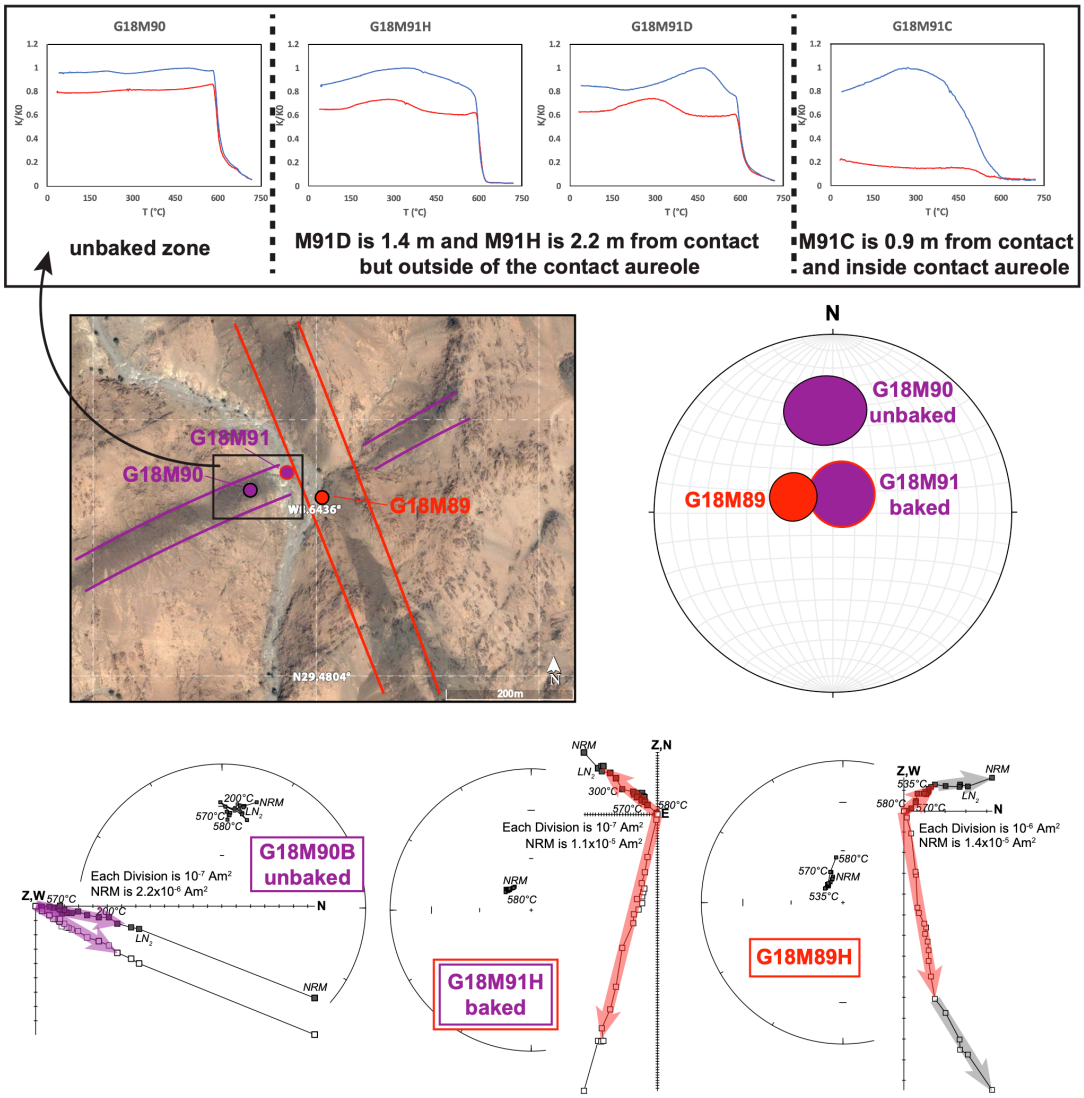

Figure S5 Results of the inverse baked-contact test for the magnetization of 1.4-1.36 Ga dikes. The Google Earth™ satellite image shows the sampling location, where the dike G18M90 (shown in purple) is cut by the younger N-S dike G18M89 (shown in red). The baked site G18M91 is within 2.2 m from the west margin of the dike G18M89. Stereographic projection and Zijderveld diagrams show that the baked samples carry the same remanent magnetization as the younger dike (red), whereas the unbaked samples have a different remanent magnetization (purple). Grey arrows indicate the low-temperature, secondary magnetizations. The inset figure shows the K-T curves of the baked

and unbaked samples. The baked (overprinted) samples G18M91D-H that are outside the contact-metamorphic aureole (~1-m wide) have a similar magnetic mineralogy as the unbaked site G18M90, while the baked sample G18M91C is inside the metamorphic aureole and represents the three most proximal exocontact samples of site G18M90 that are not stably magnetized, carrying a different magnetic mineralogy from the most distant samples of the same older dike (whether baked or unbaked).

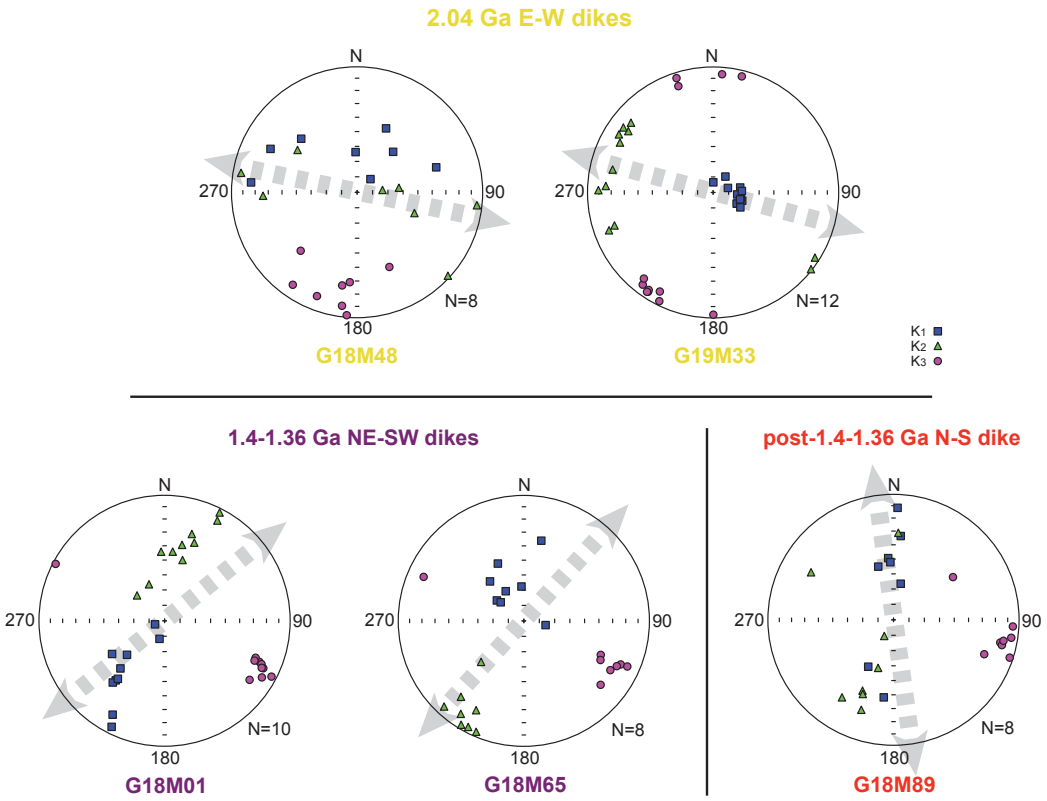

Figure S6 Stereographic projection of the anisotropy of magnetic susceptibility (AMS) data of representative sites from the 2.04 Ga E-W dikes (shown in yellow), the 1.4-1.36 Ga NE-SW dikes (shown in purple), and the post-1.4-1.36 Ga N-S dike (shown in red). The squares, triangles, and circles show the maximum (K_1), intermediate (K_2), and minimum (K_3) axes of AMS ellipsoids. N is the number of samples in one site. The grey dashed arrows indicate the general strikes of the dikes either measured in the field or inferred from the Google Earth™ satellite images.

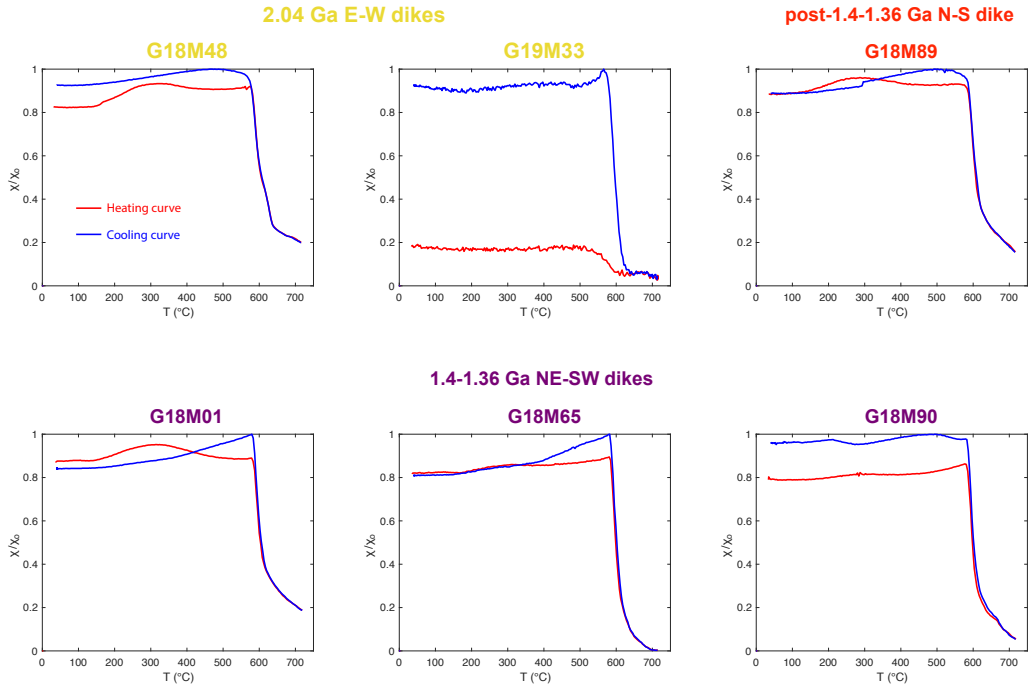

Figure S7 Magnetic susceptibility versus temperature curves on representative samples from the 2.04 Ga E-W dikes (shown in yellow), the 1.4-1.36 Ga NE-SW dikes (shown in purple), and the post-1.4-1.36 Ga N-S dike (shown in red). The red and blue curves show the changes in magnetic susceptibility during heating and cooling, respectively. Except for the sample G19M33, which was heated in air, all other samples were heated in an argon gas environment.

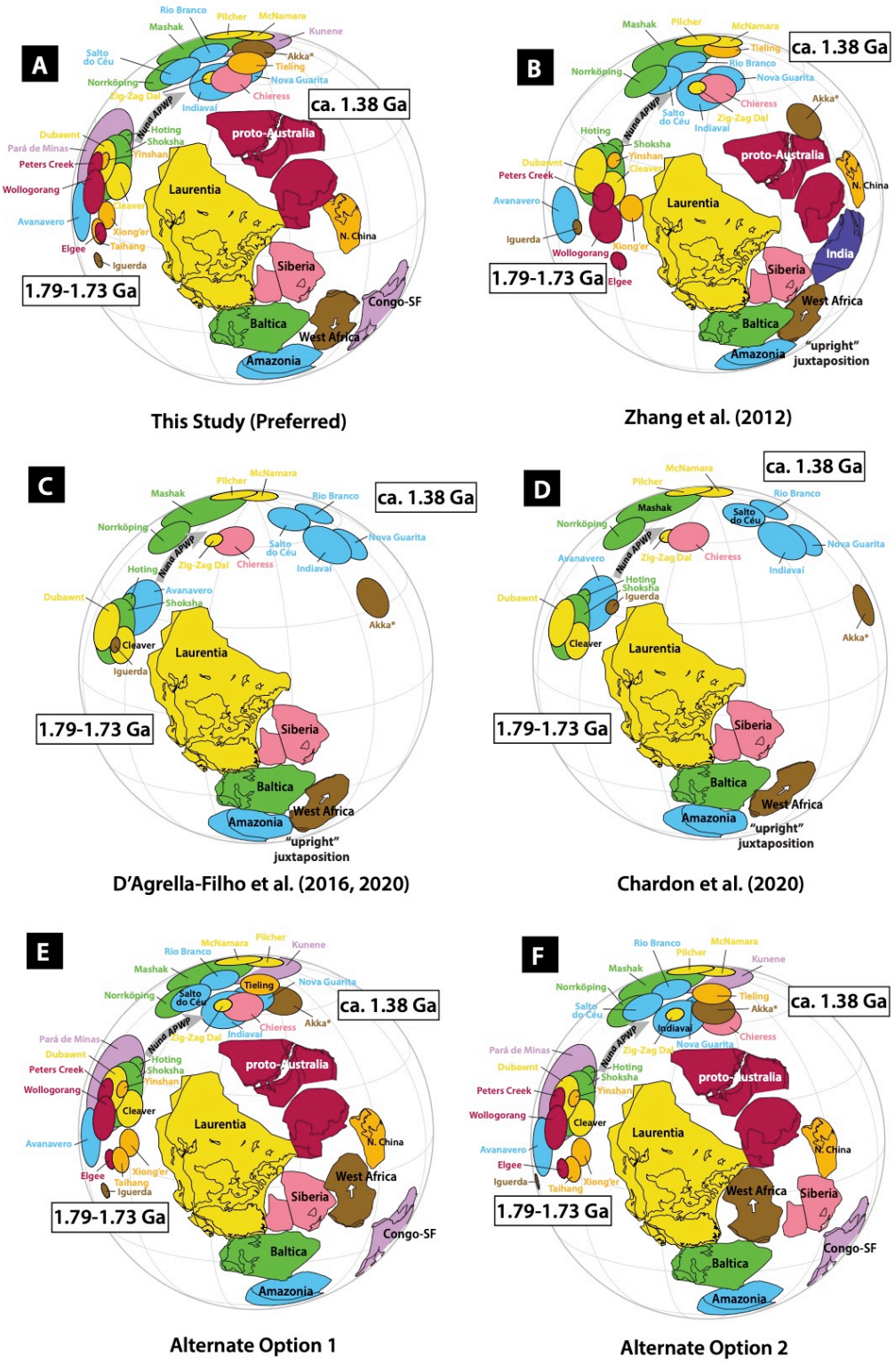

Figure S8 Different paleogeographic reconstructions of supercontinent Nuna. (A) the preferred inverted between West African Craton (WAC) and Amazonia in this study. The

"upright"-sense models of (B) Zhang et al. (2012), (C) D'Agrella-Filho et al. (2016, 2020), and (D) Chardon et al. (2020). It is clearly demonstrated that our newly obtained 1.4-1.36 Ga pole from WAC does not support an "upright"-sense of WAC-Amazonia connection in Nuna. Alternate options of Nuna reconstruction, paleomagnetically permitting the "upright" orientation, are shown to require substantial separation between WAC and Amazonia, in either of two possibilities for the sake of illustration: (E) WAC lies to the east of Siberia, and (F) WAC and Siberia switch their positions. Neither of these options fits the basement age provinces or LIP records as well as our preferred model in panel (A). Two clusters of paleomagnetic poles occur at 1.79-1.73 Ga and ca. 1.38 Ga. The grey arrow shows the younging direction of apparent polar wander path (APWP) of Nuna. The white arrow indicates the present-day north of WAC. The selected paleomagnetic poles of each craton are listed in Table S3, of which the colors are in correspondence with those of the cratons. The pole marked by the asterisk is from this study.

Table S1 U-Pb baddeleyite TIMS data from the dike G18M01.

Analysis no. (number of grains)	U/ Th	Pbc/ Pbtot[1)]	$^{206}Pb/^{204}Pb$ raw[2)]	$^{207}Pb/^{235}U$	± 2s % err	$^{206}Pb/^{238}U$ [corr][3)]	± 2s % err	$^{207}Pb/^{235}U$ [age, Ma]	$^{206}Pb/^{238}U$ [age, Ma]	$^{207}Pb/^{206}Pb$ [age, Ma]	± 2s	Concord-ance
Bd-a (2 grains)	19.6	0.054	1176.4	2.4897	0.43	0.20752	0.39	1269.1	1215.6	1360.8	3.1	0.893
Bd-b (2 grains)	10.9	0.250	210.3	2.7066	0.67	0.22538	0.54	1330.3	1310.2	1362.7	6.8	0.961
Bd-c (3 grains)	14.6	0.068	921.7	2.6194	0.43	0.21892	0.37	1306.1	1276.1	1355.6	4.3	0.941
Bd-d (1 grain)	15.0	0.281	199.1	2.6300	1.83	0.21808	1.42	1309.1	1271.7	1370.7	22.4	0.928

[1)] Pbc = common Pb; Pbtot = total Pb (radiogenic + blank + initial).

[2)] measured ratio, corrected for fractionation and spike.

[3)] isotopic ratios corrected for fractionation (0.1% per amu for Pb), spike contribution, blank (0.3 pg Pb and 0.03 pg U), and initial common Pb. Initial common Pb corrected with isotopic compositions from the model of Stacey and Kramers (1975) at the age of the sample.

Table S2 Paleomagnetic results of the 2.04 Ga E-W dikes, the 1.4-1.36 Ga NE-SW dikes, and the post-1.4-1.36 Ga N-S dike.

Inlier	Site No.	Slat (°N)	Slon (°E)	Strike (°)	Age	Dec (°)	Inc (°)	α_{95}	k	n/N	L+G	Polarity	Vlat (°)	Vlon (°)	A_{95}
2.04 Ga dikes															
Zenaga	G18M48,49	30.3702	-7.3049	102	2040 ± 2 Ma[#]	306.5	-7.5	14.1	9.6	13/18	4+9	reversed	-28.6	58.7	10
Tagragra de Tata	G19M33	29.9059	-7.9885	105	2040 ± 6 Ma*	116.7	35.5	19.6	10.4	7/12	4+3	normal	-11.5	51.2	17.2
Tagragra de Tata	G19M34	29.9099	-7.9959	87		138.7	33.5	8.7	36.0	9/10	8+1	normal	-27.5	36.9	7.5
Tagragra de Tata	G19M35	29.9151	-8.0150	99		123.9	12.1	10.3	29.9	8/10	7+1	normal	-25.3	57.9	7.5
Tagragra de Tata	G19M36	29.9161	-8.0129	103		129.2	29.4	11.9	26.7	7/10	4+3	normal	-23.1	46.2	9.8
Tagragra de Tata	G19M37	29.9169	-8.0148	102		132.2	42.8	18.2	14.5	6/10	4+2	normal	-18.6	37.2	17.7
Tagragra de Tata	G19M38	29.9276	-8.0154	101		318.7	-24.9	12.0	106.6	3/10	3+0	reversed	-31.4	40.9	9.4
Tagragra de Tata	G19M39	29.9295	-8.0165	106		114.4	26.9	16.2	59.0	3/10	3+0	normal	-12.9	57	13
Tagragra de Tata	G19M40	29.9231	-8.0179	122		118.5	15.6	8.2	40.4	9/10	9+0	normal	-19.9	59.8	6
1.4-1.36 Ga dikes															
Tagragra d'Akka	G18M01	29.2638	-8.8218	51	1.4-1.36 Ga*	17.1	58.7	8.7	41.5	8/10	8+0	reversed	72.7	40.8	11.2
Tagragra d'Akka	G18M65	29.3398	-8.7844	42		3.8	44.9	4.5	152.5	8/8	8+0	reversed	85.6	120.7	4.5
Tagragra d'Akka	G18M66	29.3419	-8.7872	46		359.3	38.5	8.0	48.9	8/8	6+2	reversed	82.3	176.1	7.3
Tagragra d'Akka	G18M68	29.3452	-8.7919	66		2.9	50.3	4.4	159.5	8/9	8+0	reversed	87	46.1	4.8
Tagragra d'Akka	G18M69	29.3461	-8.7918	59		352.5	61.8	5.2	99.0	9/9	9+0	reversed	75.1	329.4	7.1
Tagragra d'Akka	G18M71	29.3551	-8.7946	56		10.5	54.6	6.5	139.5	5/8	5+0	reversed	79.4	45.4	7.7
Tagragra d'Akka	G18M74	29.3598	-8.8071	53		195.6	-56.1	10.0	31.6	8/9	5+3	normal	75.1	47.9	12.1
Tagragra d'Akka	G18M86	29.4132	-8.6524	69		347.9	31.8	16.1	23.5	5/8	5+0	reversed	73.5	216.3	13.6
Tagragra d'Akka	G18M90	29.4831	-8.6445	67		355.9	41.9	18.4	25.9	4/8	3+1	reversed	83.5	206.8	17.7

Tagragra d'Akka	G18M91 baked by G18M89	29.4833	-8.6440	67		24.9	80.4	14.9	39.0	4/8	4+0	reversed	46	2.6	28.1
post 1.4-1.36 Ga N-S dike															
Tagragra d'Akka	G18M89	29.4827	-8.6438	352		292.4	70.4	10.9	26.8	8/8	8+0	reversed	36.4	309.6	17.5

*Note: Slat = site latitude, Slon = site longitude, Dec = magnetic declination, Inc = magnetic inclination, α_{95} = radius of 95% confidence cone of site-mean direction, k = precision parameter, n = number of samples used to calculate site-mean directions, N = number of samples subjected to thermal demagnetization, L = least-square fit, G = great circle fit, Vlat = virtual geomagnetic pole latitude, Vlon = virtual geomagnetic pole longitude, A_{95} = radius of 95% confidence cone of virtual geomagnetic pole. # marks the SHRIMP zircon age, * marks ID-TIMS baddeleyite ages.*

Table S3 Quality-filtered paleomagnetic poles used in paleogeographic reconstruction.

Rock unit / Pole name	Abbreviation	Age (Ma)	Plat (°N)	Plon (°E)	A_{95} (°)	Q-score	R-score	References
West African Craton								
Ivory Coast TTG plutons	IC1	2100-2070	-82.0	112.0	13.0	(0110100)3	(0110100)3	Nomade et al. (2003)
Tarkwa dolerite intrusions	Tarkwa	2100-2000	-53.0	36.0	13.5	(0110110)4	(0010110)3	Piper and Lomax (1973)
Obuasi dolerite dike	Obuasi	2100-2000	-56.0	69.0	7.9	(0010100)2	(0010100)2	Piper and Lomax (1973)
Ferke batholith	IC2	~2000	-25.0	83.0	16.0	(0010001)2	(0010001)2	Nomade et al. (2003)
Nimba-Harper metamorphic rocks	NiA	~2000	-18.0	89.0	13.0	(1110001)4	(0110001)3	Onstott and Dorbor (1987)
Tagragra de Tata E-W dikes	Tata	2040 ± 2; 2040 ± 6	-22.3	49.6	7.1	(1110110)5	(1110100)4	this study
Aftout plutons	Aftout	1982-1950	-6.0	90.0	8.0	(0110001)3	(0110001)3	Lomax (1975)
Harper amphibolite	HaA1	2000-1900	-10.0	73.0	7.0	(1010001)3	(0010001)2	Onstott et al. (1984)
Iguerda NW-SE dike VGP	Iguerda	1747 ± 4	-4.0	262.1	2.5	(1010101)4	(1010101)4	Neres et al. (2016)
Tagragra d'Akka NE-SW dikes	Akka	1400-1360	87.4	44.7	7.0	(1111111)7	(0111101)5	this study
Amazonia								
Tampok-Mataroni-Approuague River granite	GF1	2070-2050	1.8	292.5	11.2	(1010011)4	(1010011)4	Theveniaut et al. (2006)
Armontabo River granite	ARMO	2080 ± 4	-2.7	346.3	14.2	(1011010)4	(1010011)4	Theveniaut et al. (2006)
Oyapok granitoids	OYA	2050-2022	-28.0	346.0	13.8	(1110000)3	(1010000)2	Nomade et al. (2003)
Costal Lake granite	GF2	2050-1970	-58.5	30.2	5.8	(1110010)4	(0110010)3	Theveniaut et al. (2006)
Imataca Complex-Encrucijada pluton mean	CA1	~1970	-43.2	21.9	16.5	(0110010)3	(0110010)3	Bispo-Santos et al. (2014)
Avanavero intrusions	Avanavero	1794 ± 4	48.4	207.9	9.6	(1111101)6	(1111101)6	Bispo-Santos et al. (2014)
Rio Branco sedimentary rocks	Rio Branco	1544-1440	45.5	90.0	6.5	(1011111)6	(0011111)5	D'Agrella-Filho et al. (2016)
Salto do Céu intrusions	Salto do Céu	1439 ± 4	56.0	98.5	7.9	(1111110)6	(1111110)6	D'Agrella-Filho et al. (2016)
Nova Guarita dikes	Nova Guarita	1419 ± 4	47.9	65.9	7.0	(1111110)6	(1111110)6	Bispo-Santos et al. (2012)
Indiavaí gabbro	Indiavaí	1416 ± 7	57.0	69.7	8.6	(1110000)3	(1110000)3	D'Agrella-Filho et al. (2012)
Siberia								
Chieress dike VGP	Chieress	1384 ± 2	4.0	258.0	6.7	(1010101)4	(1010101)4	Ernst and Buchan (2000)
Laurentia								
Dubawnt Group	Dubawnt	1820-1750	7.0	277.0	8.0	(1111110)6	(0111110)5	Park et al. (1973)
Cleaver dikes	Cleaver	1745-1736	19.4	276.7	6.1	(1111101)6	(1111101)6	Irving et al. (2004)
McNamara Formation	McNamara	1401 ± 6	-13.5	208.3	6.7	(1111111)7	(1111111)7	Elston et al. (2002)
Pilcher Formation	Pilcher	1385 ± 23	-19.2	215.3	7.7	(1111101)6	(0111101)5	Elston et al. (2002)
Zig-Zag Dal basalt & & associated intrusions	Zig-Zag Dal	1382 ± 2	11.0	229.0	3.0	(1111111)7	(1011111)6	Marcussen and Abrahamsen (1983)

								recal. by Evans and Mitchell (2011)
Baltica								
Hoting gabbro mean	Hoting	1786 ± 10	43.0	233.3	10.9	(1111101)6	(1111101)6	Elming et al. (2009)
Shoksha Formation	Shoksha	1770 ± 12	39.7	221.1	4.0	(1111111)7	(1111111)7	Pisarevsky and Sokolov (2001)
Norrköping dikes	Norrköping	1411 ± 9	18.8	200.9	7.8	(1110100)4	(1010100)3	Elming et al. (2014)
Mashak suite	Mashak	1384 ± 3; 1366 ± 6	1.8	193.0	14.8	(1001110)4	(1001110)4	Lubnina (2009)
North China Craton								
Xiong'er Group	Xiong'er	1790-1770	50.2	263.0	4.5	(1111111)7	(1011111)6	Zhang et al. (2012)
Taihang dikes	Taihang	1772-1766	48.0	274.0	4.2	(1111111)7	(1011111)6	Xu et al. (2014)
Yinshan dikes	Yinshan	1780	35.5	245.2	2.4	(1111101)6	(1111101)6	Halls et al. (2000); Xu et al. (2014)
Tieling Formation	Tieling	1458-1416	11.6	187.1	6.3	(1111101)6	(0111101)5	Wu (2005)
São Francisco-Congo								
Pará de Minas dikes	Pará de Minas	1798 ± 4; 1793 ± 18; 1791 ± 7	-39.8	196.8	17.0	(1011100)4	(1011100)4	D'Agrella-Filho et al. (2020)
Kunene anorthosite	Kunene	1376 ± 2; 1371 ± 3	3.3	75.3	18.0	(1000011)3	(1000011)3	Piper (1974)
North Australia								
Elgee-Pentecost (combined)	Elgee	1790-1734	-5.4	211.8	3.2	(1111100)5	(0111100)4	Schmidt and Williams (2008)
Peters Creek Volcanics (upper part)	Peters Creek	1729-1725	-26.0	221.0	4.8	(1111111)7	(1111111)7	Idnurm (2000)
Wollogorang Formation (high temp. comp.)	Wollogorang	1730-1723	-17.9	218.2	7.2	(1011110)5	(1011110)5	Idnurm et al. (1995)

Note: Plat = paleomagnetic pole latitude, Plon = paleomagnetic pole longitude, A_{95} = radius of 95% confidence cone of paleomagnetic pole, Q-score = reliability criteria of paleomagnetic poles following Van der Voo (1990), R-score = reliability criteria of paleomagnetic poles following Meert et al. (2020).

Table S4 Euler poles used in paleogeographic reconstruction of supercontinent Nuna.

			Elat (°N)	Elon (°E)	Angle (°)	References
Baltica	to	Laurentia	47.5	1.5	49.0	Evans and Pisarevsky (2008)
Siberia-Aldan	to	Siberia-Anabar	60.0	115.0	25.0	Evans (2009)
Siberia-Anabar	to	Laurentia	78.0	99.0	147.0	Evans and Mitchell (2011)
North China Craton	to	Laurentia	36.9	14.6	38.2	Kirscher et al. (2021)
South + West Australia	to	North Australia	-20.0	135.0	40.0	Li and Evans (2011)
North Australia	to	Laurentia	37.8	90.2	102.7	Kirscher et al. (2019)
Amazonia	to	Laurentia	53.0	-67.0	127.0	Zhang et al. (2012) based on Johansson (2009)
São Francisco-Congo	to	Laurentia	13.8	56.2	-156.6	this study
West African Craton	to	Amazonia	0.8	-18.3	128.5	this study

Note: Elat = Euler pole latitude, Elon = Euler pole longitude. Euler pole of Laurentia to absolute reference: 0.0°N, -173.0°E, 83.0° (1800 Ma Dubawnt Group; Park et al., 1973); 0.0°N, -173.4°E, 70.0° (1740 Ma Cleaver dikes; Irving et al., 2004); 0.0°N, 127.5°E, 91.5° (1460 Ma Michikamau anorthosites; Emslie et al., 1976); 0.0°N, 118.3°E, 103.5° (1350 Ma McNamara Formation; Elston et al., 2002).

Table S5 Global records of large igneous provinces (LIPs) at 1.79-1.75 Ga and ca. 1.38 Ga.

1.79-1.75 Ga

#	Craton	Age (Ga)	LIPs	References
1	Baltica	1.79	Tomashgorod dikes	Bogdanova et al. (2013)
2	Baltica	1.76-1.75	AMCG intrusions	Bogdanova et al. (2013)
3	Amazonia	1.79	Avanavero dikes	Reis et al. (2013)
4	WAC	1.75	Iguerda NW-SE dikes	Youbi et al. (2013)
5	WAC	1.76	Kédougou dikes	Baratoux et al. (2019)
6	WAC	1.79	Libiri dikes	Baratoux et al. (2019)
7	North China Craton	1.78	Taihang dikes & Xiong'er volcanics	Peng (2010)
8	Siberia	1.75	Timpton dikes	Gladkochub et al. (2010)
9	Laurentia	1.75	Cleaver-Hadley Bay-Kivalliq dikes	Ernst and Bleeker (2010)
10	SF-Congo	1.79	Pará de Minas	Chaves and Rezende (2019); D'Agrella-Filho et al. (2020)
11	SF-Congo	1.76-1.75	Januária dikes	Chaves and Rezende (2019)
12	NAC	1.79	Hart dolerite sills	Kirscher et al. (2019)

ca. 1.38 Ga

#	Craton	Age (Ga)	LIPs	References
1	Laurentia	1.38	Zig-Zag Dal volcanics & associated intrusions	Upton et al. (2005)
2	Laurentia	1.38	Victoria Land dikes	Ernst et al. (2008)
3	Laurentia	1.38	Salmon River sills	Ernst et al. (2008)
4	Laurentia	1.38	Hart River sills	Ernst et al. (2008)
5	Siberia	1.38	Chieress dikes	Ernst et al. (2008)
6	Baltica	1.38	Mashak volcanics	Puchkov et al. (2013)
7	WAC	1.4-1.36	Bas Drâa dikes & Tagragra d'Akka NE-SW dikes	El Bahat et al. (2013); Söderlund et al. (2013); this study
8	SF-Congo	1.38	Kunene anorthosite	Maier et al. (2013); Ernst et al. (2013)
9	SF-Congo	1.37	Lake Victoria dikes	Mäkitie et al. (2014)

Note: WAC = West African Craton, SF = São Francisco, NAC = North Australian Craton, AMCG = anorthosite-mangerite-charnockite-granite.

References cited

Baratoux, L., Metelka, V., Naba, S., Jessell, M.W., Grégoire, M., and Ganne, J., 2011, Juvenile Paleoproterozoic crust evolution during the Eburnean orogeny (~2.2–2.0 Ga), western Burkina Faso: Precambrian Research, v. 191(1-2), p. 18-45.

Baratoux, L., Söderlund, U., Ernst, R.E., De Roever, E., Jessell, M.W., Kamo, S., Naba, S., Perrouty, S., Metelka, V., Yatte, D., and Grenholm, M., 2019, New U–Pb baddeleyite ages of mafic dyke swarms of the West African and Amazonian cratons: Implication for their configuration in supercontinents through time, *in* Srivastava, R.K., Ernst, R.E., and Peng, P., eds., Dyke Swarms of the World: A Modern Perspective, p. 263-314.

Bispo-Santos, F., D'Agrella-Filho, M.S., Trindade, R.I., Elming, S.Å., Janikian, L., Vasconcelos, P.M., Perillo, B.M., Pacca, I.I., da Silva, J.A., and Barros, M.A., 2012, Tectonic implications of the 1419 Ma Nova Guarita mafic intrusives paleomagnetic pole (Amazonian Craton) on the longevity of Nuna: Precambrian Research, v. 196, p. 1-22.

Bispo-Santos, F., D'Agrella-Filho, M.S., Janikian, L., Reis, N.J., Trindade, R.I., and Reis, M.A.A., 2014, Towards Columbia: Paleomagnetism of 1980–1960 Ma Surumu volcanic rocks, Northern Amazonian Craton: Precambrian Research, v. 244, p. 123-138.

Bogdanova, S.V., Gintov, O.B., Kurlovich, D.M., Lubnina, N.V., Nilsson, M.K., Orlyuk, M.I., Pashkevich, I.K., Shumlyanskyy, L.V., and Starostenko, V.I., 2013, Late Palaeoproterozoic mafic dyking in the Ukrainian Shield of Volgo-Sarmatia caused by rotation during the assembly of supercontinent Columbia (Nuna): Lithos, v. 174, p. 196-216.

Boyden, J.A., Müller, R.D., Gurnis, M., Torsvik, T.H., Clark, J.A., Turner, M., Ivey-Law, H., Watson, R.J., and Cannon, J.S., 2011, Next-generation plate-tectonic reconstructions using GPlates: Geoinformatics, p. 95-113.

Cahen, L., Snelling, N.J., Delhal, J., Vail, J.R., Bonhomme, M., and Ledent, D., 1984, The geochronology and evolution of Africa: Oxford, Oxford University Press, 512 p.

Chardon, D., Bamba, O., and Traoré, K., 2020, Eburnean deformation pattern of Burkina Faso and the tectonic significance of shear zones in the West African craton: BSGF-Earth Sciences Bulletin, v. 191, 2, p. 1-18.

Chaves, A.O., and Rezende, C.R., 2019, Fragments of 1.79-1.75 Ga Large Igneous Provinces in reconstructing Columbia (Nuna): A Statherian supercontinent-superplume coupling? Episodes Journal of International Geoscience, v. 42(1), p. 55-67.

D'Agrella-Filho, M.S., Trindade, R.I., Elming, S.Å., Teixeira, W., Yokoyama, E., Tohver, E., Geraldes, M.C., Pacca, I.I., Barros, M.A., and Ruiz, A.S., 2012, The 1420 Ma Indiavaí mafic intrusion (SW Amazonian Craton): Paleomagnetic results and implications for the Columbia supercontinent: Gondwana Research, v. 22(3-4), p. 956-973.

D'Agrella-Filho, M.S., Trindade, R.I., Queiroz, M.V., Meira, V.T., Janikian, L., Ruiz, A.S., and Bispo-Santos, F., 2016, Reassessment of Aguapeí (Salto do Céu) paleomagnetic pole, Amazonian Craton and implications for Proterozoic supercontinents: Precambrian Research, v. 272, p. 1-17.

D'Agrella-Filho, M.S., Bispo-Santos, F., Trindade, R.I.F., and Antonio, P.Y.J., 2016, Paleomagnetism of the Amazonian Craton and its role in paleocontinents: Brazilian Journal of Geology, v. 46(2), p. 275-299.

D'Agrella-Filho, M.S., Teixeira, W., da Trindade, R.I., Patroni, O.A., and Prieto, R.F., 2020, Paleomagnetism of 1.79 Ga Pará de Minas mafic dykes: Testing a São Francisco/Congo-North China-Rio de la Plata connection in Columbia: Precambrian Research, v. 338, p. 105584.

El Bahat, A., Ikenne, M., Söderlund, U., Cousens, B., Youbi, N., Ernst, R., Soulaimani, A., and Hafid, A., 2013, U–Pb baddeleyite ages and geochemistry of dolerite dykes in the Bas Drâa Inlier of the Anti-Atlas of Morocco: Newly identified 1380 Ma event in the West African Craton: Lithos, v. 174, p. 85-98.

Elming, S.Å., Moakhar, M.O., Layer, P., and Donadini, F., 2009, Uplift deduced from remanent magnetization of a proterozoic basic dyke and the baked country rock in the Hoting area, Central Sweden: a palaeomagnetic and $^{40}Ar/^{39}Ar$ study: Geophysical Journal International, v. 179(1), p. 59-78.

Elming, S.Å., Pisarevsky, S.A., Layer, P., and Bylund, G., 2014, A palaeomagnetic and $^{40}Ar/^{39}Ar$ study of mafic dykes in southern Sweden: A new early Neoproterozoic key-pole for the Baltic Shield and implications for Sveconorwegian and Grenville loops: Precambrian Research, v. 244, p. 192-206.

Elston, D.P., Enkin, R.J., Baker, J., and Kisilevsky, D.K., 2002, Tightening the Belt: Paleomagnetic-stratigraphic constraints on deposition, correlation, and deformation of the Middle Proterozoic (ca. 1.4 Ga) Belt-Purcell Supergroup, United States and Canada: Geological Society of America Bulletin, v. 114(5), p. 619-638.

Emslie, R.F., Irving, E., and Park, J.K., 1976, Further paleomagnetic results from the Michikamau intrusion, Labrador: Canadian Journal of Earth Sciences, v. 13(8), p. 1052-1057.

Ernst, R.E., Buchan, K.L., Hamilton, M.A., Okrugin, A.V., and Tomshin, M.D., 2000, Integrated paleomagnetism and U-Pb geochronology of mafic dikes of the eastern Anabar Shield region, Siberia: Implications for Mesoproterozoic paleolatitude of Siberia and comparison with Laurentia: The Journal of Geology, v. 108(4), p. 381-401.

Ernst, R.E., Wingate, M.T.D., Buchan, K.L., and Li, Z.X., 2008, Global record of 1600–700 Ma Large Igneous Provinces (LIPs): Implications for the reconstruction of the proposed Nuna (Columbia) and Rodinia supercontinents: Precambrian Research, v. 160(1-2), p. 159-178.

Ernst, R., and Bleeker, W., 2010, Large igneous provinces (LIPs), giant dyke swarms, and mantle plumes: Significance for breakup events within Canada and adjacent regions from 2.5 Ga to the Present: Canadian Journal of Earth Sciences, v. 47(5), p. 695-739.

Ernst, R.E., Pereira, E., Hamilton, M.A., Pisarevsky, S.A., Rodriques, J., Tassinari, C.C., Teixeira, W., and Van-Dunem, V., 2013, Mesoproterozoic intraplate magmatic 'barcode' record of the Angola portion of the Congo Craton: Newly dated magmatic events at 1505 and 1110 Ma and implications for Nuna (Columbia) supercontinent reconstructions: Precambrian Research, v. 230, p. 103-118.

Evans, D.A.D., and Pisarevsky, S.A., 2008, Plate tectonics on early Earth? Weighing the paleomagnetic evidence, *in* Condie, K.C., and Pease, V., eds., When did plate tectonics begin on planet Earth: The Geological Society of America Special Paper, v. 440, p. 249-263.

Evans, D.A.D., 2009, The palaeomagnetically viable, long-lived and all-inclusive Rodinia supercontinent reconstruction: Geological Society, London, Special Publications, v. 327(1), p. 371-404.

Evans, D.A.D., and Mitchell, R.N., 2011, Assembly and breakup of the core of Paleoproterozoic–Mesoproterozoic supercontinent Nuna: Geology, v. 39(5), p. 443-446.

Fisher, R.A., 1953, Dispersion on a sphere: Proceedings of the Royal Society of London. Series A. Mathematical and Physical Sciences, v. 217(1130), p. 295-305.

Gehring, A.U., Fischer, H., Louvel, M., Kunze, K., and Weidler, P.G., 2009, High temperature stability of natural maghemite: a magnetic and spectroscopic study: Geophysical Journal International, v. 179(3), p. 1361-1371.

Gladkochub, D.P., Pisarevsky, S.A., Ernst, R., Donskaya, T.V., Söderlund, U., Mazukabzov, A.M., and Hanes, J., 2010, Large igneous province of about 1750 Ma in the Siberian Craton: Doklady Earth Sciences, v. 430(2), p. 168-171.

Grenholm, M., Jessell, M., and Thébaud, N., 2019, A geodynamic model for the Paleoproterozoic (ca. 2.27–1.96 Ga) Birimian Orogen of the southern West African Craton–Insights into an evolving accretionary-collisional orogenic system: Earth-science reviews, v. 192, p. 138-193.

Halls, H.C., Li, J., Davis, D., Hou, G., Zhang, B., and Qian, X., 2000, A precisely dated Proterozoic palaeomagnetic pole from the North China craton, and its relevance to palaeocontinental reconstruction: Geophysical Journal International, v. 143(1), p. 185-203.

Hrouda, F., 1982, Magnetic anisotropy of rocks and its application in geology and geophysics: Geophysical Surveys, v. 5(1), p. 37-82.

Idnurm, M., Giddings, J.W., and Plumb, K.A., 1995, Apparent polar wander and reversal stratigraphy of the Palaeo-Mesoproterozoic southeastern McArthur Basin, Australia: Precambrian Research, v. 72(1-2), p. 1-41.

Idnurm, M., 2000, Towards a high resolution Late Palaeoproterozoic-earliest Mesoproterozoic apparent polar wander path for northern Australia: Australian Journal of Earth Sciences, v. 47(3), p. 405-429.

Irving, E., Baker, J., Hamilton, M., and Wynne, P.J., 2004, Early Proterozoic geomagnetic field in western Laurentia: Implications for paleolatitudes, local rotations and stratigraphy: Precambrian Research, v. 129(3-4), p. 251-270.

Jaffey, A.H., Flynn, K.F., Glendenin, L.E., Bentley, W.T., and Essling, A.M., 1971, Precision measurement of half-lives and specific activities of ^{235}U and ^{238}U: Physical Review C, v. 4(5), p. 1889-1906.

Jones, C.H., 2002, User-driven integrated software lives: "Paleomag" paleomagnetics analysis on the Macintosh: Computers & Geosciences, v. 28(10), p. 1145-1151.

Kirscher, U., Liu, Y., Li, Z.X., Mitchell, R.N., Pisarevsky, S.A., Denyszyn, S.W., and Nordsvan, A., 2019, Paleomagnetism of the Hart Dolerite (Kimberley, Western Australia)–A two-stage assembly of the supercontinent Nuna? Precambrian Research, v. 329, p. 170-181.

Kirscher, U., Mitchell, R.N., Liu, Y., Nordsvan, A.R., Cox, G.M., Pisarevsky, S.A., Wang, C., Wu, L., Murphy, J.B., and Li, Z.X., 2021, Paleomagnetic constraints on the

duration of the Australia-Laurentia connection in the core of the Nuna supercontinent: Geology, v. 49(2), p. 174-179.

Kirschvink, J.L., 1980, The least-squares line and plane and the analysis of palaeomagnetic data: Geophysical Journal International, v. 62(3), p. 699-718.

Kirschvink, J.L., Kopp, R.E., Raub, T.D., Baumgartner, C.T., and Holt, J.W., 2008, Rapid, precise, and high-sensitivity acquisition of paleomagnetic and rock-magnetic data: Development of a low-noise automatic sample changing system for superconducting rock magnetometers: Geochemistry, Geophysics, Geosystems, v. 9(5), p. 1-18.

Letsch, D., Large, S.J., Bernasconi, S.M., Klug, C., Blattmann, T.M., Winkler, W., and von Quadt, A., 2019, Northwest Africa's Ediacaran to early Cambrian fossil record, its oldest metazoans and age constraints for the basal Taroudant Group (Morocco): Precambrian Research, v. 320, p. 438-453.

Li, Z.X., and Evans, D.A.D., 2011, Late Neoproterozoic 40° intraplate rotation within Australia allows for a tighter-fitting and longer-lasting Rodinia: Geology, v. 39(1), p. 39-42.

Lomax, K., 1975, Palaeomagnetic studies of Proterozoic rocks in Britain and West Africa [Ph.D. thesis]: University of Leeds, 76 p.

Lubnina, N.V., 2009, The East European Craton in the Mesoproterozoic: new key paleomagnetic poles: Doklady Earth Sciences, v. 428(2), p. 252-257.

Ludwig, K.R., 2012, User's Manual for Isoplot 3.75. A Geochronological Toolkit for Microsoft Excel: Berkeley Geochronology Center Special Publication, v. 5, p. 1-75.

Maier, W.D., Rasmussen, B., Fletcher, I.R., Li, C., Barnes, S.J., and Huhma, H., 2013, The Kunene anorthosite complex, Namibia, and its satellite intrusions: Geochemistry, geochronology, and economic potential: Economic Geology, v. 108(5), p. 953-986.

Mäkitie, H., Data, G., Isabirye, E., Mänttäri, I., Huhma, H., Klausen, M.B., Pakkanen, L, and Virransalo, P., 2014, Petrology, geochronology and emplacement model of the giant 1.37 Ga arcuate Lake Victoria Dyke Swarm on the margin of a large igneous province in eastern Africa: Journal of African Earth Sciences, v. 97, p. 273-296.

Maloof, A.C., Schrag, D.P., Crowley, J.L., and Bowring, S.A., 2005, An expanded record of Early Cambrian carbon cycling from the Anti-Atlas Margin, Morocco: Canadian Journal of Earth Sciences, v. 42(12), p. 2195-2216.

Marcussen, C., and Abrahamsen, N., 1983, Palaeomagnetism of the Proterozoic Zig-Zag Dal basalt and the Midsommersø dolerites, eastern North Greenland: Geophysical Journal International, v. 73(2), p. 367-387.

McFadden, P.L., and McElhinny, M.W., 1988, The combined analysis of remagnetization circles and direct observations in palaeomagnetism: Earth and Planetary Science Letters, v. 87(1-2), p. 161-172.

McFadden, P.L., and McElhinny, M.W., 1990, Classification of the reversal test in palaeomagnetism: Geophysical Journal International, v. 103(3), p. 725-729.

McFarlane, H.B., Ailleres, L., Betts, P., Ganne, J., Baratoux, L., Jessell, M.W., and Block, S., 2019, Episodic collisional orogenesis and lower crust exhumation during the Palaeoproterozoic Eburnean Orogeny: Evidence from the Sefwi Greenstone Belt, West African Craton: Precambrian Research, v. 325, p. 88-110.

Meert, J.G., Pivarunas, A.F., Evans, D.A., Pisarevsky, S.A., Pesonen, L.J., Li, Z.X., Elming, S.Å., Miller, S.R., Zhang, S., and Salminen, J.M., 2020, The magnificent seven: A proposal for modest revision of the quality index: Tectonophysics, v. 790, p. 228549.

Michard, A., Saddiqi, O., Chalouan, A., and de Lamotte, D.F., 2008, Continental evolution: The geology of Morocco: Structure, stratigraphy, and tectonics of the Africa-Atlantic-Mediterranean triple junction, v. 116, 426 p.

Müller, R.D., Cannon, J., Qin, X., Watson, R.J., Gurnis, M., Williams, S., Pfaffelmoser, T., Seton, M., Russell, S.H., and Zahirovic, S., 2018, GPlates: building a virtual Earth through deep time: Geochemistry, Geophysics, Geosystems, v. 19(7), p. 2243-2261.

Muxworthy, A.R., and McClelland, E., 2000, The causes of low-temperature demagnetization of remanence in multidomain magnetite: Geophysical Journal International, v. 140(1), p. 115-131.

Neres, M., Silva, P.F., Ikenne, M., Martins, S., Hafid, A., Mata, J., Almeida, F., Youbi, N., and Boumehdi, M.A., 2016, Evidences for multiple remagnetization of Proterozoic dykes from Iguerda inlier (Anti-Atlas Belt, Southern Morocco): Studia Geophysica et Geodaetica, v. 60(4), p. 700-730.

Nomade, S., Chen, Y., Pouclet, A., Féraud, G., Théveniaut, H., Daouda, B.Y., Vidal, M., and Rigolet, C., 2003, The Guiana and the West African shield Palaeoproterozoic grouping: New palaeomagnetic data for French Guiana and the Ivory Coast: Geophysical Journal International, v. 154(3), p. 677-694.

Onstott, T.C., and Dorbor, J., 1987, $^{40}Ar/^{39}Ar$ and paleomagnetic results from Liberia and the Precambrian APW data base for the West African Shield: Journal of African Earth Sciences, v. 6(4), p. 537-552.

Onstott, T.C., Hargraves, R.B., York, D., and Hall, C., 1984, Constraints on the motions of South American and African Shields during the Proterozoic: I. $^{40}Ar/^{39}Ar$ and paleomagnetic correlations between Venezuela and Liberia: Geological Society of America Bulletin, v. 95(9), p. 1045-1054.

Park, J.K., Irving, E., and Donaldson, J.A., 1973, Paleomagnetism of the Precambrian Dubawnt Group: Geological Society of America Bulletin, v. 84(3), p. 859-870.

Peng, P., 2010, Reconstruction and interpretation of giant mafic dyke swarms: A case study of 1.78 Ga magmatism in the North China craton: Geological Society, London, Special Publications, v. 338(1), p. 163-178.

Piper, J.D.A., and Lomax, K., 1973, Palaeomagnetism of Precambrian Birrimian and Tarkwaian rocks of West Africa: Geophysical Journal International, v. 34(4), p. 435-450.

Pisarevsky, S.A., and Sokolov, S.J., 2001, The magnetostratigraphy and a 1780 Ma palaeomagnetic pole from the red sandstones of the Vazhinka River section, Karelia, Russia: Geophysical Journal International, v. 146(2), p. 531-538.

Puchkov, V.N., Bogdanova, S.V., Ernst, R.E., Kozlov, V.I., Krasnobaev, A.A., Söderlund, U., Wingate, M.T., Postnikov, A.V., and Sergeeva, N.D., 2013, The ca. 1380 Ma Mashak igneous event of the Southern Urals: Lithos, v. 174, p. 109-124.

Reis, N.J., Teixeira, W., Hamilton, M.A., Bispo-Santos, F., Almeida, M.E., and D'Agrella-Filho, M.S., 2013, Avanavero mafic magmatism, a late Paleoproterozoic LIP in the Guiana Shield, Amazonian Craton: U–Pb ID-TIMS baddeleyite, geochemical and paleomagnetic evidence: Lithos, v. 174, p. 175-195.

Ruiz, G.M., Helg, U., Negro, F., Adatte, T., and Burkhard, M., 2008, Illite crystallinity patterns in the Anti-Atlas of Morocco: Swiss Journal of Geosciences, v. 101(2), p. 387-395.

Schmidt, P.W., and Williams, G.E., 2008, Palaeomagnetism of red beds from the Kimberley Group, Western Australia: Implications for the palaeogeography of the 1.8 Ga King Leopold glaciation: Precambrian Research, v. 167(3-4), p. 267-280.

Schofield, D.I., Horstwood, M.S.A., Pitfield, P.E.J., Crowley, Q.G., Wilkinson, A.F., and Sidaty, H.C.O., 2006, Timing and kinematics of Eburnean tectonics in the central Reguibat Shield, Mauritania: Journal of the Geological Society, v. 163(3), p. 549-560.

Söderlund, U., and Johansson, L., 2002, A simple way to extract baddeleyite (ZrO_2): Geochemistry, Geophysics, Geosystems, v. 3(2), p. 1-7.

Söderlund, U., Ibanez-Mejia, M., El Bahat, A., Ernst, R.E., Ikenne, M., Soulaimani, A., Youbi, N., Cousens, B., and Hafid, A., 2013, Reply to Comment on "U–Pb baddeleyite ages and geochemistry of dolerite dykes in the Bas-Drâa inlier of the Anti-Atlas of Morocco: Newly identified 1380 Ma event in the West African Craton" by André Michard and Dominique Gasquet: Lithos, v. 174, p. 101-108.

Soulaimani, A., and Burkhard, M., 2008, The Anti-Atlas chain (Morocco): The southern margin of the Variscan belt along the edge of the West African Craton: Geological Society, London, Special Publications, v. 297(1), p. 433-452.

Stacey, J.S., and Kramers, J.D., 1975, Approximation of terrestrial lead isotope evolution by a two-stage model: Earth and Planetary Science Letters, v. 26(2), p. 207-221.

Théveniaut, H., Delor, C., Lafon, J.M., Monié, P., Rossi, P., and Lahondère, D., 2006, Paleoproterozoic (2155–1970 Ma) evolution of the Guiana Shield (Transamazonian

event) in the light of new paleomagnetic data from French Guiana: Precambrian Research, v. 150(3-4), p. 221-256.

Torsvik, T.H., Van der Voo, R., Preeden, U., Mac Niocaill, C., Steinberger, B., Doubrovine, P.V., Van Hinsbergen, D.J., Domeier, M., Gaina, C., Tohver, E., and Meert, J.G., 2012, Phanerozoic polar wander, palaeogeography and dynamics: Earth-Science Reviews, v. 114(3-4), p. 325-368.

Upton, B.G.J., Rämö, O.T., Heaman, L.M., Blichert-Toft, J., Kalsbeek, F., Barry, T.L., and Jepsen, H.F., 2005, The Mesoproterozoic Zig-Zag Dal basalts and associated intrusions of eastern North Greenland: Mantle plume–lithosphere interaction: Contributions to Mineralogy and Petrology, v. 149(1), p. 40-56.

Van der Voo, R., 1990, The reliability of paleomagnetic data: Tectonophysics, v. 184, p. 1-9.

Wu, H., 2005, New Paleomagnetic Results from Mesoproterozoic Successions in Jixian Area, North China Block, and Their Implications for Paleocontinental Reconstructions [Ph.D. thesis]: China University of Geosciences, Beijing, 133 p.

Xu, H., Yang, Z., Peng, P., Meert, J.G., and Zhu, R., 2014, Paleo-position of the North China craton within the supercontinent Columbia: Constraints from new paleomagnetic results: Precambrian Research, v. 255, p. 276-293.

Youbi, N., Kouyaté, D., Söderlund, U., Ernst, R.E., Soulaimani, A., Hafid, A., Ikenne, M., El Bahat, A., Bertrand, H., Chaham, K.R., and Abbou, M.B., 2013, The 1750 Ma magmatic event of the west African craton (Anti-Atlas, Morocco): Precambrian Research, v. 236, p. 106-123.

Zhang, S., Li, Z.X., Evans, D.A.D., Wu, H., Li, H., and Dong, J., 2012, Pre-Rodinia supercontinent Nuna shaping up: A global synthesis with new paleomagnetic results from North China: Earth and Planetary Science Letters, v. 353, p. 145-155.

Zijderveld, J.D.A., 1967, AC Demagnetization of Rocks: Analysis of Results, *in* Methods in Palaeomagnetism, p. 254-286.